Czech University of Life Sciences Prague

Faculty of Forestry and Wood Science

Department of Forest Genetics and Physiology

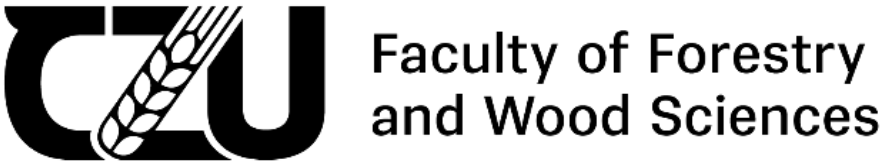

Application of novel methods in genetic evaluation using advanced phenotyping

Dissertation thesis

Author: Ing. Daniel Provazník

Supervisor: doc. Ing. Jan Stejskal, Ph.D.

4 Attachments

Prague 2025

CZECH UNIVERSITY OF LIFE SCIENCES PRAGUE

Faculty of Forestry and Wood Sciences

Ph.D. THESIS ASSIGNMENT

Ing. Daniel Provazník

Forest Biology

Thesis title

Application of novel methods in genetic evaluation using advanced phenotyping

---

Objectives of thesis

The topic of the dissertation theses was chosen based on the current needs of the forest sector. For the acceleration of breeding programs, applying the most effective strategies based on advanced phenotyping methods using molecular markers is necessary. These are the main foundations for ensuring quality reproduction material for the future. The main aim of the dissertation theses is primarily to connect genetics and tree physiology in the context of tree breeding. The physiological and morphological properties of chosen populations will be monitored in different experimental plots. All obtained information will be used for thorough statistical analyses.

Main aims:

Evaluation of the experimental plots based on growth and physiological traits.

To connect genetics and tree physiology in the context of tree breeding – a study of phenotype and genotype correlations between growth and physiological parameters (including genotype and environment interactions).

A novel aspect will be the study of phenotypic and genotypic correlations between growth, physiological parameters, and adaptive traits of chosen populations.

Hypotheses:

There are significant genetic correlations between physiological, production, and adaptive traits, which can be further used for early indirect selection.

Methodology

Experimental material will be obtained mainly from seed orchards in Czechia and other European countries. The tree species of interest will be chosen based on suitable experimental sites with significant genetic variation, the current needs of forestry, and in the context of climate change. The species of interest

will likely be Pinus sylvestris, Fagus sylvatica, Alnus glutinosa, Picea abies, Abies nordmanniana, Acer pseudoplatanus, or Quercus robur.

Production parameters (diameter at breast height, height) and physiological parameters (fluorescence, reflectance, photosynthetic pigment content, leaf senescence) will be measured. The innovative aspect will be the assessment of adaptive traits.

All data will be subsequently analyzed by multivariate mixed models, which enables the estimation of genetic correlations. The presented results will be based on a model that best fits the genetic variability of the analyzed data. A novel aspect will be mainly the effective linkage of all three groups of parameters.

The proposed extent of the thesis

100 stran

Keywords

linear mixed models, reflectance, genetic variability, genetic correlations

---

Recommended information sources

CABALLERO, A. Quantitative genetics. Cambridge University Press, 2020. ISBN 978-1-108-72235-3.
EISMANN, Michael Theodore and SPIE (SOCIETY). *Hyperspectral remote sensing.* Bellingham, Wash.: SPIE Press, 2012. ISBN 9780819487872.
FALCONER, D S. – MACKAY, T F C. Introduction to quantitative genetics. Harlow: Pearson Prentice Hall, 1996. ISBN 978-0-582-24302-6.
JACQUEMOUD, S. – & Ustin, S. Leaf optical properties. Cambridge University Press, 2019. ISBN 9781108686457.
LYNCH, M. – WALSH, B. Genetics and analysis of quantitative traits. Sunderland: Sinauer, 1998. ISBN 0-87893-481-2.
WHITE, T L. – NEALE, D B. – ADAMS, W T. – C.A.B. INTERNATIONAL, ISSUING BODY. Forest genetics. Wallingford, Oxfordshire, UK: CABI, 2007. ISBN 1845932854.

Expected date

2024/25 SS – FFWS – State Doctoral Examinations

The Dissertation Thesis Supervisor

doc. Ing. Jan Stejskal, Ph.D.

Supervising department

Department of Forest Genetics and Physiology

Electronic approval: 29. 04. 2025

doc. Ing. Ivana Tomášková, Ph.D.

Head of department

Electronic approval: 03. 11. 2025

prof. Ing. Milan Lstibůrek, MSc, Ph.D.

Chairperson of Field of Study Board

Electronic approval: 07. 11. 2025

prof. Ing. Róbert Marušák, PhD.

Dean

Prague on 12. 11. 2025

Abstract

This thesis investigates the application of novel methods in genetic evaluation by integrating advanced phenotyping with quantitative genetic approaches in forest trees. Focusing on *Pinus sylvestris* L., *Fagus sylvatica* L., and *Alnus glutinosa* (L.) Gaertn., it examines the genetic variation and adaptive significance of key functional traits, including phenology, growth and structural traits, photosynthetic and stress-related physiological traits, and spectral reflectance.

A multi-experiment framework was established, combining material from seed orchards and provenance trials, some of which included family structure or clonal structure enhanced by SNP-based genomic data. The resulting datasets were analyzed using linear mixed models to estimate heritability and genetic correlations across traits, sites, and years.

The findings revealed strong genetic control of phenological traits, while growth and water-use traits exhibit moderate heritability with pronounced site dependence. A central innovation of this work was the use of hyperspectral reflectance as a high-throughput, non-destructive proxy for physiological and structural variation. Reflectance in the visible and red-edge regions exhibited high heritability and temporal stability, whereas near- and shortwave-infrared regions captured environment-driven variation. Automated imaging methods, including a newly developed bud-counting macro, further enhanced the efficiency and consistency of phenotyping.

By integrating multiple sources of phenotypic and genetic relationship information, these studies enhance the accuracy of genetic parameter estimation, enabling earlier and more reliable detection of adaptive signals. The methodological framework developed here establishes an effective link between growth, physiological, and adaptive traits in forest tree populations. This approach provides valuable tools to accelerate breeding for climate resilience, supporting a transition from traditional production-focused strategies to modern, adaptive tree improvement programs designed for a rapidly changing environment.

Keywords: forest phenotyping, genetic evaluation, hyperspectral reflectance, genetic correlations, genotype-by-environment interactions

Abstrakt

Tato práce zkoumá využití nových metod genetické evaluace prostřednictvím integrace pokročilého fenotypování s kvantitativně-genetickými přístupy u lesních dřevin. Se zaměřením na druhy *Pinus sylvestris* L., *Fagus sylvatica* L. a *Alnus glutinosa* (L.) Gaertn. tato práce analyzuje genetickou variabilitu a adaptivní význam klíčových funkčních znaků, včetně fenologie, růstových a strukturálních znaků, spektrální odrazivosti a fyziologických znaků souvisejících se stresem a fotosyntézou.

Bylo realizováno několik experimentů s využitím materiálu ze semenných sadů a provenienčních pokusů, z nichž některé obsahovaly rodinnou nebo klonální strukturou podpořenou SNP-genomickými daty. Získané soubory dat byly analyzovány pomocí lineárních smíšených modelů za účelem odhadu dědivosti a genetických korelací mezi znaky, lokalitami a roky.

Výsledky ukázaly, že fenologické znaky jsou pod silnou genetickou kontrolou, zatímco růstové znaky, či znaky související s vodním režimem vykazují střední dědivost a výraznou závislost na stanovišti. Klíčovou inovací této práce bylo využití hyperspektrální odrazivosti jako vysoce-výkonného, nedestruktivního nástroje pro odhad fyziologické a strukturální variability. Odrazivost ve viditelných a „red-edge“ pásmech vykazovala vysokou dědivost a stabilitu mezi roky, zatímco blízké a krátkovlnné infračervené pásmo zachycovalo variabilitu způsobenou prostředím. Automatizované optické zobrazovací metody, včetně nově vyvinutého makra pro počítání pupenů, ještě zvýšily efektivitu a konzistenci fenotypování.

Integrací více zdrojů fenotypových a genetických informací tyto studie zvyšují přesnost odhadů genetických parametrů a umožnují dřívější a spolehlivější detekci adaptačních signálů. Vyvinutý metodologický rámec vytváří účinné propojení mezi růstem, fyziologickými a adaptačními znaky populací lesních dřevin. Tento přístup poskytuje cenné nástroje pro urychlení šlechtění k odolnosti vůči změně klimatu a podporuje přechod od tradičních produkčně orientovaných strategií k moderním adaptivním programům šlechtění dřevin přizpůsobeným rychle se měnícím podmínkám prostředí.

Klíčová slova: fenotypování lesních dřevin, genetická evaluace, hyperspektrální odrazivost, genetické korelace, interakce genotypu s prostředím

Abstrakt

Denne afhandling undersøger anvendelsen af nye metoder til genetisk evaluering i træforædlingen gennem brug af avanceret fænotypning kombineret med kvantitative genetiske analyser og med fokus på Pinus sylvestris L., Fagus sylvatica L. og Alnus glutinosa (L.) Gaertn. Afhandlingen undersøger den genetiske variation i- og adaptive betydning af centrale funktionelle træk, herunder fænologi, vækst- og strukturelle træk, fotosyntetiske og stressrelaterede fysiologiske træk, samt spektral reflektans.

Afhandlingen er baseret på en række eksperimenter, der omfatter materiale fra frøplantager og proveniensforsøg, nogle med familiestruktur eller klonstruktur, i flere tilfælde fundet- og forfinet vha. af SNP-baserede genomiske data. Data fra eksperimenterne er blevet analyseret ved hjælp af lineære blandede modeller for at estimere arvelighed og genetiske korrelationer på tværs af egenskaber, lokaliteter og år.

Resultaterne viser en stærk genetisk kontrol af fænologi, mens vækst- og vandudnyttelseseffektivitet (water use efficiency) udviser moderat arvelighed afhængig af lokalitet. En central innovation i dette arbejde er brugen af hyperspektral reflektans som en højkapacitets, ikke-destruktiv proxy for fysiologisk og strukturel variation.

Reflektans i områder med synligt og rødt lys, udviste høj arvelighed og tidsmæssig stabilitet, hvorimod reflektans i nær- og kortbølge-infrarøde områder viste stor miljøvariation. Automatiserede billedanalysemetoder, herunder en ny knoptællende makro, forbedrede yderligere effektiviteten og konsistensen i fænotypningen.

Ved at integrere flere fænotypiske målinger og forbedre kendskabet til slægtskaberne i træerne vha. genetiske markører, forbedrede denne undersøgelse nøjagtigheden i estimeringen af genetiske parametre, hvilket muliggjorde tidlig og mere pålidelig detektion af adaptive signaler. Den metodologiske ramme, der er udviklet her, etablerer en effektiv forbindelse mellem vækst, fysiologiske og adaptive egenskaber i skovtræer. Denne tilgang giver værdifulde værktøjer til at accelerere forædlingen for klimamodstandsdygtighed og understøtter en overgang fra traditionelle produktionsfokuserede strategier til moderne træforædlingsprogrammer der sigter mod tilpasningsdygtighed i forhold til et hurtigt skiftende miljø.

Nøgleord: Fænotypning, genetisk evaluering, hyperspektral reflektans, genetiske korrelationer, genotype-miljø vekselvirkninger

Résumé

Cette thèse étudie l'application de méthodes innovantes d'évaluation génétique en intégrant un phénotypage avancé à des approches de génétique quantitative chez les arbres forestiers. En se concentrant sur *Pinus sylvestris* L., *Fagus sylvatica* L., et *Alnus glutinosa* (L.) Gaertn., elle examine la variation génétique et l'importance adaptative de traits fonctionnels clés, notamment la phénologie, la croissance et les traits structuraux, les caractéristiques physiologiques liées à la photosynthèse et au stress, ainsi que la réflectance spectrale.

Un cadre multi-expérimental a été établi, combinant du matériel provenant d'arboretums à graines et d'essais de provenances, certains présentant une structure familiale ou clonale renforcée par des données génomiques SNP. Les jeux de données obtenus ont été analysés à l'aide de modèles linéaires mixtes afin d'estimer l'héritabilité et les corrélations génétiques entre traits, sites et années.

Les résultats révèlent un fort contrôle génétique des traits phénologiques, tandis que les traits de croissance et liés à l'usage de l'eau montrent une héritabilité modérée avec une dépendance marquée au site. Une innovation centrale de ce travail est l'utilisation de la réflectance hyperspectrale comme indicateur non destructif à haut débit des variations physiologiques et structurelles. La réflectance dans les régions visibles et rouges a montré une héritabilité et une stabilité temporelle élevées, tandis que les régions infrarouges proches et courtes ont capturé les variations liées à l'environnement. Les méthodes d'imagerie automatisées, notamment une nouvelle macro de comptage des bourgeons, ont encore amélioré l'efficacité et la cohérence du phénotypage.

En intégrant plusieurs sources d'informations sur les relations phénotypiques et génétiques, cette étude a amélioré la précision de l'estimation des paramètres génétiques, permettant une détection plus précoce et plus fiable des signaux adaptatifs. Le cadre méthodologique développé ici établit un lien efficace entre les caractéristiques de croissance, physiologiques et adaptatives des populations d'arbres forestiers. Cette approche fournit des outils précieux pour accélérer la sélection en faveur de la résilience climatique, favorisant ainsi la transition entre les stratégies traditionnelles axées sur la production et les programmes modernes d'amélioration adaptative des arbres conçus pour un environnement en rapide évolution.

Mots-clés: phénotypage forestier, évaluation génétique, réflectance hyperspectrale, corrélations génétiques, interactions génotype × environnement

Declaration

I hereby declare that I have done this final thesis entitled „ Application of novel methods in genetic evaluation using advanced phenotyping “, independently, all text in this thesis is original, and all the sources have been quoted and acknowledged by means of complete references and according to Citation rules of the FTA. I declare that I have used AI tools in accordance with the university's internal regulations and the principles of academic integrity and ethics.

Prague, 16.11.2025

Signature

Acknowledgements

I would first like to express my sincere gratitude to doc. Ing. Jan Stejskal, Ph.D., for his supervision, guidance, and constructive feedback throughout my doctoral studies, as well as during my master's degree. I am also profoundly thankful to Jon Kehlet Hansen, Ph.D., for his supervision not only during my research stay in Denmark, but also for his valuable insights and feedback on all my experiments. My sincere thanks go to Prof. Markku Keinänen, Ph.D., for providing me with the opportunity to work with and learn from him during my internship in Finland. For the data used in Experiment 2, I would like to thank Ole Kim Hansen, Ph.D., and his students for designing the experimental layout, as well as Ing. Ivana Tomášková, Ph.D., and doc. Ing. Jan Stejskal, Ph.D., for measuring the photosynthetic parameters in 2018. I would also like to acknowledge RNDr. Jaroslav Čepl, Ph.D., mainly for his assistance with the analytical aspects of my experiments, and I extend my appreciation to all my co-authors, both of published and yet unpublished work, for their collaboration and support.

On a more personal note, I am profoundly grateful to my family for their unwavering encouragement and patience throughout the long course of my studies, even when it may have seemed endless to some of them. My heartfelt thanks go to my girlfriend, Julia, for her constant support, love, and willingness to share her expertise beyond her own field, even while preparing her own Ph.D. thesis. Last but not least, I would like to thank my friend Lance for his expert knowledge of his mother tongue, which significantly improved the language quality of my publications, and for providing us with a creative refuge in his new home on Prince Edward Island, where the first chapters of this thesis took shape.

Table of Contents

1 INTRODUCTION 22

2 OBJECTIVES AND HYPOTHESIS 24

3 LITERATURE REVIEW 26

3.1 Climate Change and Tree Species Distribution 26

3.2 Overview of Selected Species 29

3.2.1 Scots Pine (Pinus sylvestris L.) 29

3.2.2 European Beech (Fagus sylvatica L.) 30

3.2.3 European Black Alder (Alnus glutinosa [L.] Gaertn.) 32

3.3 Phenotyping in Forest Trees 35

3.3.1 Traditional Approaches 35

3.3.2 Functional Traits in Phenotyping 36

3.3.2.1 Structural Functional Leaf Traits 37

3.3.2.2 Photosynthetic Pigments 37

3.3.2.3 Phenology 38

3.3.3 Novel Phenotyping Methods for Forest Trees 39

3.3.3.1 Laboratory Spectroscopy 40

3.3.3.2 Imaging Spectroscopy 43

3.3.3.3 Spectral Tools for Forest Genetics and Physiology 44

3.3.3.4 Imaging-Based Phenotyping for Conifer Seedling Phenology 45

3.3.3.5 Variable Chlorophyll *a* Fluorescence 47

3.3.3.6 Measurements of Foliage Photosynthetic Rates 49

3.4 Forest Genetics, Tree Breeding, and Genetic Evaluation 50

3.4.1 Heritability 51

3.4.2 Breeding Values 52

3.4.3 Phenotypic and Genetic Correlations 53

3.4.3.1 Phenotypic Correlation 53

3.4.3.2 Type A Genetic Correlation 53

3.4.3.3 Type B Genetic Correlation and Genotype-by-Environment Interactions 53

3.4.3.4 Age-to-Age (Year-to-Year) Correlations 54

3.4.4 Indirect Selection 55

3.4.5 Linear Mixed Models 55

3.4.5.1 Parental (Family) Models 56

3.4.5.2 Individual Tree (Animal) Models 57

3.4.6 REML and Variance Component Estimation 58

3.4.7 Estimation of Fixed and Random Effects 58

3.4.8 Multivariate Linear Mixed Models 59

4 METHODOLOGY 61

4.1 METHODOLOGY FOR EXPERIMENT 1 – SCOTS PINE CLONES – SEED ORCHARDS 62

4.1.1 Plant Material 62

4.1.2 Needle Level Reflectance 63

4.1.3 Canopy Level Reflectance 64

4.1.4 Measurement of Needle Functional Traits 66

4.1.5 SNP Genotyping Array 67

4.1.6 Genomic Data 67

4.1.7 Statistical Analysis and Genetic Parameters 68

4.2 METHODOLOGY FOR EXPERIMENT 2 – EUROPEAN BEECH PROVENANCES 71

4.2.1 Plant Material 71

4.2.2 Chlorophyll Fluorescence Kinetics 72

4.2.3 Gas Exchange 75

4.2.4 Bud Flushing 75

4.2.5 Senescence Scores 76

4.2.6 Statistical Analyses 76

4.3 METHODOLOGY FOR EXPERIMENT 3 – SCOTS PINE PROVENANCES - SEEDLINGS 78

4.3.1 Plant Material 78

4.3.2 HSI System Setup and Acquisition Parameters 79

4.3.3 Image Processing 79

4.3.4 Image Classification 80

4.3.5 Macro for Bud Counting 81

4.3.6 Partial Least Squares Discriminant Analysis (PLS-DA) 81

4.3.7 F-Score 82

4.4 METHODOLOGY FOR EXPERIMENT 4 – BLACK ALDER PROVENANCES 84

4.4.1 Plant Material 84

4.4.2 Bud Burst 88

4.4.3 Precipitation 88

4.4.4 Hyperspectral Reflectance 90

4.4.5 Statistical Analysis 90

5 RESULTS 95

5.1 RESULTS OF EXPERIMENT 1 – SCOTS PINE CLONES – SEED ORCHARD 95

5.1.1 Genetic Variation in Needle Functional Traits 95

5.1.2 Spectral Reflectance 97

5.1.3 Year-to-Year Genetic Correlations of Canopy-Level Reflectance 101

5.1.4 Genotype-by-Environment Interaction in Needle- and Canopy-Level Reflectance 102

5.1.5 Genetic Correlations Among the Spectra and NFTs 105
5.2 Results of Experiment 2 – European Beech Provenances 109
5.2.1 Photosynthetic Performance 109
5.2.2 Provenance Pairwise Comparison 111
5.2.3 Bud Flushing 114
5.2.4 Senescence 117
5.3 Results of Experiment 3 – Scots Pine Provenances - Seedlings 118
5.3.1 Background Removal and Mean Reflectance Extraction 118
5.3.2 Classification 119
5.3.3 Partial Least Squares Discriminant Analysis 121
5.3.4 Bud Count 124
5.4 Results of Experiment 4 – Black Alder Provenances 126
5.4.1 Survival Rates 126
5.4.2 Bud Burst 126
5.4.3 Heritability Estimates for Growth Increment 127
5.4.4 Family Performance in Height Increment Across Sites and Years 127
5.4.5 Genotype-by-Environment Interactions 135
5.4.6 Provenance Evaluation Across Sites and Years 137
5.4.7 Spectral Reflectance 139
6 DISCUSSION 141
6.1 Phenology and Seasonal Timing 143
6.1.1 Bud Burst and Flushing Dynamics Across Broad-Leaved Species 143
6.1.2 Autumn Senescence and Coloration 144
6.1.2.1 Supervised Classification Captures Adaptive Phenology in Scots Pine 145
6.1.2.2 Short-day Treatment Differences Revealed by Hyperspectral Data 146
6.1.3 Autumn Bud Set in Scots pine Seedlings 147
6.2 Growth and Leaf (Needle) Structural Traits 148
6.2.1 Genetic Variation of Needle Structural Traits 148
6.2.2 Genetic Variation in Early Growth of Black Alder 149
6.3 Physiological Stress-Related Traits 151
6.3.1 Photosynthetic Pigments and Physiological Indicators 151
6.3.2 Water Use Stress-Related Traits 152
6.3.3 Photosynthetic Activity Related to Altitude of Origin 152
6.4 Remote Sensing-Based Phenotyping and Spectral Reflectance 155
6.4.1 Genetic Variation in Canopy-Level and Needle-Level Reflectance 155
6.4.2 Robust Background Removal and Spectra-based Differentiation 156

6.5 TRAIT-BASED PATTERNS OF PROVENANCE DIFFERENTIATION 158
6.5.1 European Beech Provenances Separated by Photosynthetic Parameters 158
6.5.2 Hyperspectral Signatures Reveal Physiological Differentiation Among Scots Pine Origins 159
6.5.3 Provenance Variation and Local Adaptation in Black Alder Growth Performance 161
6.5.3.1 General Performance of Provenances and Families Across the Environment 162
6.6 GENETIC CORRELATIONS 164
6.6.1 Genetic Correlation Between NFTs and Spectra 164
6.6.2 Gene-by-Environment Interactions 165
6.6.2.1 Gene-by-Environment Interactions in Spectral Reflectance 165
6.6.2.2 Climatic and Soil Conditions Related to G×E in Black alder 165
6.6.3 Age-to-Age Genetic Correlations 166
6.6.3.1 Spectral Reflectance Year-to-Year Genetic Correlations 166
6.6.3.2 Age-to-Age Interactions in Growth Increment 167
6.7 NOVELTIES RELATED TO PLANT PHENOTYPING, THEIR ADVANTAGES AND LIMITATIONS 169
6.7.1 Importance of Genomic Data in the Estimation of Genetic Parameters for Needle Functional Traits Related to Environmental Variation 169
6.7.2 Novel Hyperspectral Imaging Setup: Advantages and Limitations 169
6.7.3 Automated Bud Set Detection in Scots Pine 170
7 CONCLUSIONS 172
8 REFERENCES 173
ATTACHMENTS 196
ATTACHMENT 1 - EXPERIMENT 1 – SOIL ANALYSES IN SEED ORCHARDS 196
ATTACHMENT 2 - EXPERIMENT 1 – SEED ORCHARD LAYOUTS 197
ATTACHMENT 3 - EXPERIMENT 2 – EXPERIMENTAL LAYOUT 198
ATTACHMENT 4 – EXPERIMENT 4 – EXPERIMENTAL LAYOUTS OF EACH SITE 199

List of used symbols and abbreviations

ABS/RC – Average absorbed photon flux per PSII reaction center

A1270 - Provenance subgroup - Aspromonte, 1270 m a.s.l., Italy (Exp. 2)

A1900 - Provenance subgroup - Aspromonte, 1900 m a.s.l., Italy (Exp. 2)

ANOVA – Analysis of Variance

BLUP – Best Linear Unbiased Prediction

C-G CPH – Copenhagen common garden site (Exp. 2)

car – Total carotenoids

car:chl T – Ratio of total carotenoids to total chlorophyll

CEF - C.E. Flensborg (Seedling seed orchard 506 C.E. Flensborg Plantation)

Chl a – Chlorophyll *a*

Chl b – Chlorophyll *b*

Chl T – Total chlorophyll (*a* + *b*)

κ – Cohen's Kappa coefficient (measure of inter-rater agreement)

DBH – Diameter at Breast Height

DI_0/RC – Dissipated energy flux per reaction center

DK-F13 – Provenance from Stenderup Midtskov seed stand, Denmark (Exp. 2)

DK-F419 – Provenance from Holstenshuus seed stand, Denmark (Exp. 2)

DRA – Draved Skov-Vest provenance (Exp. 4)

DY – Dybvig Skov provenance (Exp. 4)

EWT – Equivalent Water Thickness

F_0 – Minimal fluorescence intensity from a dark-adapted leaf (50 µs)

F_i – Fluorescence intensity at I-step (30 ms)

F_j – Fluorescence intensity at J-step (2 ms)

F_m – Maximal fluorescence intensity

F_m/F_0 – Fluorescence ratio (maximal to minimal)

FP657 – Tophøj clonal seed orchard (Denmark) (Exp. 4)

FP658 – Laugesen clonal seed orchard (Denmark) (Exp. 4)

FP850 – Kollaberga clonal seed orchard (Sweden) (Exp. 4)

FP851 – Ignaberg clonal seed orchard (Sweden) (Exp. 4)

FP852 – Trolleholm clonal seed orchard (Sweden) (Exp. 4)

FUS – Fussingø provenance (Exp. 4)

F_v – Maximal variable fluorescence (Fv = Fm − F0)

F829 – Skjoldenæsholm Seed lot from FP851(Denmark) (Exp. 4)

F840 – Tusenæs seed lot from F.2 Gråsten (Denmark) (Exp. 4)

G×E – Genotype × Environment interaction

GBLUP – genomic best linear unbiased prediction

GE – Gas exchange

GIS – Geographic Information System

GPS – Global Positioning System

GRM – Genomic Relationship Matrix

H^2 – Broad-sense heritability

h^2 – Narrow-sense heritability

HALD – Hald Sø-Vestende provenance (Exp. 4)

HTP – High-Throughput Phenotyping

IBD – Identity by Descent

LCP – Light compensation point [μmol (photons) m^{-2} s^{-1}]

LIV – Livø provenance (Exp. 4)

LMA – Leaf Mass per Area

LOU – Lounkær provenance (Exp. 4)

LRT – Likelihood Ratio Test

LSP_{95} – Light saturation point for $P_N + R_D$ equal to 95 % of P_{Nmax}

M_0 – Approximated initial slope of the fluorescence transient

NFT – Needle Functional Trait

NIR – Near-Infrared (spectral region)

NL – Needle Length

NWC – Needle Water Content

OJIP – Chlorophyll fluorescence transient curve steps

PAR – Photosynthetically Active Radiation

PCA – Principal Component Analysis

PI_{ABS} – Multi-parameter photosynthetic performance index

PI_{TOTAL} – Performance index for energy conservation from photons absorbed by PSII antenna until PSI reduction

PLS-DA – Partial Least Squares Discriminant Analysis

PLSR – Partial Least Squares Regression

P_N – Net assimilation of CO_2 [µmol m^{-2} s^{-1}]

PSI / PSII – Photosystem I / II

QTL – Quantitative Trait Locus

R^2 – Coefficient of Determination

RAV – Ravnholt provenance

RC – Reaction center

R_D – Dark respiration rate

RU - Runde Mølle provenance (Exp. 4)

RYD – Rydhave skov provenance (Exp. 4)

SG1300 - Provenance subgroup - Sila Grande, 1300 m a.s.l., Italy (Exp. 2)

SG1900 - Provenance subgroup - Sila Grande, 1900 m a.s.l., Italy (Exp. 2)

SLET – Slette Å provenance (Exp. 4)

SLOT – Slotsved Skov provenance (Exp. 4)

SNP – Single Nucleotide Polymorphism

SWIR – Short-Wave Infrared (spectral region)

t_{Fm} – Time to reach Fm (ms)

TR_0/RC – Maximum trapped exciton flux per PSII RC

TRUE – True Skov provenance (Exp. 4)

UAV – Unmanned Aerial Vehicle

VIS – Visible (spectral region)

V_J – Relative variable fluorescence intensity at J-step

V_I – Relative variable fluorescence intensity at I-step

δ_{R0} – Efficiency with which an electron can move from reduced intersystem acceptors to PSI end acceptors

φ_{D0} – Quantum yield of energy dissipation

φ_{E0} – Quantum yield of electron transport

φ_{P0} – Maximum quantum yield of primary photochemistry

φ_{Pav} – Average quantum yield of primary photochemistry

φ_{R0} – Quantum yield of reduction of PSI end acceptors

ψ_0 – Probability that a photon trapped by PSII will enter the electron transport chain

List of Tables

Table 1: Overview of experiments presented in the thesis. 61

Table 2: Summary of flight conditions when canopy-level data were acquired. Published in Provazník et al. (2025). 65

Table 3: Characteristics of locations of origin and the common garden experimental plot in Copenhagen (C-G CPH), where the experiment was conducted. Published in Provazník et al. (2024). 72

Table 4: Seedlings count and survival rate at the end of the vegetation season in 2018 and 2020. The survival rate for SG1900 cannot be calculated because not all seedlings from this provenance subgroup were replanted into the new permanent site in 2019 due to a higher seedling count in relation to other provenances. Published in Provazník et al. (2024). 73

Table 5: List of ChlF parameters and their formulas. The parameters used in the analyses are in bold letters. Published in Provazník et al. (2024). 74

Table 6: List of GE parameters. Parameters in bold were later used for further analyses. Published in Provazník et al. (2024). 75

Table 7: The provenance of the Pinus sylvestris seedling grown in the experiment. 79

Table 9: Plant material origin. Provenances with family (half-siblings) structures are in bold, material without family structure (from seed stands and clonal seed orchards) is in normal font. 85

Table 10: Broad-sense heritability (H^2), standard errors (SE), and type B genetic correlations (a measure of GxE) across sites in 2021 of pigment-related NFTs. NS = non-significant. Chl a – chlorophyll a, chl b – chlorophyll b, chl T – total chlorophyll a+b, car – total carotenoids, car:chl T – ratio of total carotenoids to total chlorophyll. Concentrations of photosynthetic pigments are related to dry weight marked with an $_M$ lower index [mg/g] (first four columns on the left) and to needle area projection marked with an $_A$ lower index [µg/cm^2] (following four columns to the right). Published in Provazník et al. (2025). 96

Table 11: Broad-sense heritability (H^2), standard errors (SE), and type B genetic correlations across sites in 2021 of structural and water-related NFTs. NL – needle length, LMA – Leaf Mass per Area, NWC – needle water content, EWT - Equivalent Water Thickness, NS – non-significant. Published in Provazník et al. (2025). 96

Table 12: Predicted means of ChlF parameters with standard errors (SE) of each provenance subgroup (based on LMM). Published in Provazník et al. (2024). 110

Table 13: Predicted means of GE parameters with standard errors (SE) of each provenance subgroup (based on LMM). Provenance effects were significant ($\alpha = 0.05$) for parameters shown in bold, later used for further analyses. Published in Provazník et al. (2024). 111

Table 14: Two-sided Wilcoxon signed-rank test of flushing scores between pairs of provenances and provenance subgroups scored in May 2018 and April 2020. Published in Provazník et al. (2024). 115

Table 15: Partial Least Squares discriminant analysis results for differently processed data grouped by geographical groups and individual provenances. 121

Table 16: Narrow-sense heritability estimates for height increments in specific years at individual sites. 127

Table 17: Genotype-by-environment interactions as type B genetic correlations from the MELMM. 136

Table 18: Age-to-age correlation coefficients between increments from different years at individual sites. 137

List of Figures

Figure 1: The spectral reflectance curve of vegetation. The major absorption and reflectance features are indicated 42

Figure 2: Reflectance curves for healthy vs. stressed vegetation (Roman & Ursu, 2016). 43

Figure 3: Example of fluorescence transients labeled at the O, J, I, and P steps (Bussotti et al., 2010). 48

Figure 4: Graphical abstract illustrating the workflow of individual measurements and analyses conducted for specific years and sites. Published in Provazník et al. (2025). 63

Figure 5: Flow diagram of the proposed pipeline. 83

Figure 6: Map of trials and provenance origins. Clonal seed orchards and seed stands are not included. 87

Figure 7: Total monthly precipitation at climate data stations nearest to the experimental sites. A: data from Havnø station situated between 504 and 505, B: data from Års Syd station located north of 506, and C: data from Sjælsmark station located south-east of 507. Hourly precipitation data is provided by the Danish Meteorological Institute (DMI), an open data portal licensed under CC BY 4.0. 89

Figure 8: Estimated broad-sense heritability (H^2) with standard errors (SE) for needle-level spectra, shown alongside the mean needle-level reflectance of all clones at the Plasy (A) and Nepomuk (B) sites in 2021. Published in Provazník et al. (2025). 98

Figure 9: Estimated broad-sense heritability (H^2) with standard errors (SE) for canopy-level spectra, shown alongside the mean canopy-level reflectance of all clones at Plasy 2020 (A), Plasy 2021 (B), and Nepomuk 2021 (C). Published in Provazník et al. (2025) 100

Figure 10: Year-to-year genetic correlations with standard errors (SE) estimated at Plasy between 2020 and 2021 are shown in panel A, alongside the mean canopy-level reflectance of all clones in these 2 years. Panels B, C, and D display the stability of clonal values, representing the predicted genetic component of spectral reflectance, for three representative wavelengths (450, 690, and 852 nm) across the two years. These wavelengths (e.g., from VIS, red edge, and NIR regions) were selected to illustrate typical patterns of clonal ranking consistency and variability across the spectral range. Published in Provazník et al. (2025). 102

Figure 11: Type B genetic correlation between Plasy 2021 and Nepomuk 2021 as a proxy for GxE interaction in canopy-level (A) and needle-level (F) reflectance. The reflectance plotted is the mean of all clones across the sites.

Panels B, C, D, and E illustrate the stability of clonal ranking for representative wavelengths (533, 697, 852, 1440 nm) across the environment. For needle-level reflectance, SE was not estimated in VIS, where the type B genetic correlation was significant because the model converged at a boundary. The SE in regions with insignificant type B genetic correlations was high and is not visualized. Published in Provazník et al. (2025). 104

Figure 12: Genetic correlations between needle-level reflectance spectra and photosynthetic pigments estimated from pooled data (Plasy 2021, Nepomuk 2021). Chl a – chlorophyll a, chl b – chlorophyll b, car – total carotenoids, car:chl T – ratio of total carotenoids to total chlorophyll. Concentrations of photosynthetic pigments are related to dry weight marked with an $_{M}$ lower index [mg/g] and to needle area projection marked with an $_{A}$ lower index [μg/cm^2]. The standard error of genetic correlation reached the average value of 0.3 (not shown). The significance of the genetic correlation was expressed by shades of pink. The reflectance plotted is the mean of all clones across the sites. Published in Provazník et al. (2025). 106

Figure 13: Genetic correlations between needle-level reflectance spectra and needle structural and water-related traits estimated from pooled data (Plasy 2021, Nepomuk 2021). NL – needle length, LMA – Leaf Mass per Area, NWC – needle water content, EWT - Equivalent Water Thickness. The standard error reached the average value of 0.3 around the genetic correlation value (not shown). The significance of the genetic correlation was expressed by shades of pink. The reflectance plotted is the mean of all clones across the sites. Published in Provazník et al. (2025). 107

Figure 14: Genetic correlations between canopy-level reflectance spectra and needle functional traits (NFTs) estimated from pooled data (Plasy 2021, Nepomuk 2021). chl T $_{M}$ – total chlorophyll a+b (related to dry weight [mg/g]), EWT – Equivalent Water Thickness. The standard error (SE) reached the average value of 0.3 around the genetic correlation value (not shown). The significance of the genetic correlation was expressed by shades of pink. The reflectance plotted is the mean of all clones across the sites. Published in Provazník et al. (2025). .. 108

Figure 15: Heatmap of LSD test p-values comparing all pairs of provenance subgroups based on ChlF and GE parameters (without correction for multiple testing) (based on LMM). Published in Provazník et al. (2024). .. 113

Figure 16: Density plots of flushing scores among provenance subgroups scored in May 2018 (A) and April 2020 (B). Published in Provazník et al. (2024). 116

Figure 17: Density plots of leaf senescence scores of individual provenances and the altitudinal subgroups assessed at the beginning of November 2020. Published in Provazník et al. (2024). 117

Figure 18: Visualization of the mean reflectance spectra of the three geographical groups. Data was later used for PLS-DA analyses. 118

Figure 19: Visualization of the 1st derivative of mean reflectance spectra of the three geographical groups. Data was later used for PLS-DA analyses. 119

Figure 20: Image results from different stages of data processing represented by examples from provenances of each geographical group. The figure shows RGB rendered (640nm, 562nm, 470nm) images of original datacubes (A,D,G), processed datacubes that were used for classification (B,E,H), and the classified images (C,F,I). 120

Figure 21: PLS-DA score plot for individual provenances based on the classified image data (predicting with the highest accuracy = 0.45; κ = 0.36)..... 122

Figure 22: PLS-DA score plot for geographical groups based on the classified image data (predicting with the highest accuracy = 0.95; κ = 0.92)..... 122

Figure 23: PLS-DA score plot for short-day treatment based on the 1st derivative of mean spectra (predicting with accuracy = 0.76; κ = 0.51). The individual provenances within the treatment and control are visualized with shapes. 123

Figure 24: Visualization of the bud-count processing workflow. A is a cropped part of an RGB rendered (640nm, 562nm, 470nm) image of the original datacube, B is a cropped equivalent of the classified image, and C is a cropped equivalent of the mask from Fiji (ImageJ), which was used in the proposed macro for bud count. Yellow represents correctly counted buds; the red bud was incorrectly omitted by the macro (false negative), and the blue bud was not counted due to proximity conditions preventing a double count of split buds (obscured by a needle). The white color in the mask represents pixels incorrectly classified as blue in the classified image (B). 125

Figure 25: Violin plot of the maximum level of budburst (bud burst scores) for provenances at site 506 on 24th April 2024..... 126

Figure 26: Predicted family means with provenance effect at site 504. For each year, the increment is presented by a different color. The black lines on top of each increment bar are visualizing the standard errors. 130

Figure 27: Predicted family means with provenance effect at site 505. For each year, the increment is presented by a different color. The black lines on top of each increment bar are visualizing the standard errors. 131

Figure 28: Predicted family means with provenance effect at site 506. For each year, the increment is presented by a different color. The black lines on top of each increment bar are visualizing the standard errors. 132

Figure 29: Predicted family means with provenance effect at site 507. For each year, the increment is presented by a different color. The black lines on top of each increment bar are visualizing the standard errors. 133

Figure 30: Genotype–by-environment interaction denoted by biplot showing performance of families across site–year combinations in height increment. Families are represented as points (units) and site–year combinations as vectors, based on the first two principal components of predicted values (BLUPs) from the single-site LMMs. Only families present at all sites are included. Data were standardized to visualize genotype × environment interactions. 135

Figure 31: Rankings of provenances derived from their respective BLUEs from single sit LMMs. 139

Figure 32: Mean hyperspectral reflectance for 10 selected provenances at sites 504, 505, and 507 in spring (S) and autumn/fall (F) 2023. 140

1 Introduction

Forests provide essential ecological and economic services, including carbon sequestration, water regulation, and biodiversity protection. Their stability and productivity are increasingly threatened by climate change, manifested through rising temperatures, altered precipitation, and more frequent extreme events. These changes pose serious challenges for long-lived tree species, whose adaptive capacity is limited by slow generation turnover (Buras and Menzel, 2019; Chakraborty et al., 2024; Dyderski et al., 2018).

Traditional tree breeding has focused mainly on growth and wood quality traits (White et al., 2007). While effective in terms of production, these approaches are often slow, labor-intensive, and limited in their ability to assess and integrate complex adaptive traits contributing to resilience. Accelerating breeding cycles and improving selection accuracy are essential as climate pressures intensify (Aitken and Whitlock, 2013; Grattapaglia et al., 2018; Neale and Kremer, 2011).

Advances in genetics and high-throughput phenotyping now offer new possibilities to accelerate tree breeding and make it possible to incorporate a broader range of traits into selection strategies. Techniques such as hyperspectral and imaging spectroscopy allow rapid, non-destructive measurements of physiological and structural traits at leaf and canopy levels (Bian et al., 2022; Fiorani and Schurr, 2013; Grubinger et al., 2023). Combined with genomic data and advanced statistical models, these tools provide deeper insights into trait architecture and genotype–environment interactions, supporting the selection of resilient genotypes.

This dissertation applies novel phenotyping methods in the genetic evaluation of *Pinus sylvestris* L., *Fagus sylvatica* L., and *Alnus glutinosa* (L.) Gaertn. It combines provenance and clonal trials, hyperspectral reflectance, physiological measurements, and genomic data to develop a framework linking growth, physiology, and adaptive traits. Current breeding programs are constrained by slow phenotyping and limited coverage of adaptive traits (Bian et al., 2022). Climate change adds urgency to identifying resilient genotypes. Combining high-throughput phenotyping with genetic analysis improves both the rate and reliability of selection.

The primary aim of this research is to explore and apply novel phenotyping methods used for genetic evaluation of forest trees. Specifically, it seeks to evaluate growth, phenological, and physiological traits across different provenances, providing a foundation for understanding

variation in key adaptive characteristics. Linear mixed models enable deeper insight into the genetic variation of various traits. Hyperspectral reflectance is assessed as a high-throughput, non-destructive proxy for adaptive traits, supporting more efficient phenotyping (Bian et al., 2022). Furthermore, genotype–environment interactions are analyzed to capture how genetic variation is expressed under different environmental conditions. Ultimately, the study aims to develop integrative approaches that support climate-resilient breeding strategies, facilitating the selection of productive and adaptable genotypes for future forest management.

By combining phenotypic, spectral, and genomic data, this research enables early detection of adaptive signals. These methods support more efficient breeding and long-term forest resilience.

Although this study integrates advanced methods, several limitations should be acknowledged. Physiological measurements are sensitive to short-term environmental fluctuations and are labor-intensive, limiting sampling scale and temporal consistency. Hyperspectral reflectance, while high throughput, can be affected by measurement conditions and requires complex processing to separate biological signals from noise. Genetic analyses depend on data quality and balanced experimental design, and genotype-by-environment interactions may require larger datasets to fully capture their complexity. These limitations highlight the importance of careful design, rigorous data handling, and cautious interpretation.

The structure of this thesis is designed to provide both clarity and coherence across its different components. A common literature review establishes the foundation of the research, beginning with an overview of the studied species. It then introduces advanced phenotyping approaches and their applications in tree research, followed by key concepts in forest genetics and tree breeding that provide a foundation for the experimental work. The methodology and results are then presented separately for each of the four individual experiments, reflecting their distinct species, genetic materials, site conditions, phenotyping methods, and trait focus. This structure allows each experiment to be described and interpreted within its own context, improving transparency and readability while aligning methods and results closely. Finally, the joint discussion is organized by trait categories, phenology, growth and structural traits, pigment, photosynthesis-related traits, water-use or stress-related traits, and spectral reflectance, allowing for cross-species comparisons and a clearer interpretation of genetic contributions, environmental sensitivity, and adaptive significance. This integrated approach highlights both the specific findings of each experiment and their broader implications.

2 Objectives and Hypothesis

Objectives:

1) Evaluation of the experimental plots based on growth and physiological traits.
2) To connect genetics and tree physiology in the context of tree breeding - a study of phenotype and genotype correlations between growth and physiological parameters (including genotype and environment interactions).
3) A novel aspect will be the study of phenotypic and genotypic correlations between growth, physiological parameters, and adaptive traits of chosen populations.

Hypothesis:

There are significant genetic correlations between physiological, production, and adaptive traits, which can be further used for early indirect selection.

Specific Objectives of Individual Experiments

Experiment 1 – Scots Pine Clones – Seed Orchards

To evaluate genetic variation in needle- and canopy-level reflectance traits, together with NFTs in Scots pine clonal seed orchards using SNP genotyping to quantify realized genomic relationships among clones.

- Experiment 1 is based on an already published study by Provazník et al. (2025).

Experiment 2 – European Beech Provenances

To assess photosynthetic performance (gas exchange and chlorophyll *a* fluorescence) and phenology among beech provenances and their altitudinal subgroups in a common garden setting.

- Experiment 2 is based on an already published study by Provazník et al. (2024).

Experiment 3 – Scots Pine Provenances - Seedlings

To develop an optimized, high-throughput phenotyping (HTP) pipeline using open-source tools to assess key phenological traits in Scots pine seedlings.

- Experiment 3 is part of an unpublished manuscript called: From Pixels to Phenotypes: Semi-automated Classification of Autumn Reddening and Bud Set Using Hyperspectral Imaging in Scots Pine Seedlings.

Experiment 4 – Black Alder Provenances

To evaluate genetic variation and adaptive potential of black alder provenances in growth and phenology across years and sites.

- Experiment 4 is part of an unpublished manuscript called: Understanding Genetic Variation in Black Alder Growth: The Role of Soil Conditions in Genotype × Environment Interactions.

3 Literature Review

3.1 Climate Change and Tree Species Distribution

Climate change is increasingly reshaping ecosystems across the globe, with forested landscapes among the most visibly affected. In Europe and beyond, shifts in temperature and precipitation patterns, particularly during critical phases of the growing season, are altering the environmental conditions to which tree species are adapted. These climatic changes not only influence tree growth, regeneration, and survival, but also increase the frequency and intensity of disturbances such as storms, pest outbreaks, and wildfires (Dyderski et al., 2018). As a result, the geographical distribution of many tree species is changing, with some expanding into newly suitable areas while others face decline or local extinction. Tree species may respond to environmental changes through acclimatization, local adaptation, migration, or, in the worst case, mortality (Buras and Menzel, 2019; Dyderski et al., 2018; Zang et al., 2014). Together, these responses will shape the future composition and resilience of forest ecosystems.

Species distribution models have been widely used to project how tree species' ranges may shift under various climate change scenarios. Recent studies employing advanced modeling techniques and extensive distribution data have revealed that tree species exhibit differential responses to climate change. For example, late-successional species such as silver fir (*Abies alba* Mill.), European beech (*Fagus sylvatica* L.) and pedunculate oak (*Quercus robur* L.) are projected to be "winners," potentially expanding or maintaining their ranges under moderate climate scenarios (Dyderski et al., 2018; Pietrzykowski and Woś, 2021). In contrast, species like silver birch (*Betula pendula* Roth) and Norway spruce (*Picea abies* (L.) Karst.) are more likely to experience range contractions (Dyderski et al., 2018; Pietrzykowski and Woś, 2021). Introduced species such as Douglas fir (*Pseudotsuga menziesii* (Mirb.) Franco) and black locust (*Robinia pseudoacacia* L.) may also expand their ranges, posing additional ecological challenges (Dyderski et al., 2018).

Rising temperatures and shifting precipitation patterns drive changes in species' potential ranges, often causing a northward and upslope migration of suitable habitats (Buras and Menzel, 2019; European Commission. Joint Research Centre., 2016). For example, studies indicate that many European tree species are projected to experience habitat shifts and contractions, particularly in mountainous regions such as the Pyrenees, Alps, and Carpathians, with suitable areas moving up to 800 km northeast under severe climate scenarios (European

Commission. Joint Research Centre., 2016). These changes pose risks of habitat loss, species extinction, and altered forest dynamics, compounded by uncertainties in climate projections and species' dispersal capabilities.

These shifting habitat patterns are already having visible consequences in European forests, where some of the most widely planted and economically important tree species are showing signs of stress and decline. Norway spruce and Scots pine (*Pinus sylvestris* L.), in particular, are increasingly vulnerable. Norway spruce, often cultivated outside its natural range in Central Europe, is especially susceptible to site-related stress and associated disturbances such as windthrow and bark beetle outbreaks, both of which are expected to intensify in the coming decades (Hlásny and Turčáni, 2013). Scots pine, though more drought-tolerant, has also shown rising mortality under extreme conditions (Buras and Menzel, 2019; Lévesque et al., 2013; Zang et al., 2014), underscoring the need to reassess their long-term viability under future climate scenarios.

In response, forest management practices across Europe are shifting away from homogeneous conifer plantations toward more diverse, resilient, and multifunctional forest stands. Integrating broadleaved species into conifer-dominated systems has been shown to increase resistance to both abiotic stressors, such as wind, and biotic threats like bark beetles (Griess et al., 2012). This transition has brought renewed focus to species like European beech and drought-tolerant Scots pine ecotypes, which offer greater adaptability to changing climate conditions.

While much attention has centered on the vulnerability of drought-sensitive upland conifers, forest types in floodplain and riparian ecosystems are also experiencing significant declines. In these systems, biotic agents, particularly invasive pathogens, are the primary drivers of tree mortality. One of the most severe cases is the widespread dieback of Common ash (*Fraxinus excelsior* L.), which has been recorded across much of Europe in recent decades. This decline affects natural forests, urban plantings, and nursery stock alike (Bakys et al., 2009). The disease is primarily caused by the fungal pathogen *Hymenoscyphus fraxineus* (formerly *Chalara fraxinea*) (Bakys et al., 2009; Kowalski, 2006; Kowalski and Holdenrieder, 2009). Although some genotypic variation in resistance exists, particularly among selected clonal material (Mckinney et al., 2014), the disease continues to prevent many ash trees from reaching maturity, limiting their long-term ecological role.

Similarly, European elm species (*Ulmus* spp.) remain severely affected by Dutch elm disease, caused by the fungus *Ophiostoma novo-ulmi* and spread primarily by *Scolytus* bark beetles (Webber, 2008). Despite ongoing breeding efforts to develop resistant cultivars, the disease continues to pose a persistent threat to elm populations in both managed forests and urban landscapes.

A comparable dieback has been observed in alder species (*Alnus glutinosa* (L.) Gaertn.) and *Alnus incana* (L.) Moench), particularly in riparian environments. Since the 1990s, widespread mortality has been linked to *Phytophthora alni*, a novel hybrid waterborne pathogen of likely recent origin (Husson et al., 2015). Spread through river and stream networks, the pathogen has devastated alder populations in several European countries, resulting in significant ecological and economic consequences (Bjelke et al., 2016). However, as climate change alters hydrological regimes and creates new pathways for spreading, the long-term trajectory of this disease remains uncertain.

Overall, the composition of European forests is changing not only due to abiotic stressors such as drought and temperature extremes but also due to complex biotic interactions involving novel pathogens and pest outbreaks. Both conifer-dominated upland forests and species-rich riparian systems are experiencing significant declines in key species, prompting a reevaluation of traditional forest management models. Future strategies will need to emphasize not only production traits, but also species diversity, functional redundancy, and the incorporation of resistant genotypes to enhance forest resilience in the face of accelerating environmental change. To support these efforts, there is a growing need for advanced high-throughput phenotyping techniques capable of efficiently assessing large populations for production, stress responses, adaptive traits, and disease resistance. This means the new methods should accelerate the identification and deployment of superior tree genotypes in forest breeding and restoration programs.

3.2 Overview of Selected Species

In light of the increasing urgency to enhance forest resilience under climate change, the selection of species for phenotyping studies must consider ecological significance, economic value, and vulnerability to environmental stressors. This thesis focuses on the application of novel phenotyping methods to three key European forest species: Scots pine (*Pinus sylvestris* L.), European beech (*Fagus sylvatica* L.), and European black alder (*Alnus glutinosa (L.) Gaertn.*). These species represent a range of ecological niches, from upland to riparian forests, and display varied responses to drought, temperature, and biotic pressures. Each species also shows considerable intraspecific variation in adaptive traits, making them highly suitable for exploring modern phenotyping approaches aimed at supporting future breeding and forest management strategies. Both broadleaf and conifer species are included to capture the phenotyping differences associated with leaf morphology in leaf-level measurements.

3.2.1 Scots Pine (*Pinus sylvestris* L.)

Scots pine is one of the most ecologically and economically important conifer species in Europe, particularly in Nordic countries. Its relevance is expected to grow further due to ongoing climate change, which challenges forest health and productivity across Europe. Despite a general decline in coniferous forests, Scots pine continues to be a cornerstone of European forestry (Buras and Menzel, 2019; Ols and Bontemps, 2021).

As a typical pioneer species (Linder, 1972), Scots pine demonstrates exceptional ecological plasticity and extensive genetic variability. It occupies a vast natural range covering much of Eurasia, from the Iberian Peninsula to eastern Siberia, and from the Mediterranean to northern Scandinavia (Brichta et al., 2023). This wide distribution is enabled by its ability to adapt to highly diverse climatic and ecological conditions, ranging from vegetative periods of 90 to 200 days, annual precipitation of 200–1780 mm, and mean annual temperatures from 3°C to 16°C (Durrant et al., 2016).

Scots pine's wide ecological distribution has led to pronounced local adaptation, evident in its diverse growth forms, ecotypes, and physiological clines (Bruxaux et al., 2024). Trait variation along latitudinal and altitudinal gradients is well-documented, highlighting the species' capacity to adjust to a broad range of climatic conditions (Aitken and Whitlock, 2013; Bruxaux et al., 2024). Key phenotypic traits, including bud flush and set, height growth, and frost

hardiness, show considerable variation aligned with geographic and environmental gradients such as latitude, temperature, and growing season length (Repo et al., 2000; Savolainen et al., 2004; Taulavuori et al., 2010). These patterns are reinforced by long-term field studies, provenance trials, and common garden experiments. Scots pine is in some regions categorized into distinct altitudinal ecotypes, such as upland and lowland forms, based on elevation-related differences in growth characteristics and local adaptation (Šindelář et al., 2007).

Physiological traits such as needle size and pigment content have been central to evaluating adaptive variation. Provenances from colder climates typically have shorter needles, a trait with clear genetic underpinnings (Jankowski et al., 2019; Novikova and Milyutin, 2006; Pakharkova et al., 2014). Recent studies have also begun to explore chlorophyll fluorescence and photosynthetic pigment content as indicators of physiological performance (Čepl et al., 2018).

Autumn coloration, especially in first-year seedlings, is another notable phenological trait, shown to be linked to stress tolerance. This coloration results from anthocyanin accumulation, which, alongside other flavonoids, acts as an antioxidant and UV protectant (Bogolitsyn et al., 2024; Kaur et al., 2023; Nozzolillo et al., 2002). Seasonal variation in carotenoid content in Scots pine needles further reflects environmental responsiveness and stress adaptation (Linder, 1972; Miettinen et al., 2025).

Genetically, Scots pine exhibits low interpopulation differentiation but significant phenotypic clines across its range, suggesting strong local adaptation despite panmixia and high gene flow (Bruxaux et al., 2024)

3.2.2 European Beech (*Fagus sylvatica* L.)

European beech is one of the most widespread and ecologically important broad-leaved tree species in Europe. In Central Europe alone, it occupies approximately 12 million hectares (Bolte et al., 2007; Dounavi et al., 2016), and its role in mixed-species forests is growing. Over recent decades, beeches have increasingly been introduced into pure coniferous stands across Central Europe to improve forest resilience to climate-induced disturbances such as windthrow and bark beetle outbreaks (Griess et al., 2012). As a truly autochthonous species in many regions where it is being reintroduced, beech is often a natural and ecologically valuable choice in forest restoration (Ammer et al., 2008). This growing reliance has led to rising demand for

seedlings from resilient provenances and ecotypes suited to future environmental conditions (Hazarika et al., 2021).

Despite its prominence, the long-term survival of the European beech is becoming increasingly uncertain. Ongoing climate change poses a substantial threat, particularly through intensified drought events and rising temperatures, conditions to which beech is notably sensitive (Aranda et al., 2015; Bolte et al., 2007; Fotelli et al., 2009; Gessler et al., 2020; Leuschner et al., 2001). Declines in growth and vitality have already been observed and are predicted to worsen across much of its range, except for some northern margin populations (Castillo et al., 2022). Populations at the southern distribution limit are especially vulnerable, as they are exposed to the most pronounced climatic shifts, including prolonged periods of drought (Jump et al., 2006).

However, these southern and xeric populations also offer valuable adaptive traits. Studies have shown that they exhibit morphological and physiological adaptations, such as thicker leaves, higher net CO_2 assimilation, and greater drought tolerance (Aranda et al., 2015; Čater and Levanič, 2019; García-Plazaola and Becerril, 2001). Provenances from southeastern Europe also show increased adaptability to varying soil moisture regimes and faster growth compared to northwestern populations (Nielsen and Jørgensen, 2003). These traits may prove critical in selecting climate-resilient planting material for future forestry strategies.

Genetically, beech demonstrates low interpopulation but significant intrapopulation variability (Lefèvre et al., 2004; Vornam et al., 2004), emphasizing the importance of identifying and conserving genetically diverse and locally adapted populations. Of particular interest are populations in marginal and refugial areas, which are believed to harbor key elements of the species' adaptive gene pool (Hampe and Petit, 2005). While Mediterranean refugia such as the Italian Peninsula preserved beech through glacial periods (Magri et al., 2006; Pott, 1997), postglacial recolonization of central and northern Europe appears to have originated from more northern refugia in regions like southern France, the eastern Alps, and southern Moravia–Bohemia (Magri et al., 2006). These differing origins may be reflected in distinct phenological and physiological traits, including photosynthetic efficiency and growth rhythms.

A critical aspect of beech's climate adaptability is its phenological plasticity. Variations in bud burst, leaf senescence, and growth duration have been linked to latitude, altitude, and local climate, with southern and lowland populations generally flushing earlier than northern or high-

altitude counterparts (Nielsen and Jørgensen, 2003; Robson et al., 2013). However, separating the effects of geographic and elevational factors remains challenging due to the overlapping nature of provenance origins. Studies also show that beech maintains stable flushing patterns even after replanting in new environments, suggesting strong genetic control over phenological traits (Robson et al., 2013). Long photoperiods have been shown to accelerate bud development (Basler and Körner, 2014), while phenological phase timing can vary markedly between years depending on spring temperatures (Bednářová and Merklová, 2007; Slovíková and Bednářová, 2014; Vitasse et al., 2009).

Studies across diverse environmental conditions further reveal substantial ecotypic differentiation in beech populations. Provenance trials and common garden experiments have shown distinct patterns in growth timing, morphology, and biomass allocation between montane and lowland populations (Chmura et al., 2002). Photosynthetic performance also varies by climate and altitude of origin (Kučerová et al., 2018; Kurjak et al., 2019; Pšidová et al., 2018; Robson et al., 2012).

The European beech plays a central role in the ecological functioning and management of European forests. Yet, its future under climate change will depend on the identification, conservation, and utilization of resilient genotypes, particularly from xeric and marginal populations. Advances in phenotyping technologies, especially high-throughput and non-invasive methods, are essential for characterizing this intraspecific variation and supporting informed decisions in forest restoration, assisted migration, and genetic resource management.

3.2.3 European Black Alder (*Alnus glutinosa* [L.] Gaertn.)

Black alder is naturally distributed across a wide range in Europe, from central Scandinavia in the north to North Africa in the south, extending from the western Iberian Peninsula to the mountainous regions of Turkey in the east (Vacek et al., 2022). It typically occurs in lowlands and middle altitudes, thriving in water-influenced habitats such as wetlands, riverbanks, and marshy areas where soil moisture is high (De Kort et al., 2016; Hrivnák et al., 2023; Lukyanets et al., 2022). Black alder is a water-demanding species with leaves that lack mechanisms to control transpiration, making it dependent on high precipitation or access to groundwater, with a minimum annual precipitation requirement of about 1500 mm if groundwater is unavailable (Claessens et al., 2010; Rutkowski and Konatowska, 2019). The species is well adapted to wet and anaerobic soils, with a root system capable of penetrating waterlogged substrates, allowing

it to survive flooding better than many other temperate trees (Claessens et al., 2010; Rutkowski and Konatowska, 2019). Climate change is expected to influence its distribution, with alder stands likely to spread to higher altitudes and northern regions while declining in southern and lower altitude areas due to changing hydrological conditions (Vacek et al., 2022). Black alder also forms monodominant stands in stable water regimes such as mires and riparian forests, where periodic flooding and soil oxygen availability shape its habitat preferences (Hrivnák et al., 2023).

The black alder is a keystone species in temperate riparian ecosystems, valued for its essential roles in nitrogen fixation, soil stabilization, and habitat provision for a wide array of aquatic and terrestrial organisms (Vacek et al., 2022; Verbylaitė et al., 2023). Its capacity to fix atmospheric nitrogen enhances soil fertility, supports stream food webs via nutrient-rich leaf litter (Handa et al., 2014), and allows its use in the reclamation of degraded sites such as post-mining landscapes (Kuznetsova et al., 2011). Furthermore, black alder demonstrates ecological flexibility by persisting in brackish coastal zones (Deptuła et al., 2020) and is being explored as a substitute species in forest areas impacted by ash dieback (Broome et al., 2019).

Despite relatively low genetic differentiation among populations, there is strong evidence of adaptive differentiation, particularly in phenological traits such as bud burst, which are closely tied to local temperature regimes (De Kort et al., 2016, 2014). High intrapopulation genetic diversity likely reflects ongoing long-distance gene flow, while phenotypic clines suggest selection for local adaptation.

Climate change poses a growing threat to A. glutinosa populations by altering precipitation regimes, soil moisture availability, and temperature patterns, especially at the edges of the species' range, where even autumn temperatures affect flowering and leaf-out timing (Rojo et al., 2021). Recent diebacks linked to biotic stressors and environmental extremes further highlight the urgency of identifying climate-resilient genotypes.

Growth traits in A. glutinosa are significantly influenced by genotype-environment (G × E) interactions, particularly with respect to soil moisture, nutrient availability, and temperature (Rodríguez-González et al., 2014; Rojo et al., 2021; Vacek et al., 2022). Studies have revealed substantial phenotypic plasticity, enabling adaptation to diverse habitats (De Kort et al., 2016; Pliûra, 2004), yet also emphasize the importance of genetic background in shaping local responses (De Kort et al., 2014; Verbylaitė et al., 2023). For instance, low-latitude provenances

tend to exhibit earlier bud burst and reduced chilling requirements, while northern populations often show greater plasticity under changing conditions (De Kort et al., 2016). Broad-sense heritability for bud burst varies considerably, indicating significant evolutionary potential in these traits (De Kort et al., 2016; Heide, 2003).

Understanding and managing G × E interactions in A. glutinosa is also essential for enhancing resilience under climate change. Factors such as soil pH, moisture content, and nutrient status significantly affect growth and phenology (Rutkowski and Konatowska, 2019; Usta et al., 2014), while susceptibility to pathogens can further modulate genotype performance (Redondo et al., 2020). To accurately assess these interactions, it is crucial to integrate detailed climate and soil microclimate data into phenological and genetic analyses.

Modern phenotyping approaches offer new opportunities to track health status and phenological patterns in riparian forests dominated by black alder (Guerra-Hernández et al., 2021). Together with common garden experiments and genotypic data, these tools can inform adaptive forest management and conservation strategies aimed at maintaining the ecological functions and genetic diversity of this vital species.

3.3 Phenotyping in Forest Trees

Phenotyping refers to the measurement of observable plant traits: morphological, physiological, biochemical, or performance-related, influenced by both its genetic constitution (genotype) and the environment in which it grows. The phenotype results from the interaction between genotype and environment, and phenotyping aims to assess these traits to understand how much variation is due to genetic differences versus environmental influences (Eriksson, 2006). In forest trees, these traits serve as vital proxies for understanding tree growth, productivity, stress responses, and adaptive capacity. Given the complexity, size, and long lifespan of forest trees, phenotyping is both an essential and particularly challenging component of forest research and breeding programs (Bian et al., 2022; Dungey et al., 2018).

Forest phenotyping is critical for improving tree breeding, guiding silvicultural practices, optimizing genotype-site performance, and enhancing the resilience and productivity of forests under climate change (Bian et al., 2022; Neale and Kremer, 2011). By enabling the assessment of traits such as height, diameter, phenology, photosynthetic performance, and wood quality, and other traits, phenotyping helps in identifying superior genotypes and understanding their plastic responses to environmental variation.

3.3.1 Traditional Approaches

In many countries, it is often taken for granted that the primary goal of silviculture is to produce high-quality raw materials for sawmills, the pulp and paper industry, and other wood-based markets (Eriksson, 2006). This objective has shaped the foundation of traditional tree improvement programs, which aim to enhance both the quantity and quality of forest products. Tree improvement involves the application of forest genetics, tree biology, silviculture, and economic principles to develop genetically superior varieties of forest trees (White et al., 2007). Much like breeding programs in agriculture or livestock, forestry breeding programs focus on selecting and propagating trees that exhibit desirable traits such as fast growth, straight stems, disease resistance, and wood quality.

Traditional phenotyping for growth traits plays a central role in this context. Measuring traits such as height, diameter at breast height (DBH), stem form, and volume increment has long served as the cornerstone of selection decisions in tree breeding. These observable traits offer a direct link between genotype and end-product value, making them vital targets in early

selection stages and in long-term genetic gain assessments. Despite being time-consuming and labor-intensive, this manual approach has provided robust datasets that have shaped the trajectory of forest improvement across many regions.

3.3.2 Functional Traits in Phenotyping

Functional traits are measurable characteristics of plants that influence their growth, reproduction, and survival, serving as indicators of performance across varying environmental conditions. These traits reflect both the ecological strategies of individual species and their responses to environmental pressures. Functional traits are widely used to characterize ecological communities, interpret patterns in forest composition and structure, and predict ecosystem processes such as productivity, nutrient cycling, and carbon sequestration. In applied contexts, they support the management of forest systems for multiple objectives, including biodiversity conservation and climate resilience (Russell et al., 2014).

Accurate measurement of functional traits is essential even when developing novel and high-throughput methods for indirect selection in breeding programs, especially the leaf or needle functional traits. These traits serve as critical reference points, or ground truth, enabling researchers to validate and calibrate remote sensing or imaging-based proxies (Švik et al., 2023). By measuring them directly, one can assess how well spectral or structural features captured through high-throughput phenotyping correspond to actual biological performance.

Moreover, these conventional trait measurements are necessary for identifying meaningful genetic correlations. Understanding the relationships between easily measurable spectral features and more complex physiological or developmental traits allows us to select individuals based on surrogate indicators, thus improving selection efficiency. Without this foundational data, high-throughput methods risk losing their biological relevance, making it difficult to link what is observed remotely to traits that truly influence plant fitness, productivity, or stress adaptation. In this way, traditional trait data remains indispensable for building reliable, scalable phenotyping frameworks that can inform selection decisions in large and genetically diverse populations.

3.3.2.1 Structural Functional Leaf Traits

Structural functional traits such as leaf mass per area (LMA), specific leaf area (SLA), leaf morphology, and water-related characteristics are fundamental indicators of plant strategies for resource use, growth, and adaptation to environmental conditions. LMA and SLA, which represent the dry mass investment per unit leaf area and its inverse, respectively, are particularly informative of leaf structure and efficiency in capturing light and utilizing resources. These traits are tightly linked to photosynthetic capacity and growth rates, reflecting how plants balance investment in durable tissues with the need for rapid resource acquisition (Kothari et al., 2023; Švik et al., 2023) Leaf morphology, encompassing anatomical features such as mesophyll structure and the presence of specialized tissues, influences the efficiency of light capture and gas exchange, directly affecting physiological performance under varying environmental conditions (Lhotáková et al., 2025). Water-related traits like equivalent water thickness (EWT) and overall leaf water content are critical for maintaining cellular functions and turgor pressure, particularly under drought stress, and provide insight into species' drought tolerance strategies (Kothari et al., 2023; Švik et al., 2023). Together, these structural traits not only reflect ecological adaptation across gradients of light, temperature, and moisture but also serve as measurable proxies for ecosystem functioning, enabling scalable assessments through both laboratory and remote sensing techniques.

3.3.2.2 Photosynthetic Pigments

Photosynthetic pigments in trees, primarily chlorophylls and carotenoids, are fundamental to capturing light energy and driving the photosynthetic process. Chlorophyll *a* serves as the central pigment in both photosystems *I* and *II*, enabling the conversion of light into chemical energy during photochemical reactions. Accessory pigments like chlorophyll *b* and carotenoids expand the range of absorbed light wavelengths and contribute significantly to photoprotection, safeguarding the photosynthetic apparatus from photooxidative damage (Bogolitsyn et al., 2024; Linder, 1972).

These pigments are not static but undergo seasonal changes. Chlorophyll and carotenoid concentrations typically peak in late summer, corresponding to maximum photosynthetic activity, and gradually decline during winter and early spring. This fluctuation reflects physiological adjustments to environmental cues such as photoperiod, temperature, and light

intensity (Linder, 1972). Concurrently, shifts in the chlorophyll-to-carotenoid ratio occur, often associated with enhanced photoprotection under stress, including high light or low temperature (Bogolitsyn et al., 2024). During winter, photosystem *I* becomes more dominant due to lower light levels, and carotenoid accumulation helps dissipate excess energy and mitigate oxidative stress, further supported by the presence of phenolic compounds (Bogolitsyn et al., 2024; Linder, 1972).

The regulation of pigment content is also responsive to spectral light quality. Different wavelengths influence both primary and secondary pigment accumulation, modulating antioxidant activity and protective responses. For example, red light has been observed to increase reactive oxygen species and stimulate flavonoid synthesis, while blue light enhances levels of key antioxidants such as ascorbate and glutathione (Pashkovskiy et al., 2023). These responses underline a finely tuned balance between light harvesting and defense, with pigment dynamics playing a central role in the acclimation of trees to their ever-changing environments (Bogolitsyn et al., 2024; Pashkovskiy et al., 2023)

3.3.2.3 Phenology

Phenology, the timing of seasonal biological events such as bud burst, bud set, leaf senescence, and dormancy, is a fundamental aspect of plant fitness and survival in temperate forest ecosystems. These traits are tightly regulated by environmental cues, particularly day length and temperature, and serve as essential mechanisms for synchronizing growth and developmental processes with seasonal climatic variability (Repo et al., 2000; Savolainen et al., 2004). In long-lived forest trees, phenological variation across geographic and climatic gradients reflects local adaptation, enabling populations to optimize growth and survival in diverse environments. Understanding this variation is critical for predicting species resilience under changing climate conditions and for informing adaptive forest management strategies (Aitken and Whitlock, 2013).

Phenology is also closely linked to variation in photosynthetic pigment concentrations, which influence leaf reflectance properties throughout the growing season (Linder, 1972). In deciduous and evergreen species alike, pigments such as chlorophylls, carotenoids, and anthocyanins undergo seasonal fluctuations that correspond to key phenological stages, particularly during senescence. These changes not only reflect shifts in physiological status but also affect spectral characteristics of foliage. Monitoring pigment dynamics using

hyperspectral reflectance data allows for quantitative assessment of phenological development, species discrimination, and broader evaluations of plant health and productivity (Blackburn, 1998).

The role of pigments extends beyond reflectance and phenological tracking; they are also central to stress protection and ecological function. For example, autumn reddening in young seedlings, driven by anthocyanin accumulation, is a common response in the first year of growth and serves as an indicator of stress tolerance (Kaur et al., 2023; Nozzolillo et al., 2002). Flavonoids, including anthocyanins, function as antioxidants and UV protectants, providing a critical defense mechanism for conifer needles (Bogolitsyn et al., 2024). Carotenoids also contribute to photoprotection and antioxidative defense, with their content showing marked seasonal shifts influenced by needle age and environmental conditions (Linder, 1972; Bogolitsyn et al., 2024; Miettinen et al., 2025). Provenance studies consistently show that northern populations initiate bud set and frost hardening earlier than southern ones, a clear sign of local adaptation to shorter growing seasons and colder climates (Repo et al., 2000; Savolainen et al., 2004).

From a breeding perspective, knowledge of flowering phenology is a prerequisite for successful selection and crossing efforts. Without flowering, no controlled breeding can occur, and it is essential to understand the conditions that promote reproductive development. This task is generally more straightforward in temperate and boreal zones, where distinct seasonal changes govern reproductive timing, compared to tropical regions with less pronounced seasonality (Eriksson, 2006). Phenology differences are also essential for the fitness of trees (Robson et al., 2013).

3.3.3 Novel Phenotyping Methods for Forest Trees

Traditional phenotyping methods are time-consuming, labor-intensive, often destructive, and prone to error. These limitations are especially pronounced in forest trees due to their size, connected to long generation times. Most conventional phenotyping in forest trees has relied on progeny or common garden trials aimed at assessing growth traits, which, while useful, do not capture the full spectrum of functional or physiological traits critical for stress resistance and adaptation (Singh et al., 2021; White et al., 2007).

Recent technological developments are beginning to overcome these limitations through the advent of high-throughput phenotyping (HTP) systems. HTP leverages automated sensor-based approaches, such as imaging, spectroscopy, LiDAR, and thermography, to collect large volumes of data with high precision and spatial-temporal resolution (Bian et al., 2022). Other methods enabling repeated, non-invasive measurements of physiological parameters, such as chlorophyll fluorescence, gas exchange, and water use efficiency, are particularly valuable for monitoring plant responses under dynamic environmental conditions, though they typically offer lower throughput compared to imaging-based phenotyping approaches (Fiorani and Schurr, 2013; Haworth et al., 2018).

Phenotyping data are central to unraveling the genetic architecture of complex quantitative traits such as growth, drought tolerance, flowering phenology, bud burst, or bud set. These traits often exhibit varying degrees of heritability and environmental plasticity, and understanding their expression across ecological gradients is essential for both breeding and conservation (Climent et al., 2024; Neale and Kremer, 2011).

The future of forest phenotyping depends on interdisciplinary collaboration across genetics, physiology, ecology, and engineering to develop standardized and scalable high-throughput phenotyping platforms that are both cost-effective and adaptable. Mobile and non-invasive tools suitable for diverse field conditions are especially needed. At the same time, advances in environmental monitoring and bioinformatics are essential to manage complex datasets and enable multivariate models that integrate phenotypic, genotypic, and environmental data, supporting precision forestry and climate-resilient forest management.

Among the methods discussed, this thesis specifically focuses on laboratory and imaging spectroscopy, chlorophyll *a* fluorescence, and gas exchange, examining their relationships with growth, physiological, and phenological traits.

3.3.3.1 Laboratory Spectroscopy

Spectroscopy is a physics-based approach that investigates the properties of electromagnetic spectra in interaction with the examined samples. In laboratory settings, this typically involves the use of spectroradiometers to acquire high-resolution spectral curves across the 350–2500 nm range (Albrechtová et al., 2017). Reflectance at a specific wavelength is defined as the ratio of reflected light intensity to the intensity of the incident light (Cavender-Bares et al., 2016).

Spectroradiometers provide stable, detailed measurements that support the estimation of photosynthetic pigments like chlorophyll, enabling the non-destructive assessment of plant physiological condition (Croft et al., 2014; Lhotáková et al., 2013). Conventional biochemical analyses of leaf traits are often laborious, costly, and destructive. Spectroscopy offers a non-destructive and rapid alternative to model relationships between spectral signatures and physiological characteristics (Jacquemoud and Ustin, 2019; Lhotáková et al., 2013). Light reflectance and absorption by leaves depend on their biochemical and structural properties, primarily pigment content and water status (Croft et al., 2014; Jacquemoud and Ustin, 2019; Kureel et al., 2022). Spectral reflectance curves reveal how plant leaves interact with light across the visible (VIS), near-infrared (NIR), and shortwave infrared (SWIR) regions of the electromagnetic spectrum.

Healthy leaves absorb 70–90% of visible radiation, particularly in the blue (~450 nm) and red (~670 nm) regions, and reflect most green light (~533 nm), which explains their green appearance. Photosynthetic pigments such as chlorophyll are primarily responsible for these absorption patterns, and visible (VIS) bands are strongly correlated with pigment content (Gitelson & Solovchenko, 2018). In contrast, the near-infrared (NIR) region (700–1300 nm) is largely reflected and transmitted due to scattering by cell walls and internal leaf structures (Roman & Ursu, 2016), and is associated with structural features (Buschmann et al., 2012). Water content influences characteristic dips in reflectance around 1450 nm and 1950 nm in the shortwave infrared (SWIR) region and can also be detected in the green spectrum (~550 nm) (Granlund et al., 2018). The red-edge region (680–800 nm), where reflectance rapidly shifts between red and NIR wavelengths, is especially sensitive to chlorophyll concentration, plant stress, and phenological changes (Baranoski and Rokne, 2005; Campbell et al., 2019; Curran et al., 1995; Jacquemoud and Ustin, 2019; Neuwirthová et al., 2021). Recent advances in hyperspectral remote sensing have significantly improved the ability to monitor vegetation traits and ecosystem dynamics (Zhang et al., 2022a). Spectral properties of different materials can be described using the spectral reflectance curve. The spectral reflectance curve of vegetation is shown in Fig. 1.

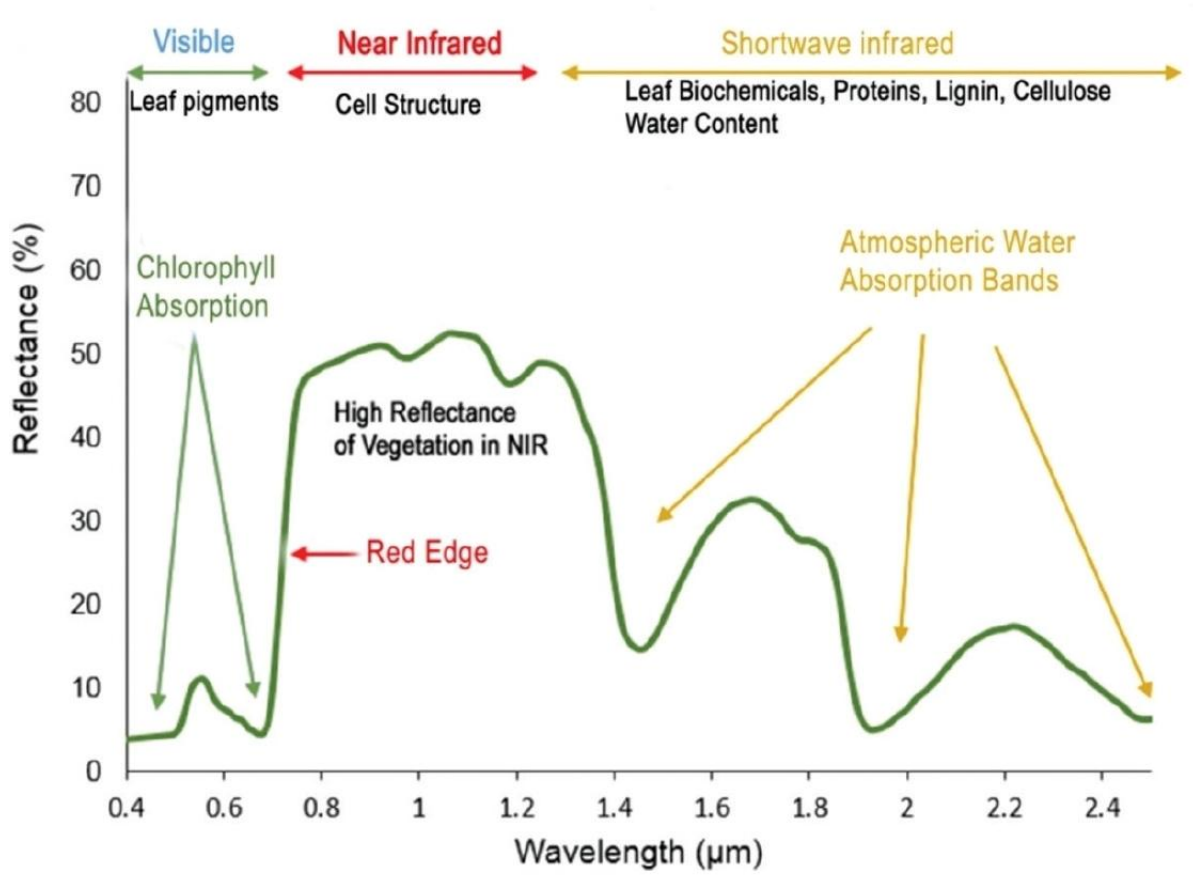

Figure 1: The spectral reflectance curve of vegetation. The major absorption and reflectance features are indicated (Roman & Ursu, 2016).

Stressed vegetation exhibits altered spectral signatures, including increased yellowing in the VIS region and decreased NIR reflectance (Roman and Ursu, 2016). These differences can be used to differentiate plant health status or physiological stress responses. Vegetation indices, quantitative measures derived from combinations of spectral bands, translate raw spectral data into interpretable traits such as chlorophyll content, pigment degradation, or water stress, particularly when based on red and NIR bands, which are especially useful for monitoring plant vigor, quality, and stress (Croft et al., 2014; Roman and Ursu, 2016). The different spectral properties of healthy and stressed vegetation are shown in Fig. 2.

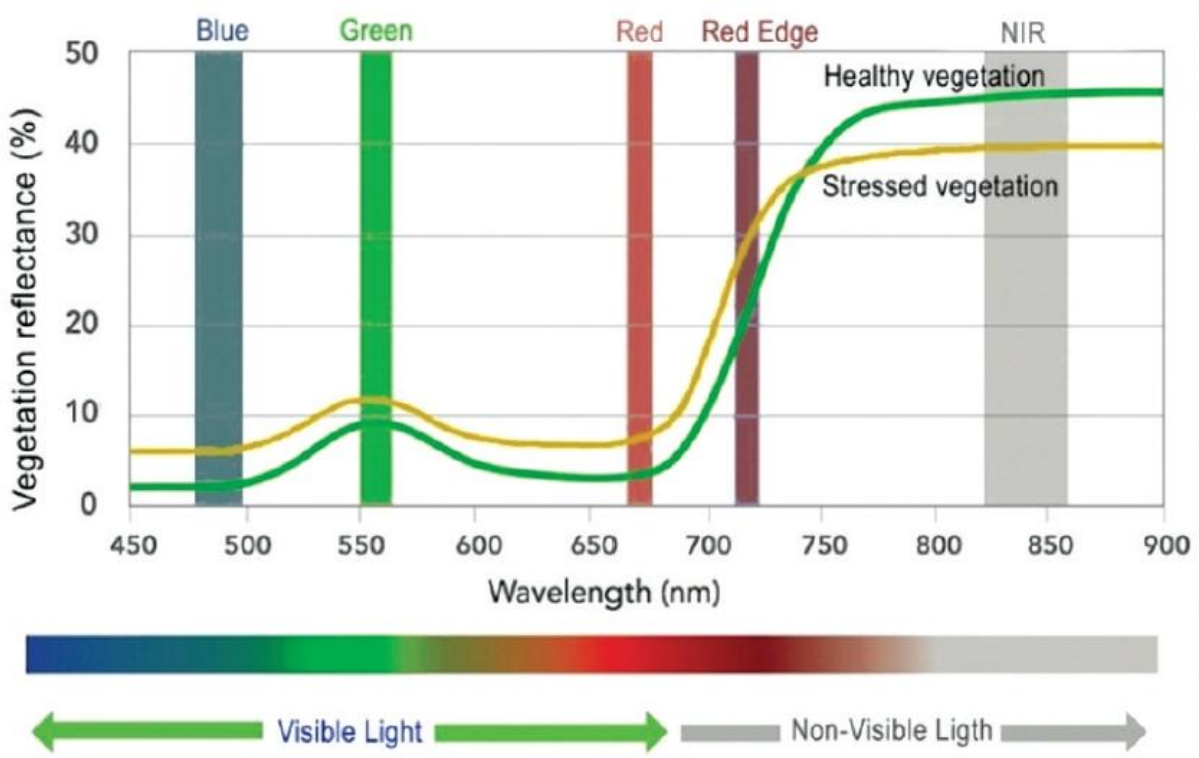

Figure 2: Reflectance curves for healthy vs. stressed vegetation (Roman & Ursu, 2016).

Spectral traits derived from these measurements serve as proxies for various physiological characteristics and are especially valuable for forest tree research. For example, spectral reflectance has been used to detect chlorophyll degradation in Scots pine at high elevations (Dengel et al., 2013) and to distinguish between provenances, revealing patterns of ecotypic variation and adaptability (Čepl et al., 2018; Danusevicius et al., 2014). Structural information from the NIR spectrum has even been used to identify population origin (Stejskal et al., 2023).

These spectral proxies are increasingly being used in breeding programs for indirect selection, helping to estimate trait heritability and genetic correlations that would otherwise require destructive, time-consuming methods (Bian et al., 2022). Lab-based spectroradiometry, although precise, remains resource-intensive and low-throughput when applied to large populations or breeding trials.

3.3.3.2 Imaging Spectroscopy

Imaging spectroscopy offers a distinct advantage over traditional spectroradiometers by combining high spectral resolution (multispectral or hyperspectral) with spatial detail, enabling pixel-level analysis of heterogeneous plant traits across complex canopies or seedling

populations. Hyperspectral cameras mounted on UAVs (unmanned aerial vehicles) allow for rapid, high-resolution data acquisition over extensive field plots, significantly increasing the throughput of phenotyping efforts (Eismann, 2012; Grubinger et al., 2023). These systems typically capture reflectance across the visible (VIS), near-infrared (NIR), and sometimes also shortwave infrared (SWIR) bands, each linked to distinct physiological attributes: VIS bands correlate with pigment content (Gitelson and Solovchenko, 2018), NIR bands with structural integrity (Buschmann et al., 2012), and SWIR bands with water status (Granlund et al., 2018).

Imaging spectroscopy also presents specific challenges. Data quality is influenced by spatial resolution and ambient lighting (Feduck et al., 2018), and image segmentation is complicated by shadows and understory vegetation (Kopačková-Strnadová et al., 2021). However, innovations such as snapshot cameras address some of these limitations by capturing full spectral images in a single exposure, thereby improving efficiency in the field (Faehn et al., 2024). However, its design requires a stationary setup, which limits its use in UAV-based applications.

Multimodal approaches that integrate RGB and hyperspectral imagery with machine learning have further enhanced classification accuracy, for example, in species identification or fruit maturity detection (Garillos-Manliguez and Chiang, 2021; Liu et al., 2022)

3.3.3.3 Spectral Tools for Forest Genetics and Physiology

While remote sensing is well established in ecological studies, its application in tree physiology and forest genetics remains limited (Čepl et al., 2018; D'Odorico et al., 2023; Wong et al., 2019). Understanding genotype-by-environment interactions (GxE) is essential for forest management, as GxE can cause substantial performance variation if not accounted for (Zobel and Talbert, 1984). Though GxE has been studied for traits like height and vitality in Scots pine (Calleja-Rodriguez et al., 2019; Hejtmánek et al., 2023), its influence on hyperspectral reflectance remains underexplored.

Bridging this gap will require a multidisciplinary approach integrating quantitative genetics, genomics, plant physiology, and remote sensing (Cavender-Bares et al., 2020). Hyperspectral tools show potential within such frameworks, already demonstrating utility in predicting biochemical traits (Song et al., 2024), evaluating drought response and seasonal adaptation (Grubinger et al., 2023), and assessing population differentiation (Stejskal et al., 2023).

Advancements in UAV-based phenotyping and digital imaging have improved scalability and reduced observer bias (Cloutier et al., 2024; Hu et al., 2022). However, most platforms remain tailored to agriculture and lack the precision or adaptability required for forests, tree seedlings, or the specifics of conifers. Future phenotyping systems must accommodate fine-scale morphological and physiological variability, while remaining portable, efficient, and robust under diverse environmental conditions (Araus and Cairns, 2014; Pieruschka and Schurr, 2019).

Spectral information has been applied to forest trees, including Scots pine, to assess ecotypic variation and physiological responses. For instance, (Dengel et al., 2013) demonstrated chlorophyll degradation in Scots pine at high elevations through needle spectral reflectance. Other studies have shown that needle reflectance can distinguish between provenances, indicating adaptability at the intra-population scale (Čepl et al., 2018; Danusevicius et al., 2014). Moreover, NIR-based structural information can help identify population origin (Stejskal et al., 2023).

Spectral phenotyping has shown promise for assessing physiological traits and nutrient dynamics in the alder species, though studies remain relatively scarce. Near-infrared (NIR) spectroscopy has been used to non-destructively differentiate nitrogen sources in black alder, detecting biochemical differences between symbiotically fixed and soil-derived nitrogen not captured by conventional chlorophyll measurements (Georgopoulos et al., 2025). During autumn senescence, black alder retains high chlorophyll levels and remains green, contrasting with species like rowan (*Sorbus aucuparia* L.), which rapidly loses chlorophyll and turns red, reflecting distinct nutrient resorption strategies (Taulavuori, 2006). A rare study on grey alder (*Alnus incana* (L.) Moench) highlights continuous seasonal spectral changes, with chlorophyll indices increasing late into the growing season and complex red-edge dynamics that challenge the use of REIP as a stable proxy (Mottus et al., 2014).

3.3.3.4 Imaging-Based Phenotyping for Conifer Seedling Phenology

Although phenological traits in forest trees are crucial for both ecological research and breeding programs, they are still most often assessed through manual visual scoring. This approach requires frequent site visits during transitional periods, relies on trained personnel, and introduces subjectivity and variation between observers (Vilhar et al., 2013). While this method

can provide valuable insights, it becomes increasingly impractical and error-prone when applied to large-scale experiments or long-term monitoring.

Recent developments in indirect phenotyping techniques expanded the ability to monitor plant traits at scale (Cloutier et al., 2024; Hu et al., 2022). These methods reduce observer bias, allow for higher throughput, and can provide temporally resolved data at finer spatial scales. However, current applications are predominantly optimized for agricultural crops and canopy-level assessments. As a result, these setups often lack the spatial resolution, species-specific adaptability, and classification precision needed for seedling-scale studies in forest trees, especially conifers.

To address these limitations, plant phenotyping requires scalable, image-based tools capable of capturing subtle morphological and physiological variation across genetically diverse seedlings and under varied environmental treatments (Omari et al., 2020). Such tools must generate repeatable, quantitative outputs while accommodating the large sample sizes typical of breeding programs and common garden trials (Pieruschka and Schurr, 2019). Moreover, spatially explicit visualizations, such as mapping red needle area or detailing bud morphology, can provide critical insight into plant-environment interactions. For practical deployment, any phenotyping pipeline must be computationally efficient, accessible, and robust to variation in imaging conditions, or alternatively, designed so that the imaging setup can be relocated closer to the experimental site to establish unified conditions (Araus and Cairns, 2014).

Hyperspectral imaging (HSI) has become an increasingly powerful tool in plant phenotyping, offering non-destructive, high-resolution insights into plant structure and physiology. Traditional HSI systems, such as line-scan or pushbroom configurations, require mechanical scanning of either the object or the camera, which can slow down data acquisition and complicate experimental workflows and relocation of the setup. In contrast, snapshot hyperspectral cameras capture full spectral images in a single exposure without the need for spatial scanning, streamlining the imaging process and reducing mechanical complexity. The VNIR SNAPSCAN camera (imec, Leuven, Belgium) is one such device that integrates line-scan and snapshot functionality using on-chip filter technology. This hybrid approach improves usability across various plant imaging contexts and has recently been demonstrated as effective in root phenotyping studies (Faehn et al., 2024), where it enabled accurate classification of root, soil, and rhizosheath interfaces at both macro- and microscale levels. Although initially

developed for below-ground traits, this methodology provides a valuable framework for broader applications in plant science.

Recent advances in hyperspectral image classification using the VNIR SNAPSCAN system highlight the power of integrating spectral and spatial information with advanced machine learning techniques. For instance, multimodal deep learning approaches that fuse RGB and hyperspectral data have significantly improved fruit maturity classification across multiple developmental stages in a study by Garillos-Manliguez and Chiang (2021). Similarly, lightweight convolutional neural networks trained on hyperspectral bands have been shown to outperform traditional RGB-based classifiers for live plant species identification by capturing subtle spectral features in red-edge and near-infrared ranges (Liu et al., 2022). In outdoor applications, spectral reflectance estimation under variable illumination has improved weed detection accuracy, even under inconsistent lighting conditions, highlighting the importance of robust image acquisition strategies (Amziane et al., 2021). These findings reinforce the adaptability of HSI for diverse plant phenotyping challenges and support its implementation in semi-automated phenological monitoring of tree seedlings.

3.3.3.5 Variable Chlorophyll *a* Fluorescence

Chlorophyll fluorescence (ChlF) kinetics, particularly fast induction dynamics known as the OJIP transient, have become a vital tool for evaluating photosynthetic performance, stress responses, genetic variation, and ecological adaptation in plants (Akinyemi et al., 2023; Mishra, 2018; Murchie and Lawson, 2013). The shape of the OJIP curve and associated parameters provide an indirect yet highly sensitive representation of the photosynthetic process (Jalink and Schoor, 2015; Jansen et al., 2009) and a plant's adaptive capacity under varying environmental conditions (Baker and Rosenqvist, 2004). Each phase of the OJIP transient reflects a specific physiological process: the O–J rise corresponds to the reduction of the PSII acceptor side, the J–I phase relates to plastoquinone pool dynamics, and the I–P phase reflects the re-reduction of plastocyanin (PC^+) and $P700^+$ in PSI (Oukarroum et al., 2009). An example of an OJIP transient is visualized in Fig. 3. This physiological mapping enables the detection of distinct stress responses and environmental sensitivities across phases (Bussotti et al., 2020, 2010; Kalaji et al., 2016; Perboni et al., 2012; Strasser et al., 2004).

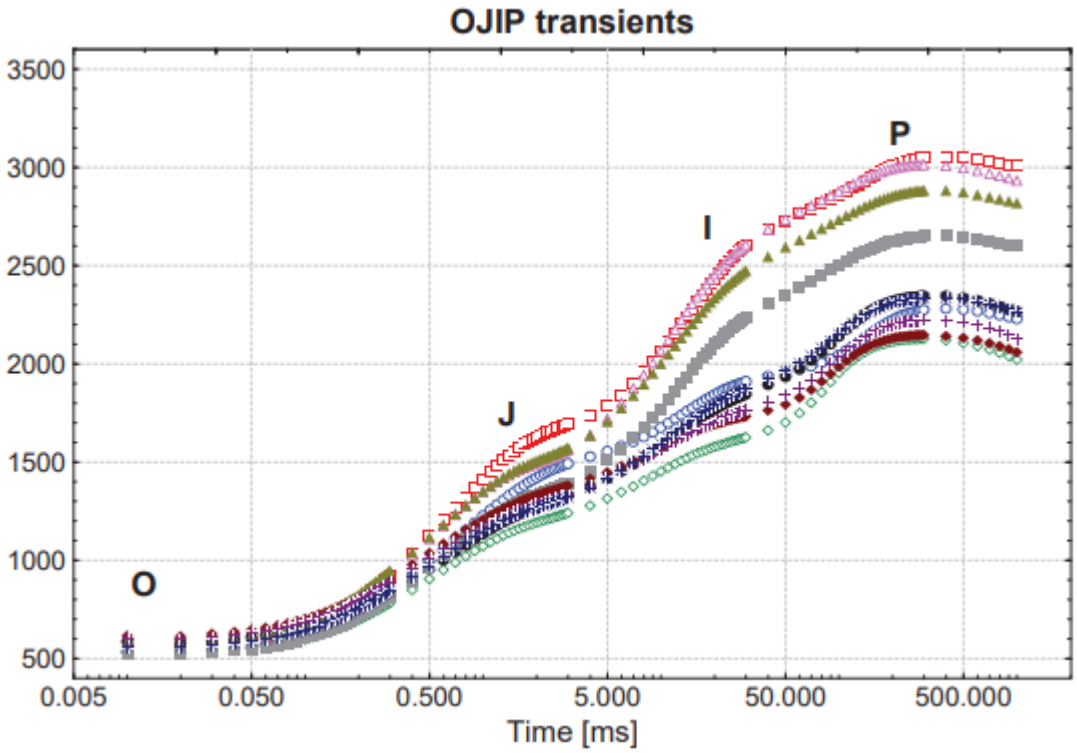

Figure 3: Example of fluorescence transients labeled at the O, J, I, and P steps (Bussotti et al., 2010).

A wide range of fluorescence indices can be derived from the OJIP curve, each capturing distinct aspects of the photosynthetic apparatus and offering varying sensitivities to physiological status, environmental stress, or genetic variation (Strasser et al., 2004). Among ChlF-derived metrics, the maximum quantum yield of PSII (F_v/F_m) is the most commonly used indicator of early stress, while the performance index on an absorption basis (PI_{ABS}) provides a more integrative view of photosynthetic efficiency (Kalaji et al., 2011; Parammal et al., 2019). These metrics are particularly useful for diagnosing plant stress before visible symptoms or growth reductions occur (Fiorani and Schurr, 2013). The ability to localize changes along the OJIP curve enhances its diagnostic potential, not only under stress but also under non-stress conditions where genetic differences may be apparent (Čepl et al., 2016). ChlF measurements are rapid, non-invasive, and feasible in the field, making them well-suited for ecological and breeding studies. For instance, research on European beech has demonstrated provenance-specific differences in ChlF parameters based on environmental origin, such as altitude (Pšidová et al., 2018) or climatic background (Kučerová et al., 2018; Kurjak et al., 2019; Robson et al., 2012).

3.3.3.6 Measurements of Foliage Photosynthetic Rates

Photosynthesis is the primary driver of plant productivity, underpinning growth, biomass accumulation, and nutrient assimilation. The capacity to maintain photosynthetic carbon dioxide and nitrate assimilation under environmental stress is fundamental for sustained plant performance (Tilman et al., 1996). Various techniques are used to study photosynthesis, ranging from growth analysis and detailed in vitro biochemical assays to biophysical measurements. Among these, gas exchange remains one of the most widely used approaches, providing macroscopic insights into plant-environment interactions (Busch et al., 2024; Wang et al., 2012). Importantly, photosynthesis is not measured directly; rather, it is calculated based on gas concentrations, flow rates, and other parameters (Field et al., 1989; Hussain et al., 2024). Rapid, non-invasive alternatives such as carbon uptake monitoring and chlorophyll fluorescence analysis can also offer valuable indicators of plant physiological status (Niinemets, 2010; Song and Zhu, 2024). The overall efficiency of photosynthesis is critical across agriculture, forestry, and ecology. It is influenced by numerous factors, including photosynthetically active radiation (PAR), temperature, water availability, nutrient status, photorespiration, and exposure to pollutants such as heavy metals. Understanding how these factors interact with changing environmental conditions remains a central focus of both applied and fundamental research (Tamayo et al., 2001).

3.4 Forest Genetics, Tree Breeding, and Genetic Evaluation

Forest genetics is a specialized branch of genetics that investigates hereditary variation and the inheritance of traits in forest tree species, aiming to understand how genetic factors influence growth, adaptation, and survival in diverse environments (Eriksson, 2006; White et al., 2007; Zobel and Talbert, 1984). Despite their large size and long-life cycles, which make forest trees less conventional as genetic model organisms, their ecological and economic significance underscores the importance of studying their genetic makeup (Grattapaglia et al., 2009; White et al., 2007). Central to forest genetics is the analysis of genetic variation within and among populations, the dynamics of gene flow, and the role of natural selection in shaping genetic structure (Eriksson, 2006). This understanding provides the foundation for tree breeding, which applies genetic principles to improve the target traits.

Progeny trials, where offspring of selected “plus trees” are planted and evaluated over time to estimate the heritability and genetic control of desirable traits, are a key element in breeding cycles (Bilir and Ozbey, 2022; Zobel and Talbert, 1984). These trials are essential for identifying superior genotypes that are then propagated in seed orchards through grafting and controlled pollination to produce improved seeds (Zobel and Talbert, 1984). The breeding process is refined over successive generations by roguing fewer desirable clones and advancing the most promising individuals into second-generation breeding populations, thereby maximizing genetic gain and enhancing the long-term performance and adaptability of forest plantations (Eriksson, 2006; White et al., 2007).

Forest tree breeding mostly targets quantitative (polygenic) traits (e.g., growth traits, bud set, bud burst, frost hardiness, and wood density) (Eriksson, 2006; Sederoff et al., 2009). These traits are highly relevant for assessing adaptive potential and evolutionary responses, particularly in the face of environmental variability and climate change (Aitken et al., 2008). Because specific genotypes can't be identified for polygenic traits (in contrast to qualitative traits where phenotypes are identifiable and environmental variation negligible), statistical methods of quantitative genetics are used to quantify phenotypic variation, estimate genetic and environmental contributions, and predict the total genetic value of each individual, family, or clone (Caballero, 2020; Falconer and Mackay, 1996; Grattapaglia et al., 2009; Lynch and Walsh, 1998).

Phenotyping plays a critical role in studying quantitative traits for several reasons. Firstly, it enables the detection of natural variation, which is typically not expressed in discrete Mendelian patterns (in qualitative traits) but rather as continuous variation across populations (Eriksson, 2006; Falconer and Mackay, 1996). Secondly, it provides the empirical data necessary to estimate key quantitative genetic parameters, such as heritability, genetic correlations, breeding values, and genotype-by-environment interactions (Caballero, 2020; Falconer and Mackay, 1996; Lynch and Walsh, 1998). These parameters are all essential for predicting how traits will respond to selection and for making informed decisions in breeding programs.

3.4.1 Heritability

Heritability is a central concept in quantitative genetics, describing the proportion of phenotypic variation in a trait that is due to genetic differences among individuals. It is commonly expressed in two forms: narrow-sense heritability (h^2) and broad-sense heritability (H^2) (Eriksson, 2006; Falconer and Mackay, 1996; White et al., 2007; Zobel and Talbert, 1984).

Narrow-sense heritability (h^2) can be interpreted in three equivalent forms (Falconer and Mackay, 1996; White et al., 2007):

1. As the proportion of phenotypic variance (V_P) explained by additive genetic variance (V_A):

$$h^2 = \frac{V_A}{V_P},$$

   or variance in breeding values, reflecting only the transmissible portion of genetic variance.

2. As the regression coefficient of breeding value on phenotype, which indicates how much the breeding value is expected to change per unit change in phenotype.

3. As a measure of the resemblance between parents and their sexual offspring. When h^2 is close to 1.0, the phenotype reliably reflects the breeding value, and offspring performance is expected to closely mirror that of the parent.

4. As the probability that parents and offspring share the same position in the trait distribution, (how often offspring in the selected part of the phenotype range come from parents in that same range). When this parent–offspring matching rate is high, it

indicates high narrow-sense heritability because the trait is being consistently transmitted across generations (Lstibůrek et al., 2018).

These same interpretations apply to broad-sense heritability as to narrow-sense heritability, with additive variance, breeding value, and sexual offspring replaced by total genetic variance, clonal value, and clonal offspring, respectively (White et al., 2007). Broad-sense heritability is the ratio of total genetic variance (V_G) to total phenotypic variance (V_P), capturing the full genetic contribution, including additive, dominance, and epistatic effects (White et al., 2007):

$$H^2 = \frac{V_G}{V_P}$$

It is important to note that heritability is population- and environment-specific. Accurate estimation requires well-designed, replicated trials to properly separate genetics from environmental sources of variation. High heritability suggests that phenotypic selection will be effective, whereas low heritability indicates that more rigorous testing (e.g., progeny trials) is needed to identify superior genotypes (Bernardo, 2020).

3.4.2 Breeding Values

Breeding values are fundamental concepts in quantitative genetics and tree breeding, representing the genetic worth of an individual. The breeding value of a tree (if mated to a number of individuals taken at random from the population) is defined as twice the deviation of its progeny mean from the overall population mean, reflecting the additive genetic contribution that the individual passes on to its offspring (Eriksson, 2006; Falconer and Mackay, 1996). This value is dependent on the specific population and environmental conditions under which the progeny is tested, making it a relative estimate. The variance of breeding values within a population is known as the additive genetic variance, which is crucial for predicting the potential for genetic improvement through selection (Caballero, 2020; Eriksson, 2006; Falconer and Mackay, 1996).

General Combining Ability (GCA) is closely related to breeding values and refers to the average performance of a parent in hybrid combinations, independent of the specific mating partner. It is estimated as the average deviation of a parent's progeny from the grand mean in a mating design such as a diallel (Caballero, 2020; Eriksson, 2006). Specific Combining Ability (SCA), on the other hand, captures deviations in progeny performance that are specific to

particular parental combinations and not explained by GCA alone (Eriksson, 2006). While SCA reflects non-additive gene action, the breeding values of progenies are determined solely by the additive genetic effects they receive from their parents. In quantitative genetic terms, a progeny's breeding value represents the sum of the average additive effects contributed by each parent, and therefore only the GCA component of parental performance directly contributes to progeny breeding values (Falconer and Mackay, 1996; White et al., 2007).

In modern breeding programs, these additive effects are most accurately estimated using animal models (described later), a class of mixed linear models that incorporate pedigree or genomic relationships among individuals. Through Best Linear Unbiased Prediction, animal models partition phenotypic variation into fixed environmental effects and random additive genetic effects, yielding estimated breeding values for each progeny (Walsh and Lynch, 2018).

3.4.3 Phenotypic and Genetic Correlations

3.4.3.1 Phenotypic Correlation

When two different traits are measured in a forest tree population, there may be an association between them. This indicates a phenotypic association between the traits, which is quantified by the phenotypic correlation (r_p), a measure of the strength and direction of their observed relationship (White et al., 2007).

3.4.3.2 Type A Genetic Correlation

Genetic correlations refer to the relationship between two different quantitative traits that may be influenced by the same alleles or loci. This concept is important in tree breeding because selecting for one specific trait can affect other traits due to their genetic linkage or pleiotropy (when one gene influences multiple, seemingly unrelated traits in an organism) (Mode and Robinson, 1959). Genetic correlations are typically calculated as the correlation of breeding values between two traits and are denoted as (r_a) (Caballero, 2020; Eriksson, 2006).

3.4.3.3 Type B Genetic Correlation and Genotype-by-Environment Interactions

Type B genetic correlations refer to the genetic correlations of the same trait expressed in different environments or under different environmental conditions. These correlations measure the consistency of genetic effects across environments and are important for

understanding genotype-by-environment interactions (Eriksson, 2006; Walsh and Lynch, 2018; White et al., 2007).

In the context of forest genetics, type B correlations indicate how well the genetic performance of a trait in one environment predicts its performance in another environment. A high type B genetic correlation suggests that the genetic control of the trait is stable across environments, while a low type B genetic correlation indicates significant genotype-by-environment (G×E) interaction, meaning that different genotypes perform differently depending on the environment (Eriksson, 2006).

The essence of G×E interaction is the inconsistency in the relative performance of genotypes across different environments. This can take two forms: rank change interaction, where genotype rankings differ between environments, and scale effect interaction, where rankings remain the same but the magnitude of differences in performance varies across environments (White et al., 2007).

Type B correlations are crucial in tree breeding and selection because they affect the reliability of selecting superior genotypes in one environment for deployment in another. If type B correlations are low, breeding programs may need to conduct multi-environment trials to identify genotypes with stable performance.

The following equation represents the type B genetic correlation (rg_B^2):

$$rg_B^2 = \frac{V_a}{V_a + V_{axs}},$$

where $V_a$is the additive genetic variance, and $V_{a\times s}$ is the variance due to the interaction between the additive genetic effect and site (G×E interaction). If the interaction term $V_{a\times s}$is 0, the Type B genetic correlation corresponds to 1, indicating no G×E interaction.

3.4.3.4 Age-to-Age (Year-to-Year) Correlations

Age-age correlations (also called juvenile-mature correlations) refer to the genetic correlation between the same trait measured at different ages in a tree's life (White et al., 2007). If the same gene loci largely influence the trait across ages, the genetic correlation will be high, and early selection will reliably predict mature performance. However, if different genes influence the trait at different stages, the correlation will be lower, making early selection less effective. The success of juvenile selection depends on the strength of this age-age genetic correlation

(White et al., 2007). Early testing has long been explored as a way to accelerate breeding cycles, but juvenile–mature correlations for growth traits have historically been inconsistent, with some studies reporting strong relationships while many others found weak or no predictive value (Eriksson, 2006).

3.4.4 Indirect Selection

Indirect selection is a breeding strategy in which individuals are selected based on one trait (the measured trait) to improve another genetically correlated trait (the target trait) (Eriksson, 2006; Falconer and Mackay, 1996; White et al., 2007). This approach is especially useful when the target trait is difficult, costly, or time-consuming to measure, but shows a strong genetic correlation with a more easily assessed trait (Eriksson, 2006).

In forest genetics, indirect selection can be effective when the measured trait has high heritability and is positively correlated with the target trait. However, care must be taken to avoid negative genetic correlations, which can lead to unintended or undesirable changes in the target trait (Eriksson, 2006). Several surrogate traits, which are simple and rapid measurements used as proxies for more difficult or costly assessments, are widely applied in forestry and wood science. For example, Pilodyn penetration and acoustic velocity have been used to estimate solid wood properties in standing Norway spruce trees (Chen et al., 2015), and near infrared (NIR) spectroscopy has been applied to predict a range of wood physical, mechanical, and chemical traits (Tsuchikawa and Kobori, 2015).

3.4.5 Linear Mixed Models

Linear mixed models (LMMs) are a flexible extension of classical linear models, well-suited for the complex and unbalanced data typical in plant breeding programs, enabling more accurate estimation and prediction of various genetic parameters mentioned above (Bernardo, 2020). However, many of these parameters require a complex modelling approach (MET trials, bivariate models estimating genetic correlations between traits, etc.). LMMs are statistical models that extend classical linear models by incorporating both fixed effects and random effects. In the context of plant breeding and quantitative genetics, LMMs are used to analyze phenotypic and genetic data, especially when data are unbalanced or when there is relatedness among individuals (Bernardo, 2020).

A typical linear mixed model can be expressed as:

$$Y_{ij} = \mu + g_i + e_j + (ge)_{ij} + \varepsilon_{ij}$$

where:

- μ is the grand mean (fixed effect),
- g_i is the effect of genotype i (can be modeled as fixed or random),
- e_j is the effect of environment j (fixed effect),
- $(ge)_{ij}$ is the genotype × environment interaction effect (random effect),
- ε_{ij} is the residual error.

In LMMs, factors are classified as either fixed or random effects based on the objective of the experiment. Fixed effects refer to factors where interest lies in the specific levels used in the experiment, which are treated as constants without associated variance or covariance. Common fixed effects include: (1) treatment effects such as fertilizers, irrigation, and planting density; (2) environmental effects related to the experimental design, like location, year, or block; and (3) fixed genetic effects, also known as group effects, such as provenance, seed source, or generation of selection (Falconer and Mackay, 1996; White et al., 2007).

In contrast, a random effect represents a factor whose levels are considered a random sample from a larger population, and the goal is to make inferences about that broader population or predict future performance. In forest genetics, genetic effects such as families, breeding values, and clonal values are always treated as random effects in LMM analysis, as they reflect underlying genetic variation and are associated with variance components that contribute to phenotypic prediction (Caballero, 2020; Walsh and Lynch, 2018; White et al., 2007).

Additionally, significant spatial variation is common in forestry genetic trials. Incorporating *x* and *y* coordinates into mixed model analyses through spatial analysis can help account for this variation, reducing experimental error and improving the accuracy of results. This approach often leads to higher heritability estimates and greater genetic gain from selection, making it a valuable tool in forest genetics (Walsh and Lynch, 2018; White et al., 2007).

3.4.5.1 Parental (Family) Models

Historically, quantitative genetics in forestry and crop breeding has relied on parental models, where genetic effects are defined by the influence of parents on their offspring. These models,

commonly used for half-sib and full-sib families, include family effects that trace back to the genetic contribution of parents (White et al., 2007).

Parental models have been widely used in forest genetics and dominate the literature. However, their application depends on several key assumptions: (1) parents are unrelated and non-inbred; (2) they represent a random, unselected sample from the population; (3) they come from the same generation; (4) mating is random; and (5) a single, consistent mating design is used. Additionally, the models assume regular diploid inheritance (Falconer and Mackay, 1996).

3.4.5.2 Individual Tree (Animal) Models

Traditional parental models predict breeding values only for parents, not for the measured trees themselves. To overcome this limitation, individual tree models (also known as animal models in animal breeding) were developed. These models treat the breeding value of each measured tree as a random effect, allowing simultaneous prediction of breeding values for offspring, parents, and ancestors (White et al., 2007).

This is achieved using a pedigree file and an additive genetic relationship matrix (Identity by Descent). Identity by Descent (IBD) refers to alleles in two individuals that are inherited from a common ancestor without mutation, and it forms the basis for calculating additive genetic relationship matrices used in quantitative genetic analyses (Caballero, 2020; Lynch and Walsh, 1998). These relationship matrices quantify the expected proportion of shared genetic material among individuals and therefore define their genetic relatedness. By incorporating these IBD-based relationships, data from all measured trees contribute to a unified prediction of breeding values across generations, enabling consistent selection decisions regardless of pedigree depth (White et al., 2007). These models can also accommodate complex mating designs, clonal tests, and integration with quantitative trait loci (QTL) data.

The additive genetic relationship matrix (often denoted as A) captures the expected proportion of alleles shared between individuals due to common ancestry. This matrix allows information to flow across related individuals, improving the accuracy of breeding value predictions. It also supports the inclusion of related, inbred, or selected individuals from different generations, making the model robust and flexible for complex breeding programs (White et al., 2007).

3.4.6 REML and Variance Component Estimation

Restricted Maximum Likelihood (REML) (Patterson and Thompson, 1971) is an iterative method used to estimate variance components by maximizing the likelihood of the residuals rather than the raw observations, thereby removing fixed-effect bias from variance estimates. REML is particularly advantageous in forest genetic analyses because it yields unbiased estimates of variance components even in unbalanced datasets, a common feature of long-term field trials where missing trees, heterogeneous environments, or incomplete pedigrees often occur. In this respect, REML offers a modern and statistically robust alternative to classical analysis of variance (ANOVA) methods, which require strict balance and homogeneity of variance and are therefore unsuitable for many forestry datasets (White et al., 2007). By estimating additive genetic, environmental, and interaction variance components, REML enables LMMs to generate accurate estimates of heritability and to support the prediction of breeding values using Best Linear Unbiased Prediction (BLUP), a framework originally developed by Henderson, (1975). When REML-derived variance components are combined with BLUP, all available phenotypic, pedigree, and genomic marker information (when included) is optimally integrated to produce the most accurate predictions of additive genetic merit (Caballero, 2020; Lynch and Walsh, 1998). In forestry applications, this combination of REML and BLUP has become the standard approach for genetic evaluation across generations and environments because it can accommodate complex mating designs, spatial variability, clonal replications, and incomplete data structures, enabling robust and biologically meaningful inference about genetic parameters and breeding values (Bernardo, 2020; White et al., 2007).

3.4.7 Estimation of Fixed and Random Effects

Estimation of random and fixed effects, as well as variance components, in the context of quantitative genetics for plant breeding, is effectively handled using mixed-model analysis. This approach involves best linear unbiased estimation (BLUE) for fixed effects and best linear unbiased prediction (BLUP) for random effects (Bernardo, 2020).

BLUP refers to the prediction of random effects in a mixed model. In plant breeding, BLUP is commonly used to predict genetic values (such as genotypic values of lines, clones, or hybrids) by incorporating information from relatives through covariance matrices of random genetic

effects. BLUP accounts for relatedness and shrinks estimates toward the population mean to improve prediction accuracy. A key extension of this framework is the use of the realized relationship matrix, which quantifies the actual genomic relationships among individuals based on marker data rather than relying solely on expected pedigree relationships. This matrix improves accuracy by capturing Mendelian sampling variation and cryptic relatedness and forms the basis of genomic prediction models such as GBLUP (genomic best linear unbiased prediction) (VanRaden, 2008). BLUP treats genetic effects as random variables and provides the best linear unbiased predictions of these effects, making it a central tool in both traditional pedigree-based evaluations and modern genomic selection approaches (Bernardo, 2020).

BLUE refers to the estimation of fixed effects in a mixed model. Fixed effects might include overall means, environmental effects, or known major gene effects. BLUE provides the best linear unbiased estimates of these fixed parameters, assuming the model and variance components are correctly specified. Unlike BLUP, BLUE treats effects as fixed and does not shrink estimates (Bernardo, 2020).

3.4.8 Multivariate Linear Mixed Models

In some situations, a multivariate linear model is more appropriate than a univariate approach, especially when analyzing multiple traits or when the same trait is measured across different environments. In such cases, measurements from each test site are treated as distinct variables within the model. This allows for more flexible modeling of site-specific genetic effects, capturing variation that may be masked in simpler models (Calleja-Rodriguez et al., 2019; White et al., 2007).

This approach is particularly valuable when genetic control of a trait differs across test environments. Indicators of such variation include: substantially different heritability estimates among sites, measurements taken at different ages, and uneven levels of G × E interaction between site pairs (Li et al., 2017; White et al., 2007). Treating each environment or age as a separate variable enables the estimation of unique variance structures, such as environment-specific heritability, improving the biological relevance and predictive power of the model (White et al., 2007).

In some cases, edaphoclimatic data and exploratory analysis reveal logical groupings of test sites. If genotype × environment interaction is high between groups but low within them, it is

effective to treat each group as a separate variable while pooling data within each group. This allows for both flexibility across environments and efficiency within similar conditions, enhancing the utility of multivariate models in forest genetics (Li et al., 2017; Poupon et al., 2023; White et al., 2007).

4 Methodology

The methods section of the thesis is divided into four individual experiments for clarity and provides a structured approach for each experiment, reflecting the distinct characteristics and objectives of each experiment. Each experiment represents a distinct species, genetic material, site conditions, phenotyping methods, and trait focus. This variation leads to unique experimental designs, data types, and research questions that are best understood when presented independently. Structuring the methods by experiments aligns with the organization of results, thereby improving the thesis's overall readability and scientific transparency. The thesis comprises four distinct experiments, which are summarized in Table 1.

Experiment Number	Plant Material	Genetic entries	Seasons of Measurements	Number of Sites	Novel Phenotyping Methods	Supporting measurement	Location
1	**Scots pine** (clonal seed orchard - graftings)	clones	2 (UAV imaging in 1 site), 1 (other traits)	2	hyperspectral reflectance (spectroradiometer, UAV - imaging)	photosynthetic pigments, needle morphology	Czechia
2	**European beech** (juvenile trees)	proven-ances	1 (physiological traits), 2 (phenology)	1	chlorophyll *a* fluorescence, gas exchange	phenology, senescence, survival	Denmark
3	**Scots pine** (seedlings)	proven-ances	1	1	hyperspectral imaging (Imec Snapscan), short-day treatment	ion leakage (not included in the thesis)	Finland
4	**black alder** (juvenile trees)	proven-ances, half-sib families	4 (growth traits), 1 (phenological traits)	4	hyperspectral reflectance (spectroradiometer)	bud burst, hyperspectral reflectance	Denmark

Table 1: Overview of experiments presented in the thesis.

4.1 Methodology for Experiment 1 – Scots Pine Clones – Seed Orchards

4.1.1 Plant Material

Two first-generation clonal seed orchards of Scots pine (*Pinus sylvestris* L.) were selected for this experiment. The orchards are referred to by their neighboring towns, Plasy and Nepomuk, located in the western part of Czechia at 49°54′31.543″ N, 13°26′33.860″ E (Plasy) and at 49°28′53.747″ N, 13°31′38.760″ E (Nepomuk), approximately 50 km apart. Both orchards were established by grafting scions from plus trees, i.e., phenotypically superior individuals selected for their growth performance and overall vitality. The sites are situated within the same geographic region but differ slightly in soil characteristics, particularly in magnesium, phosphorus, nitrogen content, and carbon-to-nitrogen ratio (Supplementary Table 1). The Plasy orchard was established in 1980 and consists of 87 grafted clones and 1165 ramets, covering an area of 6.48 ha. The Nepomuk orchard was established in 1975 and consists of 45 clones and 410 ramets, covering 2.24 ha. Twenty-four genotyped clones were common to both orchards. The spatial layout of all genotyped clones is shown in Supplementary Figure 1 (Plasy) and Supplementary Figure 2 (Nepomuk).

Sampling was conducted during the 2021 growing season. At Plasy, samples were collected from 148 ramets representing 29 clones, and at Nepomuk from 200 ramets representing 31 clones. A maximum of seven ramets per clone was targeted to ensure adequate representation. In some cases, fewer ramets were available due to mortality or limited planting density; for one clone at Plasy, only a single ramet was sampled. Leaf-level data collected in 2020 were excluded from the analyses due to insufficient replication of clones, which would have limited the reliability of the genetic evaluation. Fully sun-exposed branches were collected from the mid-to-upper crown on the southern side of each tree using telescopic pole scissors. Sampling was performed between 10:00 AM and 4:00 PM during a single day at each site. Branches were at least 100 cm in length to minimize water loss, and the cut ends were wrapped in moistened towels immediately after collection. At the end of each collection day, all samples were transported to the laboratory, stored at approximately 4 °C, and processed the following morning. Collection times were recorded to ensure consistent processing order, and all spectral measurements were completed within 24 hours of cutting. This sampling protocol was based on previous work, which demonstrated stable chlorophyll fluorescence and reflectance values in evergreen conifers for up to 48 hours after branch excision (Čepl et al., 2018, 2016;

Richardson and Berlyn, 2002). A schematic overview of the methodological workflow is presented in Fig. 4.

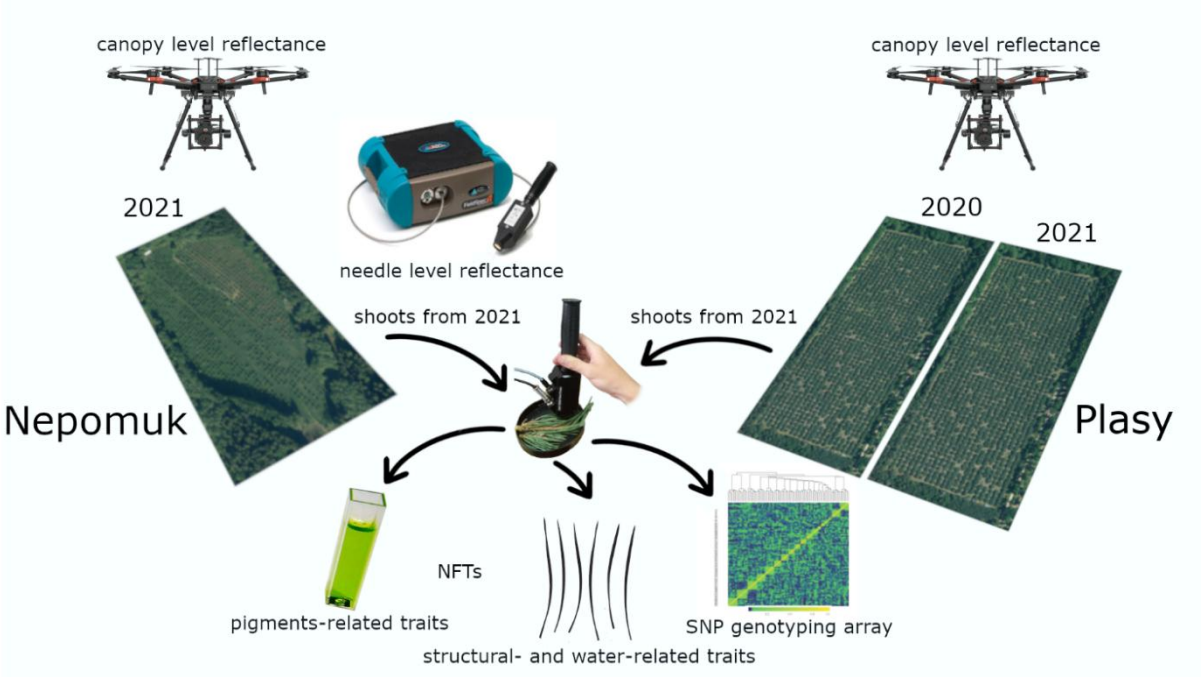

Figure 4: Graphical abstract illustrating the workflow of individual measurements and analyses conducted for specific years and sites. Published in Provazník et al. (2025).

4.1.2 Needle Level Reflectance

Needle-level spectral reflectance was measured using a FieldSpec 4 Wide-Res portable spectroradiometer (Malvern Panalytical Ltd., United Kingdom) equipped with a detachable contact probe. The probe includes an internal light source, enabling measurements across the 350–2500 nm spectral range. The spectroradiometer contains three detectors covering 350–1000 nm (spectral resolution 3 nm), 1000–1800 nm (8 nm), and 1800–2500 nm (8 nm). Instrument calibration was performed every 15 minutes using a Spectralon® white reference panel (SphereOptics, Herrsching am Ammersee, Germany), which provides approximately 99% reflectance across all measured wavelengths. For measurements, shoots (also used for NFT measurements) with attached needles were placed on a measurement plate coated with a low-reflectance black surface (NEXTEL Velvet-Coating 811-21). Needles from the upper part of the branch were arranged tightly to fully cover the probe aperture, following previously established protocols (Čepl et al., 2018; Hejtmánek et al., 2022). The scan average on the spectroradiometer was set to 25. Reflectance was calculated as the ratio between the radiance measured from the sample and that of the white reference panel. For each sample, five

measurements were taken, with branch rotation and needle rearrangement between measurements to reduce positional variability. The median reflectance from the five replicates was used for further analyses. All spectral reflectance and NFT measurements were performed within 24 hours of branch collection to ensure data quality and consistency.

4.1.3 Canopy Level Reflectance

Hyperspectral image data were acquired using a Nano-Hyperspec camera (Headwall Photonics Inc., Fitchburg, Massachusetts, USA) mounted on a DJI Matrice 600 Pro UAV. The camera operates in the spectral range of 400–1000 nm and is divided into 269 spectral bands. All flights were conducted around midday to maximize solar elevation. At Plasy, data were collected in September 2021 under overcast conditions. Although cloudy skies reduce the signal-to-noise ratio (SNR), diffuse illumination can enhance vegetation spectral features (Arroyo-Mora et al., 2021; Shoshany et al., 2019). The flight altitude was 68.9 m above ground level, resulting in a ground sampling distance of approximately 3 cm. A 40% side overlap between flight lines was applied to ensure complete crown coverage of each tree.

Radiometric and basic geometric corrections were carried out using SpectralView – Hyperspec v3.1.0 (Headwall Photonics Inc.). Radiometric calibration was performed using a portable fabric reflectance target with known reflectance (Group 8 Technology, Inc., Provo, UT, USA) placed in the scanned area. Geometric corrections were based on GNSS and IMU logs recorded by the UAV. Orthorectification employed a global digital elevation model (pixel size 0.0083°) provided by the Headwall software, as no digital surface model including trees was available. Since the orchard terrain is flat, an orthophotomosaic was not generated. All parameters used for data acquisition are summarized in Table 2.

seed orchard/year	Plasy 2020	Plasy 2021	Nepomuk 2021
date	05/08/2020	17/09/2021	25/08/2021
local time	11:59-14:30	12:33-13:18	13:09-13:39
weather conditions	clear sky	overcast	clear sky
exposure	3.996 ms	5.995 ms	5.995 ms
number of flights	4	2	2
number of flight lines	16	16	11

Table 2: Summary of flight conditions when canopy-level data were acquired. Published in Provazník et al. (2025).

Initial data processing focused on classifying five surface cover classes: green canopy needles, branches, undergrowth vegetation, soil, and shadows. Object-Based Image Analysis (OBIA) was performed in ENVI (version 5.5) using the Feature Extraction toolbox. Segmentation was carried out with a scale level of 30 and a merge level of 85, based on all spectral bands and spatial attributes (Jin, 2012). The scale parameter defined the size of image segments, while the merge level controlled the merging of adjacent segments. For training and validation, 50 samples were visually selected for each class and split into a 3:2 ratio, with 30 samples used for training and 20 for validation. OBIA classification employed a Support Vector Machine (SVM) with a radial basis function kernel. Input features included spectral (mean, standard deviation, minimum, maximum), texture (range, mean, variance, entropy), and spatial attributes (area, length, compactness, convexity, solidity).

Classification results demonstrated high accuracy, with overall accuracy exceeding 85% for both sites. For the target class (green canopy needles), producer's accuracy was 94% and user's accuracy 90% for Plasy, and 92% and 88% for Nepomuk, respectively. Mean reflectance values for each tree crown (green canopy needles only) across all 269 bands were extracted using the Zonal Statistics Multiband Toolbox from the Dymaxion Labs plugin in QGIS (QGIS Development Team, 2024).

To address systematic fluctuations in every second wavelength, each pair of neighboring bands was averaged, resulting in smoother spectral curves. The first 13 and last 36 bands were removed to eliminate spectral noise, leaving 220 bands (429–919 nm) for further analyses.

Hyperspectral data were acquired for the entire seed orchard area, covering all trees. For subsequent analyses, only ramets of genotyped clones were included: 984 ramets representing 67 clones at Plasy and 261 ramets representing 25 clones at Nepomuk. Spatial visualization of these clones is provided in Supplementary Figure 1 (Plasy) and Supplementary Figure 2 (Nepomuk).

4.1.4 Measurement of Needle Functional Traits

Needle samples for NFT assessment were collected from the same branches used for needle-level reflectance measurements. Branches with current-year shoots were sampled. From each shoot, two needle samples (three current-year needles per sample) were collected: one sample for pigment content analysis and the other for water content and leaf mass per area (LMA) determination.

The first needle sample was used for the biochemical assessment of photosynthetic pigments, including chlorophyll a (chl a), chlorophyll b (chl b), total chlorophylls (chl T), and total carotenoids (car). Needles were cut into 2–3 mm segments, sealed in plastic vials, and stored at –20 °C until biochemical analysis. Pigments were extracted in the dark at 4 °C for seven days using N-dimethylformamide (Porra et al., 1989). Absorbance of the extracts at 480, 647, 664, and 750 nm was measured spectrophotometrically using an Evolution 201 spectrophotometer (Thermo Fisher Scientific, Waltham, MA, USA). Pigment concentrations were calculated according to (Wellburn, 1994) and expressed per unit of dry mass (mg pigment g^{-1} dry mass). The carotenoid-to-chlorophyll ratio (car:chl T) was also derived from the measured values.

The second needle sample was used to determine water content and LMA. Measurements were carried out in the laboratory the day after field collection (see Section 2.1). Needles were weighed fresh, scanned using an EPSON Perfection V600 Photo scanner with an upper lamp at 800 dpi in grayscale, and then dried at 60 °C to constant weight. Needle projection area and length were determined from binary images in ImageJ (National Institutes of Health, Bethesda, Maryland, USA). LMA was calculated as the ratio of dry weight to needle projection area (g cm^{-2}). LMA values were also used to convert pigment and water contents to area-based units, following standard practices in remote sensing and spectroscopy (Kattenborn et al., 2019).

Photosynthetic pigment contents were expressed relative to both dry needle mass (mg g^{-1}; e.g., chl aM for chlorophyll a per dry mass) and needle projection area (µg cm^{-2}; e.g., chl aA for chlorophyll a per area). Needle water content (NWC) was calculated as the percentage difference between fresh and dry weights. Equivalent water thickness (EWT) was calculated as the amount of water per needle area (g cm^{-2}).

4.1.5 SNP Genotyping Array

The clones included in this experiment were sampled in 2022 for subsequent genotyping. Approximately 100 mg of needles per sample were cut into small pieces with a scalpel and immediately preserved in liquid nitrogen. The frozen material was then homogenized for three minutes at 30 Hz using an MM400 mixer mill (Retsch, Haan, Germany). Total genomic DNA was extracted using the NucleoSpin Plant II kit (Macherey-Nagel, Düren, Germany) according to the manufacturer's instructions. DNA concentration and purity were measured with a NanoDrop 2000 spectrophotometer (Thermo Fisher Scientific, Madison, WI, USA), and a subset of samples was additionally quantified using a Qubit assay (Thermo Fisher Scientific, Madison, WI, USA) for validation. DNA integrity was assessed by electrophoresis on a 0.8% agarose gel. Undiluted aliquots of 45 µL DNA (mean concentration 116 ng μL^{-1}, 260/280 ratio between 1.56 and 1.93) were pipetted into 96-well PCR plates. The plates were shipped on dry ice to SGS INSTITUT FRESENIUS GmbH, Germany, for genotyping. SNP genotyping was performed using the PiSy50k SNP chip Axiom array following (Kastally et al., 2022). The resulting raw data were delivered in CEL file format.

4.1.6 Genomic Data

74 Scots pine clones were genotyped using the PiSy50k SNP chip array (Kastally et al., 2022) and standard filtering procedures were applied to ensure high-quality SNP data. Markers with low quality, low minor allele frequency, significant deviations from Hardy–Weinberg equilibrium ($p < 0.001$), or heterozygosity exceeding 60% were removed. After filtering, 20,216 SNPs were retained and used to construct the genomic relationship matrix (GRM) K following the method of Yang et al. (2010), implemented in the AGHmatrix R package (Amadeu et al., 2016).

The genomic relationship matrix allowed us to identify genetically related clones that likely originated from plus trees located in close proximity within seed stands of naturally regenerated

forests. All ramets belonging to the same clone were assumed to share an identical genotype and were treated accordingly in the analysis. In total, 68 genotyped clones were included in the final analysis of canopy-level reflectance.

4.1.7 Statistical Analysis and Genetic Parameters

A linear mixed model (LMM) was fitted to evaluate genotype-by-environment interaction in terms of type B genetic correlations (Burdon, 1977) implemented in the ASReml-R package (Butler et al., 2017) as follows:

$$\boldsymbol{y} = \boldsymbol{X\beta} + \boldsymbol{Zu} + \boldsymbol{e},$$

where $\boldsymbol{y}$ is a vector with the measurements, $\boldsymbol{\beta}$ is a vector of fixed effects including overall mean, site, and population within site, and $\boldsymbol{u}$ is a vector of random effects including additive genetic effects nested within site, following $\boldsymbol{u} \sim N(\mathbf{0}, \mathbf{G})$, where $\boldsymbol{G}$ variance/covariance structure is defined as follows:

$$\boldsymbol{G} = \begin{bmatrix} \sigma^2_{a_{S_1}} & \sigma_{a_{S_1}S_2} \\ \sigma_{a_{S_1}S_2} & \sigma^2_{a_{S_2}} \end{bmatrix} \otimes \boldsymbol{K},$$

where $\sigma^2_{a_{S_1}}$ and $\sigma^2_{a_{S_2}}$ are additive genetic variances at site 1 and site 2, $\sigma_{a_{S_1}S_2}$ is additive genetic covariances between sites 1 and 2, $\boldsymbol{K}$ is the genomic relationship matrix described earlier, $\boldsymbol{e}$ is a vector of residuals following $\boldsymbol{e} \sim N(\mathbf{0}, \boldsymbol{R})$, where $\boldsymbol{R}$ is the residual variance/covariance structure defined as follows:

$$\boldsymbol{R} = \begin{bmatrix} \sigma^2_{\xi_{S_1}}[AR1(p_{col}) \otimes AR1(p_{row})] + \sigma^2_{\eta_{S_1}}\boldsymbol{I} & 0 \\ 0 & \sigma^2_{\xi_{S_2}}[AR1(p_{col}) \otimes AR1(p_{row})] + \sigma^2_{\eta_{S_2}}\boldsymbol{I} \end{bmatrix},$$

where $\sigma^2_{\xi_{S_1}}$ and $\sigma^2_{\xi_{S_2}}$ are variances for spatially dependent residus at sites 1 and 2, $\sigma^2_{\eta_{S_1}}$ and $\sigma^2_{\eta_{S_2}}$ are variances for independent residuals (nugget) at sites 1 and 2, AR1(p_{col}) and AR1(p_{row}) are first-order autoregressive correlation matrices in column and row directions, $\boldsymbol{I}$ is the identity matrix (Dutkowski et al., 2002), $\boldsymbol{X}$ and $\boldsymbol{Z}$ are incidence matrices associating fixed and random effects.

The genetic correlations between different traits (e.g., type-a correlation) or between the same trait measured at various ages (*e.g.*, age-by-age correlation in this case, limited to the two

following years and, thus, further referred to as year-to-year correlation) were estimated on pooled data using a bivariate mixed linear model implemented with the ASReml-R package (Butler et al., 2009) as follows:

$$\boldsymbol{y} = \boldsymbol{X\beta} + \boldsymbol{Zu} + \boldsymbol{e},$$

where **y** is a vector with measurements stacked, $\boldsymbol{\beta}$ is a vector of fixed effects including mean for each trait (or age) and population within trait (or age) nested within trait (or age), $\boldsymbol{u}$ is a vector of additive genetic effects nested within trait (or age) following $\boldsymbol{u} \sim N(\mathbf{0}, \mathbf{G})$, where $\boldsymbol{G}$ variance/covariance structure is defined as follows:

$$\boldsymbol{G} = \begin{bmatrix} \sigma^2_{a_{T_1}} & \sigma_{a_{T_1}T_2} \\ \sigma_{a_{T_1}T_2} & \sigma^2_{a_{T_2}} \end{bmatrix} \otimes \boldsymbol{K},$$

where $\sigma^2_{a_{T_1}}$ and $\sigma^2_{a_{T_2}}$ are additive genetic variances at trait (or age) 1 and trait (or age) 2, $\sigma_{a_{T_1}T_2}$ is the additive genetic covariances between trait (or age) 1 and trait (or age) 2, $\boldsymbol{K}$ is the genomic relationship matrix described earlier, $\boldsymbol{e}$ is a vector of residuals nested within trait (or age) following $\boldsymbol{e} \sim N(\mathbf{0}, \boldsymbol{R})$, where $\boldsymbol{R}$ is residual variance/covariance structure defined as follows:

$$\boldsymbol{R} = \begin{bmatrix} \sigma^2_{e_{T_1}} & \sigma_{e_{T_1}T_2} \\ \sigma_{e_{T_1}T_2} & \sigma^2_{e_{T_2}} \end{bmatrix} \otimes \boldsymbol{I},$$

where $\sigma^2_{e_{T_1}}$ and $\sigma^2_{e_{T_2}}$ are residual variances at trait (or age) 1 and trait (or age) 2, $\sigma_{e_{T_1}T_2}$ is the residual covariances between trait (or age) 1 and trait (or age) 2, $\boldsymbol{I}$ is the identity matrix.

All estimated genetic parameters, including genetic correlations, were tested using a likelihood ratio test (LRT), which compares the final model with a baseline model where the tested parameters are fixed to zero.

Best Linear Unbiased Predictors (BLUPs) of genotypic (clonal) effects were extracted from the fitted linear mixed models to estimate the performance of individual clones. These BLUPs account for random effects and are used to derive clonal rankings based on genetic merit. Clones are ranked according to their BLUPs, providing a basis for selection decisions (usually in breeding programs) (White et al., 2007).

Broad-sense heritability (H^2) is calculated using the following equation:

$$H^2 = \frac{\sigma^2_g}{\sigma^2_p},$$

where σ_g^2 is the total genetic variation, and σ_p^2 is the total phenotypic variation estimated from LMM described above. Heritability values range from 0 to 1, where a value of 0 indicates that observed variation is entirely due to environmental or residual effects (i.e., no genetic contribution), and a value of 1 indicates that all phenotypic variation is attributable to genetic differences.

4.2 Methodology for Experiment 2 – European Beech Provenances

This experiment, which was published by Provazník et al. (2024), aimed to assess variation in photosynthetic performance among European beech (*Fagus sylvatica* L.) seedlings of different geographic and altitudinal origins. The experiment was conducted in a Danish common garden and included plant material from three Italian provenances from the Calabria region, each with subgroups based on elevation, as well as two local Danish provenances. Seedlings were monitored for key physiological and phenological traits, including chlorophyll *a* fluorescence (ChlF), gas exchange (GE), bud flushing, leaf senescence, and survival after 2 years. The design allowed for the evaluation of both within-provenance variation related to altitude and broader inter-provenance differences across geographic origins.

4.2.1 Plant Material

European beech seedlings, aged 1–2 years, were sourced from both Denmark and Calabria, Italy, and used to establish a common garden experiment. The experimental setup included three Italian provenances from distinct mountain ranges, each with subgroups based on elevation, and two Danish provenances representing local populations. In September 2016, seedlings were transplanted into HerkuPlast Quick Pot 12 T/18 trays (produced by Kubern GmbH, Germany) and placed in an outdoor common garden at the University of Copenhagen nursery. Seedlings from the same provenance subgroup were grouped within trays, initially arranged as 3 × 4 plants per tray. Each block in the garden contained at least nine Italian subgroups (from the three provenances), forming an incomplete randomized block design with 9 trays in each of 20 incomplete blocks. Replication of Italian provenances ranged from 9 to 15 trays, while Danish provenances were replicated in two blocks using 3 and 4 trays containing 12 seedlings each. Some plant mortality occurred after transplanting, which disrupted the original design prior to measurement. The layout of the experiment as of September 2018 is shown in Supplementary Figure 3. Design imbalances caused by mortality were adjusted for using REML analysis (Butler et al., 2018), with statistical model details provided in the relevant analysis section.

For this experiment, a subset of plant material was chosen, including two Italian provenances, Aspromonte and Sila Grande, each with two subgroups based on altitude: Aspromonte (1270 and 1900 m a.s.l.) and Sila Grande (1300 and 1900 m a.s.l.). Danish plant material included

seedlings from two seed stands: F13 – Stenderup Midtskov and F419 – Holstenshuus. The geographic coordinates of all provenances and the location of the experimental site are listed in Table 3 together with bioclimatic data associated with the provenance origins, taken from WorldClim version 2.1 for the period 1970–2000 (Fick and Hijmans, 2017).

Primary measurements, chlorophyll *a* fluorescence (ChlF) and gas exchange (GE), were taken between September 10 and 14, 2018, marking the end of the seedlings' second growing season in the common garden. Precipitation levels were adequate at the end of August 2018, and the weather during the measurement period was mostly overcast with intermittent rainfall. There were no visible signs of stress in the trees during data collection.

Location	A1270	A1900	SG1300	SG1900	DK-F13	DK-F419	C-G CPH
Altitude [m.a.s.l.]	1270	1900	1300	1900	20	80	8
Latitude (WGS84)	38.11225	38.16074	39.24688	39.28361	55.48083	55.10828	55.68615
Longitude (WGS84)	15.83665	15.91953	16.55135	16.45029	9.6505	10.30975	12.54405
Annual Mean Temperature [°C]	10.2	7.8	9.8	6.6	7.7	8	8.5
Mean Temperature of Warmest Quarter [°C]	17.8	15.6	17.3	14.1	15.2	15.4	16.6
Mean Temperature of Coldest Quarter [°C]	3.4	1	3	-0.2	0.5	0.9	1
Annual Precipitation [mm]	821	849	874	860	722	654	622
Precipitation of Wettest Month [mm]	112	113	121	113	81	71	67
Precipitation of Driest Month [mm]	20	22	22	25	39	37	34

Table 3: Characteristics of locations of origin and the common garden experimental plot in Copenhagen (C-G CPH), where the experiment was conducted. Published in Provazník et al. (2024).

4.2.2 Chlorophyll Fluorescence Kinetics

Chlorophyll *a* fluorescence (ChlF) kinetics were assessed using the FluorPen FP110 device (Photon Systems Instruments, Brno, Czech Republic). Measurements were conducted on all

320 surviving seedlings representing the six provenance subgroups (see Table 4). The ChlF induction curve (OJIP) was recorded following dark adaptation, achieved by placing detachable leaf clips on the leaves approximately 20 minutes prior to measurement. Once the FluorPen was attached to the leaf clip, a saturating blue light pulse (470 nm) with an intensity of 3000 μmol m^{-2} s^{-1} was applied. The rapid fluorescence response was recorded within the first second after exposure. OJIP parameters were computed using FluorPen software based on the method described by Strasser et al. (2010). Additional parameters related to the I–P phase were derived from raw fluorescence data following the approach outlined by Oukarroum et al. (2009). A full list of measured and calculated fluorescence parameters is provided in Table 5.

Provenance	Count 2018	Survival 2018	Count 2020	Survival 2020
A1270	41	28%	40	28%
A1900	52	31%	48	29%
DK-F13	20	56%	17	47%
DK-F419	29	60%	28	58%
SG1300	53	49%	52	48%
SG1900	125	69%	59	NA

Table 4: Seedlings count and survival rate at the end of the vegetation season in 2018 and 2020. The survival rate for SG1900 cannot be calculated because not all seedlings from this provenance subgroup were replanted into the new permanent site in 2019 due to a higher seedling count in relation to other provenances. Published in Provazník et al. (2024).

F_0	Minimal fluorescence intensity from a dark-adapted leaf (50 μs)
F_j	Fluorescence intensity at J-step (at 2 ms)
F_i	Fluorescence intensity at I-step (at 30 ms)
F_m	Maximal fluorescence intensity; PSI, photosystem I; PSII, photosystem II; RC, reaction center
F_v	Maximal variable fluorescence $F_v = F_m - F_0$
V_J	Relative variable fluorescence intensity at J-step $V_J = (F_j - F_0) / (F_m - F_0)$
V_I	Relative variable fluorescence intensity at I-step $V_I = (F_i - F_0) / (F_m - F_0)$
t_{Fm}	Time to reach F_m (in ms)
F_m/F_0	Ratio of maximal and minimal fluorescence intensity
M_0	Approximated initial slope of the fluorescence transient $M_0 = 4\ (F_{300} - F_0) / (F_m - F_0)$
S_M	S_M = Area / $(F_m - F_0)$ (multiple turn-over)
F_v/F_m (φ_{P0})	The maximum quantum yield of primary photochemistry. $F_v/F_m = \varphi_{P0} = 1\text{-}F_0 / F_m$
ψ_0	The probability that a photon trapped by the PSII reaction center will enter the electron transport chain. $\psi_0 = 1 - V_J$
φ_{E0}	$\varphi_{E0} = (1\text{-}(F_0 / F_m)) * \psi_0$
φ_{D0}	$\varphi_{D0} = F_0 / F_m$
φ_{Pav}	$\varphi_{Pav} = \varphi_{P0}\ (S_M / t_{Fm})$
ABS/RC	Average absorbed photon flux per PSII RC (apparent antenna size of an active PSII) $(M_0 / V_J)\ (1 / Fv / Fm)$
TR_0/RC	Maximum trapped exciton flux per PSII RC. $TR_0/RC = M_0 / V_J$
ET_0/RC	Electron-transport flux from Q_A to Q_B per PSII RC. $ET_0/RC = (M_0 / V_J)\ 1 - V_J$
DI_0/RC	Dissipated energy flux per RC. $DI_0/RC = (ABS / RC) – (TR_0 / RC)$
δ_{R0}	Efficiency with which an electron can move from the reduced intersystem electron acceptors to the PSI end electron acceptors. $\delta_{R0} = (1–V_I) / (1–V_J)$
φ_{R0}	Quantum yield of reduction of end acceptors of PSI. $\varphi_{R0} = \varphi_{P0} * \psi_0 * \delta_{R0}$
PI_{ABS}	Multi-parameter photosynthetic performance index expressing energy conservation from absorption of light by an antenna. $PI_{ABS} = [(V_J / M_0) * (Fv / Fm)] * (Fv / Fo) * [(1\text{-}V_J) / V_J]$
PI_{TOTAL}	Performance index for energy conservation from photons absorbed by PSII antenna until the reduction of PSI acceptors. $PI_{TOTAL} = PI_{ABS} \cdot \delta_{R0} / (1 – \delta_{R0})$
ΔV_{IP}	Decrease of the relative contribution of the I-P phase. $\Delta V_{IP} = 1–V_I = (F_m–F_i)/(F_m–F_0)$

Table 5: List of ChlF parameters and their formulas. The parameters used in the analyses are in bold letters. Published in Provazník et al. (2024).

4.2.3 Gas Exchange

Gas exchange (GE) measurements, reflecting net photosynthetic activity, were carried out on a subset of 84 randomly selected seedlings spanning all six provenance subgroups: A1270 (14 individuals), A1900 (17), SG1300 (19), SG1900 (19), DK-F13 (7), and DK-F419 (8). Measurements were performed using the LI-6400XT gas exchange system (LI-COR Biosciences, Nebraska, USA) equipped with a 6400-02B LED light source, which provided consistent and uniform illumination within the chamber. Leaf samples were taken from the upper canopy region of each seedling. The chamber temperature was adjusted to match ambient outdoor conditions, and the reference CO_2 concentration was maintained at 415 µmol m^{-2} s^{-1}. A light response curve was generated by exposing leaves to a decreasing sequence of light intensities: 1500, 1000, 500, 250, 120, 60, 40, 20, 10, and 0 µmol m^{-2} s^{-1}.

Net photosynthesis rates were plotted against the corresponding light intensities and fitted using the equation proposed by Prado and De Moraes (1997) for woody species:

$$P_N = \{P_{gmax}[1 - exp(-k(I - I_{comp})]\} - R_D,$$

where P_N represents the net photosynthetic rate [µmol(CO_2) m^{-2} s^{-1}], P_{gmax} is the maximum gross photosynthesis rate, k is the curve-fitting constant, I is the photosynthetic photon flux density, I_{comp} is the light compensation point, and R_D is the dark respiration rate. Model constants were optimized by minimizing residual sum of squares using the Solver function in Microsoft Excel, following the procedure outlined by Lobo et al. (2013). The final gas exchange parameters used in subsequent analysis are summarized in Table 6.

P_N	net assimilation of CO_2 [µmol.m^{-2}.s^{-1}]
LCP	light compensation point [µmol (photons) m^{-2}.s^{-1}]
LSP_{95}	light saturation point for $P_N + R_D$ equal to 95% of P_{Nmax} [µmol (photons) m^{-2}.s^{-1}]
R_D	dark respiration rate [µmol (CO_2) m^{-2}.s^{-1}]
ϕ_{I0}	quantum yield at I = 0 µmol(photon) m^{-2}.s^{-1} [µmol (CO_2) μmol^{-1} (photons)]

Table 6: List of GE parameters. Parameters in bold were later used for further analyses. Published in Provazník et al. (2024).

4.2.4 Bud Flushing

Bud flushing was assessed twice during the experiment period. The first evaluation occurred in May 2018, marking the start of the seedlings' second growing season. A second assessment was conducted in April 2020 at a permanent forest site near the original common garden, where

the seedlings had been replanted in 2019. The initial flushing evaluation included only the Italian provenances, while the second assessment in 2020 covered all provenance groups. A total of 361 seedlings were scored in the first assessment and 247 in the second. Bud flushing was evaluated using a 7-point scale based on the system described by (Robson et al., 2013):

1. Dormant buds
2. Buds swollen and elongated
3. First green visible from bud scales, buds adopt a silver-grey sheen
4. First folded hairy leaves visible but remain partially held by the bud
5. Entire leaves cascade from the bud; the leaves are still folded and flaccid
6. Leaves unfolded but still corrugated, fan-shaped and hairy
7. Leaves fully unfolded, smooth, and flat

4.2.5 Senescence Scores

Leaf senescence was evaluated in early November 2020 for all 244 seedlings located at the permanent experimental site. The assessment used a 10-point visual scoring scale (ranging from 0 to 9) based on the condition of the majority of leaves on each individual. A score of 0 indicated fully green leaves with no visible senescence symptoms; scores from 1 to 4 denoted increasing degrees of yellowing; scores from 4 to 8 reflected progressive development of necrosis; and a score of 9 corresponded to completely dry and dead foliage.

4.2.6 Statistical Analyses

Statistical analyses were performed using R software (R Core Team, 2014). To evaluate the photosynthetic traits, a linear mixed model (LMM) was applied with the following structure:

$$Y = \mu + Xa + Z_1 S_i + Z_2 S_i{:}\, S_j + e,$$

In this model, Y represents the response variable; μ is the overall mean; X is the incidence matrix corresponding to the fixed effect; a denotes the fixed effect of individual provenance; Z_1 and Z_2 are incidence matrices for random effects; S_i is the random effect of block; S_j is the random effect of box nested within block; and e is the residual error term, assumed to follow a normal and independent distribution. Model fitting was conducted using the ASReml-R package (Butler et al., 2018). Outliers, typically ranging from 0 to 10 per trait and attributed to measurement errors, were removed after model fitting. Pairwise comparisons of GE and ChlF parameters were performed using custom R scripts based on the least significant difference (LSD) method, with no adjustment for multiple testing.

To assess the fixed effect of country of origin, the fixed term *a* in the model was redefined to represent pooled Danish vs. Italian provenances. Wald tests (W-values) were used to evaluate this effect across all measured traits.

4.3 Methodology for Experiment 3 – Scots Pine Provenances - Seedlings

4.3.1 Plant Material

The plant material used in this experiment consisted of Scots pine (*Pinus sylvestris L.*) container seedlings originating from eight European provenances listed in Table 7. The provenances were assigned to three geographical groups corresponding to European regions with similar climatic conditions. The seedlings were grown for one season in low-humified *Sphagnum* peat in hard plastic containers (trays) (Plantek PL81F, 81 cells per tray, cell volume 85 cm^3) on raised metal pallets at Natural Resources Institute Finland Suonenjoki nursery (62° 39´N, 27°03'E). The seeds were sown on May 21, 2024, and grown in a greenhouse until the end of July, after which they were moved outdoors. The seedlings were irrigated and fertilized according to standard nursery practice. The provenances were assigned to three geographical groups corresponding to European regions with similar climatic conditions. Half of the seedlings from each seed lot from the Central-Eastern and Southern regions were short-day treated (September 17 to 27; 14 h night length).

The total number of seedlings was 4366, grown in 57 trays (81 seedlings each). Since provenances were not mixed in trays, one tray is considered an experimental unit in this experiment. The trays were moved and had no permanent spot. The hyperspectral images of the seedlings were taken on the 21st of October 2024.

Provenance	Group	Number of trays	Number of seedlings
Finland - Patasalo	North (N)	8	616
Norway - Romedal	North (N)	8	646
Czechia - Děčín	Central-East (C-E)	4	251
Romania - Cozia	Central-East (C-E)	8	641
Romania - Tulnici	Central-East (C-E)	8	619
Switzerland - Maienfeld	South (S)	8	647
Italy - Monte Duro	South (S)	6	425
Spain - Pirineo Navarro	South (S)	7	521

Table 7: The provenance of the Pinus sylvestris seedling grown in the experiment.

4.3.2 HSI System Setup and Acquisition Parameters

The HSI system used in this experiment consisted of an Imec SNAPSCAN VNIR camera equipped with a Schneider Optics APO-Xenoplan 21-1071371 2.0/24mm Standard Anti Shading 1.3″ lens. Illumination was provided by ARRI ARRILITE 750 Plus lights (MAN, 220-250V, IP20), ensuring uniform lighting during imaging. Hyperspectral images were acquired using the HSI SNAPSCAN software (version 1.8.1.1). The white reference image was obtained by scanning the white reference target covering the entire frame under the same settings as the samples, with reflectance calibrated to 95%. The dark reference image was captured using the built-in mechanical shutter. The imaging system was configured to capture hyperspectral images of the Scots pine seedlings under controlled lighting conditions. The acquired images were in 2048x2048 spatial resolution with 150 bands ranging from 470 nm to 900 nm.

4.3.3 Image Processing

Spatial cropping was applied to the images using Spectronon software (Resonon, Bozeman, MT, USA), resulting in a total of 1993 samples cropping out the area on the edge of the images

not covered by the white reference correctly. Savitzky-Golay filtering with a window size of 19 and polynomial order of 2 was applied to smooth the hyperspectral data and reduce noise.

The processed images were loaded to Fiji (ImageJ) (Schindelin et al., 2012) using the MSTools plug-in to load the images in the software. Negative values resulting from hyperspectral data acquisition were saturated to zero to prevent erroneous data interpretation.

A Fiji (ImageJ) macro was created to automate hyperspectral image processing. The macro prompts the user to select a folder containing ENVI files, then scans the folder for files with the right filename extensions. It opens each valid file, using the MSTools plug-in, with the "use saturate" option to saturate negative values to zero to prevent erroneous data interpretation. The 95th slice of each image stack (corresponding to 741nm wavelength) is duplicated and scaled between -0.01 and 1.25. Automatic thresholding using the Shanbhag method segments the image, creating a binary mask that is converted to an 8-bit image. This mask is multiplied with the original image stack to isolate relevant portions, and the result is saved as a new file with background pixels having a NaN value.

The resulting images with NaN background were used for an average tray reflectance acquisition. Selection of all seedlings in a tray was created with the Freehand selections tool, as not all of the background was correctly replaced by NaN (mainly marking paper tape for tray placement at edges of the image and some weeds in trays containing fewer seedlings). Then the Plot Z-axis profile function was used to save the average reflectance data from the selection of all seedlings from a given tray into a data file.

Another macro was applied to replace NaN values with zeros across all image slices to make the images without background readable for the Spectronon software, in which the classification was done.

4.3.4 Image Classification

In the Spectronon software, the free-form pixel selection tool was used to select pixels for each class (background, green needles, red needles, dry needles, and buds) from all provenances (not all trays). Datacubes from these selections were created and appended together within a given class to create data cubes used for the supervised classification. In the batch processor, the Auto Classifier tool was selected, and the class data cubes were loaded for training. The *Auto Classifier* tool simplifies hyperspectral image classification by automatically performing

feature engineering with the concatenation of first derivatives to Savitsky-Golay smoothed spectra, dimensionality reduction via PCA, and classification using a Random Forest model, producing probability maps for each class. With the *Classification to Color Map* tool, the classified images were created, colors were adjusted to visualize the different classes, and they were exported as RGB images.

4.3.5 Macro for Bud Counting

A Fiji (ImageJ) macro was employed to process the preprocessed image files and selectively retain Regions of Interest (ROIs) based on specific morphological and spatial criteria. Images were converted to the HSB (Hue, Saturation, Brightness) color space and split into individual channels. Thresholding was applied to the Hue channel (169–171) to select only the blue pixels from the classified image. Binary masks were generated for each channel and combined using logical AND operations to create a final mask highlighting relevant areas. Particle analysis was then performed on the final mask to detect ROIs exceeding 50 pixels in size with circularity between 0.05 and 1.0. Detected ROIs were filtered by shape descriptors, retaining only those with solidity ≥ 0.4, roundness ≥ 0.4, and aspect ratio (AR) ≤ 2.3. Additionally, spatial filtering was applied to exclude ROIs located within 100 pixels of previously accepted centroids to prevent clustering. The macro reported the total number of accepted ROIs.

4.3.6 Partial Least Squares Discriminant Analysis (PLS-DA)

Partial Least Squares Discriminant Analysis (PLS-DA) is a classification technique derived from Partial Least Squares Regression (PLSR). It transforms the regression results of PLS into a set of latent variables, which can be used to predict the dependent variable (i.e., class membership). PLS-DA was employed to classify geographical groups within the dataset based on spectra or pixel counts in each class from the classified images. The analysis was performed using the Caret package (Kuhn, 2008) in R (R Core Team, 2014). The Caret package provides an accuracy of the PLS-DA model prediction and Cohen's Kappa coefficient (κ). κ is a metric that accounts for the agreement occurring by chance and provides a more robust measure compared to simple accuracy. κ is calculated as:

$$\kappa = \frac{p_o - p_e}{1 - p_e}$$

p_o is the observed agreement p_e is the expected agreement by chance, calculated based on the marginal probabilities of each class.

4.3.7 F-Score

To evaluate the segmentation accuracy and bud detection using the custom macro and classification data, three metrics were employed: precision (*p*), recall (*re*), and F-score (*F*). Precision (*p*) measures the accuracy of tree segmentation by calculating the ratio of true positives (*TP*) to the sum of true positives and false positives (*FP*), as described by the formula:

$$p = \frac{TP}{TP + FP}$$

Recall (*re*) quantifies the detection rate of trees by determining the ratio of true positives to the sum of true positives and false negatives (*FN*), expressed as:

$$re = \frac{TP}{TP + FN}$$

The F-score (*F*) provides an overall accuracy assessment by harmonically balancing precision and recall, calculated as:

$$F = \frac{2 \times p \times re}{p + re}$$

Here, TP represents the number of correctly detected trees, *FP* refers to the number of falsely detected trees, and *FN* denotes the number of missed trees. The precision metric reflects the accuracy of tree segmentation, recall indicates the detection rate, and the F-score represents the overall accuracy, accounting for both *FP* and *FN*.

The pipeline of the methods used is visualized in Fig. 5.

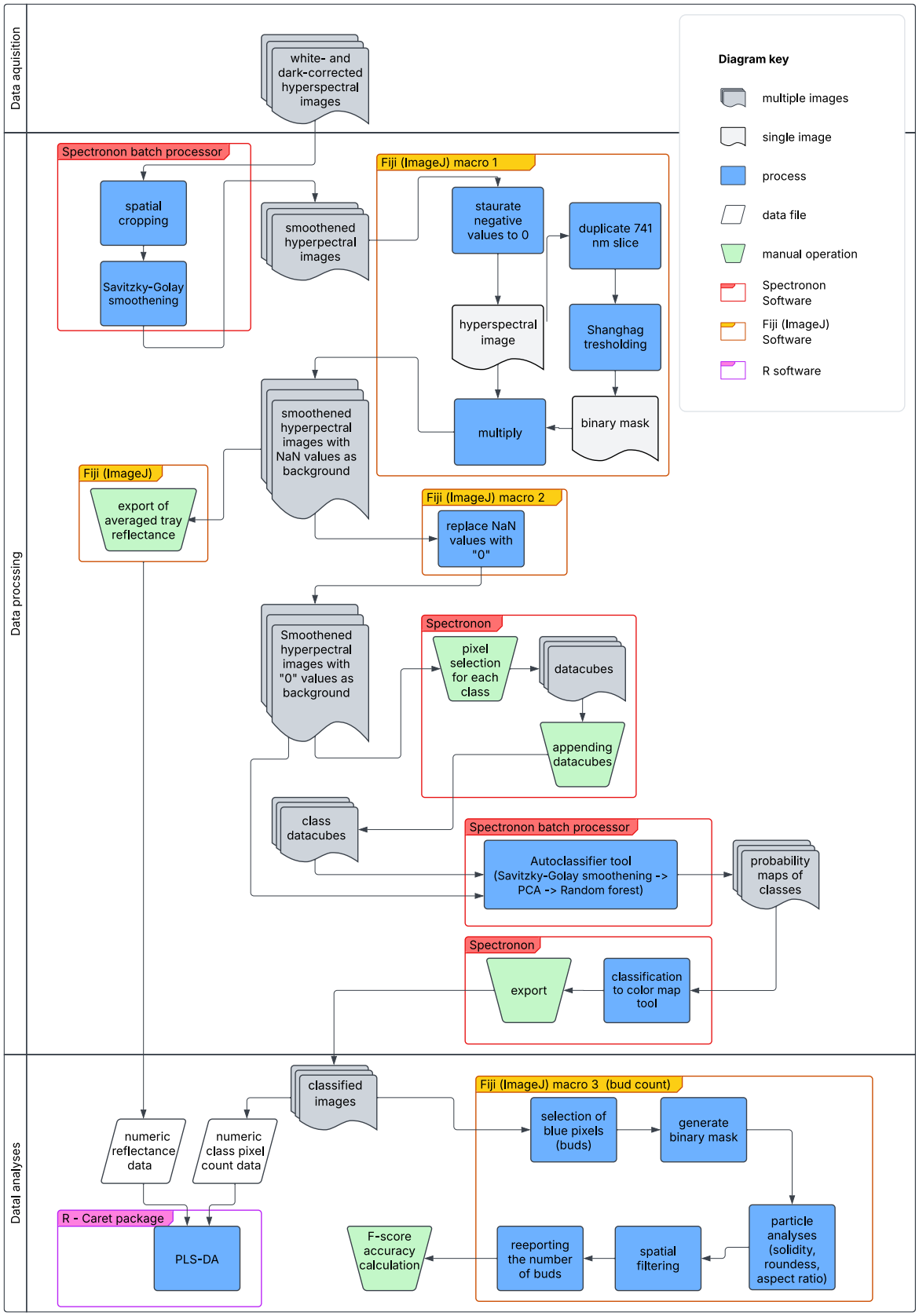

Figure 5: Flow diagram of the proposed pipeline.

4.4 Methodology for Experiment 4 – Black Alder Provenances

4.4.1 Plant Material

The plant material originated from open-pollinated (half-siblings) selected plus trees (trees with superior phenotype) from 12 Danish provenances of black alder (*Alnus glutinosa* L. Gaertn.), which are listed in Table 9 in bold together with abbreviations by which they are referred to. 10 provenances originated from natural stands, provenance RAV originated from a seed lot, and provenance TRUE originated from a stand that already originates from selected plus trees. The 12 provenances are shown in Fig. 6 in hollow shapes.

Experimental sites also contain additional Black Alder plant material from seven officially approved seed sources (two seed stands and five clonal seed orchards, including three Swedish seed orchards and one Swedish seed stand. This additional plant material does not have a recorded family structure and, therefore, is included only in provenance effect comparison. Details about the additional plant material are also presented in Table 9.

Full name	Abbrevation	Origin	Country
Draved Skov-Vest	**DRA**	**Natural stand**	**DK**
Dybvig Skov, Genner Bugt	**DY**	**Natural stand**	**DK**
Fussingø	**FUS**	**Natural stand**	**DK**
Hald Sø-Vestende	**HALD**	**Natural stand**	**DK**
Livø	**LIV**	**Natural stand**	**DK**
Lounkær	**LOU**	**Natural stand**	**DK**
Ravnholt, Sønderskov	**RAV**	**From seed lot**	**DK**
Runde Mølle ved Genner	**RU**	**Natural stand**	**DK**
Rydhave Skov	**RYD**	**Natural stand**	**DK**
Slette Å	**SLET**	**Natural stand**	**DK**
Slotsved Skov	**SLOT**	**Natural stand**	**DK**
True Skov	**TRUE**	**Stand of selected plus trees**	**DK**
FP. 658 Laugesen	FP658	Clonal seed orchard	DK
FP. 657 Tophøj	FP657	Clonal seed orchard	DK
F.840 Tusenæs	F840	Seed lot from F.2 Gråsten	DK
FP.850 Kollaberga	FP850	Clonal seed orchard (FP851 copy)	S
FP.852 Trolleholm	FP852	Clonal seed orchard	S
F.829 Skjoldenæsholm	F829	Seed lot from FP.851	DK
FP.851 Ignaberg	FP851	Clonal seed orchard	S

Table 8: Plant material origin. Provenances with family (half-siblings) structures are in bold, material without family structure (from seed stands and clonal seed orchards) is in normal font.

Four experimental plantations were established from the plant material: three seedling seed orchards (505, 506, and 507) and one combined provenance–progeny trial 504. Seedling seed orchards are foreseen as future seed sources when their fructification starts. However, they also serve as provenance–progeny trials. The experimental sites are shown in Fig. 6 in filled shapes. All sites were planted with the same genetic material to estimate genotype-by-environment interactions. Individual families (open-pollinated half-siblings) of different provenances are differentiated with a number added to the provenance abbreviation, e.g., SLOT1, SLOT2, etc. There are 4 to 10 families per provenance, depending on the experimental site. Each experimental site contains all provenances (except for DY at 504), but some families are not present at all sites. The four experimental sites differ substantially in soil conditions and water availability.

Provenance–progeny trial 504 Lounkær Forest (Eastern Jutland) is established on a typical alder site with high groundwater levels. The soil is classified as saltwater silt. Due to the abundance of natural alder in the neighboring forest, a seed orchard is not feasible in this location because of the high risk of external pollen contamination. It was established as a combined provenance-progeny trial with an experimental design slightly different from the other sites – family plots nested in provenance plots and blocks. The experimental design can be seen in Supplementary Figure 4.

Seedling seed orchard 505 Hanehøj Plantation (Eastern Jutland) is located on nutrient-poor, former conifer stand with soil classified as meltwater sand that quickly dries out. The seedling seed orchard is organized in single-tree plots in blocks. The experimental design can be seen in Supplementary Figure 5.

Seedling seed orchard 506 C.E. Flensborg Plantation (Central Jutland) is established on former agricultural land with soil classified as sandy till. The seedling seed orchard is organized in single-tree plots in blocks. The experimental design can be seen in Supplementary Figure 6.

Seedling seed orchard 507 Wendelholm (North Zealand) is planted on former agricultural land with soils classified as meltwater sand, similar to site 505. The seedling seed orchard is organized in single-tree plots in blocks. The experimental design can be seen in Supplementary Figure 7.

All trials and seedling seed orchards were established in spring 2022. Tree height was recorded before and after the growing seasons of 2022, 2023, and 2024 at 504 Lounkær Forest, 505 Hanehøj Plantation, and 507 Wendelholm, while measurements at 506 C.E. Flensborg Plantation were collected for the 2023 and 2024 growing seasons only.

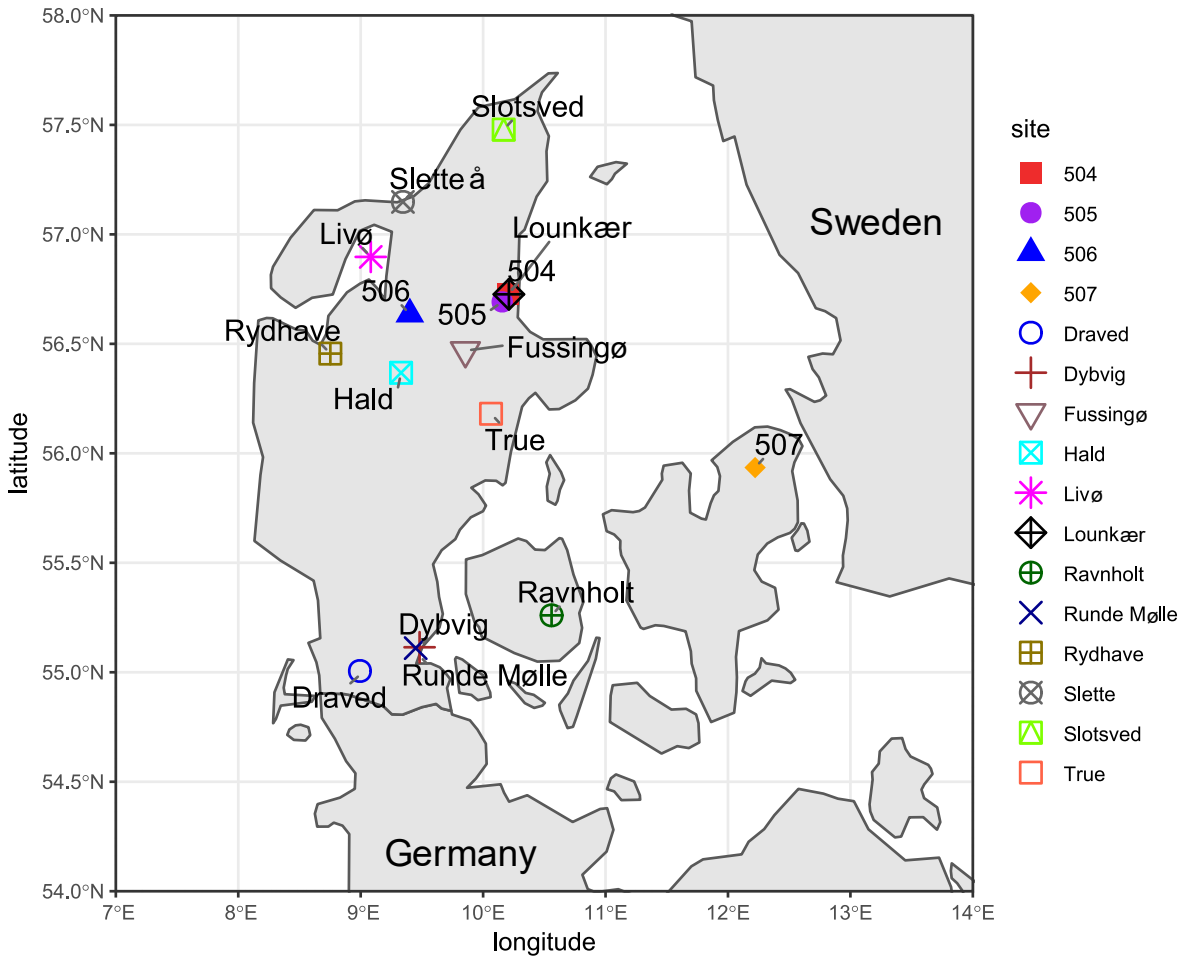

Figure 6: Map of trials and provenance origins. Clonal seed orchards and seed stands are not included.

4.4.2 Bud Burst

Bud burst was assessed 24th of April 2024 in the Seedling Seed Orchard 506 C.E. Flensborg Plantation as a maximum degree of bud burst of the individual. The developmental stage of each tree was scored on a scale from 0 to 9, where 0 represented trees in winter dormancy with no visible sprouting, and 9 indicated trees with fully developed leaves.

4.4.3 Precipitation

To further illustrate conditions on different experimental sites, monthly precipitation totals are presented in Fig. 7. Data were provided as hourly precipitation by the Danish Meteorological Institute (DMI), Open Data portal, licensed under CC BY 4.0. For sites 504 and 505 the data were collected from Havnø station (56°42'56.5"N 10°09'51.8" E) situated between the two experimental sites circa 2.5 km away from each. For site 506, the data were gathered from Års Syd station (56°45'20.9"N 9°30'24.1" E) located circa 15 km north of the site (Fig 2B). For the site 507, the data were obtained from Sjælsmark station (55°52'35.0"N 12°24'43.6" E) located 13.5 km south-east of 507.

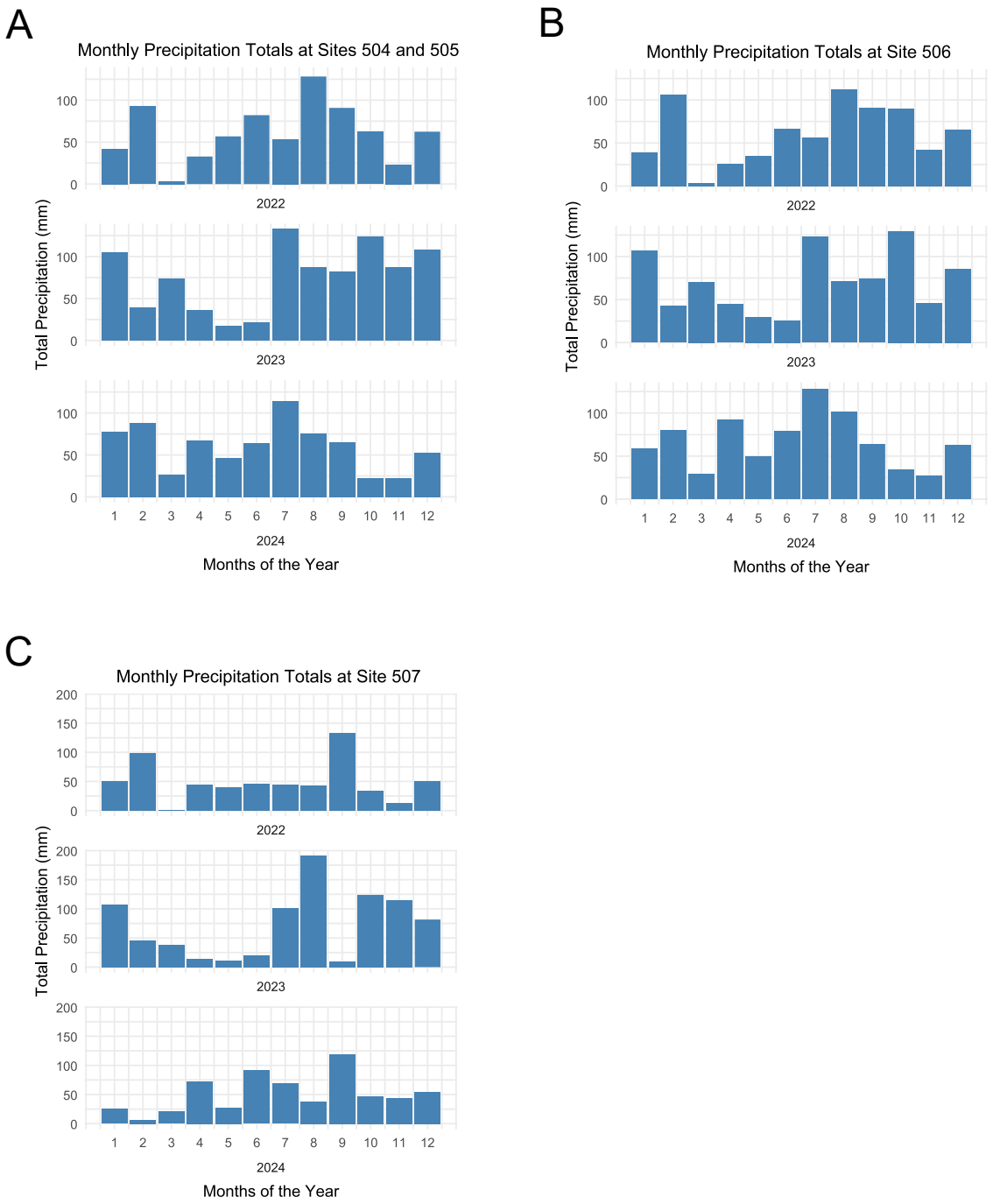

Figure 7: Total monthly precipitation at climate data stations nearest to the experimental sites. A: data from Havnø station situated between 504 and 505, B: data from Års Syd station located north of 506, and C: data from Sjælsmark station located south-east of 507. Hourly precipitation data is provided by the Danish Meteorological Institute (DMI), an open data portal licensed under CC BY 4.0.

4.4.4 Hyperspectral Reflectance

To evaluate leaf-level reflectance, the FieldSpec 4 Wide-Res portable spectroradiometer (Malvern Panalytical Ltd., United Kingdom) equipped with a plant probe and leaf clip attachment (Malvern Panalytical Ltd., United Kingdom) was used. The plant probe contains an internal light source, enabling measurements across the 350–2500 nm spectral range. The spectroradiometer is fitted with three sensors covering 350–1000 nm (spectral resolution 3 nm), 1000–1800 nm (8 nm), and 1800–2500 nm (8 nm).

Calibration was performed every 15 minutes using the Gore-Tex white PTFE reflector background incorporated into the leaf clip.. Leaf reflectance was measured directly in the field on living trees by inserting leaves into the leaf clip to ensure full coverage of the measurement window. The scan average was set to 25. Reflectance was calculated as the ratio between the radiance measured from the sample and that of the white reference panel. Three leaves per plant were measured. The reflectance measurements were made only at 504, 505, and 507 in spring and autumn of 2023 for a subset of 10 provenances, each comprising 4 families of 6 individuals (240 trees). The specific measurement days were 24th-27th of May for spring, and 20th-23rd of September for autumn.

4.4.5 Statistical Analysis

Single-Site Models

A linear mixed model (LMM) for single sites (505, 506, and 507) was fitted using the ASReml-R package (Butler et al., 2017), and is specified as follows

$$y = X\beta + Zu + e,$$

where y is the vector of phenotypic observations, β is a vector of fixed effects including the overall mean, provenance, and block, and u is a vector of random effects. The random effects included family, row within block, column within block, and individual units, such that

$$u \sim N(0, G),$$

with *G* a block-diagonal covariance matrix corresponding to the specified random terms. The residual term **e** was modeled using a two-dimensional first-order autoregressive process to account for spatial correlation among neighboring trees within each trial. Specifically,

$$e \sim N(0, R),$$

where R represents the residual variance–covariance structure defined as:

$$R = \sigma_{\xi}^2[AR1(p_{\text{col}}) \otimes AR1(p_{\text{row}})] + \sigma_{\eta}^2 I$$

Here, σ_{ξ}^2 denotes the variance associated with spatially correlated residuals, and σ_{η}^2 represents the variance of independent (nugget) residuals. $AR1(p_{\text{col}})$and $AR1(p_{\text{row}})$ are first-order autoregressive correlation matrices describing the correlation between observations in the column and row directions, respectively, and **I** is the identity matrix. The Kronecker product ($\otimes$) combines the two one-dimensional autoregressive processes into a two-dimensional spatial structure (Dutkowski et al., 2002). This specification captures spatial dependence among residuals arising from local environmental heterogeneity or micro-site effects within each experimental block. Missing values were retained in both response and explanatory variables and handled directly within the ASReml-R estimation procedure.

For site 504, the model specification differed by including additional random terms due to a different design: family effects within provenance plots nested in blocks and provenance plot effects nested in blocks, in addition to the family, unit, and residual spatial effects described above.

Obvious outliers were identified and removed after visual inspection of diagnostic plots from the fitted model.

Narrow-sense heritability (h^2) was calculated as

$$h^2 = \frac{\sigma_a^2}{\sigma_p^2},$$

where σ_a^2 is the additive genetic variance, and σ_p^2 is the total phenotypic variance estimated from the mixed model described above. Heritability values range from 0 to 1, where a value of 0 indicates that phenotypic variation is entirely due to environmental or non-additive effects, and a value of 1 indicates that all phenotypic variation is explained by additive genetic differences.

Predicted values were obtained using the *predict.asreml* function in *ASReml-R*, with *family* and *provenance* specified as classification factors. This produced best linear unbiased predictions (BLUPs) that were adjusted for the best linear unbiased estimate (BLUE) of the fixed provenance effect for each relevant family–provenance combination derived from the fitted

mixed model. The prediction table was extracted from the *$pvals* element of the prediction object for further analyses.

A genotype–environment biplot (Fig. 30) was generated using the *ASRtriala* package, with families as units and site-year combinations as vectors, using height increment as the response. Predicted values (BLUPs) for each family–provenance combination, obtained as described above using the *predict.asreml* function in *ASReml-R*, were used in this analysis. Only families present at all sites were retained, and relevant columns were converted to factors while site and year columns were removed. The first two principal components were plotted with standardization applied, and both family and vector labels were displayed to facilitate visualization of *genotype* × *environment* interactions across sites and years.

The BLUEs of provenances, including those from the seed stand and clonal seed orchard material, were used to establish provenance rankings, enabling comparison between them, as the provenance effect was highly significant.

Multi-environment trial analyses

A multi-environment linear mixed model (MELMM) was fitted using the ASReml-R package (Butler et al., 2017) to analyze data across sites. The model was specified as

$$y = X\beta + Zu + e$$

where y is the vector of phenotypic observations, β is a vector of fixed effects including site and provenance within site, and u is a vector of random effects. The random effects included: family within site, block within site, and individual units within site.

The residual term **e** was modeled with a site-specific two-dimensional spatial structure to account for autocorrelation among neighboring trees within each trial. Specifically,

$$\mathrm{e} \sim N(0, \mathrm{R}),$$

where R represents a block-diagonal residual variance–covariance matrix defined as

$$R = dsum\left(\sigma^2_{\xi_{S_i}}[AR1(pcol) \otimes AR1(prow)] + \sigma^2_{\eta_{S_i}} \mid site\ i\right).$$

Here, $\sigma^2_{\xi_{S_i}}$ denotes the variance of spatially correlated residuals at site i, $\sigma^2_{\eta_{S_i}}$ the variance of independent (nugget) residuals, $AR1(p_{\mathrm{col}})$and $AR1(p_{\mathrm{row}})$the first-order autoregressive correlation matrices in the column and row directions, respectively, and **I**the identity matrix.

The Kronecker product (⊗) combines the two one-dimensional autoregressive processes into a two-dimensional spatial structure (Dutkowski et al., 2002). This formulation allows for site-specific residual variances and correlations, effectively capturing local environmental heterogeneity within each experimental site.

Type-B genetic correlations were estimated by modeling additive genetic effects as a site-specific, correlated random effect. The vector of additive genetic effects u was partitioned by site and assumed to follow a structured multivariate normal distribution, $\boldsymbol{u} \sim N(\mathbf{0}, \mathbf{G})$, where the genetic covariance matrix $G$is

$$G = \begin{bmatrix} \sigma^2_{aS_1} & \sigma_{aS_1S_2} \\ \sigma_{aS_1S_2} & \sigma^2_{aS_2} \end{bmatrix} \otimes K.$$

Here, $\sigma^2_{aS_1}$and $\sigma^2_{aS_2}$are the additive genetic variances specific to sites 1 and 2, $\sigma_{aS_1S_2}$is the between-site additive genetic covariance, and $K$is the pedigree-relationship matrix. The type-B genetic correlation was then computed as:

$$r_B = \frac{\sigma_{aS_1S_2}}{\sqrt{\sigma^2_{aS_1}\,\sigma^2_{aS_2}}},$$

which quantifies the consistency of genetic expression across environments (values near 1 indicating low G×E interaction). Significance of the covariance component, and thus of the type-B correlation, was evaluated using a likelihood-ratio test (LRT) by comparing the full model with a reduced model in which $\sigma_{aS_1S_2}$was fixed to zero. Missing values were retained in both response and explanatory variables and handled directly within the ASReml-R estimation procedure.

Age-to-age analyses

The same multi-environment linear mixed model was used for repeated measures, replacing site with season to perform age-to-age analyses. Fixed effects included season and provenance within season, while random effects accounted for family within season, block within season, and individual units within season. Residuals were modeled with a season-specific two-dimensional spatial structure, analogous to the site-specific structure described above, to account for spatial autocorrelation among neighboring trees within each season. In this formulation, genotype-by-environment interaction was modeled in the same way as in the multi-site analysis, with season treated as the environmental factor, allowing the estimation of

age-to-age genetic correlations through a season-specific genetic variance–covariance structure. Age-to-age correlations were tested using a likelihood ratio test (LRT), which compares the final model with a baseline model where the tested parameters are fixed to zero.

5 Results

5.1 Results of Experiment 1 – Scots Pine Clones – Seed Orchard

5.1.1 Genetic Variation in Needle Functional Traits

The broad-sense heritability (H^2) of needle functional traits (NFTs) was estimated using clonal replications from both seed orchards sampled in 2021. Traits were divided into two groups: (1) photosynthetic pigment-related traits (chl a, chl b, car, chl T, car:chl T; Table 10) and (2) structural and water-related traits (NL, NWC, LMA, EWT; Table 11).

At Nepomuk, pigment-related traits expressed on a mass basis showed moderate heritability values: 0.14 for chlorophyll a, 0.15 for chlorophyll b, 0.14 for carotenoids, and 0.12 for total chlorophyll. Area-based heritability values were slightly higher for most traits, with the exception of chl a. The highest heritability among pigment traits was observed for the carotenoid-to-total chlorophyll ratio (car:chl T), reaching 0.29. In contrast, at Plasy, H^2 values for most pigment traits were lower or not statistically significant, but car:chl T again showed the highest value (0.25).

When data from both sites were pooled, heritability estimates remained moderate overall, with consistently higher values for area-based traits compared to mass-based traits. The highest H^2 across all pigment traits was again found for car:chl T (0.26). A very high type B genetic correlation (0.99) between the two sites for this trait indicates strong and stable genetic control. Pooling the data also reduced the standard errors of the heritability estimates, on average by 0.02.

Structural and water-related traits showed higher heritability than pigment-related traits. Across both sites, the highest H^2 was estimated for NL (0.29, SE = 0.07), while the highest single-site value was observed for needle water content (NWC) at Plasy (H^2 = 0.38, SE = 0.10). Type B genetic correlations were significant for all structural traits except NL, reaching 0.99 for LMA and EWT and 0.72 for NWC. These high values indicate minimal genotype-by-environment interaction and stable expression of structural traits across sites (Table 11).

	chl a_M [mg/g]	chl b_M [mg/g]	chl T_M [mg/g]	car_M [mg/g]	chl a_A [µg/cm^2]	chl b_A [µg/cm^2]	chl T_A [µg/cm^2]	car_A [µg/cm^2]	car:chl T
H^2 Plasy (SE)	0.13 (0.09)	NS	NS	NS	0.12 (0.08)	NS	0.10 (0.08)	0.11 (0.08)	0.25 (0.08)
H^2 Nepomuk (SE)	0.14 (0.07)	0.15 (0.07)	0.12 (0.07)	0.14 (0.07)	0.13 (0.07)	0.22 (0.08)	0.16 (0.08)	0.19 (0.08)	0.29 (0.09)
H^2 both sites (SE)	0.14 (0.06)	0.13 (0.05)	0.11 (0.05)	0.12 (0.05)	0.13 (0.05)	0.17 (0.06)	0.14 (0.06)	0.16 (0.06)	0.26 (0.07)
type B gen. corr. (SE)	NS	NS	NS	NS	NS	NS	NS	NS	0.99 (NA)

Table 9: Broad-sense heritability (H^2), standard errors (SE), and type B genetic correlations (a measure of GxE) across sites in 2021 of pigment-related NFTs. NS = non-significant. Chl a – chlorophyll a, chl b – chlorophyll b, chl T – total chlorophyll a+b, car – total carotenoids, car:chl T – ratio of total carotenoids to total chlorophyll. Concentrations of photosynthetic pigments are related to dry weight marked with an $_M$ lower index [mg/g] (first four columns on the left) and to needle area projection marked with an $_A$ lower index [µg/cm^2] (following four columns to the right). Published in Provazník et al. (2025).

	NL	LMA	NWC	EWT
H^2 Plasy (SE)	0.35 (0.10)	0.21 (0.09)	0.38 (0.10)	0.15 (0.09)
H^2 Nepomuk (SE)	0.24 (0.09)	NS	0.15 (0.07)	0.23 (0.09)
H^2 both sites (SE)	0.29 (0.07)	0.14 (0.05)	0.28 (0.07)	0.20 (0.06)
type B gen. corr. (SE)	NS	0.99 (NA)	0.72 (0.24)	0.99 (NA)

Table 10: Broad-sense heritability (H^2), standard errors (SE), and type B genetic correlations across sites in 2021 of structural and water-related NFTs. NL – needle length, LMA – Leaf Mass per Area, NWC – needle water content, EWT - Equivalent Water Thickness, NS – non-significant. Published in Provazník et al. (2025).

5.1.2 Spectral Reflectance

The broad-sense heritability (H^2) was estimated for each wavelength across the spectral range of 350–2500 nm at the needle level and 429–919 nm at the canopy level. In 2021, needle-level reflectance was analyzed for clones present at both Nepomuk and Plasy orchards. A lower sample size at Plasy in 2021 resulted in slightly higher standard errors, which is reflected in the wider error bars at this site (Fig. 8A) compared to those at Nepomuk (Fig. 8B).

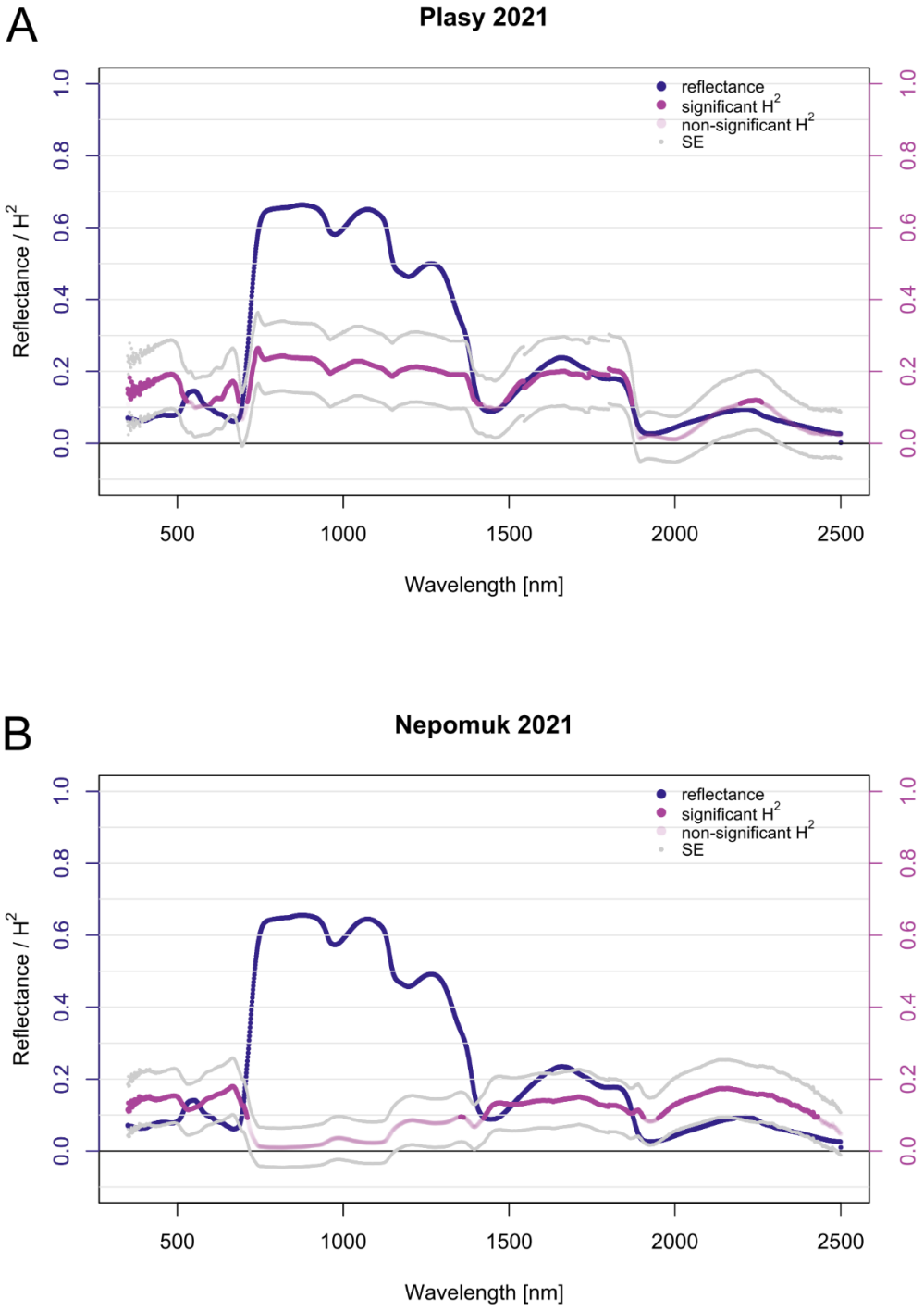

Figure 8: Estimated broad-sense heritability (H^2) with standard errors (SE) for needle-level spectra, shown alongside the mean needle-level reflectance of all clones at the Plasy (A) and Nepomuk (B) sites in 2021. Published in Provaznik et al. (2025).

At both Nepomuk and Plasy in 2021, broad-sense heritability (H^2) of needle-level reflectance across individual wavelengths ranged from 0.10 to 0.25, with Plasy generally exhibiting slightly higher values. Significant H^2 estimates were observed across the VIS, NIR, and SWIR regions, although most NIR wavelengths at Nepomuk did not exceed the significance threshold ($\alpha = 0.05$).

For the canopy-level analysis, all clones and their replications were included in the UAV campaigns at both sites. The smaller size of the Nepomuk orchard and the lower number of clones and ramets (Supplementary Figure 2) resulted in a higher standard error for heritability estimates (Fig. 9C). Heritability remained significant across the full analyzed spectral range (429–919 nm) at the canopy level (Fig. 9).

In the VIS region, H^2 values were typically higher between 429 and 500 nm and lower around 520 nm, particularly at Plasy in 2021. While the heritability patterns at Plasy 2020 and Nepomuk 2021 were relatively flat with consistently higher values, Plasy 2021 displayed a more distinct spectral trend that closely resembled the needle-level reflectance heritability pattern.

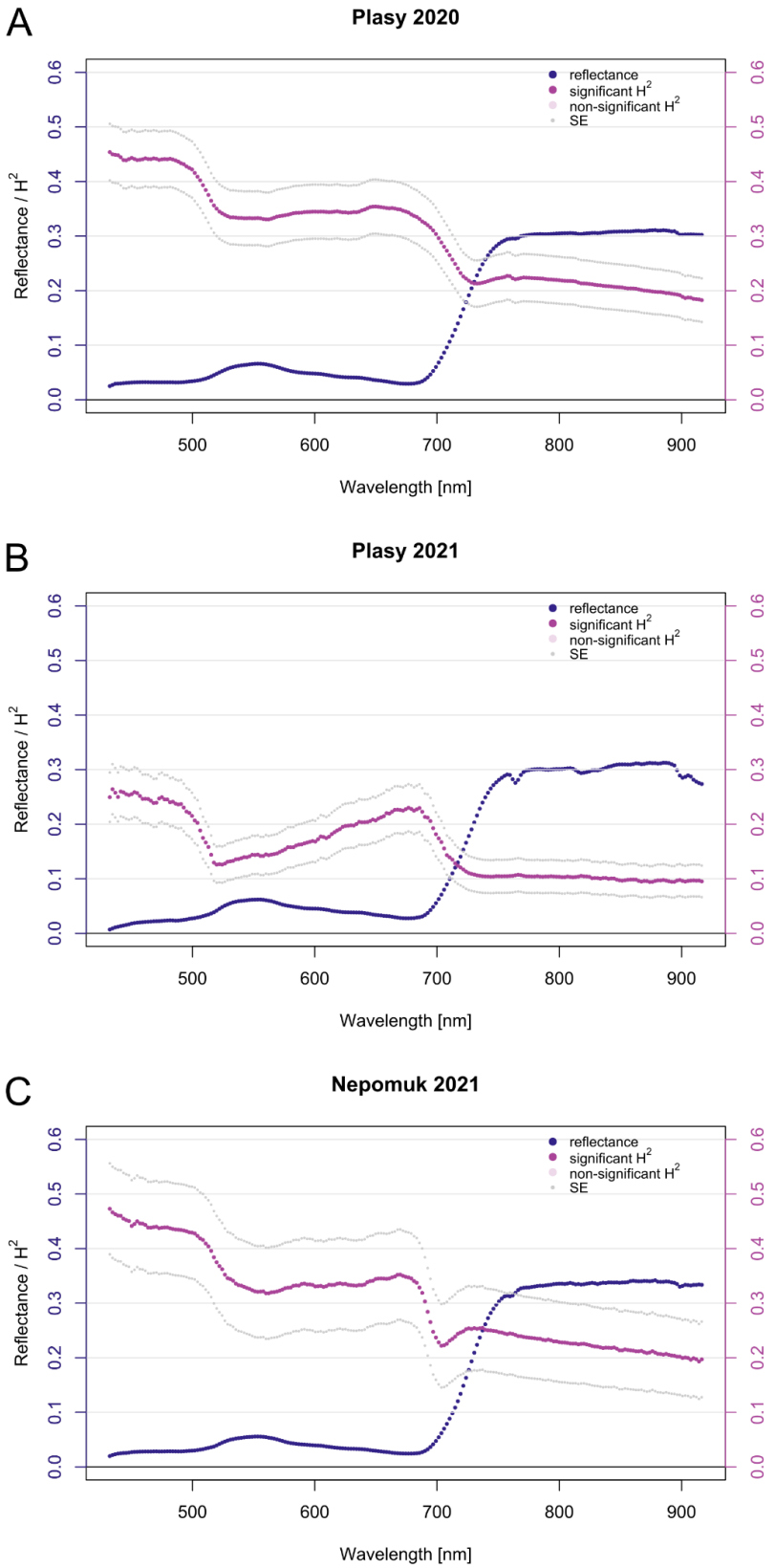

Figure 9: Estimated broad-sense heritability (H^2) with standard errors (SE) for canopy-level spectra, shown alongside the mean canopy-level reflectance of all clones at Plasy 2020 (A), Plasy 2021 (B), and Nepomuk 2021 (C). Published in Provaznik et al. (2025).

5.1.3 Year-to-Year Genetic Correlations of Canopy-Level Reflectance

Spectral data at the canopy level were collected at Plasy in 2020 and 2021, allowing for a detailed assessment of year-to-year genetic correlations across the spectral range captured by the hyperspectral sensor. The substantial sample size and replicated clonal structure at this site provided a robust basis for these analyses.

Significant positive genetic correlations were observed primarily in the VIS region, with correlation values gradually decreasing with increasing wavelength, from 0.93 at 450 nm to 0.59 at 690 nm (Fig. 10A). At 450 nm (Fig. 10B), clonal rankings based on BLUP-estimated genetic values remained highly consistent across years, reflecting strong genetic stability and aligning with the highest year-to-year genetic correlation. In contrast, at 690 nm (Fig. 10C), the genetic correlation reached its minimum (0.59), corresponding to more pronounced shifts in clonal ranking between years.

Following this minimum in the red edge region, genetic correlation values increased again, forming a local peak of 0.73. Across the NIR region, year-to-year genetic correlations remained stable at approximately 0.68. However, this level of correlation was insufficient to maintain stable clonal rankings over time (Fig. 10D).

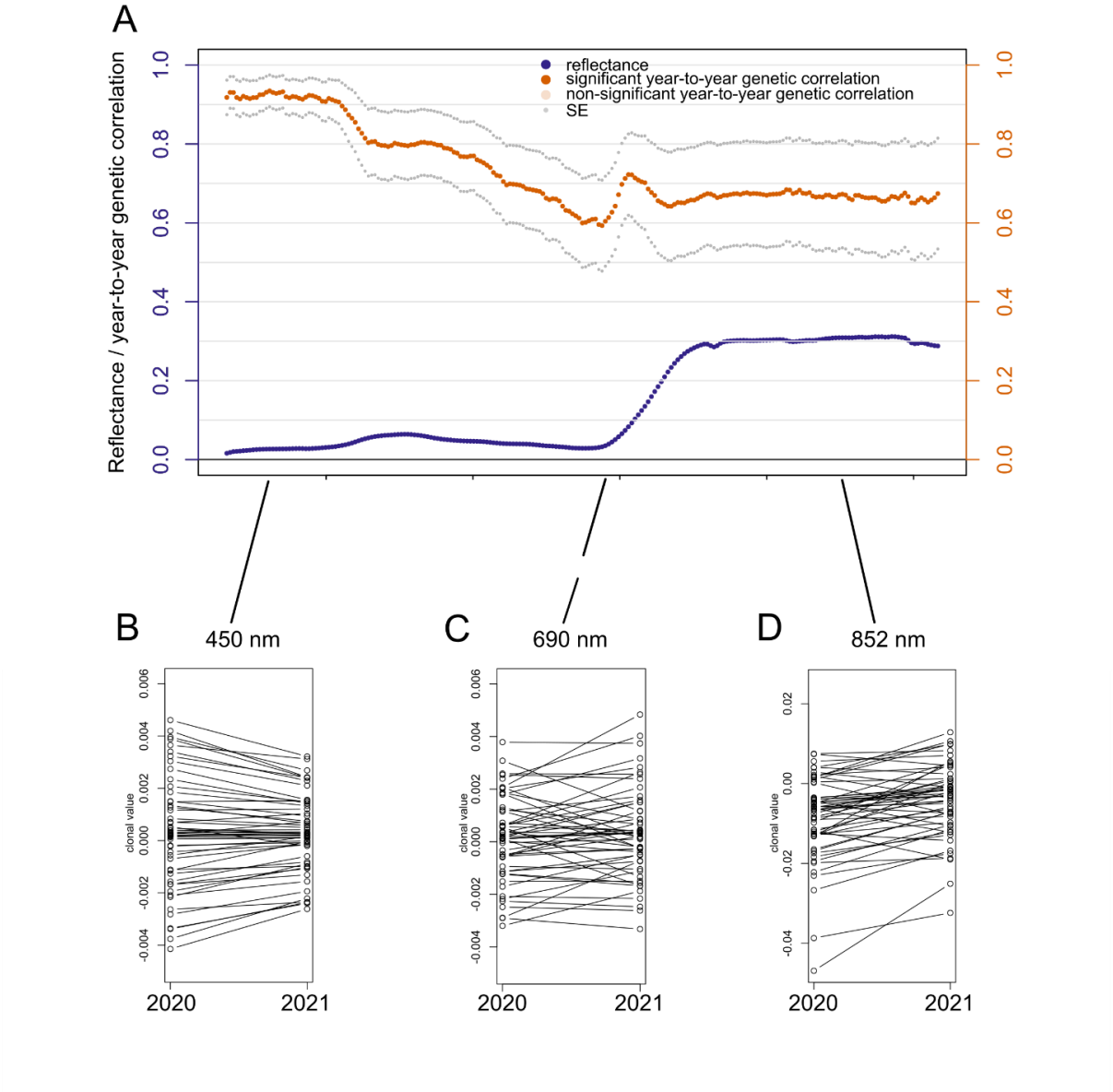

Figure 10: Year-to-year genetic correlations with standard errors (SE) estimated at Plasy between 2020 and 2021 are shown in panel A, alongside the mean canopy-level reflectance of all clones in these 2 years. Panels B, C, and D display the stability of clonal values, representing the predicted genetic component of spectral reflectance, for three representative wavelengths (450, 690, and 852 nm) across the two years. These wavelengths (e.g., from VIS, red edge, and NIR regions) were selected to illustrate typical patterns of clonal ranking consistency and variability across the spectral range. Published in Provazník et al. (2025).

5.1.4 Genotype-by-Environment Interaction in Needle- and Canopy-Level Reflectance

Type B genetic correlations of hyperspectral reflectance at both the needle and canopy levels across Nepomuk and Plasy in 2021 were estimated to assess G×E interactions.

At the canopy level, significant positive type B genetic correlations were observed across the VIS region, ranging from 0.72 to 0.99, indicating small to negligible G×E effects (Fig. 11A). Clonal rankings remained highly consistent across sites at wavelengths 533 nm and 697 nm, where the correlations were highest (Fig. 11B, 11C). The strongest correlation was observed at 697 nm, corresponding to the most stable clonal ranking across environments (Fig. 11C). In contrast, in the NIR region, type B genetic correlations declined to zero or negative values, indicating considerable G×E interactions. This was evident at 852 nm, where clonal rankings diverged between sites and certain genotypes performed well in one environment but not in the other (Fig. 11D).

At the needle level, similar strong type B genetic correlations were found in the VIS region, again followed by a sharp decrease to zero and negative values in the NIR (Fig. 11F). A distinct pattern was also observed in the SWIR region, where type B genetic correlations reached one (though statistically insignificant) around major water absorption bands at 1440 nm, 1900 nm, and 2500 nm. At 1440 nm, clonal rankings were consistent across sites, but the variance between Nepomuk and Plasy differed, indicating heterogeneous genetic variance despite stable rank order (Fig. 11E).

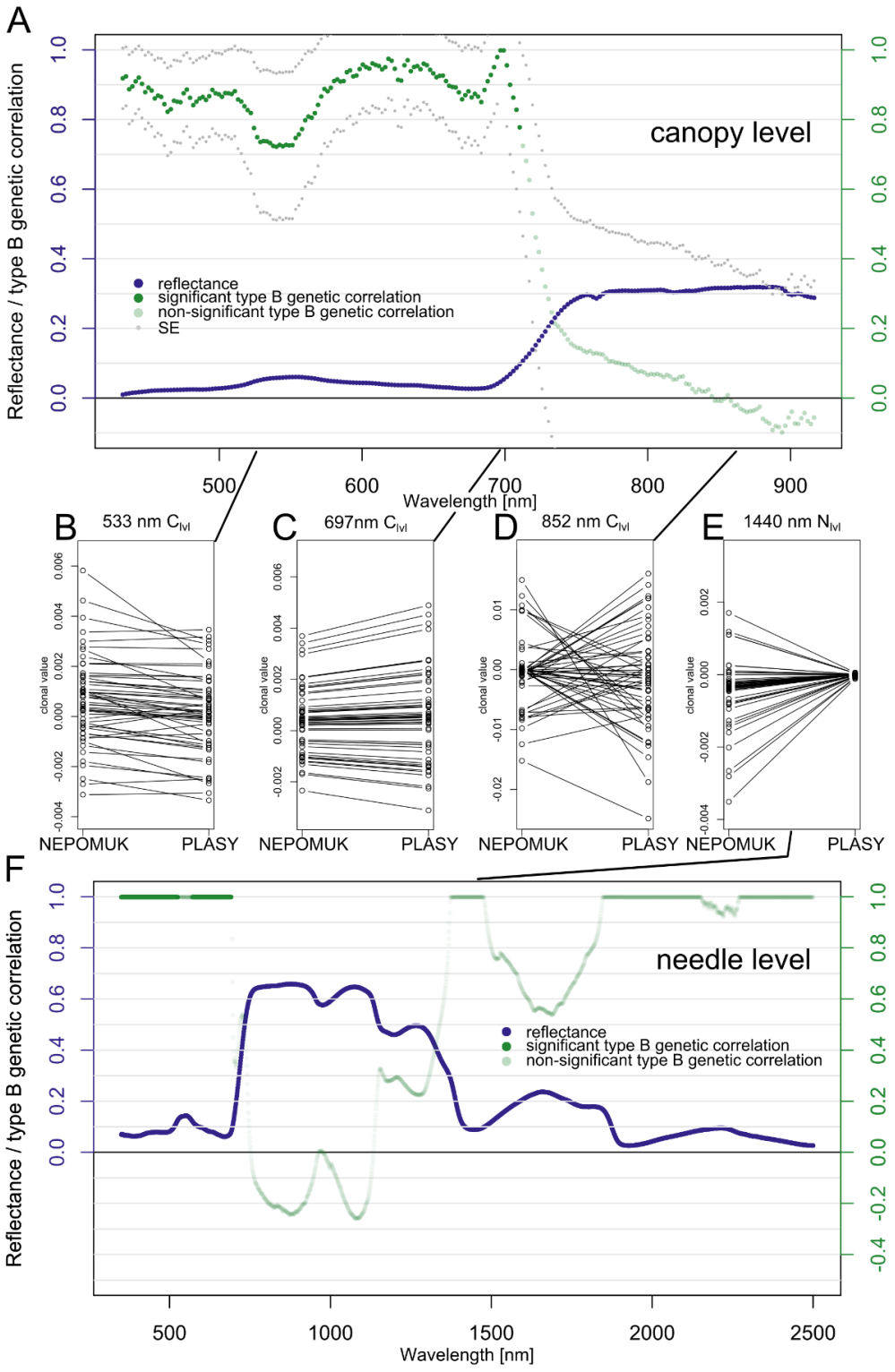

Figure 11: Type B genetic correlation between Plasy 2021 and Nepomuk 2021 as a proxy for GxE interaction in canopy-level (A) and needle-level (F) reflectance. The reflectance plotted is the mean of all clones across the sites. Panels B, C, D, and E illustrate the stability of clonal ranking for representative wavelengths (533, 697, 852, 1440 nm) across the environment. For needle-level reflectance, SE was not estimated in VIS, where the type B genetic correlation was significant because the model converged at a boundary. The SE in regions with insignificant type B genetic correlations was high and is not visualized. Published in Provazník et al. (2025).

5.1.5 Genetic Correlations Among the Spectra and NFTs

Type A genetic correlations describe the genetic association between two traits, offering insight into their shared biological pathways and potential causal relationships. These correlations between needle- and canopy-level reflectance and both photosynthetic pigment content and structural or water-related needle traits were estimated in Experiment 1.

At the needle level, significant genetic correlations were detected between reflectance and all analyzed photosynthetic pigments (Fig. 12). Pigment traits expressed on a dry mass basis showed strong, significant, positive correlations in the SWIR region. In contrast, pigment traits expressed on a needle area basis exhibited strong, significant, negative correlations in the red edge region. The carotenoid-to-total chlorophyll ratio (car:chl T) did not show significant genetic correlations with reflectance across the needle-level spectral range (350–2500 nm).

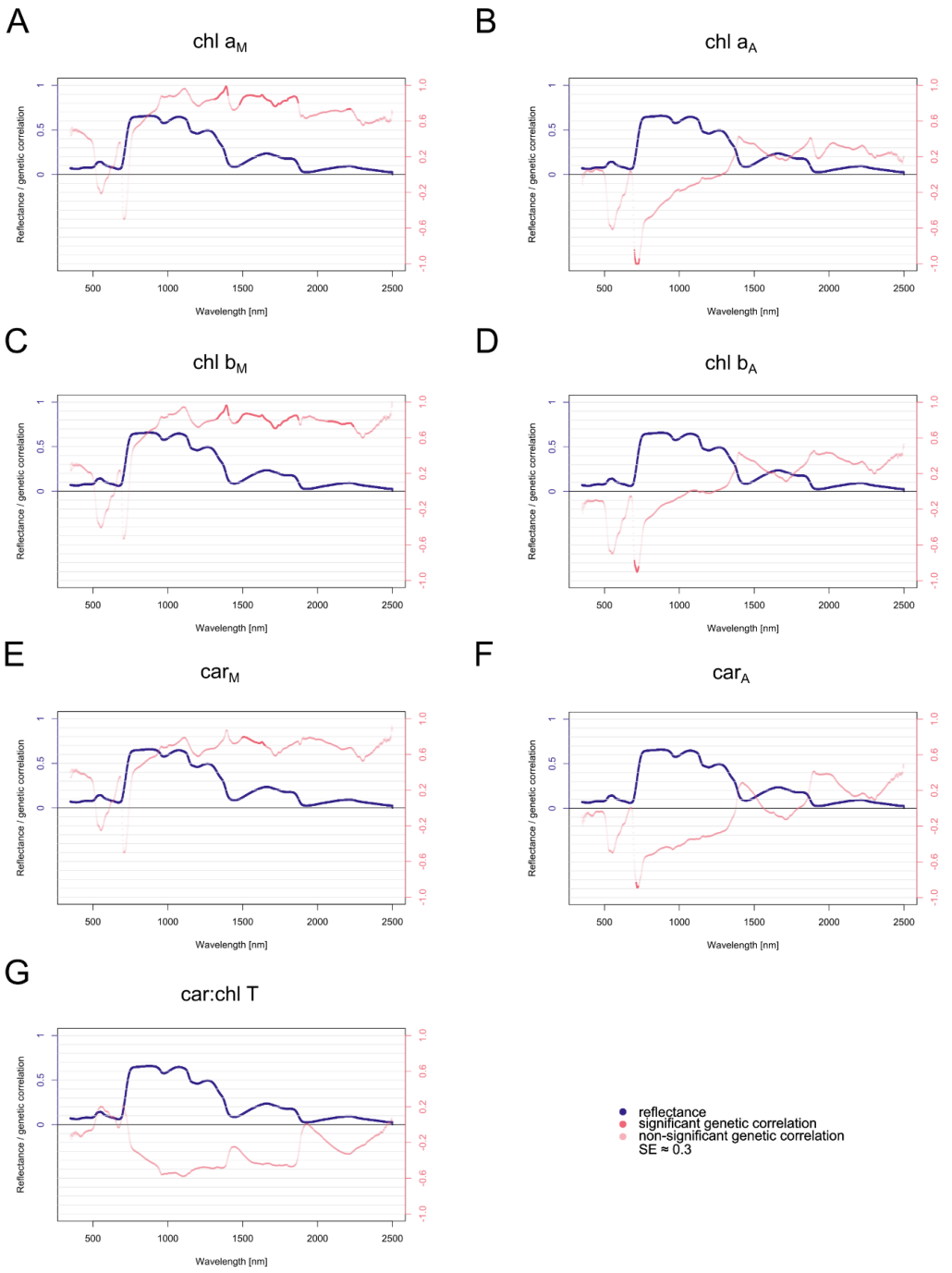

Figure 12: Genetic correlations between needle-level reflectance spectra and photosynthetic pigments estimated from pooled data (Plasy 2021, Nepomuk 2021). Chl a – chlorophyll a, chl b – chlorophyll b, car – total carotenoids, car:chl T – ratio of total carotenoids to total chlorophyll. Concentrations of photosynthetic pigments are related to dry weight marked with an $_M$ lower index [mg/g] and to needle area projection marked with an $_A$ lower index [µg/cm^2]. The standard error of genetic correlation reached the average value of 0.3 (not shown). The significance of the genetic correlation was expressed by shades of pink. The reflectance plotted is the mean of all clones across the sites. Published in Provazník et al. (2025).

Leaf mass per area (LMA) showed strong, significant, negative genetic correlations with needle-level reflectance in the NIR and at the beginning of the SWIR region (Fig. 13). Needle water content (NWC) exhibited significant, strong, positive correlations in the NIR, while equivalent water thickness (EWT) displayed significant, strong, negative correlations in the later part of the NIR and at the beginning of the SWIR region (Fig. 13). In contrast, needle length (NL) showed no significant genetic correlations with reflectance across the analyzed spectral range (Fig. 13).

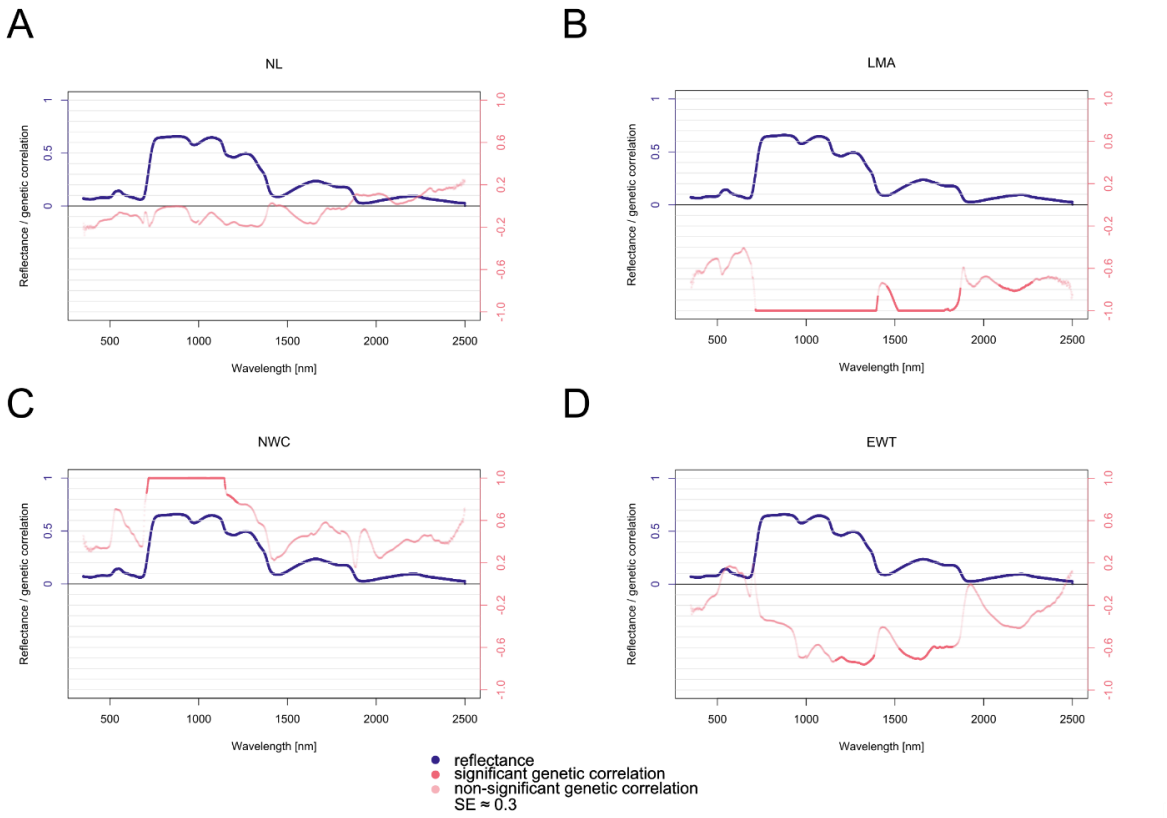

Figure 13: Genetic correlations between needle-level reflectance spectra and needle structural and water-related traits estimated from pooled data (Plasy 2021, Nepomuk 2021). NL – needle length, LMA – Leaf Mass per Area, NWC – needle water content, EWT - Equivalent Water Thickness. The standard error reached the average value of 0.3 around the genetic correlation value (not shown). The significance of the genetic correlation was expressed by shades of pink. The reflectance plotted is the mean of all clones across the sites. Published in Provazník et al. (2025).

At the canopy level, significant genetic correlations were observed only with total chlorophyll content expressed on a mass basis (chl T_M) and equivalent water thickness (EWT) (Fig. 14A, 14B). Chl T_M exhibited a strong negative genetic correlation in the red edge region (around 720 nm) and in the adjacent NIR wavebands, reaching –0.99. Because the model reached the boundary, standard errors could not be estimated for these correlations.

EWT showed a positive genetic correlation at the green reflectance peak (around 540 nm) in the VIS spectrum and across most of the NIR region, with values around 0.9 and standard errors ranging from 0.23 to 0.30. For comparison, leaf mass per area (LMA) exhibited a similar correlation pattern to EWT, but the values dropped to zero in the NIR region and did not reach statistical significance (results not shown).

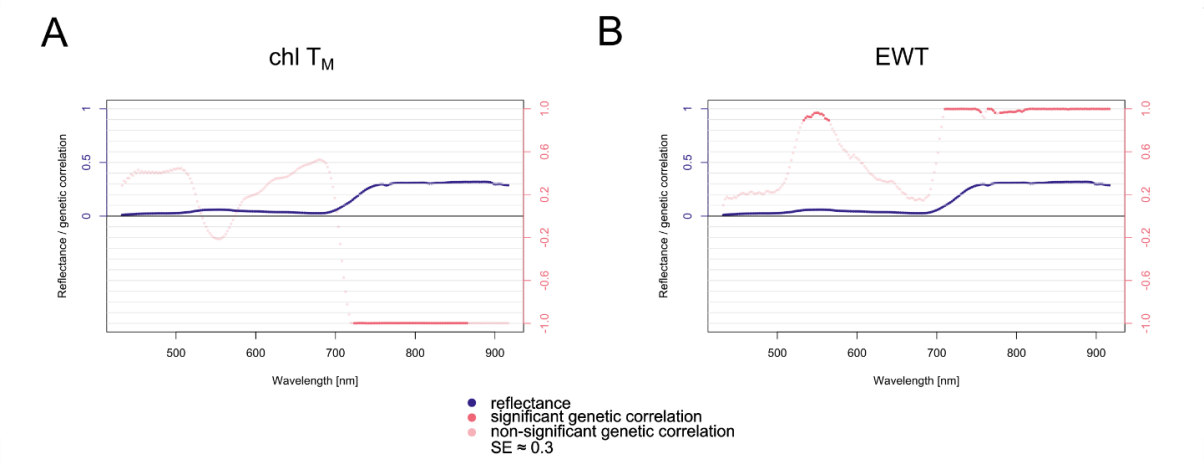

Figure 14: Genetic correlations between canopy-level reflectance spectra and needle functional traits (NFTs) estimated from pooled data (Plasy 2021, Nepomuk 2021). chl T_M – total chlorophyll a+b (related to dry weight [mg/g]), EWT – Equivalent Water Thickness. The standard error (SE) reached the average value of 0.3 around the genetic correlation value (not shown). The significance of the genetic correlation was expressed by shades of pink. The reflectance plotted is the mean of all clones across the sites. Published in Provazník et al. (2025).

5.2 Results of Experiment 2 – European Beech Provenances

5.2.1 Photosynthetic Performance

The Italian provenances exhibited significantly higher average values than the Danish provenances for most chlorophyll fluorescence (ChlF) parameters: F_m/F_0 ($W = 1.55 \times 10^{-6}$), F_v/F_m ($W = 3.93 \times 10^{-7}$), ψ_0 ($W = 1.53 \times 10^{-5}$), φ_{E0} ($W = 7.27 \times 10^{-8}$), δ_{R0} ($W = 0.001$), φ_{R0} ($W = 2.76 \times 10^{-7}$), PI_{ABS} ($W = 5.16 \times 10^{-8}$), PI_{TOTAL} ($W = 6.58 \times 10^{-7}$), and ΔV_{IP} ($W = 3.75 \times 10^{-6}$). Conversely, the Italian provenances showed significantly lower average values than the Danish provenances for φ_{D0} ($W = 3.76 \times 10^{-7}$), ABS/RC ($W = 4.24 \times 10^{-7}$), TR_0/RC ($W = 1.47 \times 10^{-5}$), and DI_0/RC ($W = 8.81 \times 10^{-9}$). No significant differences were detected for ET_0/RC ($W = 0.721$) or φPav ($W = 0.259$). Model-predicted means of ChlF parameters for each provenance subgroup are summarized in Table 12.

	A1270	A1900	DK-F13	DK-F419	SG1300	SG1900
F_m/F_0	4.765 (0.113)	5.065 (0.104)	3.921 (0.194)	4.528 (0.234)	4.804 (0.114)	4.976 (0.092)
F_v/F_m (φ_{P0})	0.786 (0.005)	0.801 (0.005)	0.742 (0.009)	0.778 (0.011)	0.789 (0.005)	0.797 (0.004)
ψ_0	0.600 (0.012)	0.625 (0.011)	0.534 (0.020)	0.547 (0.024)	0.602 (0.011)	0.614 (0.009)
φ_{E0}	0.472 (0.011)	0.501 (0.010)	0.384 (0.019)	0.427 (0.022)	0.474 (0.011)	0.490 (0.087)
φ_{D0}	0.214 (0.005)	0.199 (0.005)	0.258 (0.009)	0.222 (0.011)	0.211 (0.005)	0.202 (0.004)
φ_{Pav}	937.1 (2.010)	934.6 (1.813)	941.1 (3.578)	935.7 (3.767)	937.6 (2.020)	932.0 (1.464)
ABS/RC	1.508 (0.034)	1.457 (0.031)	1.842 (0.060)	1.638 (0.068)	1.557 (0.034)	1.493 (0.026)
TR_0/RC	1.196 (0.226)	1.165 (0.021)	1.393 (0.041)	1.272 (0.043)	1.228 (0.023)	1.190 (0.018)
ET_0/RC	0.701 (0.019)	0.726 (0.018)	0.738 (0.033)	0.690 (0.039)	0.739 (0.020)	0.729 (0.016)
DI_0/RC	0.325 (0.014)	0.292 (0.013)	0.474 (0.025)	0.364 (0.029)	0.330 (0.014)	0.303 (0.011)
δ_{R0}	0.558 (0.010)	0.565 (0.009)	0.506 (0.017)	0.504 (0.016)	0.533 (0.010)	0.577 (0.008)
φ_{R0}	0.258 (0.009)	0.282 (0.008)	0.194 (0.015)	0.214 (0.018)	0.256 (0.009)	0.282 (0.007)
PI_{ABS}	4.039 (0.316)	4.838 (0.294)	1.461 (0.546)	2.465 (0.661)	3.985 (0.324)	4.507 (0.259)
PI_{TOTAL}	5.073 (0.495)	6.464 (0.460)	1.597 (0.854)	2.538 (1.028)	4.905 (0.510)	6.228 (0.405)
ΔV_{IP}	0.333 (0.010)	0.353 (0.009)	0.271 (0.017)	0.275 (0.019)	0.325 (0.010)	0.354 (0.008)

Table 11: Predicted means of ChlF parameters with standard errors (SE) of each provenance subgroup (based on LMM). Published in Provaznik et al. (2024).

In terms of gas exchange (GE) traits, the Italian provenances displayed significantly higher average values for LSP_{95} ($W = 7.90 \times 10^{-8}$) and P_N ($W = 2.64 \times 10^{-5}$), indicating that under identical irradiation, Italian provenances reached their maximum assimilation rate more rapidly and achieved a higher net assimilation compared to Danish provenances. No significant differences were observed for the light compensation point (LCP) ($W = 0.764$) or dark respiration (R_D) ($W = 0.309$). All provenances required a similar photon flux density to achieve net positive carbon assimilation. Additionally, no differences were detected in the quantum

yield of photosynthesis (ϕ_{I0}) (W = 0.701), suggesting that the molar ratio between assimilated carbon and absorbed photons did not differ between provenance groups. Model-predicted means of GE parameters for each provenance subgroup are presented in Table 13.

	A1270	**A1900**	**DK-F13**	**DK-F419**	**SG1300**	**SG1900**
LCP [µmol (photons) $m^{-2}.s^{-1}$]	6.648 (0.51)	6.332 (0.48)	6.316 (0.87)	5.438 (1.33)	6.256 (0.48)	6.062 (0.47)
R_D [µmol (CO_2) $m^{-2}.s^{-1}$]	0.134 (0.033)	0.164 (0.032)	0.100 (0.055)	0.101 (0.077)	0.150 (0.034)	0.104 (0.031)
LSP_{95} [µmol (photons) $m^{-2}.s^{-1}$]	**685.9 (30.2)**	**683.4 (27.7)**	**373.2 (47.4)**	**423.6 (46.1)**	**587.6 (26.7)**	**598.8 (26.3)**
P_N [µmol.$m^{-2}.s^{-1}$]	**14.06 (0.64)**	**13.67 (0.59)**	**7.61 (1.07)**	**8.67 (1.11)**	**12.21 (0.58)**	**12.05 (0.56)**
ϕ_{I0} [µmol (CO_2) µmol^{-1} (photons)]	0.063 (0.0016)	0.061 (0.0015)	0.061 (0.0024)	0.063 (0.0025)	0.063 (0.0015)	0.063 (0.0014)

Table 12: Predicted means of GE parameters with standard errors (SE) of each provenance subgroup (based on LMM). Provenance effects were significant (α = 0.05) for parameters shown in bold, later used for further analyses. Published in Provazník et al. (2024).

5.2.2 Provenance Pairwise Comparison

All provenance subgroup pairs were compared for both chlorophyll fluorescence (ChlF) and gas exchange (GE) parameters (Fig. 15). Clear differentiation between Italian and Danish provenances was evident across both measurement types.

Among the Italian provenances, several ChlF parameters, D_{I0}/RC, φ_{R0}, PI_{TOTAL}, and ΔV_{IP}, showed significant differences between subgroups originating from different altitudes (Fig. 15, pink). In contrast, GE parameters LSP_{95} and P_N distinguished between Italian provenances from different geographic locations (Aspromonte vs. Sila Grande; Fig. 15, gray and red). No clear altitudinal pattern was observed in the GE data, while ChlF measurements did not fully discriminate between geographically distant Italian provenances.

A different pattern emerged when comparing the two local Danish provenances. Here, seven ChlF parameters (F_m/F_0, F_v/F_m, φ_{E0}, φ_{D0}, ABS/RC, TR_0/RC, and DI_0/RC) were sufficient to distinguish between the two Danish subgroups (Fig. 15, light green), whereas GE parameters did not reveal any significant differences. Notably, the only parameter capable of differentiating both the altitudinal subgroups within the Italian provenances and the two Danish

provenances was D_{10}/RC (Fig. 15, pink and light green), highlighting its sensitivity to variation both within and between provenance groups.

Figure 15: Heatmap of LSD test p-values comparing all pairs of provenance subgroups based on ChlF and GE parameters (without correction for multiple testing) (based on LMM). Published in Provazník et al. (2024).

5.2.3 Bud Flushing

In May 2018, significant differences in bud flushing scores were observed between provenances from the two mountain ranges, Sila Grande (SG) and Aspromonte (A) ($p = 1.92 \times 10^{-15}$). The more southern Aspromonte provenance exhibited more advanced bud development at the time of assessment. Within the Sila Grande provenance, a clear altitudinal effect was detected, with SG1900 showing significantly less developed buds than SG1300 ($p = 2.87 \times 10^{-14}$). No significant differences were observed between altitudinal subgroups within Aspromonte. Detailed pairwise comparisons for May 2018 are provided in Table 14, and the distribution of flushing scores illustrating these differences is shown in Fig. 16A.

The flushing assessment conducted in April 2020 on the surviving trees revealed the same overall pattern (Fig. 16B). Although the trees were at an earlier flushing stage during this later assessment, differences between provenances and their subgroups remained significant for the same pairs, except for SG1300 and A1270 (Table 14). The overall difference between Aspromonte and Sila Grande persisted clearly (Fig. 16, red vs. green).

In 2020, bud flushing was also evaluated for the Danish provenances. Both Danish provenances were in a more advanced flushing stage than the Italian ones, except for SG1300, which exhibited a delayed flushing pattern more similar to the Danish beech. The statistical significance of all pairwise comparisons is presented in Table 14.

Year	2018	2020
Compared pair	**p-value**	**p-value**
SG x A	**1.92e-15**	**0.0009**
I x DK	**-**	**5.316e-07**
SG1300 x SG1900	**8.80e-13**	**6.197e-07**
SG1300 x A1270	**0.0107**	0.9836
SG1300 x A1900	0.4440	0.5887
SG1900 x A1900	**4.46e-14**	**7.547e-07**
SG1900 x A1270	**2.87e-14**	**0.0001**
A1270 x A1900	0.0503	0.6287
DK-F13 x A1270	-	**0.0014**
DK-F13 x A1900	-	**0.0001**
DK-F13 x SG1300	-	**9.407e-05**
DK-F13 x SG1900	-	0.1598
DK-F419 x A1270	-	**0.0002**
DK-F419 x A1900	-	**4.09e-06**
DK-F419 x SG1300	-	**2.706e-06**
DK-F419 x SG1900	-	0.1615
DK-F13 x DK-F419	-	0.7061

Table 13: Two-sided Wilcoxon signed-rank test of flushing scores between pairs of provenances and provenance subgroups scored in May 2018 and April 2020. Published in Provazník et al. (2024).

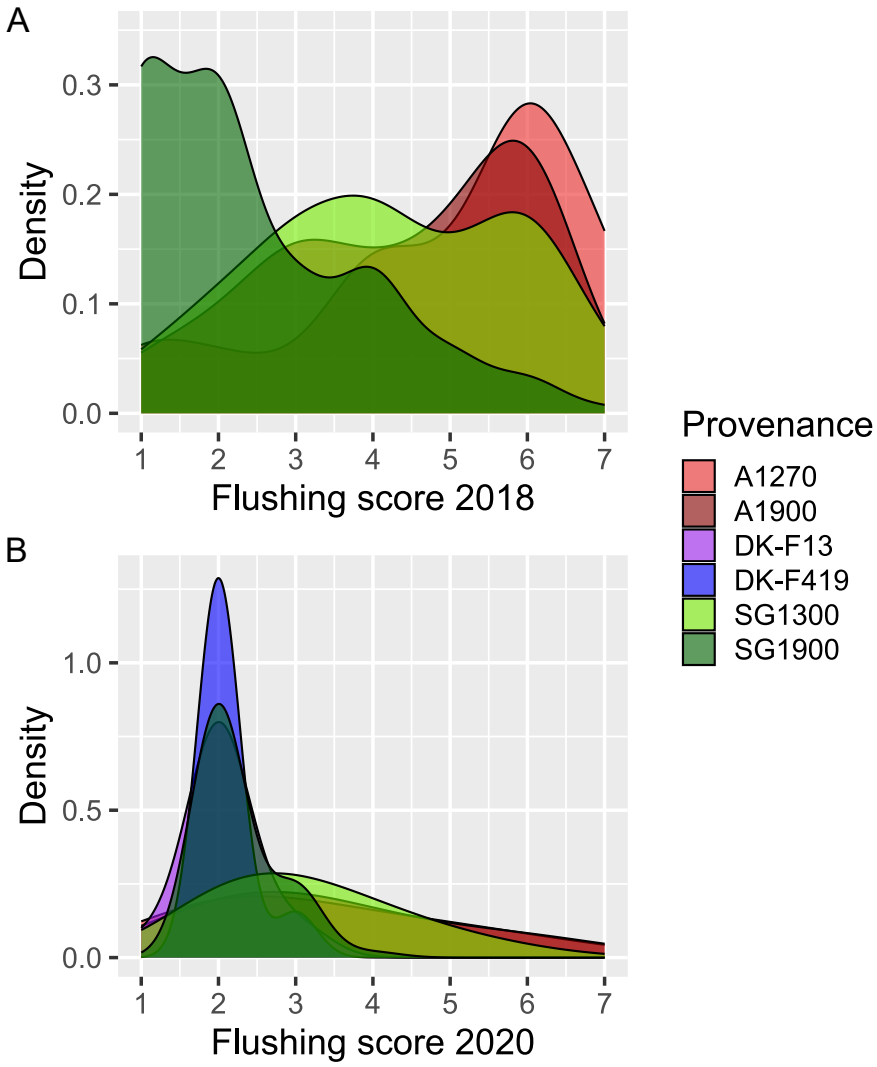

Figure 16: Density plots of flushing scores among provenance subgroups scored in May 2018 (A) and April 2020 (B). Published in Provaznik et al. (2024).

5.2.4 Senescence

At the beginning of November 2020, all provenances exhibited clear signs of senescence, with most leaves showing yellowing across nearly all assessed trees. No significant differences in senescence scores were detected between provenance subgroups. The distribution of senescence scores for each provenance subgroup is presented in Fig. 17.

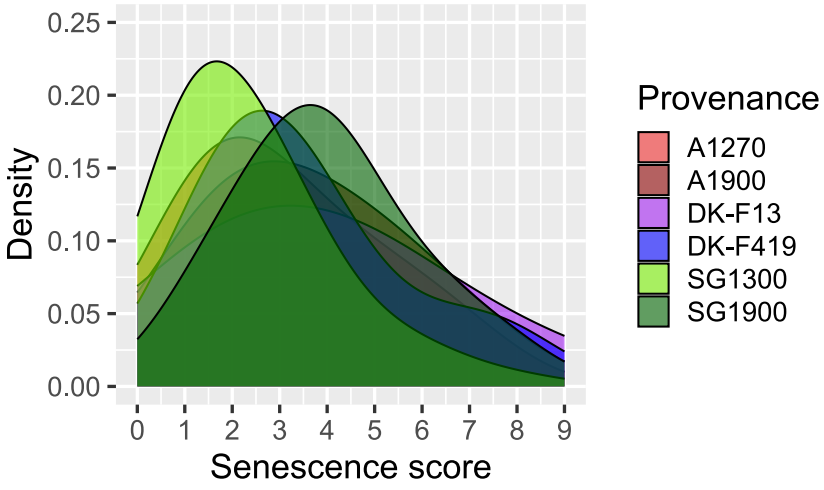

Figure 17: Density plots of leaf senescence scores of individual provenances and the altitudinal subgroups assessed at the beginning of November 2020. Published in Provazník et al. (2024).

5.3 Results of Experiment 3 – Scots Pine Provenances - Seedlings

5.3.1 Background Removal and Mean Reflectance Extraction

The first outcomes of the proposed pipeline are smoothed hyperspectral images with empty (NaN according to ImageJ) background pixels. These images can already be visually interpreted in Spectronon software by selecting combinations of any 3 wavelengths. It can be a standard RGB or any other possible wavelength combination ranging from 470 to 900 nm. To demonstrate the potential use, mean reflectance values for each tray corresponding to seedling provenances were extracted. Subsequently, the provenances were grouped into three geographical groups of origin (Fig. 18). In the next step, the first derivative of these spectra was calculated (Fig. 19). Both plots show a clear separation among the three geographical groups in both visible (VIS) and near infrared (NIR) spectral regions. The numerical values of mean reflectance and the respective 1st derivative were used for PLS-DA analyses.

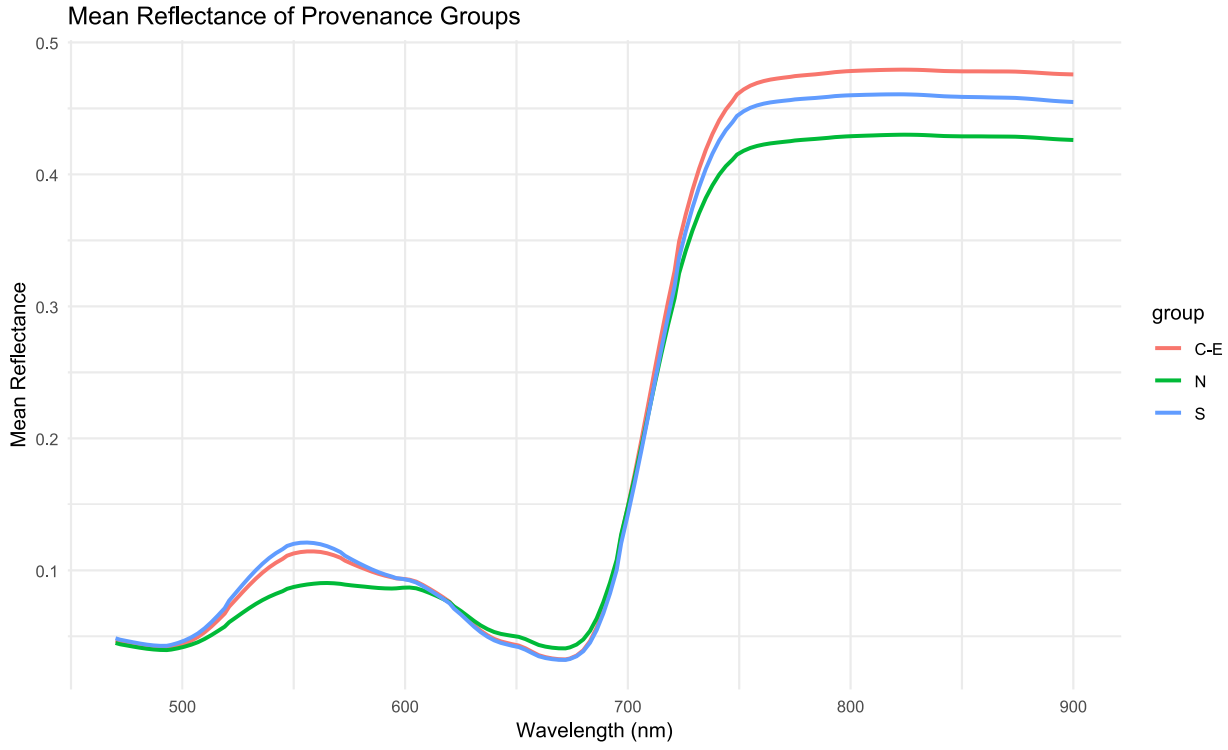

Figure 18: Visualization of the mean reflectance spectra of the three geographical groups. Data was later used for PLS-DA analyses.

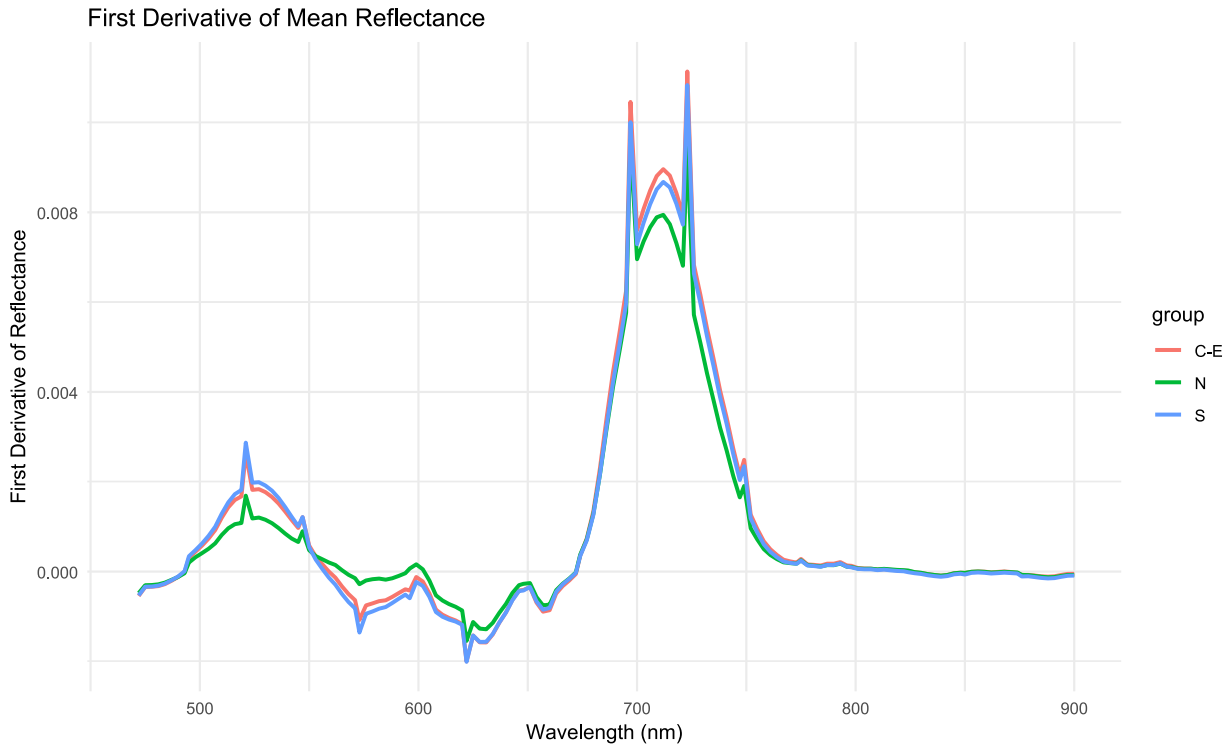

Figure 19: Visualization of the 1st derivative of mean reflectance spectra of the three geographical groups. Data was later used for PLS-DA analyses.

5.3.2 Classification

Three provenances representing three distinct geographical groups were chosen to demonstrate classification results in Figure 19. From the original datacubes (Fig. 20 – A, D, G), smoothed hyperspectral images with empty background pixels were produced (Fig. 20 – B, E, H). A supervised classification model was created using representative pixels for five categories: background, green needles, red needles, dry needles, and buds (Fig. 20 – C, F ,I). In the entire figure, one can clearly observe the differentiation among provenances from distinct geographical groups, mainly due to autumn phenology. The main benefit after the classification is the precise quantification of the autumn reddening (bright orange) and bud set (blue) within the classified images (Fig. 20 - C, F, I).

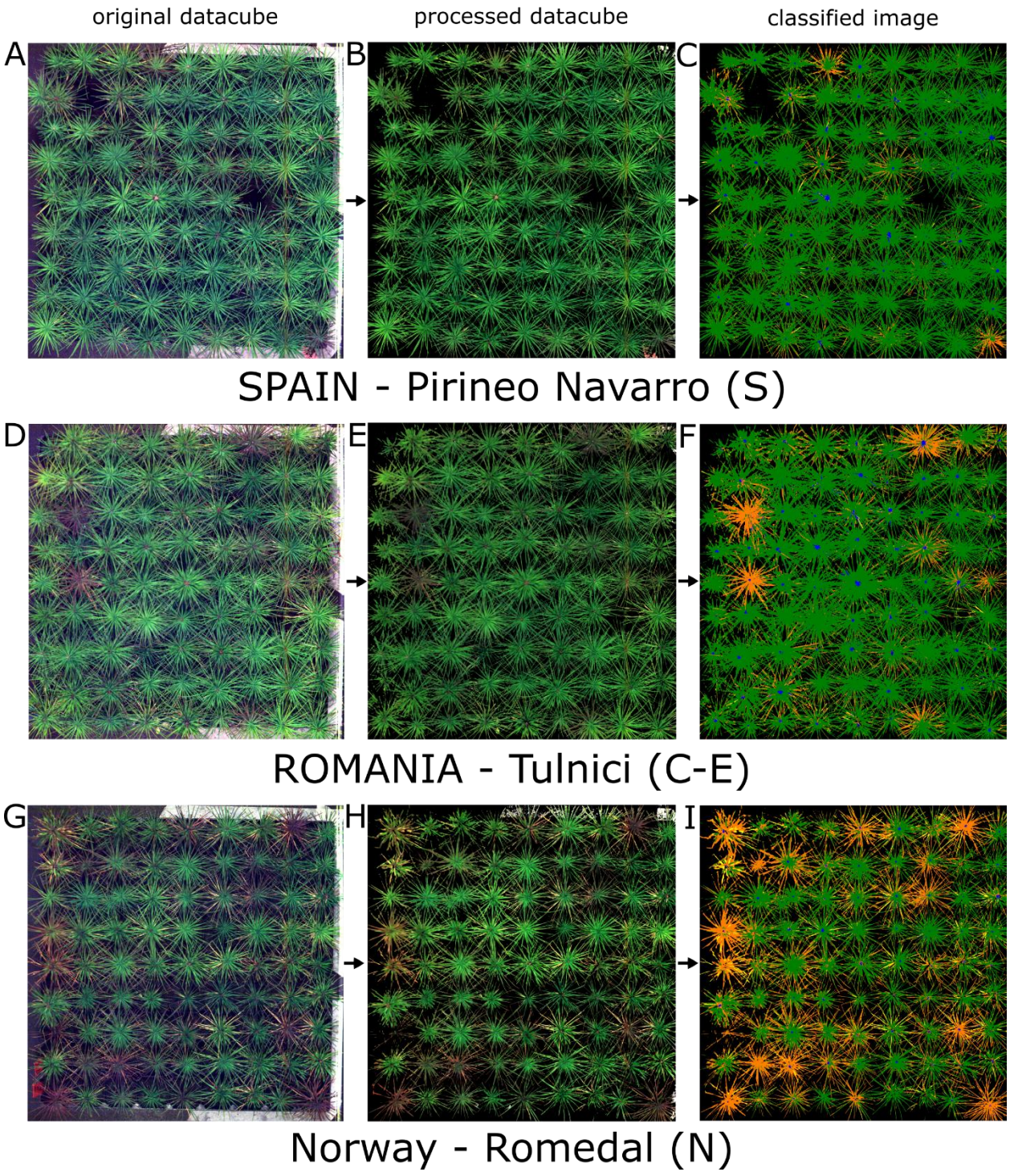

Figure 20: Image results from different stages of data processing represented by examples from provenances of each geographical group. The figure shows RGB rendered (640nm, 562nm, 470nm) images of original datacubes (A,D,G), processed datacubes that were used for classification (B,E,H), and the classified images (C,F,I).

5.3.3 Partial Least Squares Discriminant Analysis

The PLS-DA model predicting individual provenances' origin performed best on classified images (with 45% accuracy, PLS-DA score plot shown in Fig. 21). In comparison, on raw spectra, it achieved 40% accuracy, and on the first-derivative spectra, it reached 43% accuracy. The PLS-DA of classified images performed even better when predicting the geographical groups of origin (with 95% accuracy, PLS-DA score plot shown in Fig. 22). In comparison, models based on raw spectral data achieved 82% accuracy, while the first-derivative spectra reached 93% accuracy when predicting geographical groups.

While data from the classified images cannot reliably separate the treatment and control, the mean spectra and the 1st derivative of the mean spectra predict the short-day treatment in the treated provenances with similar accuracy. The PLS-DA from the 1st derivative of mean spectra achieves an accuracy of 0.76, and its PLS-DA score plot is shown in Fig. 23.

All the numerical values of the resulting accuracies and agreement scores (κ) from the PLS-DA predicting provenances, groups, and treatment are listed in Table 15 for comparison.

data for PLS-DA	accuracy (provenances)	κ (provenances)	accuracy (groups)	κ (groups)	accuracy (treatment)	κ (treatment)
mean spectra	**0.40**	0.33	**0.82**	0.73	**0.71**	0.43
1st derivative of mean spectra	**0.43**	0.36	**0.93**	0.89	**0.76**	0.51
pixel counts of classified images	**0.45**	0.36	**0.95**	0.92	**0.56**	0.13

Table 14: Partial Least Squares discriminant analysis results for differently processed data grouped by geographical groups and individual provenances.

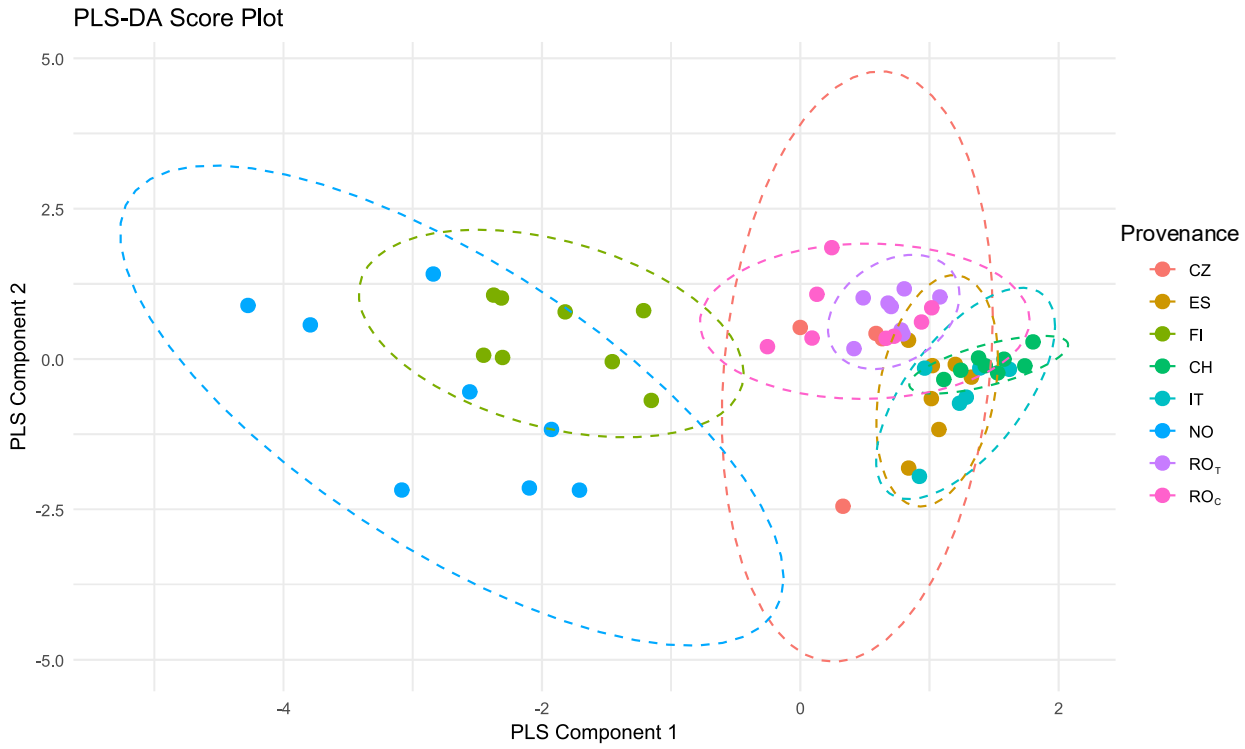

Figure 21: PLS-DA score plot for individual provenances based on the classified image data (predicting with the highest accuracy = 0.45; κ = 0.36)

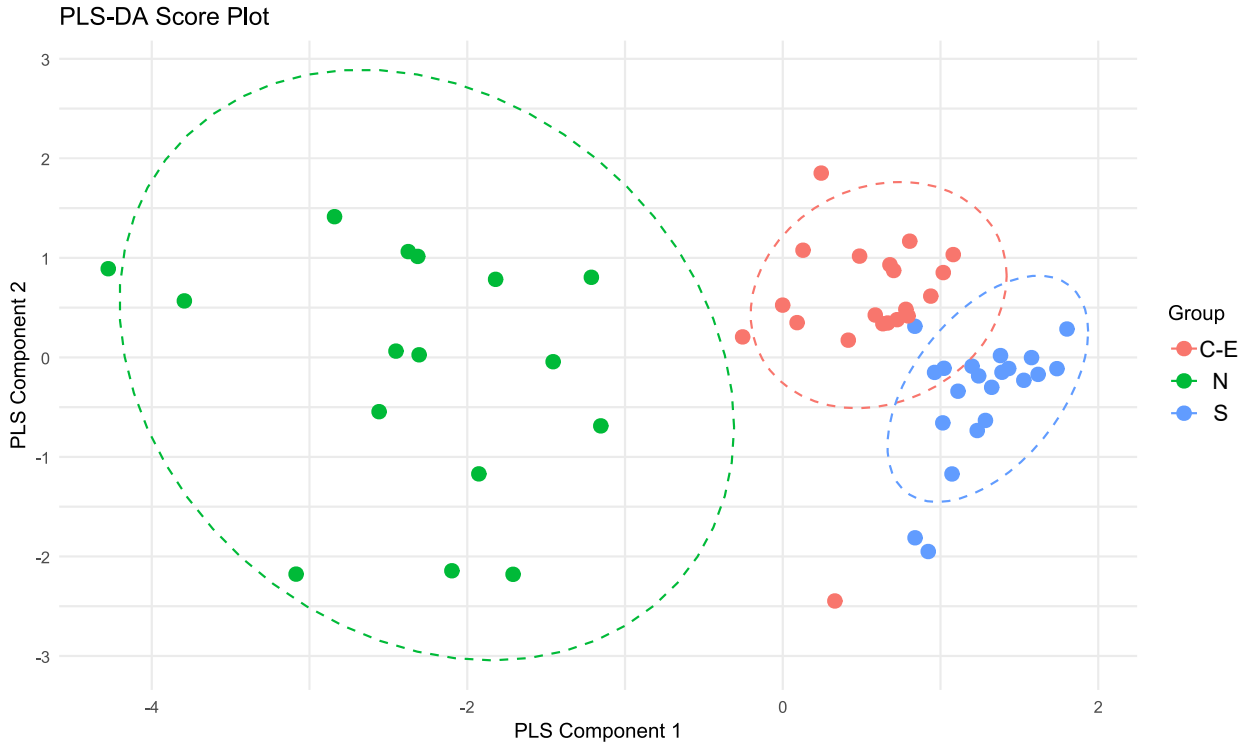

Figure 22: PLS-DA score plot for geographical groups based on the classified image data (predicting with the highest accuracy = 0.95; κ = 0.92)

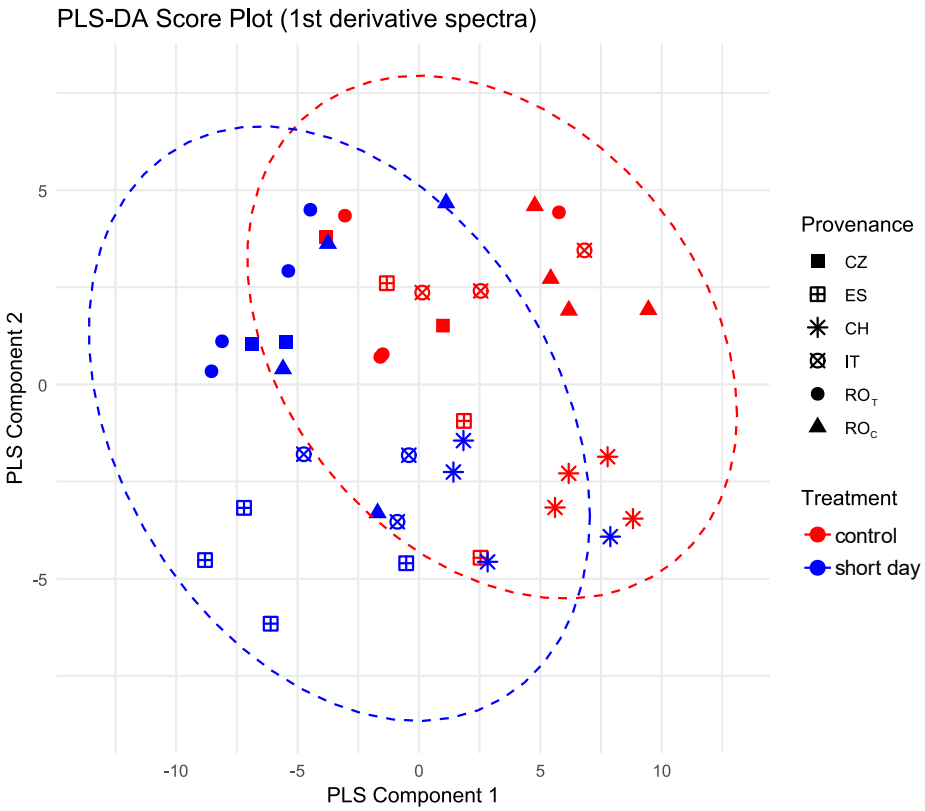

Figure 23: PLS-DA score plot for short-day treatment based on the 1st derivative of mean spectra (predicting with accuracy = 0.76; κ = 0.51). The individual provenances within the treatment and control are visualized with shapes.

5.3.4 Bud Count

Additionally, a macro to automatically count visible terminal buds from the classified images was developed, achieving a counting accuracy of 93 %. Fig. 24 provides an example of close-up image processing at various stages of the analysis workflow. The macro provides the user with the final number of buds that satisfy the predefined filtering criteria. Additionally, an image displaying tissue regions classified as buds is generated for the user (Fig. 24C), allowing visual inspection of pixel groups to verify which regions were identified as buds and which did not meet the specified criteria. The filtering conditions (defined in the methods section) can be modified based on the age of the trees or species in question.

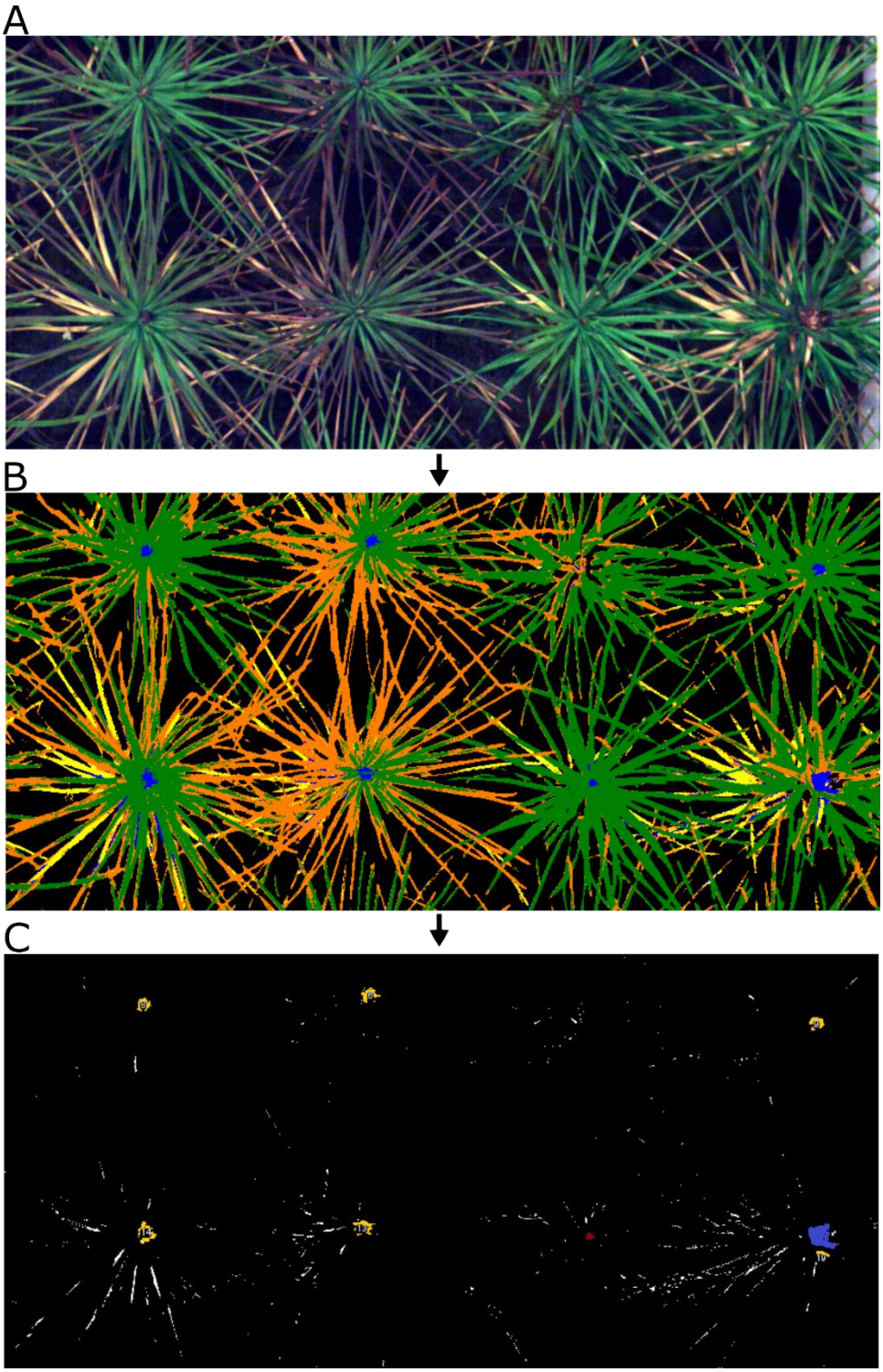

Figure 24: Visualization of the bud-count processing workflow. A is a cropped part of an RGB rendered (640nm, 562nm, 470nm) image of the original datacube, B is a cropped equivalent of the classified image, and C is a cropped equivalent of the mask from Fiji (ImageJ), which was used in the proposed macro for bud count. Yellow represents correctly counted buds; the red bud was incorrectly omitted by the macro (false negative), and the blue bud was not counted due to proximity conditions preventing a double count of split buds (obscured by a needle). The white color in the mask represents pixels incorrectly classified as blue in the classified image (B).

5.4 Results of Experiment 4 – Black Alder Provenances

5.4.1 Survival Rates

After three growing seasons, survival rates from spring 2022 to autumn 2024 were assessed. Negligible mortality, mainly due to browsing, was excluded from the survival rate calculations. Survival rates were 93% in F504 Lounkær Forest, 98% in F505 Hanehøj Plantation, 99% in F506 C.E. Flensborg Plantation, and 96% in F507 Wendelholm. These consistently high survival rates, combined with a low incidence of top dieback (<2%), enabled meaningful genetic evaluation of growth increments.

5.4.2 Bud Burst

For bud burst at 506, a high heritability of 0.74 with a standard error (SE) of 0.13 was estimated. Most performances had a similar level of leaf development except TRUE, which showed slightly earlier budburst compared to other provenances, as apparent from Fig. 25. Trees from seedling seed orchards FP657 and FP851, on the other hand, displayed later leaf development. Significant Pearson correlation of $r = 0.45$ ($p = 1.76e\text{-}6$) was obtained between the predicted mean values of height increment and bud burst among individual families.

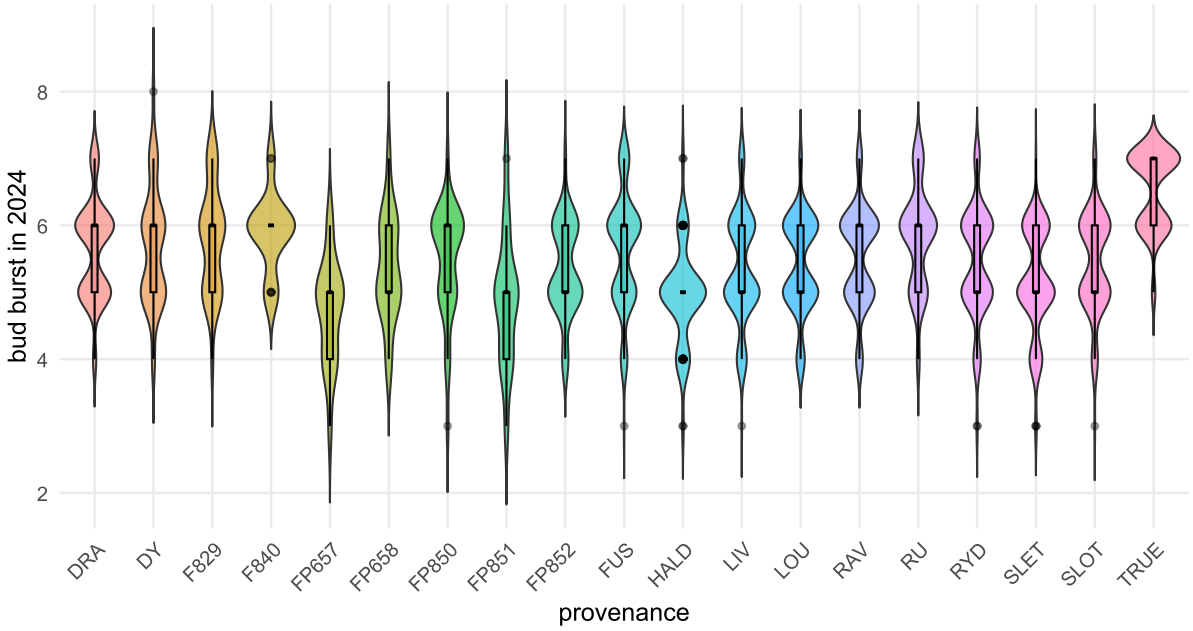

Figure 25: Violin plot of the maximum level of budburst (bud burst scores) for provenances at site 506 on 24th April 2024.

5.4.3 Heritability Estimates for Growth Increment

To minimize the influence of initial nursery conditions, yearly height increment was considered as the primary growth trait for analysis. h^2 estimates for height increment reached from 0.10 to 0.28 with SE between 0.04 and 0.09. The highest and most consistent h^2 was estimated at site 507. All the estimates for individual sites in different growing seasons are presented in Table 16.

	H^2 2022	SE 2022	H^2 2023	SE 2023	H^2 2024	SE 2024
504	**0.28**	0.09	**0.17**	0.07	**0.11**	0.06
505	**0.10**	0.06	**0.15**	0.07	**0.15**	0.07
506	**NA**	NA	**0.17**	0.05	**0.13**	0.04
507	**0.28**	0.07	**0.28**	0.06	**0.21**	0.05

Table 15: Narrow-sense heritability estimates for height increments in specific years at individual sites.

5.4.4 Family Performance in Height Increment Across Sites and Years

To evaluate the height increments of individual families at each site, the family means were predicted. The effect of provenances was significant at each site and has been added to the predictions to allow for comparison between families from different provenances. The predicted family means can be seen in Figures 26, 27, 28, and 29 for sites 504, 505, 506, and 507, respectively. At all sites, there is a trend of increasing increment in each following growing season, although the proportions of the increase vary by site.

At site 504, the best 5 performing families in 2022 were TRUE10, SLET6, SLET9, SLET7, and SLET8, showing the superior growth of the SLET provenance. In 2023, the families from RYD outperformed the others, with the top 5 families being RYD3, SLET9, RYD8, RYD9, and SLET7. In 2024, four out of the top five performing provenances were again from the SLET provenance: SLET7, SLET8, SLET9, SLET6, and SLOT2. Interestingly, SLOT2 performed below average in both previous growing seasons. The worst performing families in 2022 were FUS2, FUS8, FUS3, FUS1 and HALD3, in 2023 they were HALD2, HALD5, DRA3, LOU11, and LOU2. The worst-performing family in 2024 was again HALD2, followed

by RAV4, HALD5, RAV5, and DRA3. The performance in growth increments of all families at site 504 can be followed in Fig. 26.

At site 505, the provenance effect was more profound, and the top 5 performing families in growth increment were in all 3 seasons from the TRUE provenance (except 5th place in 2024 occupied by SLET9). The family that performed best in 2022 from a provenance other than TRUE was SLET9 at 11th place (after all the TRUE families). In 2023, it was SLET 8 at 6th place, and in 2024, it was SLET 9 at 5th place. The best performing family of the TRUE provenance was TRUE7. The worst-performing families in 2022 were RAV6, HALD5, RAV8, FUS8, and HALD6. In 2023, the worst-performing families were all from the RAV provenance, specifically RAV4, RAV8, RAV7, RAV2, and RAV9. In 2024, HALD 5 had the smallest increment, followed by RAV8, HALD4, RAV6, and RAV2. The performance in growth increments of all families at site 504 can be followed in Fig. 27.

At site 506, the height increment for 2022 was not measured. In 2023 however, the height increment at 506 was substantially larger than on the other sites with the average of all families being 94.9 cm, while in comparison it was 77.4 cm at 504 (typical black alder site), 37.7 cm at 505 (poor soil with generally lower increments), and 30.14 cm at 507 (comparable site to 505 with regard to soil). Despite the scale differences, the top 5 performing families at 506 are from TRUE provenance in both 2023 and 2024, similarly to site 505. The best performing family at site 506 is TRUE3. Another well-performing provenance at 506 is RYD, with families RYD2, RYD4, RYD3, RYD8, and RYD1 occupying the 9th to 13th place, respectively, in 2023. In 2024, RYD3, RYD2, and RYD1 jumped up to 6th to 9th place, respectively. Interestingly, families from SLET provenance, which performed well at all other sites, showed only average or below-average height increments at site 506 in 2024. The worst performing families were HALD5, HALD6, LIV7, HALD4 and HALD2 in 2023, and HALD5, LIV13, RAV3, DRA3, and LIV6 in 2024. The performance in growth increments of all families at site 506 can be followed in Fig. 28.

At 507, the family height increments substantially increased in 2024 to 106.0 cm, while in 2023 it was only 30.1 cm and in 2022 only 13.0 cm (as seen in Fig. 29). The best 5 performing families in 2022 were TRUE10, TRUE9, TRUE6, LIV11, and LIV10. In 2023, the best 5 performing provenances were again only from the TRUE provenance: TRUE7, TRUE10, TRUE6, TRUE9, and TRUE2. In 2024, the rowing provenances were TRUE7, TRUE5, TRUE10, TRUE1, and SLET7. The worst-performing families in 2022 were all the families

from the HALD provenance. In 2023 the worst performing families were HALD2, LIV3, RAV5, HALD5 and HALD4, and in 2024 they were HALD5, DRA1, RAV5, HALD2 and RAV7.

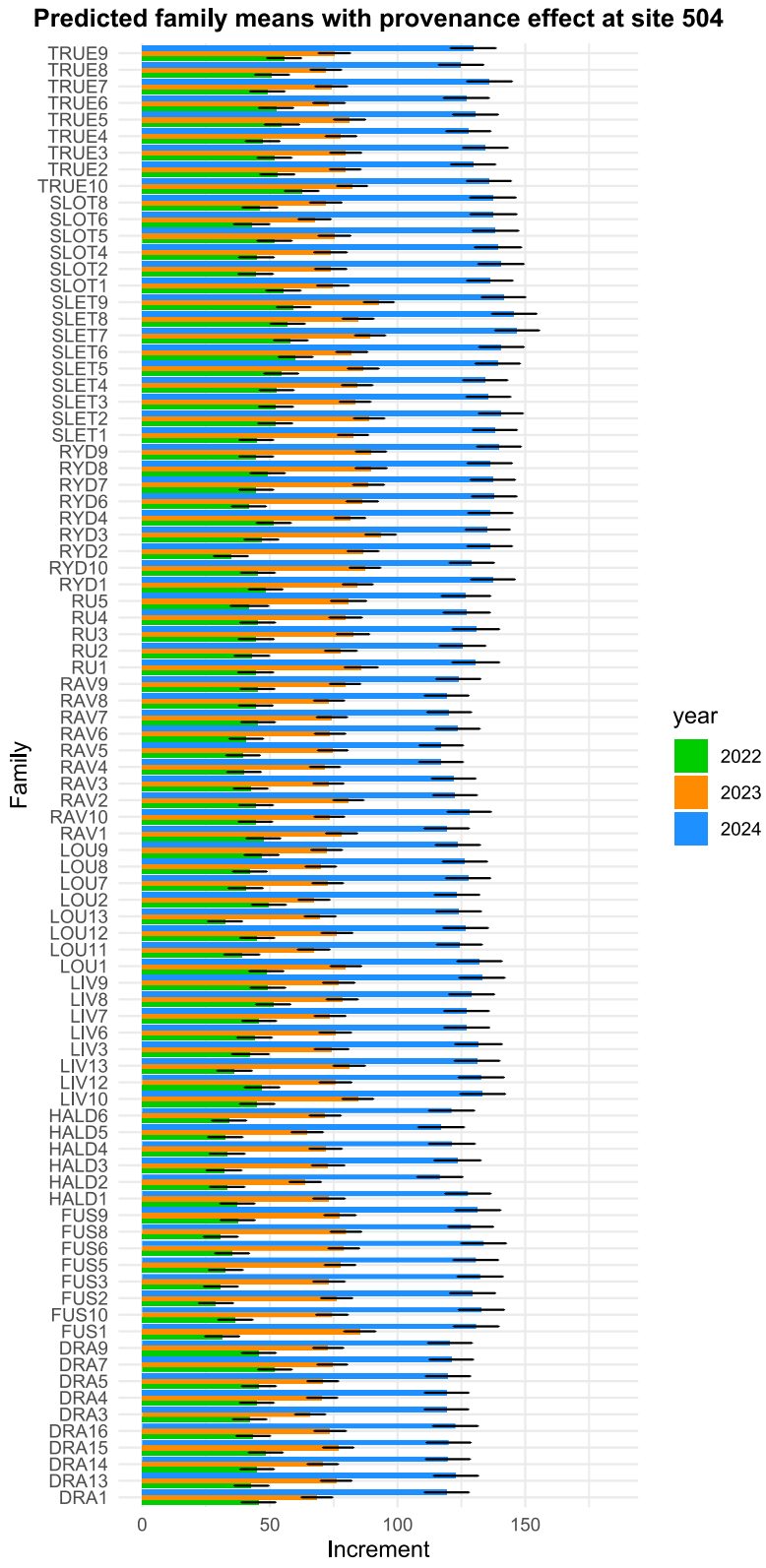

Figure 26: Predicted family means with provenance effect at site 504. For each year, the increment is presented by a different color. The black lines on top of each increment bar are visualizing the standard errors.

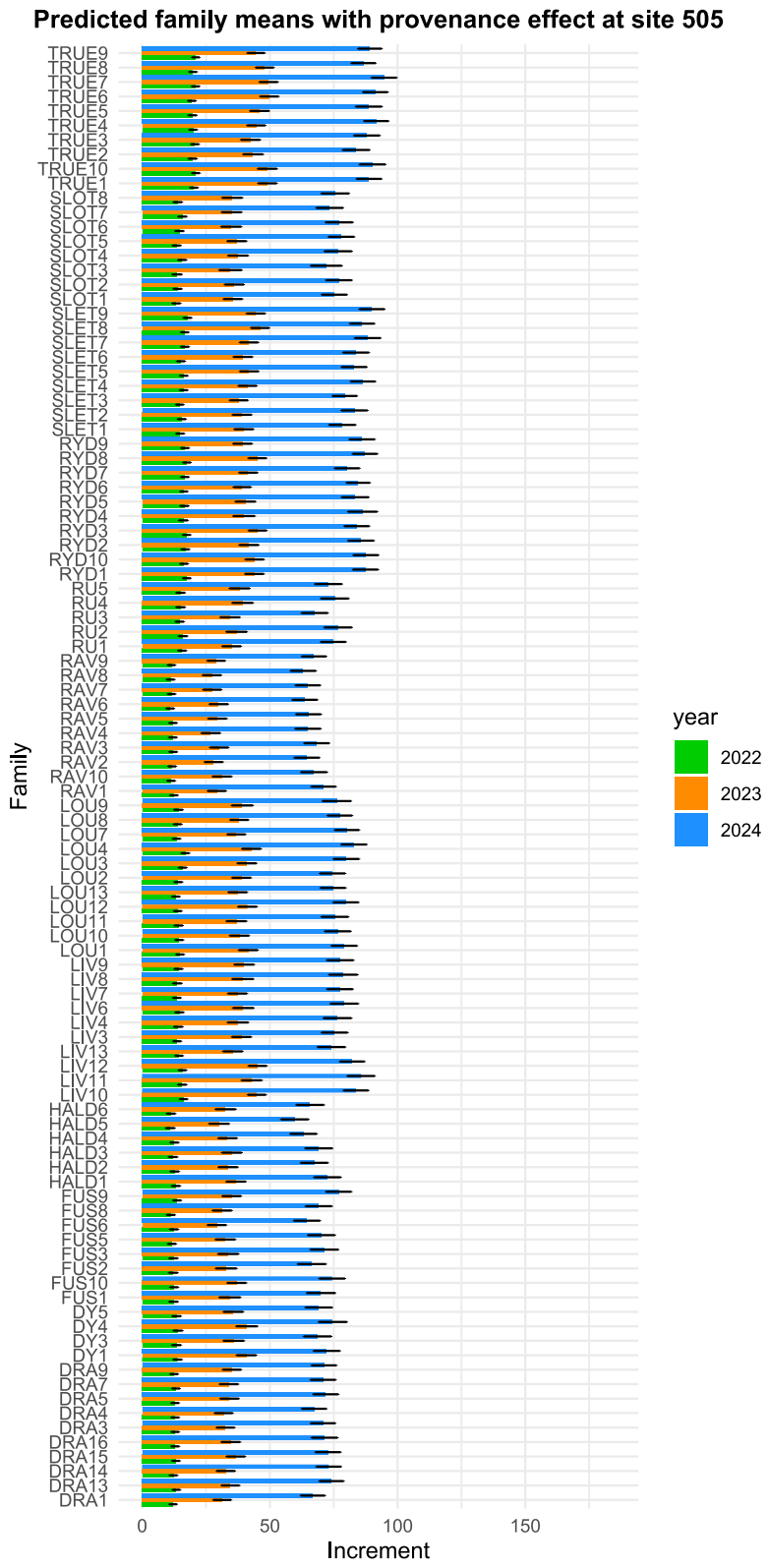

Figure 27: Predicted family means with provenance effect at site 505. For each year, the increment is presented by a different color. The black lines on top of each increment bar are visualizing the standard errors.

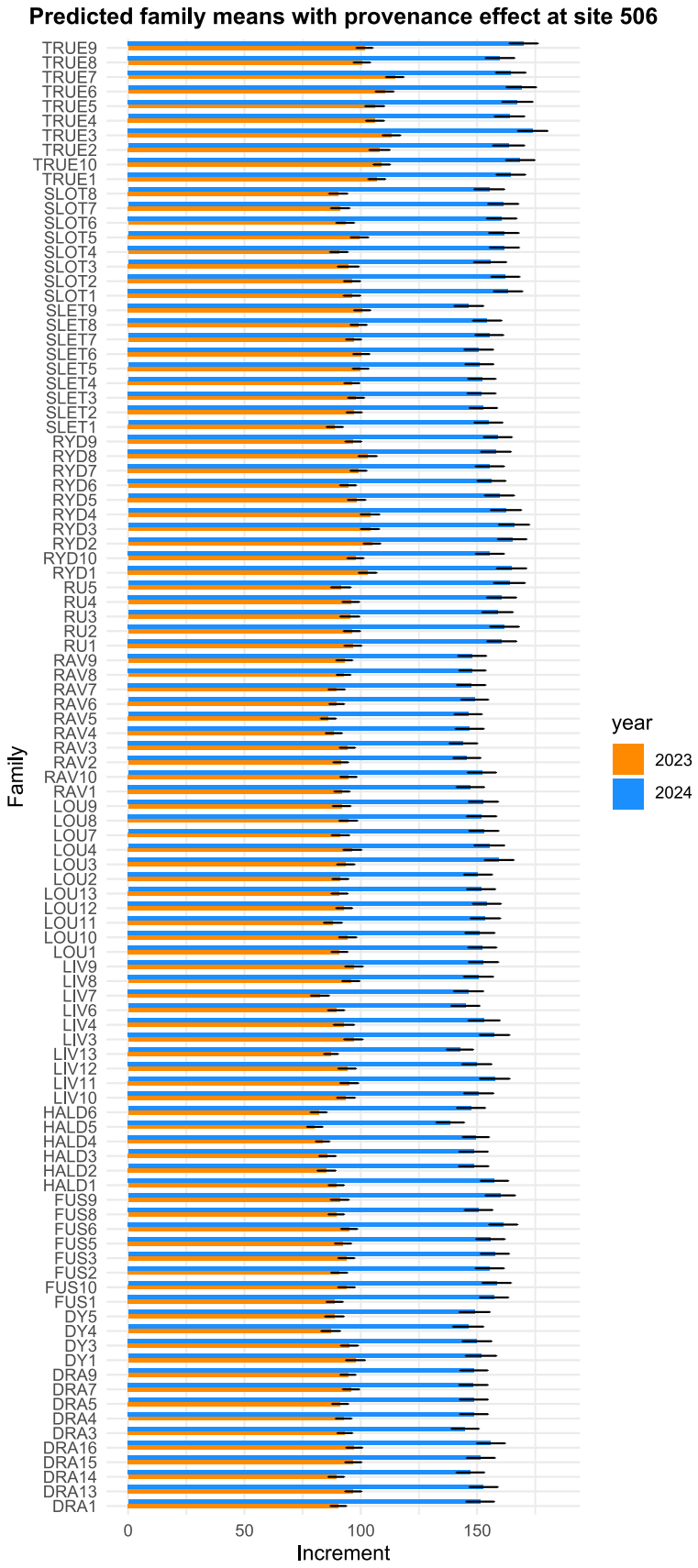

Figure 28: Predicted family means with provenance effect at site 506. For each year, the increment is presented by a different color. The black lines on top of each increment bar are visualizing the standard errors.

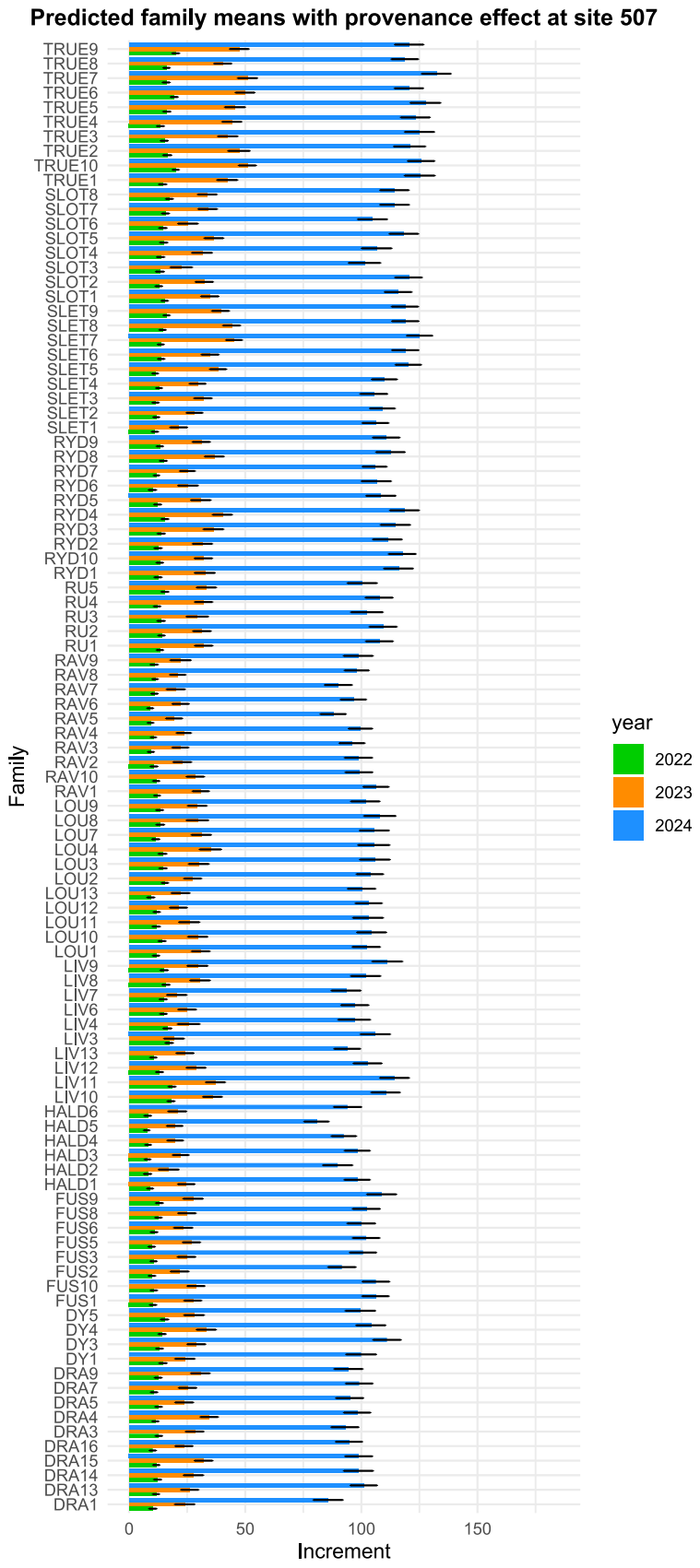

Figure 29: Predicted family means with provenance effect at site 507. For each year, the increment is presented by a different color. The black lines on top of each increment bar are visualizing the standard errors.

To display the height increment family predictions in a single figure, a biplot - a graph that shows both observations (as points) and variables (as arrows) from a dataset on the same two-dimensional plot (based on Principal Component Analysis) was constructed. In the biplot in Fig. 30, trial (site) and year combinations are vectors, and genotypes (families) are units. The closer the families are in the plot, the more similar their values are across the sites. The more a family's point lies in the direction of a site–year vector, the better its performance in that site–year. The angles between the site–year vectors indicate their type-B genetic correlation. Small angles suggest positive correlations, while large angles suggest no or negative correlation, indicating the presence of G × E. For instance, in Fig. 30, the site–years 504–2023 and 504–2024 form a larger angle with the other site–years, indicating the presence of G × E interaction. The length of the site–year vector in the biplot indicates how strongly that site–year contributes to the variation explained by the principal components. Longer vectors represent site–years with greater influence or stronger discrimination among families for height increment, while shorter vectors indicate site–years that contribute less to the overall variation or where family performance was more uniform. The biplot provides a useful visualization of the results through dimensionality reduction, but it includes only the first two principal components, which together explain 77% of the total variability.

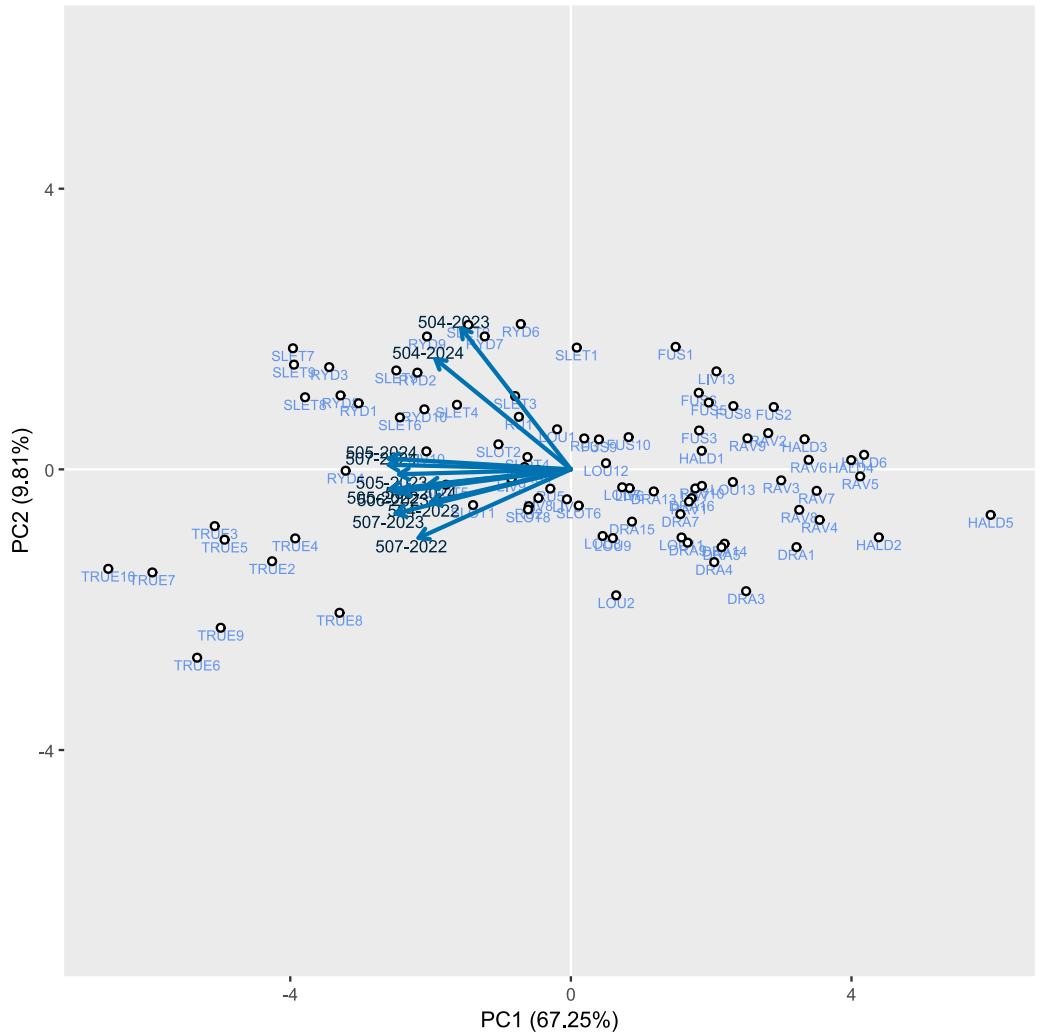

Figure 30: Genotype–by-environment interaction denoted by biplot showing performance of families across site–year combinations in height increment. Families are represented as points (units) and site–year combinations as vectors, based on the first two principal components of predicted values (BLUPs) from the single-site LMMs. Only families present at all sites are included. Data were standardized to visualize genotype × environment interactions.

5.4.5 Genotype-by-Environment Interactions

Table 17 presents the G × E interaction in the form of type B genetic correlation coefficients between sites. Highly positive type B genetic correlations indicate stable family rankings in growth performance across sites, whereas low correlations suggest the presence of G × E interactions, where family performance varies between sites.

In 2022, the type B genetic correlations are relatively high, indicating limited G × E interaction. In contrast, in 2023, correlations between site 504 and the other sites are lower, suggesting stronger G × E interactions, consistent with the patterns (vector angles) observed in Fig. 30. The 2023 data also reveal a G × E interaction between sites 505 and 506. In 2024, G × E

interactions are evident between sites 505 and 506, and between 506 and 507, with a weaker interaction observed between sites 504 and 505. Across all three seasons, correlations between sites 505 and 507 remain consistently high, indicating stable family performance rankings at these two sites.

2022	505	506	507
504 (Lounkær)	0.82	NO DATA	0.95
505 (Hanehøj)		NO DATA	0.90
506 (CEF)			NO DATA
2023	505	506	507
504 (Lounkær)	0.59	0.42	0.55
505 (Hanehøj)		0.85	0.99
506 (CEF)			0.68
2024	505	506	507
504 (Lounkær)	0.74	0.99	0.85
505 (Hanehøj)		0.57	0.99
506 (CEF)			0.65

Table 16: Genotype-by-environment interactions as type B genetic correlations from the MELMM.

Age-to-Age Interactions

Table 18 presents the age-to-age correlation coefficients. High correlations indicate consistent genotype performance across years and the absence of age-to-age interactions. At site 504, correlations between 2022 and the subsequent years are low, suggesting changes in family performance rankings in 2023 and 2024 compared to 2022. At site 505, family rankings remain consistent across all years, indicating stable performance over time. A similar pattern is observed at site 506, where correlations between 2023 and 2024 also suggest stability in family rankings. In contrast, site 507 shows age-to-age correlations similar to those at 504, indicating differences in family performance between 2022 and later years.

504	2023	2024	**505**	2023	2024
2022	0.500	0.518	2022	0.999	0.999
2023		0.999	2023		0.999
506	2023	2024	**507**	2023	2024
2022	no data	no data	2022	0.782	0.590
2023		0.999	2023		0.999

Table 17: Age-to-age correlation coefficients between increments from different years at individual sites.

Provenance was a significant factor in all evaluated models and represented a major source of variation in height increments across years and sites. When assessing provenance performance, trees from Danish and Swedish clonal seed orchards and seed stands were also included. Provenance rankings for height increment across sites and years are presented in Fig. 31.

5.4.6 Provenance Evaluation Across Sites and Years

The TRUE provenance consistently performed best, ranking first or second at all sites and years except at site 504 in 2024 and 2025 (Fig. 31A). At site 504, the top-performing provenances were SLET and RYD. SLOT performed well in 2022 and 2024 but declined in 2023, whereas RYD and RU performed best in 2023, with RYD maintaining strong performance across all years. Trees from the Danish clonal seed orchard FP658 exhibited low increment in 2022 but rose to the top rankings in 2023 and 2024. A similar pattern was observed for FUS, which showed substantial improvement in later years. In contrast, TRUE, the best-performing provenance at other sites, ranked mid-range at 504 in 2023 and 2024. RAV and HALD consistently ranked at the bottom across all three growing seasons. DRA ranked fifth in 2022 but declined below average in subsequent years. The Danish seed stand F840 improved from eighth in 2022 and 2023 to second in 2024. Other Danish seed orchards (FP657) and Swedish sources (F829, FP850, FP851) generally performed poorly. The only Swedish seed orchard material performing well was FP852, which ranked within the top five across all three years. The relatively large rank changes in Fig. 31A indicate strong age-to-age interactions.

At site 505, provenance rankings were the most stable across the three growing seasons (Fig. 31B). The consistently high-performing provenances were TRUE, FP658, RYD, SLET, F840, LIV, and LOU. FP657 and RU started above average in 2022 but dropped to mid-rank positions

in later years. SLO, DY, DRA, FUS, and F829 remained stable in the middle of the rankings. The poorest performers were HALD, RAV, FP852, and the other two Swedish seed orchard materials FP850 and FP851, which are closely related (also with F.829).

At site 506, the most stable top-performing provenances were TRUE, F840, RYD, and F829 (Fig. 31C). FP657, FP658, SLET, and FP852 performed well in 2023 but dropped in 2024. RU and SLOT ranked mid-range in 2023 but rose to the top in 2024, while LOU and FUS improved from the lower ranks in 2023 to the middle in 2024. Provenances consistently ranking at the bottom in both 2023 and 2024 included DRA, DY, RAV, HALD, and FP851.

At site 507, provenance rankings were relatively stable between 2023 and 2024, but notable age-to-age interactions were evident between 2022 and 2023 (Fig. 31D). The TRUE provenance ranked first in all three years. LIV, SLOT, DY, RU, and LOU ranked among the top in 2022 but declined in 2023 and slightly further in 2024. FP658 and RYD maintained stable positions in the top half throughout all years. SLET rose from mid-ranking to second place in 2023 and 2024, while FP657 showed the most dramatic improvement, rising from 18th in 2022 to fourth in 2023 and third in 2024. FP852, F840, and FP850 remained mid-ranked across all seasons. DRA declined from a lower-half ranking to third from the bottom in 2024. The consistently poorest performers at 507 were FUS, F829, FP657, RAV, HALD, and FP851.

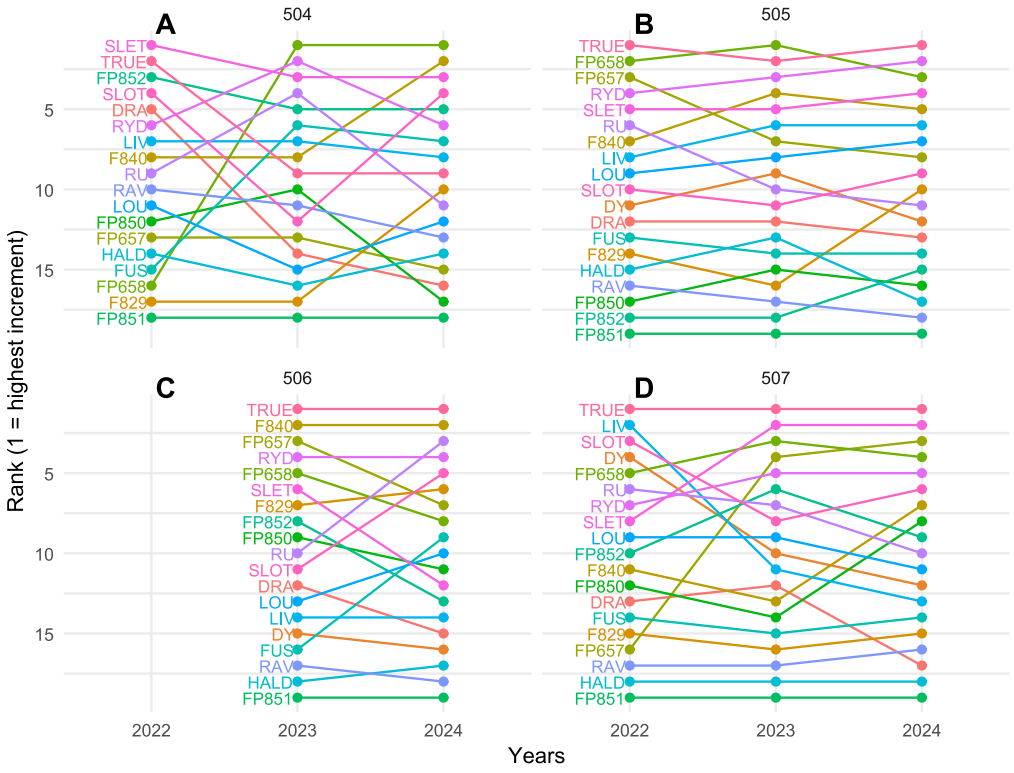

Figure 31: Rankings of provenances derived from their respective BLUEs from single sit LMMs.

5.4.7 Spectral Reflectance

The reflectance curves from 2023 for the 10 selected provenances are shown in Fig. 32. In Fig. 32 A, C, and E, which depict spring reflectance, the green peak around 550 nm is clearly more pronounced compared to the autumn measurements shown in Fig. 32B, D, and F. Differences between spring and autumn reflectance are also evident across the entire NIR region, as well as in specific SWIR bands.

The strongest provenance-related variation occurred in the green peak of the VIS region, the red-edge region (associated with photosynthetic pigments), and the NIR range (reflecting leaf structural properties), indicating that these spectral regions are particularly sensitive to differences among provenances. Hyperspectral reflectance represents a highly informative high-throughput phenotyping tool for identifying and characterizing genetic variation among and within provenances. The detailed analysis of the reflectance data combined with other physiological traits will be the focus of a subsequent study, aiming to explore their potential for early selection and trait prediction in black alder breeding programs.

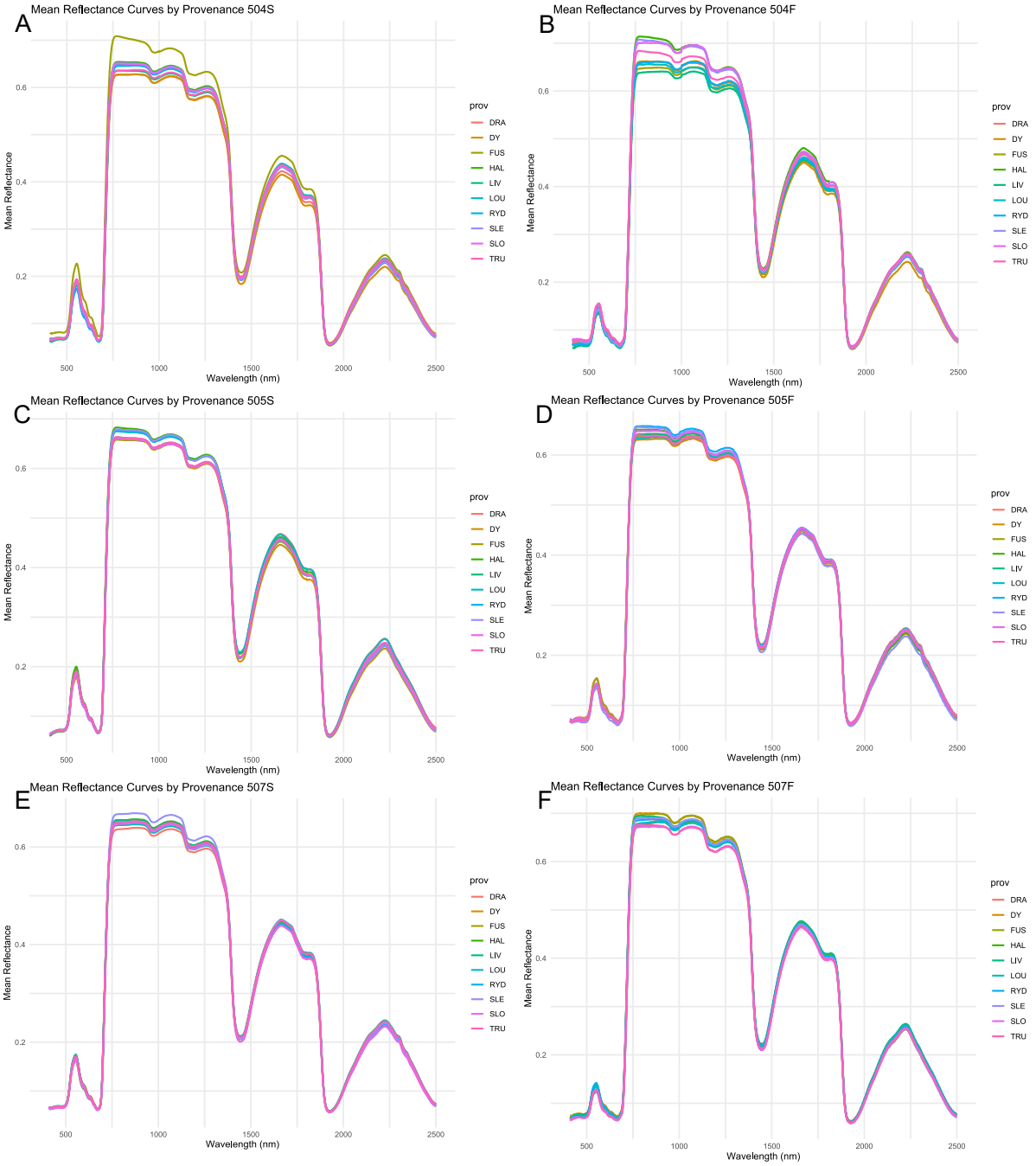

Figure 32: Mean hyperspectral reflectance for 10 selected provenances at sites 504, 505, and 507 in spring (S) and autumn/fall (F) 2023.

6 Discussion

This thesis investigates three widespread and ecologically significant European tree species: Scots pine, European beech, and black alder. To investigate the genetic and physiological underpinnings of functional trait variation using novel phenotyping methods across these species, four complementary experiments were conducted. The first experiment focused on needle functional traits and spectral reflectance in Scots pine, integrating two clonal seed orchards incorporating a novel SNP genotyping array. This approach enabled the estimation of genetic parameters, assessment of genotype × environment and year-to-year interactions, and exploration of genetic correlations between physiological and spectral traits. The second experiment examined photosynthetic performance and phenology in European beech, comparing southern and northern provenances using gas exchange and chlorophyll fluorescence methods in a common garden setting. The third experiment developed and applied a high-throughput hyperspectral imaging pipeline to detect physiological and phenological variation in pine seedlings at the end of the growing season. Finally, the fourth experiment investigated genetic variation in juvenile growth and bud burst phenology in black alder through multi-site progeny trials established across contrasting soil moisture regimes.

Understanding the genetic architecture of functional traits is central to predicting the adaptive potential of forest tree species and identifying meaningful targets for breeding and selection. Functional traits related to photosynthesis, structural investment, water use, and phenology often show substantial genetic variation, but their degree of heritability and stability across environments varies (e.g., Marguerit et al., 2014). These traits are not only important for physiological performance but are also tightly linked to survival, growth, and reproductive success. In long-lived forest trees, the timing of phenological transitions, leaf structure, water-use efficiency, and pigment composition are critical in determining how individuals cope with abiotic stress, compete for resources, and persist across variable environments (De Kort et al., 2016; Pulkkinen et al., 2011; Robson et al., 2012).

Moreover, because these traits mediate responses to temperature, water availability, and growing season length, they play a key role in resilience to changing climate conditions, including altered drought regimes and shifts in seasonal timing (Alberto et al., 2013; Pliûra, 2004). Identifying genetically controlled and environmentally robust traits can therefore support the development of adaptive breeding and management strategies aimed at maintaining forest productivity and stability under future climates. By combining clonal field trials,

provenance experiments, and high-throughput phenotyping approaches, this work provides insight into the relative genetic contribution to different categories of traits in various tree species.

By organizing the discussion mainly according to trait categories, including phenology, growth and structural traits, photosynthetic pigments, photosynthesis-related traits, water-use related traits, and spectral reflectance, this thesis aims to disentangle the relative genetic contribution, environmental sensitivity, and adaptive significance of each functional domain. This structure enables meaningful cross-species comparisons and highlights how distinct trait groups shape the adaptive capacity and resilience of forest trees under changing climatic conditions. It also offers an insight into novel methods and approaches in tree phenotyping.

6.1 Phenology and Seasonal Timing

Phenology is one of the most fundamental axes of adaptation in temperate and boreal forest trees. The timing of seasonal transitions, such as bud burst, leaf flushing, growth cessation, and autumn senescence, strongly influences survival, productivity, and stress tolerance. These traits are under strong genetic control, reflecting evolutionary responses to climatic regimes. In long-lived species like Scots pine, European beech, and black alder, phenological timing determines the length of the growing season, exposure to frost, and competitive dynamics within stands (Pliûra, 2004; Pulkkinen et al., 2011; Robson et al., 2012). Early or delayed phenological transitions can directly affect growth potential and stress avoidance, making these traits particularly relevant for understanding adaptive variation and for guiding breeding and deployment strategies under changing climatic conditions (De Kort et al., 2016; Dittmar and Elling, 2006; Nielsen and Jørgensen, 2003).

6.1.1 Bud Burst and Flushing Dynamics Across Broad-Leaved Species

Bud burst and flushing mark the onset of the growing season and are strongly linked to temperature and photoperiod cues. This was particularly evident in Experiment 2, where the southern provenance of European beech from Aspromonte exhibited significantly higher flushing scores than the Sila Grande provenance in both 2018 and 2020. In the same year, Danish provenances flushed later than Italian ones, reflecting well-established patterns of latitudinal and altitudinal adaptation in this species (Čufar et al., 2012; Dittmar and Elling, 2006; Nielsen and Jørgensen, 2003). These results are consistent with previous studies showing that flushing in beech is significantly correlated with geographic and climatic variables such as latitude, longitude, and altitude, and influenced by chilling, temperature sums, and day length (Nielsen and Jørgensen, 2003). The duration of phenological phases also varies between years, mainly in response to temperature fluctuations (Bednářová and Merklová, 2007; Slovíková and Bednářová, 2014). Similarly, research from Slovakia (Schieber et al., 2013), southern Germany (Dittmar and Elling, 2006), and Slovenia (Čufar et al., 2012) showed phenological variation with altitudinal gradients (various provenances from different altitudes); in one study, leaf unfolding was delayed by approximately 2–3 days for every 100 m increase in elevation (Dittmar and Elling, 2006). In Experiment 2, Sila Grande exhibited some altitudinal variation, while Aspromonte did not show a similar pattern. Nevertheless, the provenance-level ranking in flushing remained somewhat stable across 2018 and 2020, indicating a genetically based

adaptation of flushing behavior that is maintained under Danish climatic conditions. This stability is in line with observations that beech leaf unfolding is less temperature-sensitive than in other European tree species, suggesting that other factors, particularly photoperiod, play a major role in controlling its timing (Vitasse et al., 2009).

Similar patterns of strong genetic differentiation in bud burst were observed in black alder. In experiment 4, a high narrow-sense heritability ($h^2 = 0.74$, SE = 0.13) was estimated, indicating strong genetic control, which is within or even slightly above published ranges for black alder. Multi-site Lithuanian progeny tests reported moderate-to-high heritability for bud flushing depending on site ($h^2 \approx 0.30$ at Kaunas and 0.72 at Šiauliai) (Pliûra, 2004); clonal work across European regions estimated broad-sense heritability (H^2) for bud burst between 0.14 and 0.54 and much lower heritability for bud burst plasticity, with temperature driving reaction norms and variance components (De Kort et al., 2016). The slight earliness of TRUE provenance and delayed leaf development of FP657/FP851 are consistent with well-documented population/family differences and population × environment interactions for bud flushing in black alder (Pliûra, 2004) and with regional adaptive signals in phenology along temperature gradient patterns and potential frost-tolerance phenology trade-offs (De Kort et al., 2016). In Experiment 2, a significant Pearson correlation of $r = 0.45$ ($p = 1.76e\text{-}6$) was obtained between the predicted mean values of height increment and bud burst among individual families, accounting for provenance effects. Climate sensitivity of bud burst is further supported by evidence that spring frosts can suppress detectable family variance and weaken between-trial correlations for alder phenology, complicating inference in some years and sites (Baliuckas and Pliūra, 2008). More broadly, in red alder (*Alnus rubra* Bong.), phenological patterns show that northern families exhibit earlier bud burst and leaf drop than southern families when planted at the same site (Hamann et al., 2000; Porter et al., 2013)

6.1.2 Autumn Senescence and Coloration

Autumn senescence represents the other key phenological transition in temperate trees, marking the end of active growth and the onset of dormancy. In Experiment 3, autumn reddening associated with anthocyanin accumulation was observed to vary consistently among Scots pine provenances. Northern provenances showed earlier, and more intense coloration compared to southern ones, reflecting adaptation to shorter growing seasons and earlier frost onset. Anthocyanin accumulation is thought to play a photoprotective role during the transition

from active photosynthesis to dormancy, mitigating photooxidative stress under cold and high-light conditions (Pulkkinen et al., 2011; Toivonen et al., 1991). This trait is particularly interesting because it provides a visible and quantifiable marker of physiological transition, which can be measured non-destructively and even remotely through spectral imaging (Seyednasrollah et al., 2021).

No visible differences in leaf senescence were observed in Experiment 2 among European beech provenances and provenance subgroups at the beginning of November 2020 (Fig. 16). Based on this, the conclusion is that the photosynthetic measurements conducted at the beginning of September 2018 were not influenced by the direct onset of leaf senescence, as the senscence in November was still in an earlier (low senscence scores) stage. Senescence is closely linked to chlorophyll content, as the progressive loss of chlorophyll in deciduous trees leads to a decline in photosynthetic capacity on a leaf area basis (Adams et al., 1990). Leaves that persist longer in the season typically show more efficient nutrient translocation, and this capacity is species dependent (Niinemets and Tamm, 2005). In a related beech species (*Fagus grandifolia* Ehrh.), chlorophyll degradation during senescence was shown to be gradual rather than abrupt. The slower formation of the abscission layer allowed for extended nutrient withdrawal from leaves (Primka and Smith, 2019). Although less pronounced in black alder, autumn phenology is well-documented in these species. In beech, senescence timing shows clear provenance-level differentiation and is largely driven by photoperiod, with additional modulation by temperature and site conditions (Dittmar and Elling, 2006; Robson et al., 2012; Schieber et al., 2013). Black alder is relatively inefficient in nitrogen resorption during autumn senescence because it hosts N-fixing Frankia in its root nodules, providing a steady nitrogen supply and allowing the leaves to stay green in autumn (Taulavuori, 2006). Nonetheless, subtle differences can be detected using hyperspectral reflectance, particularly in the green peak of the VIS region, which typically decreases during the autumn period. A thorough analysis of reflectance variation among black alder provenances will be the focus of future research.

6.1.2.1 Supervised Classification Captures Adaptive Phenology in Scots Pine

The classified images from Experiment 4 presented in Figure 19 effectively demonstrate the differentiation among Scots pine provenances from three distinct geographical groups, primarily driven by variations in autumn phenology. The supervised classification model, trained on representative pixels for five categories (remaining background pixels, green

needles, red needles, dry needles, and buds), allowed for detailed semantic segmentation of the images (Fig. 19 – C, F, I). Supervised classification allows us to define biologically meaningful classes based on expert knowledge, ensuring the model targets relevant phenotypic traits. It improves accuracy by training on labeled data that reflects true variability and avoids irrelevant spectral patterns. The *Auto Classifier* tool (within Spectronon freeware) automates the complex process of hyperspectral image classification by minimizing user input, making it accessible to non-experts (without advanced programming skills), while providing probability maps instead of simple categorical labels for even more nuanced interpretation. The Auto Classifier tool runs in a batch processor, processing each image independently, which reduces the computational load of large datacubes. Despite this, it applies consistent thresholds derived from pooled pixel data across all provenances (supervised classification categories), ensuring standardized outputs. Finally, the *Classification to Color Map* tool creates classified images representing pixels of the chosen categories for easy interpretation.

Reducing hyperspectral data dimensionality by the proposed classification allows for a clear, unbiased assessment of autumn phenology. This approach aligns with recent advances in UAV-based phenotyping and deep learning techniques, which have been shown to improve the accuracy and objectivity of phenological trait monitoring in forest trees (Cloutier et al., 2024; Hu et al., 2022).

6.1.2.2 Short-day Treatment Differences Revealed by Hyperspectral Data

Short-day treatment in pines is known to induce complex physiological and biochemical changes beyond visible color differences. In Scots pine, it stops shoot elongation and advances bud set while triggering shoot-specific increases in abscisic acid and rapid changes in its turnover (Odén and Dunberg, 1984). In Chinese pine (*Pinus tabuliformis* Carr.), short-day treatment enhances chlorophyll, starch, abscisic acid, and lignin, while also elevating activities of phenylalanine ammonia lyase, polyphenol oxidase, and peroxidase, and altering needle protein expression linked to photosynthesis and stress responses (Jiang et al., 2019). Similarly, it can shift nutrient partitioning, for instance by increasing stem and foliar nitrogen and phosphorus (Pan et al., 2017). However, not all responses translate into practical benefits: early-season short-day treatment did not improve field survival or growth in Scots pine in an experiment by Luoranen and Rikala (2012).

In experiment 3, PLS-DA models based on first-derivative spectral data were able to predict short-day treated seedlings with relatively high accuracy. In contrast, classification of images alone was not sufficient, suggesting that the differences induced by short-day treatment cannot be reduced to simple categories such as the presence or absence of needle reddening. A finer classification system, or alternative approaches that capture biochemical variation, would be required.

Studies show that short-day treatment reliably induces dormancy-related and stress-associated biochemical responses in pines (Jiang et al., 2019; Odén and Dunberg, 1984; Pan et al., 2017). Yet, its practical benefits depend on species, timing, duration, fertilization, and nursery management, requiring protocols to be tailored carefully (Jiang et al., 2019; Pan et al., 2017). Importantly, hyperspectral reflectance data (particularly in first-derivative form) capture subtle changes in pigments, carbohydrates, and stress-related chemistry caused by short-day treatment. These biochemical shifts are not easily reflected in simple visual classifications such as needle reddening, highlighting the value of detailed hyperspectral data for detecting treatment effects and linking them to underlying physiological processes.

6.1.3 Autumn Bud Set in Scots pine Seedlings

Bud set, the timing of terminal bud formation, is another key phenological trait closely linked to climatic adaptation and frost hardiness. Studies have demonstrated that bud set in Scots pine exhibits strong clinal variation with latitude, with northern populations setting buds earlier than southern ones, reflecting adaptation to shorter growing seasons and earlier onset of frost (Hurme et al., 1997; Taulavuori et al., 2010). The genetic basis and heritability of bud set have been documented, with significant additive genetic variation within and between populations (Savolainen et al., 2004). In Experiment 3, clear provenance variation in bud set was observed, but as this phenomenon has already been studied, the focus of the experiment was rather to automate the bud set assessment method, as discussed later.

6.2 Growth and Leaf (Needle) Structural Traits

Growth and structural traits are key components of tree adaptive strategies and are tightly linked to resource acquisition, physiological efficiency, and competitive ability. They play a critical role in determining how trees respond to environmental conditions over their lifespan and are often under both strong genetic control and environmental modulation (Bhat et al., 2016; Donnelly et al., 2016; Marguerit et al., 2014). It is important to note that in clonal seed orchards, growth traits cannot be reliably measured due to the grafted origin of the trees and regular trimming to maintain orchard structure. As a result, direct measurements of height or diameter growth were not available for Scots pine in Experiment 1 in this context, and the focus was placed instead on structural needle traits such as needle length and leaf mass per area, which are less affected by management practices and reflect genetic differences more consistently (Rweyongeza et al., 2003; Tao et al., 2021). Similarly, early seedling development is largely supported by seed reserves rather than active photosynthesis and nutrient uptake; therefore, the seedling height was not assessed in Experiments 2 and 3.

6.2.1 Genetic Variation of Needle Structural Traits

In Experiment 1, NL exhibited consistently moderate to high heritability across sites, supporting previous findings in Scots pine (Donnelly et al., 2016). Although reported heritability values vary among studies, the overall pattern reinforces that needle morphology traits, particularly NL, are strongly influenced by genetic factors in conifers, including black pine (*Pinus nigra* subsp. *pallasiana* (Lamb.) Holmboe), and chir pine (*Pinus roxburghii* Sargent) (e.g., Bhat et al., 2016; Donnelly et al., 2016; Rweyongeza et al., 2003; Yigit et al., 2023).

Because LMA reflects key morphological features of needles, its heritability patterns are likely shaped by similar genetic factors influencing NL but remain strongly modulated by environmental conditions. In conifers, LMA is primarily determined by needle thickness, tissue density, and degree of lignification (Buraczyk et al., 2022; Houminer et al., 2022). A provenance common garden study of Scots pine demonstrated that LMA varies within populations, highlighting its value for detecting intrapopulation variability (Buraczyk et al., 2022). In Experiment 1, however, significant heritability of LMA was detected only at Plasy in 2021. This site- and year-specific expression suggests that the genetic signal underlying LMA

can be either masked or amplified by environmental factors, aligning with previous findings that phenotypic variation in LMA reflects a combination of genetic differentiation and plasticity.

The presence of significant heritability under specific conditions indicates that selection could act on LMA in certain environments, potentially contributing to adaptation to local climatic constraints. Experimental studies have linked high LMA to conservative water-use strategies and enhanced drought resistance, as species with larger LMA tend to maintain both photosynthetic capacity and midday water potential under water deficit (Bhusal et al., 2021). Similarly, hybrids and populations adapted to semi-arid sites frequently exhibit elevated LMA, supporting its role in conferring vigor and resilience in marginal environments (Houminer et al., 2022). At the physiological level, persistent xylem impairment after drought can limit the recovery of gas exchange even when water potential improves, underscoring how structural traits like LMA interact with hydraulic function to shape post-drought performance (Rehschuh et al., 2020).

Collectively, these lines of evidence highlight LMA as a key integrative trait linking leaf structure, hydraulic function, and drought resilience in Scots pine and other conifers (Bhusal et al., 2021; Buraczyk et al., 2022; Houminer et al., 2022). Beyond its physiological relevance, LMA also provides valuable information for ecosystem modeling and fire risk assessments (Féret et al., 2019), making it a practical trait for both ecological research and applied forest management.

6.2.2 Genetic Variation in Early Growth of Black Alder

As black alder has only recently gained interest from European foresters (mainly as a substitute for declining ash), only a few studies have documented its genetic variation in growth. A progeny trial in Lithuania using 85 open-pollinated families drawn from 17 populations reported narrow-sense heritability for juvenile height growth that in individual test plantations reached from 0.43 to 0.70, and h^2 of stem diameter reached 0.28 to 0.51 (Pliûra, 2004). In Experiment 4, the h^2 values for height increment in individual years and sites reached between 0.11 and 0.28. indicating substantial heritable variance which can be exploited in breeding and provenance/family selection. The former nursery planting effect often causes high heritable variation in height. The estimates in Experiment 4, based on annual increments, are generally

lower and more realistic. Other studies of black alder have addressed the heritability of phenological traits: for instance, bud burst timing and its plasticity have been found to have substantial broad-sense heritability under multiple temperature treatments (De Kort et al., 2014). In the study by Pliûra (2004), heritability estimates of bud flushing, frost resistance, and disease resistance are also presented. Because of its rapid growth and relatively early onset of flowering, black alder allows for progeny testing and early evaluation of provenances for both general and specific combining ability at an early stage of the breeding program (Onokpise and Hall, 1994).

6.3 Physiological Stress-Related Traits

Physiological traits provide valuable insights into the functional strategies and stress responses of forest trees. Unlike purely morphological or phenological traits, physiological traits respond more dynamically to environmental fluctuations and can reveal genotype-specific differences in acclimation capacity (Marguerit et al., 2014; Tao et al., 2021). The thesis examines needle pigment and needle water-related traits in Scots pine, and photosynthetic activity in European beech. Integrating these results to understand how physiological processes shape adaptive potential and resilience under variable climatic conditions.

6.3.1 Photosynthetic Pigments and Physiological Indicators

At the Nepomuk site in Experiment 1, chlorophylls and carotenoids showed low broad-sense heritability, indicating modest genetic control over pigment composition. Similar patterns were observed by Sigala et al. (2020), who reported provenance- and treatment-related pigment variation linked to differences in growth and survival, suggesting that pigment responses can influence plant fitness under water-limited conditions.

Photosynthetic pigment composition, particularly the balance between chlorophylls and carotenoids, plays a central role in drought tolerance by maintaining photosynthetic function and providing photoprotection in Scots pine (Semerci et al., 2017). Trees under drought stress that maintain higher chlorophyll levels while increasing the carotenoid-to-chlorophyll ratio can better protect their photosystems, sustaining carbon assimilation and improving water-use efficiency during acclimation (Semerci et al., 2017). Among pigment traits in Experiment 1, car:chl T showed the strongest genetic signal, suggesting that this metric could capture underlying genetic influences more effectively than individual pigments.

At the Plasy site, lower or non-significant heritability estimates likely reflected greater environmental heterogeneity and smaller sample size, both known to reduce statistical power (Visscher and Goddard, 2015). However, pooling data across sites increased precision, and car:chl T exhibited high genetic correlation between environments, indicating minimal G×E and a stable clonal ranking in this ratio.

The ecological relevance of car:chl T is well established: it responds sensitively to light intensity, and reflects acclimation strategies during plant development (Demmig-Adams and Adams, 1996; García-Plazaola et al., 2012). Moreover, the seasonal dynamics of the spectrally

detected car:chl T ratio closely tracked photosynthetic activity in lodgepole pine (*Pinus contorta*, Dougl.), under both controlled and field conditions (Gamon et al., 2016). With advances in hyperspectral imaging, this ratio can now be measured non-destructively and at scale (Gitelson, 2020; Song and Wang, 2022; Sonobe et al., 2020), making it a robust, heritable, and scalable marker for monitoring physiological performance and incorporating stress resilience into breeding strategies.

6.3.2 Water Use Stress-Related Traits

Water-related traits in Experiment 1 showed clear genetic control but generally lower heritability estimates than structural traits. However, anatomical adjustments such as shorter needles, modified mesophyll-to-phloem ratios, and reduced needle surface area can limit transpiration and improve water retention under recurrent drought (Bachofen et al., 2021), highlighting the close link between structural and water-related traits. Among the traits assessed, NWC exhibited the highest heritability, indicating meaningful genetic variation in water retention capacity. However, the values remained moderate, consistent with earlier reports for other pine species such as maritime pine (*Pinus pinaster* Ait.) (Marguerit et al., 2014). Overall, needle water-related traits can serve as useful indicators of drought strategies and recovery potential in pine species (Bachofen et al., 2021; Bhusal et al., 2021), including Scots pine (Rehschuh et al., 2020), and, when heritable, may be integrated into breeding programs targeting drought resilience.

Estimates of type B genetic correlations further illustrate the stability of trait expression across environments. Structural traits such as LMA and EWT showed high type B values, indicating low genotype × environment interaction and stable clonal performance across sites. In contrast, NWC exhibited slightly lower type B correlations, suggesting greater site-specific variability. These patterns align with previous findings on variation in needle morphology and physiology in Scots pine (Donnelly et al., 2016) and support the potential for selecting stable, heritable traits under variable environmental conditions.

6.3.3 Photosynthetic Activity Related to Altitude of Origin

Several studies have examined the photosynthetic performance of European beech provenances originating from different altitudes, often in contexts where elevation is confounded with cardinal direction (eg, Kučerová et al., 2018; Pšidová et al., 2018; Robson et al., 2013, 2012).

In such cases, the effects of altitude can be difficult to separate from latitude and longitude. In contrast, in Experiment 2, provenance subgroups were sampled from the same mountain ranges with minimal geographic distance between them, allowing us to attribute physiological differences primarily to altitudinal origin.

Chlorophyll fluorescence (ChlF) parameters are widely used to detect early stress responses before growth decline becomes apparent (Faseela et al., 2020; Fiorani and Schurr, 2013). Among these, DI_0/RC and F_v/F_m are common drought and temperature stress indicators (Fghire et al., 2015; Mathur et al., 2013; Yuan et al., 2013), though F_v/F_m is relatively robust and can be less sensitive than other parameters (Bussotti et al., 2020). Since the measurements in this experiment were made under non-stressed conditions, the observed variation in ChlF parameters primarily reflected provenance differentiation and post-replanting vitality rather than stress per se.

Within the Italian provenances, four ChlF parameters, DI_0/RC, φ_{R0}, PI_{TOTAL}, and ΔV_{IP}, differentiated subgroups along the altitudinal gradient. High-altitude subgroups exhibited higher φ_{R0}, PI_{TOTAL}, and ΔV_{IP}, whereas low-altitude subgroups showed higher DI_0/RC. Of these, DI_0/RC was the most discriminating, distinguishing both between altitudinal subgroups and between the two Danish provenances. The ΔV_{IP} parameter was of particular interest, as it reflects the loss of PSI reaction centers during the I–P phase (Oukarroum et al., 2009), which has not been extensively explored in European beech. Previous work has also highlighted F_v/F_m and ΔV_{IP} as sensitive indicators of photosynthetic efficiency and responses to environmental stress (Bussotti et al., 2020).

Findings from this experiment align with previous studies reporting mechanistic differences in ChlF kinetics among beech provenances. Kučerová et al. (2018) observed that Austrian and Polish provenances differed in F_v/F_m, while Pšidová et al. (2018) found lower ABS/RC and ψ_0 in lower-altitude provenances during heatwaves. Higher-altitude provenances showed better PSII photochemical performance (PI_{ABS}) under both dry and wet conditions. Similarly, Kurjak et al. (2019) reported that provenances from colder, wetter regions exhibited higher PSII performance than those from warmer, drier sites, with performance decreasing toward the northwestern margins. These patterns mirror the results of Experiment 2, where altitude and latitude-related differences were clearly reflected in ChlF parameters.

Gas exchange (GE) measurements provided complementary insights. Two GE parameters, LSP_{95} and P_N, effectively distinguished provenances from different Italian mountain ranges (Aspromonte vs. Sila Grande), but did not reflect an altitudinal trend. This differs from the findings of Kučerová et al. (2018), who observed a linear altitudinal effect on CO_2 assimilation across geographically distant Central European provenances, but where also latitude and longitude likely contributed to these observed differences. In Experiment 2, Aspromonte provenances exhibited higher LSP_{95} and P_N values than Sila Grande, suggesting local adaptation to their respective light and climate regimes.

Previous work shows that shade-adapted plants have lower light saturation points (Meng et al., 2014), although post-disturbance light release can reduce differences between shade-grown and sun-grown seedlings (Reynolds et al., 2003). Moreover, Čater and Levanič (2019) reported reduced shade tolerance and higher photosynthetic efficiency in southern beech populations, consistent with the observation of higher LSP_{95} in the more southerly Aspromonte provenances.

Taken together, the ChlF and GE data highlight complementary patterns of provenance differentiation. While ChlF captured altitudinal and latitudinal differences in PSII performance, GE traits distinguished provenances based on geographical origin. These findings demonstrate how integrating both approaches can reveal fine-scale variation in photosynthetic strategy, potentially linked to local adaptation and climate-of-origin effects.

However, some limitations to this experiment need to be stated. Firstly, only two provenances from Calabria, representing beech refugia, which we separated into two distinct altitudinal subgroups, and two local Danish provenances were used. Secondly, the sample size of GE measurements was smaller than that of ChlF measurements due to the extensive time consumption of the GE method. And thirdly, the experiment did not involve any stress treatment or biomass measurements, which would also be beneficial in understanding the well-being of replanted trees in new conditions.

6.4 Remote Sensing-Based Phenotyping and Spectral Reflectance

High-resolution spectroscopy can detect fine-scale trait variation, providing valuable insight into underlying genetic differences (C. Li et al., 2023). By capturing this variation spatially, spectral data can help assess the evolutionary potential of populations to adapt to environmental change. For example, studies on apple trees under drought stress have reported high broad-sense heritability for several multispectral vegetation indices, demonstrating their potential to capture genetic variation in physiological responses (Coupel-Ledru et al., 2019; Virlet et al., 2015).

6.4.1 Genetic Variation in Canopy-Level and Needle-Level Reflectance

Studies on Scots pine and slash pine (*Pinus elliottii* Engelm.) conducted under variable field conditions and using half-sib structures have generally reported low narrow-sense heritability estimates (Čepl et al., 2018; Tao et al., 2021). Experiment 1 provides new insights into the broad-sense heritability of canopy-level reflectance in Scots pine, where estimates reached moderately high values. This represents one of the first assessments of canopy-level spectral heritability in forest trees under natural field conditions. Notably, heritability estimates were consistently higher at the canopy level than at the needle level, suggesting that integrating reflectance over larger spatial scales can buffer environmental noise and better reveal underlying genetic differences.

The results also revealed persistent heritable variation in the red edge and visible (VIS) spectral regions, in line with previous findings (Čepl et al., 2018). These regions are closely linked to pigment absorption and stress-related physiological processes (Čepl et al., 2018; Curran, 1989; Curran et al., 1995; Eitel et al., 2011), reinforcing their relevance as targets for genetic and evolutionary studies. The spatial and temporal consistency of heritability patterns in these spectral regions further supports their robustness as indicators of genetic variation. For example, the low heritability observed in the NIR region at the Nepomuk site corresponded with low heritability of NWC, illustrating the close functional link between spectral signals and physiological traits.

Finally, the significant clonal differentiation in spectral traits found in this experiment complements emerging evidence of genetic variation in foliar reflectance in other tree species, including interior spruce (*Picea engelmannii* × *glauca*) (Grubinger et al., 2025) and Fremont

cottonwood (Seeley et al., 2024). Together, these findings demonstrate that reflectance traits, particularly in the VIS and red edge regions, are heritable and likely capture adaptive variation relevant to stress tolerance and resource-use efficiency, traits that are expected to be under selection in a changing climate.

6.4.2 Robust Background Removal and Spectra-based Differentiation

Accurate background removal is a critical preprocessing step in HSI pipelines, particularly when applied to plant phenotyping. Unlike in phenotyping facilities, seedlings in nurseries are often imaged against non-uniform backgrounds, usually soil, which can vary in color, texture, and moisture content. This heterogeneity introduces noise and spectral overlap that can confound the reflectance signals associated with the target plant tissues (Faehn et al., 2024). Effective separation of the plant signal from the background is crucial to ensure that subsequent analyses capture true biological variation rather than artifacts introduced by the imaging environment (Mazis et al., 2020). Soil presents a particular challenge for image-based analyses due to its spectral complexity and the overlap of its reflectance properties with those of plant tissues at certain wavelengths, complicating accurate segmentation and trait extraction (Faehn et al., 2024). Moreover, the presence of algae or various weeds growing in the soil further complicates background removal by introducing additional spectral variability that can be misclassified as the target plant material. Addressing these issues requires carefully selecting segmentation strategies and thresholds to minimize misclassification and preserve data quality.

The proposed setup in Experiment 3 provided high spatial resolution, yielding multiple pixels across the width of a single needle of the imaged seedlings. This enabled the application of more stringent thresholding criteria during pixel removal, improving the accuracy of needle segmentation and minimizing the inclusion of background noise. Wavelengths in the NIR region proved to be the best for creating the mask applied for background removal. Minor imperfections in the initial masking were subsequently resolved through supervised classification. Similarly, Faehn et al. (2024) demonstrated the effectiveness of snapshot HSI combined with supervised classification to accurately differentiate root, soil, and root-soil interfaces, underscoring the importance of precise background separation in phenotyping pipelines. Overall, the complexity of soil backgrounds in nursery imaging necessitates robust and adaptive segmentation approaches to ensure that phenotypic trait quantification is accurate

and reliable, supporting downstream analyses in plant phenotyping and breeding programs (Bian et al., 2022).

The initial outputs of the proposed pipeline already provide a robust foundation for phenotypic analysis. The numeric spectral reflectance data allow for the initial estimation of spectral differences among seedlings. By extracting mean reflectance values per tray corresponding to seedling provenance and grouping these into three geographical origin regions, distinct spectral signatures that reflect geographical group-specific traits were observed. The subsequent calculation of the first derivative of these spectra further enhanced the accuracy of the differentiation among geographical groups in both VIS and NIR regions. These clear separations underscore the sensitivity of hyperspectral data to subtle phenological and physiological variations linked to climatic adaptation or genetic differentiation among populations. This finding aligns with previous research demonstrating that leaf reflectance spectra can effectively detect genetic variation and gene-by-environment interactions in tree populations, enabling the identification of population-specific physiological responses to environmental stresses (Corbin et al., 2024; Stejskal et al., 2023).

6.5 Trait-Based Patterns of Provenance Differentiation

6.5.1 European Beech Provenances Separated by Photosynthetic Parameters

Chlorophyll fluorescence (ChlF) and gas exchange (GE) provide valuable estimates of a tree's physiological status by capturing photosynthetic assimilation rates at the leaf level (Niinemets, 2010). In Experiment 2, significant differences were detected between Italian and Danish provenances in nearly all photosynthetic parameters. As hypothesized, Italian provenances exhibited higher values for both P_N (GE method) and PI_{TOTAL} (ChlF method), indicating stronger photosynthetic performance under Danish site conditions.

Within the Italian material, provenances from higher altitudes outperformed lower-altitude ones, achieving higher P_N and PI_{TOTAL} values. This pattern suggests that trees originating from cooler, harsher environments were better adapted to the colder and wetter Danish climate. This physiological advantage was accompanied by a higher survival rate in these provenances, particularly in SG1900, which showed the highest survival in 2018, surpassing even local Danish provenances. The later bud flushing of SG1900 in 2018 may have provided additional protection against spring frost, contributing to this survival advantage. In contrast, the two Aspromonte provenances showed lower survival rates that year. Between 2018 and 2020, survival rates across provenance subgroups remained stable, with minimal additional mortality (Table 4). The initially higher survival of Danish provenances likely reflects their local adaptation and the shorter transport time before planting compared to the Italian material.

While few studies have examined altitudinal differences within similar origins, several have reported latitudinal effects on photosynthetic performance. For instance, in a common garden study, southern beech provenances maintained higher net photosynthesis rates (P_N), water-use efficiency, and growth throughout the summer compared to northern ones (Robson et al., 2012). In contrast, a Romanian provenance displayed lower absolute P_N values than a Danish provenance under varying CO_2 conditions (Leverenz et al., 1999). Additionally, xeric provenances have shown faster post-drought P_N recovery (Arend et al., 2016), and provenance differences in GE and ChlF parameters are known to become more pronounced under drought stress (Aranda et al., 2015).

In the case of Experiment 2, the higher photosynthetic activity of Italian provenances likely reflects their phenological timing and adaptive origin, as southern provenances typically

sustain growth and assimilation later into the season. This interpretation aligns with previous findings that Danish beech provenances tend to cease growth earlier than those from southern Europe under similar climatic conditions (Nielsen and Jørgensen, 2003). Flushing was unfortunately not scored for the Danish plant material in 2018, so it can only be compared in 2020.

6.5.2 Hyperspectral Signatures Reveal Physiological Differentiation Among Scots Pine Origins

PLS-DA models based on classified images outperformed those relying solely on raw or 1st derivative spectral data, underscoring the importance of visual inspection, implementing biologically meaningful categories. The limited spectral separation among individual provenances is likely a result of their close genetic relatedness. Grouping by geographic region improves differentiation by capturing broader patterns of adaptive variation, as illustrated by the comparison between Figures 4 and 5.

The results demonstrate that HSI, particularly when combined with robust background removal and image-based classification, is highly effective for differentiating the geographic origins of European Scots pine seedlings. This aligns with findings from (Miettinen et al., 2025), where HSI was effectively used to monitor pigment dynamics and spatial patterns in Scots pine under water stress, demonstrating the power of imaging spectroscopy to reveal physiological and biochemical heterogeneity within plant tissues.

The northern European Scots pine seedlings exhibit higher reflectance in the red bands of the visible spectrum, which aligns well with findings by Pulkkinen et al. (2011) and (Linder, 1972) that mention that the red/reddish coloration in conifer seedlings is more common in northern origins and is associated with increased accumulation of pigments such as flavonoids and carotenoids, which contribute to photoprotection and frost hardiness. This pigmentation is an adaptive response to the harsh high-latitude light regimes characterized by long nights and low temperatures, mitigating oxidative stress through enhanced antioxidant capacity, as also supported by the phenolic and pigment accumulation dynamics described by Bogolitsyn et al. (2024), where ambient light and temperature were identified as key climatic factors influencing pigment and phenolic compound content in Scots pine needles. Furthermore, the physiological role of these pigments in photoprotection and their seasonal dynamics are supported by the pigment analyses and remote sensing study by D'Odorico et al. (2020) and Gamon et al.

(2016), where carotenoid pigment indices were used to reveal photosynthetic phenology in evergreen conifers, emphasizing the importance of pigment composition in seasonal adaptation.

Genetic differentiation and local adaptation among Scots pine populations are evident in regional variation, as shown by Bruxaux et al. (2024) and supported by physiological studies (Linder, 1972; Miettinen et al., 2025; Pulkkinen et al., 2011). Strong local adaptation in traits such as bud set and cold hardiness is evident (Savolainen et al., 2013, 2004), which likely modulates pigment biosynthesis pathways and thus spectral signatures. These adaptive traits are crucial for survival and phenological timing in different environments. The ability to distinguish these categories is particularly important for capturing phenological events such as autumn reddening and bud set. Autumn reddening in Scots pine seedlings, associated with anthocyanin accumulation, occurs during the time period linked to frost hardiness (Pulkkinen et al., 2011; Toivonen et al., 1991). However, the relationship between needle coloration and frost hardiness remains debated. Toivonen et al. (1991) found the connection to be inconclusive, suggesting that further research is needed. In contrast, Pulkkinen et al. (2011) observed that seedlings exhibiting reddish coloration in autumn of their first vegetation season showed higher survival rates and slightly greater productivity after 14 years of growing in field trials compared to their originally green counterparts. These findings suggest that autumn reddening may serve as a useful phenotypic marker for early selection in Scots pine breeding programs.

Apart from genetic factors, epigenetic mechanisms play a crucial role in conifers' adaptive capacity by modulating gene expression in response to environmental conditions without altering the DNA sequence. This transgenerational epigenetic memory, an adaptive phenotypic plasticity inherited during embryo development, influences key phenological traits such as bud burst, bud set, and cold acclimation (Bose et al., 2020; Fossdal et al., 2024; Yakovlev et al., 2012). To fully separate these epigenetic effects, seeds would need to develop under identical climatic conditions, a challenging long-term endeavor in natural settings. However, innovative approaches like the pollen-based assisted migration strategy proposed by Chludil et al. (2025) may provide promising frameworks to design controlled experiments that isolate these effects. Furthermore, the HTP pipeline could contribute to a novel assessment of this plasticity.

6.5.3 Provenance Variation and Local Adaptation in Black Alder Growth Performance

Provenance was a significant source of variation in height increment across sites and years; a pattern also reflected in the family rankings. When comparing provenances independently, material from clonal seed orchards and seed lots without defined family structures was also included. The provenance TRUE, derived from previously selected plus trees, consistently exhibited superior growth across sites and years. This indicated that even phenotypic selection, applied twice in this case, can effectively enhance growth performance in black alder even across a range of sites, as other provenances went only through one round of phenotypic selection. Similar results were reported in a breeding study on Chinese alder (*Alnus cremastogyne* Burkill), where significant variation in growth traits was observed both among and within provenances (Zheng et al., 2023). Additionally, the superior increment growth of the TRUE provenance aligns with the highly heritable, earlier bud burst, giving the trees from this provenance an earlier start of growth within the vegetation season. Rötzer et al. (2004) showed that the timing of bud burst can significantly influence tree growth: when bud burst occurs earlier under favorable environmental conditions, trees gain an extended period for leaf-based carbon assimilation and growth, which can translate into greater biomass accumulation over the season.

In contrast, trees originating from Swedish clonal seed orchards or seed/plus-tree stands performed poorly under Danish conditions when compared with local provenances. This suggests a degree of local adaptation in the Swedish material that is not advantageous under Danish environmental conditions. Comparable provenance-by-environment interactions have been observed in red alder across seed-transfer trials in North America, where populations performed best near their origin sites, leading to clear geographic clines in growth and survival and motivating the delineation of separate breeding/seed zones to minimize maladaptation (Hamann et al., 2000; Xie, 2008). Xie (2008) found latitudinal trends in 10-year volume and survival and recommended separate northern and southern breeding zones (boundary ≈ 52°N) to limit performance loss and increased mortality with seed transfer. Hamann et al. (2000) showed significant genotype × environment interactions at population and family levels, and demonstrated how geostatistical methods (kriging, PCA, GIS) can be used to map predicted performance and associated uncertainty, thereby deriving objective seed-transfer guidelines and probability-based seed-procurement zones. Among the Danish provenances in Experiment 4, those from the northwestern regions generally performed best, whereas the southern

provenances exhibited below-average height increments. This trend likely reflects the northern location of the experimental sites, which may favor local adaptation of northern provenances. Additionally, trees derived from Danish clonal seed orchards also performed very well, particularly the material from FP658.

6.5.3.1 General Performance of Provenances and Families Across the Environment

The LMM analyses revealed a significant family effect as well as a provenance effect, indicating that genetic differences play an important role in growth performance. Within each provenance, both superior and inferior families were identified, confirming the presence of substantial genetic variability that can be exploited for selection. This variability was further influenced by environmental conditions, as family rankings differed among the four test sites and across years with contrasting climatic conditions. Some families performed particularly well on nutrient-poor or drier sites, whereas others showed superior growth under more favorable conditions, highlighting strong genotype × environment interactions. This pattern aligns with evidence that alder growth and nitrogen-fixing performance are strongly modulated by soil conditions, including nutrient status and hydrology (Claessens et al., 2010). Overall, these results indicate that black alder populations harbor both adaptive genetic variation and phenotypic plasticity, traits that may underpin resilience to site heterogeneity and future climatic shifts.

Black alder is a pioneer, light-demanding species that regenerates and grows best on disturbed, moist substrates (floodplains, marshy or alluvial soils) and shows high early growth rates on such sites (Lukyanets et al., 2022). Among the test sites, trees growing at sites 504 and 506 generally exhibited larger seasonal increments, likely reflecting more favorable environmental conditions. These locations experienced higher soil moisture availability, which was particularly beneficial during the dry early summer of 2023. The year 2023 was notably dry, with minimal rainfall in April, May, and June, in contrast to the more favorable conditions observed in 2024, which likely contributed to differences in growth performance among sites and families (Figure 2). Site 504, situated in a natural habitat with high groundwater levels accessible to tree roots, and site 506, located further west with higher precipitation levels, especially compared to site 507 in eastern Denmark (Zealand). Black alder typically prefers wet, riparian, and waterlogged sites with access to high groundwater, where soil moisture is readily available and trees are less limited by precipitation deficits (Claessens et al., 2010;

Vacek et al., 2022). In contrast, sites 507 and 505 were established on sandy soil, providing poorer growth conditions due to their lower fertility and limited water-holding capacity. Its growth is also influenced by local factors such as soil type and previous land use, so stands with stable high groundwater or regular flooding generally show better adaptation to climatic extremes than sites with lower water access (Rodríguez-González et al., 2014).

Despite these findings providing valuable insights for future selection decisions, it remains too early to determine whether heritability estimates or family rankings have stabilized sufficiently to support fully reliable selection outcomes. Nonetheless, given the rapid growth and relatively early flowering of black alder, progeny evaluations can still be conducted relatively early in the breeding program, allowing identification of provenances with general and specific combining ability in the coming years (Onokpise and Hall, 1994). Continued monitoring over subsequent years will, however, be essential to confirm the consistency and robustness of these genetic patterns.

6.6 Genetic correlations

6.6.1 Genetic Correlation Between NFTs and Spectra

Genetic correlations are often attributed to pleiotropy, where a single gene influences multiple phenotypic traits (Mode and Robinson, 1959). This principle forms the basis for indirect selection in breeding programs, where improvement in one trait can lead to correlated responses in others. However, in forest trees, studies exploring genetic correlations between spectral reflectance and physiological traits remain limited.

In Experiment 1, significant genetic correlations were identified between needle-level reflectance and key needle functional traits (NFTs), particularly in the NIR and SWIR spectral regions. These patterns are consistent with findings in crop species, where reflectance data reliably capture structural and physiological variation. For example, Montes et al. (2022) demonstrated links between SLA and leaf nitrogen in soybean and hyperspectral signatures, revealing shared genetic loci that confirmed a pleiotropic basis. Similarly, in slash pine, genetic correlations were found between growth traits (height and canopy projection area) and multispectral indices, which varied seasonally (Y. Li et al., 2023).

The results of this experiment extend this evidence to Scots pine, showing that genetic correlations between LMA and reflectance in the NIR and SWIR regions likely reflect shared genetic control over needle structure and water status. These associations align with observations in Norway spruce, where pigment-related variation was strongly linked to SWIR (Hejtmánek et al., 2022), and with studies across multiple broadleaved and coniferous species demonstrating red-edge sensitivity to pigment content (Zhang et al., 2022). The SWIR region appears to integrate signals from both structural and biochemical components, reflecting overlapping absorption features of water and other leaf constituents.

There were also genetic correlations between canopy-level reflectance and physiological traits such as EWT and chl T_M. This is one of the first reports of significant genetic correlations using UAV-derived canopy spectra in a forest tree context. Previous studies have focused on leaf-level correlations, and no comparable UAV-based analysis has been documented for trees. In crop science, a similar approach by Feng et al. (2017) found genetic correlations between image-based reflectance indices and key agronomic traits in rice, including chlorophyll content.

6.6.2 Gene-by-Environment Interactions

6.6.2.1 Gene-by-Environment Interactions in Spectral Reflectance

In Experiment 1, using type B genetic correlations to quantify G×E interactions, reflectance in the VIS region was found to be highly consistent across both sites at canopy and needle scales. This pattern mirrors the stable VIS performance previously reported for multispectral indices in slash pine (Tao et al., 2021). Such stability suggests that pigment-associated spectral features are under robust genetic control, making them promising targets for operational breeding or physiological performance monitoring.

In contrast, type B genetic correlations in the NIR region were lower, indicating substantial genotype × environment interaction or site-specific genetic variation in this spectral range. Environmental effects on needle cellular structure, influenced by factors such as nutrient status, water availability, and soil characteristics, likely explain this variability (Buschmann et al., 2012; Granlund et al., 2018). The lower type B genetic correlation in the NIR could be explained by insignificant H^2 in LMA at the Nepomuk site, as LMA reflects the needle structure. The presence of a significant genetic correlation between LMA and NIR reflectance further supports this interpretation.

In the short-wave infrared (SWIR) region, needle-level reflectance around major water absorption bands (≈1440, 1900, and 2500 nm) exhibited very high but non-significant type B genetic correlations, indicating stable reflectance expression related to water content and suggesting minimal differences in water availability between sites. However, this pattern requires further validation with larger sample sizes to confirm its robustness.

At the among-population level, significant G×E interactions have been observed in spectral indices related to photosynthetic efficiency and water content in Populus (Corbin et al., 2024). These findings indicate that population-level differences may lead to distinct adaptive strategies when genotypes are exposed to contrasting environments.

6.6.2.2 Climatic and Soil Conditions Related to G×E in Black alder

The contrasting performance across the four test sites in Experiment 4 underscores the strong influence of edaphic and climatic gradients on G×E in black alder. Sites 505 and 507, which share similar soil properties and both exhibited relatively poor productivity, likely impose

greater constraints on growth (e.g., nutrient limitation or acidity). In contrast, the more favorable soil conditions at sites 504 and 506 allowed genotypes to more fully express their potential. The fact that family rankings significantly shift across these sites signals genuine G×E interactions, rather than mere scaling effects, consistent with observations in other forest tree systems (Li et al., 2017). In radiata pine, for example, rank changes are common across contrasting soils and climates, precisely because certain genotypes are specialized for narrower niches (Gapare et al., 2015).

In Experiment 4, the moisture availability defined the G×E patterns: sites 504 and 506 were wet, either due to soil (504) or climate (506) (and likely due to deeper rooting), whereas sites 505 and 507 were dry, imposing moisture stress on families with limited drought tolerance. Families that maintained relatively stable performance across this moisture gradient in these trials are candidates for broad adaptation, yet the rank changes observed indicate that no single family dominated across the full gradient. The data suggest that some families exhibit specialized adaptation to nutrient-poor or drier sites, whereas others display broader plasticity, performing reliably across a wider range of conditions.

This pattern (specialists performing well under specific stressful edaphic conditions while other genotypes show broader plasticity) matches findings from provenance and common-garden studies showing genotype × environment interactions and family-level differences in plasticity and stability in *Alnus* and other riparian trees (Baliuckas and Pliūra, 2008; Cooper et al., 2022). More generally, experimental and observational work across tree species confirms that reduced soil moisture dampens growth responses to favorable climatic conditions and highlights genotype-specific performance differences, implying that selection for broad adaptation should favor families with stable performance under variable soil moisture (Reich et al., 2018).

6.6.3 Age-to-Age Genetic Correlations

6.6.3.1 Spectral Reflectance Year-to-Year Genetic Correlations

Year-to-year genetic correlations offer valuable insight into the temporal stability of trait expression, providing a foundation for both breeding strategies and evolutionary inference. Such correlations indicate whether genetic rankings of individuals or clones remain stable over time, an essential criterion for selecting genotypes with consistent performance across variable environmental conditions (Hong et al., 2015).

The temporal stability of canopy-level reflectance in Experiment 1 was evaluated by estimating genetic correlations across two consecutive years at a single site. Significant, highly positive correlations were observed in both the VIS and NIR spectral regions, with slightly lower values in the NIR. This pattern indicates that relative genetic rankings of clones remained largely stable between years, supporting the reliability of these spectral traits for long-term monitoring and selection.

These results are consistent with previous findings in other species. For example, Song et al. (2024) documented stable genetic variation in reflectance-derived phenolic content within a growing season in slash pine, while El-Hendawy et al. (2022) demonstrated stable spectral predictions across years and developmental stages in wheat. Although temporal scales and species differ, these studies collectively highlight the potential of spectral traits to capture heritable variation that persists over time, making them valuable indicators for breeding and adaptive studies.

6.6.3.2 Age-to-Age Interactions in Growth Increment

Age-to-age genetic correlations provide valuable insight into the stability of provenance performance over time, particularly under variable site conditions. Differences in soil type and site history played a major role in shaping early growth dynamics in Experiment 4. Sites 507 and 505, both established on sandy soils with low fertility and limited water-holding capacity, exhibited low age-to-age correlations, retaining stable early growth rankings of generally poor increments under resource-limited conditions. Growth during this period may also have been shaped by local site characteristics, as stands with stable groundwater levels or regular flooding tend to show greater resilience to climatic extremes compared to those with limited water access (Rodríguez-González et al., 2014). This effect was particularly evident at site 505, a former conifer stand where legacy needle litter likely acidified the soil, further constraining early growth.

Patterns observed in 2023, a year marked by an exceptionally dry early summer, provided further evidence of age-to-age interactions. The response was especially pronounced at site 504, where changes in provenance rankings between years suggested differential drought tolerance among provenances. Provenances that improved or declined under these conditions may reflect genetic differences in drought response, which were more apparent at this otherwise wetter site. Provenances that improved or declined in ranking under these conditions

may indicate varying levels of drought tolerance, which was especially evident at this normally wetter site. These combined findings suggest the rank shifts observed in 2023 plausibly reflect genetic variation in drought tolerance among provenances, and they underscore the value of multi-site testing, including stressful years, for detecting adaptive differences (Hamann et al., 2000). Spring 2022 was also very dry, but since the trees were planted in 2022, the initial growth increment may still have been influenced by the nursery effect, which often affects early establishment and vigor as well. Therefore, the drought effect is harder to evaluate.

6.7 Novelties Related to Plant Phenotyping, Their Advantages and Limitations

6.7.1 Importance of Genomic Data in the Estimation of Genetic Parameters for Needle Functional Traits Related to Environmental Variation

Experiment 1 estimated the broad-sense heritability of multiple needle functional traits (NFTs) using clonal replications established in seed orchards across two experimental sites in 2021. To complement phenotypic analyses, genomic data obtained with a recently developed 50K SNP genotyping array were incorporated to better characterize genetic relationships among clones. Analysis revealed weak but non-negligible relatedness, likely resulting from the selection of related plus trees in natural regeneration stands. This structure was explicitly accounted for in the statistical models to avoid bias in parameter estimation. A stringent filtering strategy ensured the reliability of SNP data for constructing a robust GRM.

The inclusion of SNP-based genotyping was driven by the need to quantify realized genomic relatedness in Scots pine clones, where historical selection from natural stands has resulted in a lack of pedigree records. In such populations, pedigree-based approaches fail to capture hidden relatedness, which can bias estimates of heritability and genetic correlations (De Los Campos et al., 2015; Grattapaglia and Resende, 2011). By constructing a GRM from high-density SNP data, this experiment integrated genomic information into mixed-model frameworks, thereby increasing the precision and biological accuracy of quantitative genetic parameter estimates.

6.7.2 Novel Hyperspectral Imaging Setup: Advantages and Limitations

The newly proposed HIS setup in Experiment 3 offers several advantages for pine seedling phenotyping and shows great potential for broader use in other experimental plant studies. Its portability enables convenient transportation and on-site deployment, eliminating the need for extensive laboratory infrastructure and prolonged seedling transport. This mobility is especially advantageous for capturing phenotypic traits near experimental sites, such as tree nurseries, where timely and context-specific data acquisition is critical for accurate assessment. The spectral resolution of the Snapscan system allows effective discrimination between species, including separating target species from weeds, enhancing the accuracy of phenotyping and weed management strategies (Amziane et al., 2021; Liu et al., 2022). The

Snapscan camera provides high spatial resolution hyperspectral images, enabling detailed capture of seedling features at a fine scale. This high resolution supports precise analysis of morphological and spectral characteristics, which is essential for distinguishing subtle differences among narrow conifer needles.

However, some disadvantages are associated with the Snapscan camera. The multishot acquisition process, which involves successive frame captures, can be sensitive to illumination variations during image acquisition, potentially affecting reflectance estimation and spectral consistency (Amziane et al., 2021). Although methods exist to mitigate these effects, such as frame-level illumination estimation, these add complexity to data processing. Furthermore, the acquisition time may limit its use in highly dynamic or large-scale field conditions. Despite these limitations, the Snapscan camera remains a robust and versatile tool for detailed phenotyping of plants and tree seedlings, combining mobility, high spatial resolution, and spectral discrimination capabilities crucial for advanced plant research.

6.7.3 Automated Bud Set Detection in Scots Pine

The proposed macro script for automated terminal bud counting represents a substantial advancement in the phenotyping of Scots pine seedlings. By leveraging classified hyperspectral images, this macro achieves a high accuracy rate of 93 %, significantly reducing the labor and subjectivity associated with manual bud counting. This is particularly important in large-scale phenotyping experiments, where manual methods are not only time-consuming but also susceptible to observer bias, potentially affecting the reproducibility and reliability of results.

The macro's visualization output, which highlights classified bud pixels, enhances transparency and allows users to verify the accuracy of the automated classification. The ability to adjust filtering conditions further increases the macro's utility, enabling its application across different developmental stages and potentially extending its use to other species with varying bud morphologies. This adaptability is crucial, as phenological traits such as bud set and frost hardiness are not only important for understanding local adaptation but also for breeding programs aimed at improving resilience to climate change (Pulkkinen et al., 2011).

Integrating automated image-based phenotyping tools, such as this macro, aligns with broader trends in plant phenotyping research, where HTP platforms are increasingly used to collect quantitative data on key traits at scale (Bian et al., 2022; Omari et al., 2020; Pieruschka and

Schurr, 2019). These technologies facilitate the collection of large, reproducible datasets necessary for genetic association studies, quantitative trait locus mapping, and the development of climate-resilient tree populations.

Altogether, this innovation offers a robust and scalable tool that not only facilitates large-scale, reproducible phenotyping of bud set in Scots pine, which could strengthen both basic research on climatic adaptation and applied breeding programs aimed at enhancing the resilience and productivity of coniferous forest resources.

7 Conclusions

This thesis demonstrates how advanced phenotyping and modern genomic approaches can substantially improve genetic evaluation in forest trees. Across Scots pine, European beech, and black alder, results revealed significant genetic variation in key adaptive traits, particularly phenology and pigment-related spectral features, while growth and water-use traits showed greater environmental sensitivity.

Hyperspectral reflectance proved to be a powerful tool for detecting heritable variation at both needle and canopy levels. VIS and red-edge reflectance exhibited stable genetic signals, whereas NIR and SWIR were more environmentally responsive, reflecting structural and water-related processes. In addition to applying established methods, this work introduced a new hyperspectral imaging setup for high-throughput trait assessment and a bud count macro, enabling precise and more automated phenology measurements.

Incorporating SNP-based genomic information improved the accuracy of genetic parameter estimation by capturing previously hidden relatedness in clonal seed orchard populations. Phenological traits emerged as particularly robust indicators of local adaptation, while physiological and structural traits highlighted both heritable components and plastic responses, underlining their importance for resilience under changing climates.

Together, these studies provide an integrated framework linking forest genetics and physiology along environmental gradients. By combining classical quantitative genetics with spectral and physiological phenotyping, this work identifies reliable trait targets for breeding and management and improves predictions of adaptive responses to future climatic shifts. This trait-based, integrative approach, strengthened by novel imaging and phenotyping tools, supports the development of resilient and adaptive forest tree populations.

8 References

Adams, W.W., Winter, K., Schreiber, U., Schramel, P., 1990. Photosynthesis and Chlorophyll Fluorescence Characteristics in Relationship to Changes in Pigment and Element Composition of Leaves of Platanus occidentalis L. during Autumnal Leaf Senescence. Plant Physiol 93, 1184–1190. https://doi.org/10.1104/pp.92.4.1184

Aitken, S.N., Whitlock, M.C., 2013. Assisted Gene Flow to Facilitate Local Adaptation to Climate Change. Annu. Rev. Ecol. Evol. Syst. 44, 367–388. https://doi.org/10.1146/annurev-ecolsys-110512-135747

Aitken, S.N., Yeaman, S., Holliday, J.A., Wang, T., Curtis-McLane, S., 2008. Adaptation, migration or extirpation: climate change outcomes for tree populations. Evol Appl 1, 95–111. https://doi.org/10.1111/j.1752-4571.2007.00013.x

Akinyemi, O.O., Čepl, J., Keski-Saari, S., Tomášková, I., Stejskal, J., Kontunen-Soppela, S., Keinänen, M., 2023. Derivative-based time-adjusted analysis of diurnal and within-tree variation in the OJIP fluorescence transient of silver birch. Photosynthesis Research. https://doi.org/10.1007/s11120-023-01033-x

Alberto, F.J., Aitken, S.N., Alía, R., González-Martínez, S.C., Hänninen, H., Kremer, A., Lefèvre, F., Lenormand, T., Yeaman, S., Whetten, R., Savolainen, O., 2013. Potential for evolutionary responses to climate change – evidence from tree populations. Global Change Biology 19, 1645–1661. https://doi.org/10.1111/gcb.12181

Albrechtová, J.;, Kupková, L., Campbell, P.K.E., 2017. Hodnocení stavu smrkových porostů. - Případové studie sledování vývoje fyziologického stavu smrkových porostů v Krušných horách v letech 1998–2013. Geographica - Česká geografická společnost.

Ammer, C., Bickel, E., Kölling, C., 2008. Converting Norway spruce stands with beech - A review of arguments and techniques. Austrian Journal of Forest Science 125, 3–26.

Amziane, A., Losson, O., Mathon, B., Dumenil, A., Macaire, L., 2021. Reflectance Estimation from Multispectral Linescan Acquisitions under Varying Illumination—Application to Outdoor Weed Identification. Sensors 21, 3601. https://doi.org/10.3390/s21113601

Aranda, I., Cano, F.J., Gascó, A., Cochard, H., Nardini, A., Mancha, J.A., López, R., Sánchez-Gómez, D., 2015. Variation in photosynthetic performance and hydraulic architecture across European beech (Fagus sylvatica L.) populations supports the case for local adaptation to water stress. Tree Physiology 35, 34–46. https://doi.org/10.1093/treephys/tpu101

Araus, J.L., Cairns, J.E., 2014. Field high-throughput phenotyping: the new crop breeding frontier. Trends in Plant Science 19, 52–61. https://doi.org/10.1016/j.tplants.2013.09.008

Arend, M., Sever, K., Pflug, E., Gessler, A., Schaub, M., 2016. Seasonal photosynthetic response of European beech to severe summer drought: Limitation, recovery and post-drought stimulation. Agricultural and Forest Meteorology 220, 83–89. https://doi.org/10.1016/j.agrformet.2016.01.011

Arroyo-Mora, J.P., Kalacska, M., Løke, T., Schläpfer, D., Coops, N.C., Lucanus, O., Leblanc, G., 2021. Assessing the impact of illumination on UAV pushbroom hyperspectral imagery collected under various cloud cover conditions. Remote Sensing of Environment 258, 112396. https://doi.org/10.1016/j.rse.2021.112396

Bachofen, C., Perret-Gentil, A., Wohlgemuth, T., Vollenweider, P., Moser, B., 2021. Phenotypic plasticity versus ecotypic differentiation under recurrent summer drought in two drought-tolerant pine species. Journal of Ecology 109, 3861–3876. https://doi.org/10.1111/1365-2745.13762

Baker, N.R., Rosenqvist, E., 2004. Applications of chlorophyll fluorescence can improve crop production strategies: an examination of future possibilities. Journal of Experimental Botany 55, 1607–1621. https://doi.org/10.1093/jxb/erh196

Bakys, R., Vasaitis, R., Barklund, P., Thomsen, I.M., Stenlid, J., 2009. Occurrence and pathogenicity of fungi in necrotic and non-symptomatic shoots of declining common ash (Fraxinus excelsior) in Sweden. Eur J Forest Res 128, 51–60. https://doi.org/10.1007/s10342-008-0238-2

Baliuckas, V., Pliūra, A., 2008. Phenogenetic variation pattern in adaptive traits of *Betula pendula, Alnus glutinosa* and *Quercus robur* in Lithuania. Biologija 54, 60–65. https://doi.org/10.2478/v10054-008-0012-x

Baranoski, G., Rokne, J., 2005. A practical approach for estimating the red edge position of plant leaf reflectance. International Journal of Remote Sensing - INT J REMOTE SENS 26, 503–521. https://doi.org/10.1080/01431160512331314029

Basler, D., Körner, C., 2014. Photoperiod and temperature responses of bud swelling and bud burst in four temperate forest tree species. Tree Physiology 34, 377–388. https://doi.org/10.1093/treephys/tpu021

Bednářová, E., Merklová, L., 2007. Results of monitoring the vegetative phenological phases of European beech (Fagus sylvatica L.) in 1991-2006 34, 77–85.

Bernardo, R., 2020. Reinventing quantitative genetics for plant breeding: something old, something new, something borrowed, something BLUE. Heredity 125, 375–385. https://doi.org/10.1038/s41437-020-0312-1

Bhat, S.S., Singh, N.B., Sankhyan, H.P., Sharma, K.R., 2016. Variability studies for needle and wood traits of different half sib progenies of Pinus roxburghii Sargent. Physiol Mol Biol Plants 22, 231–239. https://doi.org/10.1007/s12298-016-0358-y

Bhusal, N., Lee, M., Lee, H., Adhikari, A., Han, A.R., Han, A., Kim, H.S., 2021. Evaluation of morphological, physiological, and biochemical traits for assessing drought resistance in eleven tree species. Science of The Total Environment 779, 146466. https://doi.org/10.1016/j.scitotenv.2021.146466

Bian, L., Zhang, H., Ge, Y., Čepl, J., Stejskal, J., EL-Kassaby, Y.A., 2022. Closing the gap between phenotyping and genotyping: review of advanced, image-based phenotyping technologies in forestry. Annals of Forest Science 79, 22. https://doi.org/10.1186/s13595-022-01143-x

Bilir, N., Ozbey, A.A., 2022. Growth performances of seed sources in a progeny trial of Pinus brutia Ten.: Growth performances in a progeny trial of Pinus brutia Ten. REFOR 1–6. https://doi.org/10.21750/REFOR.13.01.94

Bjelke, U., Boberg, J., Oliva, J., Tattersdill, K., Mckie, B.G., 2016. Dieback of riparian alder caused by the Phytophthora alni complex: Projected consequences for stream ecosystems. Freshwater Biology. https://doi.org/10.1111/fwb.12729

Bogolitsyn, K.G., Gusakova, M.A., Krasikova, A.A., Khviyuzov, S.S., Samsonova, N.A., Selivanova, N.V., Pustynnaya, M.A., 2024. Dynamics of the processes of formation and accumulation of phenolic and pigment complexes in the needles of pine Pinus sylvestris. Plant Physiol. Rep. 29, 385–394. https://doi.org/10.1007/s40502-024-00795-3

Bolte, A., Czajkowski, T., Kompa, T., 2007. The north-eastern distribution range of European beech - A review. Forestry 80, 413–429. https://doi.org/10.1093/forestry/cpm028

Bose, A.K., Moser, B., Rigling, A., Lehmann, M.M., Milcu, A., Peter, M., Rellstab, C., Wohlgemuth, T., Gessler, A., 2020. Memory of environmental conditions across generations affects the acclimation potential of scots pine. Plant Cell & Environment 43, 1288–1299. https://doi.org/10.1111/pce.13729

Brichta, J., Vacek, S., Vacek, Z., Cukor, J., Mikeska, M., Bílek, L., Šimůnek, V., Gallo, J., Brabec, P., 2023. Importance and potential of Scots pine (L.) in 21 century. Central European Forestry Journal 69, 3–20. https://doi.org/doi:10.2478/forj-2022-0020

Broome, A., Ray, D., Mitchell, R., Harmer, R., 2019. Responding to ash dieback (*Hymenoscyphus fraxineus*) in the UK: woodland composition and replacement tree species. Forestry: An International Journal of Forest Research 92, 108–119. https://doi.org/10.1093/forestry/cpy040

Bruxaux, J., Zhao, W., Hall, D., Curtu, A.L., Androsiuk, P., Drouzas, A.D., Gailing, O., Konrad, H., Sullivan, A.R., Semerikov, V., Wang, X., 2024. Scots pine – panmixia and the elusive signal of genetic adaptation. New Phytologist 243, 1231–1246. https://doi.org/10.1111/nph.19563

Buraczyk, W., Tulik, M., Konecka, A., Szeligowski, H., Czacharowski, M., Będkowski, M., 2022. Does leaf mass per area (LMA) discriminate natural pine populations of different origins? Eur J Forest Res 141, 1177–1187. https://doi.org/10.1007/s10342-022-01500-5

Buras, A., Menzel, A., 2019. Projecting Tree Species Composition Changes of European Forests for 2061–2090 Under RCP 4.5 and RCP 8.5 Scenarios. Front. Plant Sci. 9. https://doi.org/10.3389/fpls.2018.01986

Burdon, R., 1977. Burdon RD. Genetic correlation as a concept for studying genotype-environment interaction in forest tree breeding. Silvae Genet 26: 168-175. Silvae Genetica 26, 168–175.

Busch, F.A., Ainsworth, E.A., Amtmann, A., Cavanagh, A.P., Driever, S.M., Ferguson, J.N., Kromdijk, J., Lawson, T., Leakey, A.D.B., Matthews, J.S.A., Meacham-Hensold, K., Vath, R.L., Vialet-Chabrand, S., Walker, B.J., Papanatsiou, M., 2024. A guide to photosynthetic gas exchange measurements: Fundamental principles, best practice and potential pitfalls. Plant Cell & Environment 47, 3344–3364. https://doi.org/10.1111/pce.14815

Buschmann, C., Lenk, S., Lichtenthaler, H.K., 2012. Reflectance spectra and images of green leaves with different tissue structure and chlorophyll content. Israel Journal of Plant Sciences 60, 49–64. https://doi.org/10.1560/IJPS.60.1-2.49

Bussotti, F., Desotgiu, R., Pollastrini, M., Cascio, C., 2010. The JIP test: A tool to screen the capacity of plant adaptation to climate change. Scandinavian Journal of Forest Research 25, 1–8. https://doi.org/10.1080/02827581.2010.485777

Bussotti, F., Gerosa, G., Digrado, A., Pollastrini, M., 2020. Selection of chlorophyll fluorescence parameters as indicators of photosynthetic efficiency in large scale plant ecological studies. Ecological Indicators 108. https://doi.org/10.1016/j.ecolind.2019.105686

Butler, D., Cullis, B., Gilmour, A., Gogel, B., Thompson, R., 2017. ASReml-R reference manual version 4. VSN International Ltd, Hemel Hempstead, HP1 1ES, UK.

Butler, D.G., Cullis, B.R., Gilmour, A.R., Gogel, B.J., 2009. ASReml estimates variance components under a general linear mixed model by residual maximum likelihood (REML).

Butler, D.G., Cullis, B.R., Gilmour, A.R., Gogel, B.J., Thompson, R., 2018. ASReml-R Reference Manual Version 4 ASReml estimates variance components under a general linear mixed model by residual maximum likelihood (REML).

Caballero, A., 2020. Quantitative genetics. Cambridge university press, Cambridge, United Kingdom.

Calleja-Rodriguez, A., Andersson Gull, B., Wu, H.X., Mullin, T.J., Persson, T., 2019. Genotype-by-environment interactions and the dynamic relationship between tree vitality and height in northern Pinus sylvestris. Tree Genetics & Genomes 15, 36. https://doi.org/10.1007/s11295-019-1343-8

Campbell, P.K.E., Huemmrich, K.F., Middleton, E.M., Ward, L.A., Julitta, T., Daughtry, C.S.T., Burkart, A., Russ, A.L., Kustas, W.P., 2019. Diurnal and Seasonal Variations in Chlorophyll Fluorescence Associated with Photosynthesis at Leaf and Canopy Scales. Remote Sensing 11, 488. https://doi.org/10.3390/rs11050488

Castillo, E.M. del, Zang, C.S., Buras, A., Hacket-Pain, A., Esper, J., Serrano-Notivoli, R., Hartl, C., Weigel, R., Klesse, S., Dios, V.R. de, Scharnweber, T., Dorado-Liñán, I., Maaten-Theunissen, M. van der, Maaten, E. van der, Jump, A., Mikac, S., Banzragch, B.E., Beck, W., Cavin, L., Claessens, H., Čada, V., Čufar, K., Dulamsuren, C., Gričar, J., Gil-Pelegrín, E., Janda, P., Kazimirovic, M., Kreyling, J., Latte, N., Leuschner, C., Longares, L.A., Menzel, A., Merela, M., Motta, R., Muffler, L., Nola, P., Petritan, A.M., Petritan, I.C., Prislan, P., Rubio-Cuadrado, Á., Rydval, M., Stajić, B., Svoboda, M., Toromani, E., Trotsiuk, V., Wilmking, M., Zlatanov, T., Luis, M. de, 2022. Climate-change-driven growth decline of European beech forests. Communications Biology 5. https://doi.org/10.1038/s42003-022-03107-3

Čater, M., Levanič, T., 2019. Beech and silver fir's response along the Balkan's latitudinal gradient. Scientific Reports 9. https://doi.org/10.1038/s41598-019-52670-z

Cavender-Bares, J., Gamon, J.A., Townsend, P.A. (Eds.), 2020. Remote Sensing of Plant Biodiversity. Springer International Publishing, Cham. https://doi.org/10.1007/978-3-030-33157-3

Cavender-Bares, J., Meireles, J.E., Couture, J.J., Kaproth, M.A., Kingdon, C.C., Singh, A., Serbin, S.P., Center, A., Zuniga, E., Pilz, G., Townsend, P.A., 2016. Associations of leaf spectra with genetic and phylogenetic variation in oaks: Prospects for remote detection of biodiversity. Remote Sensing 8. https://doi.org/10.3390/rs8030221

Čepl, J., Holá, D., Stejskal, J., Korecký, J., Kočová, M., Lhotáková, Z., Tomášková, I., Palovská, M., Rothová, O., Whetten, R.W., Kaňák, J., Albrechtová, J., Lstibůrek, M., 2016. Genetic variability and heritability of chlorophyll a fuorescence parameters in

Scots pine (Pinus sylvestris L.). Tree Physiology 36, 883–895. https://doi.org/10.1093/treephys/tpw028

Čepl, J., Stejskal, J., Lhotáková, Z., Holá, D., Korecký, J., Lstibůrek, M., Tomášková, I., Kočová, M., Rothová, O., Palovská, M., Hejtmánek, J., Krejzková, A., Gezan, S., Whetten, R., Albrechtová, J., 2018. Heritable variation in needle spectral reflectance of Scots pine (Pinus sylvestris L.) peaks in red edge. Remote Sensing of Environment 219, 89–98. https://doi.org/10.1016/j.rse.2018.10.001

Chakraborty, D., Ciceu, A., Ballian, D., Benito Garzón, M., Bolte, A., Bozic, G., Buchacher, R., Čepl, J., Cremer, E., Ducousso, A., Gaviria, J., George, J.P., Hardtke, A., Ivankovic, M., Klisz, M., Kowalczyk, J., Kremer, A., Lstibůrek, M., Longauer, R., Mihai, G., Nagy, L., Petkova, K., Popov, E., Schirmer, R., Skrøppa, T., Solvin, T.M., Steffenrem, A., Stejskal, J., Stojnic, S., Volmer, K., Schueler, S., 2024. Assisted tree migration can preserve the European forest carbon sink under climate change. Nat. Clim. Chang. 14, 845–852. https://doi.org/10.1038/s41558-024-02080-5

Chen, Z.-Q., Karlsson, B., Lundqvist, S.-O., García Gil, M.R., Olsson, L., Wu, H.X., 2015. Estimating solid wood properties using Pilodyn and acoustic velocity on standing trees of Norway spruce. Annals of Forest Science 72, 499–508. https://doi.org/10.1007/s13595-015-0458-9

Chludil, D., Čepl, J., Steffenrem, A., Stejskal, J., Sagariya, C., Pook, T., Schueler, S., Korecký, J., Almqvist, C., Chakraborty, D., Berlin, M., Lstibůrek, M., 2025. A Pollen-Based Assisted Migration for Rapid Forest Adaptation. Global Change Biology 31, e70014. https://doi.org/10.1111/gcb.70014

Chmura, Daniel J., Chmura, D. J., Roz, R., Kowski, ·, 2002. Variability of beech provenances in spring and autumn phenology, Silvae Genetica.

Claessens, H., Oosterbaan, A., Savill, P., Rondeux, J., 2010. A review of the characteristics of black alder (Alnus glutinosa (L.) Gaertn.) and their implications for silvicultural practices. Forestry 83, 163–175. https://doi.org/10.1093/forestry/cpp038

Climent, J., Alía, R., Karkkainen, K., Bastien, C., Benito-Garzon, M., Bouffier, L., De Dato, G., Delzon, S., Dowkiw, A., Elvira-Recuenco, M., Grivet, D., González-Martínez, S.C., Hayatgheibi, H., Kujala, S., Leplé, J.-C., Martín-Sanz, R.C., De Miguel, M., Monteverdi, M.C., Mutke, S., Plomion, C., Ramírez-Valiente, J.A., Sanchez, L., Solé-Medina, A., Soularue, J.-P., Steffenrem, A., Teani, A., Westin, J., Whittet, R., Wu, H., Zas, R., Cavers, S., 2024. Trade-offs and Trait Integration in Tree Phenotypes: Consequences for the Sustainable Use of Genetic Resources. Curr. For. Rep. 10, 196–222. https://doi.org/10.1007/s40725-024-00217-5

Cloutier, M., Germain, M., Laliberté, E., 2024. Influence of temperate forest autumn leaf phenology on segmentation of tree species from UAV imagery using deep learning. Remote Sensing of Environment 311, 114283. https://doi.org/10.1016/j.rse.2024.114283

Cooper, H.F., Best, R.J., Andrews, L.V., Corbin, J.P.M., Garthwaite, I., Grady, K.C., Gehring, C.A., Hultine, K.R., Whitham, T.G., Allan, G.J., 2022. Evidence of climate-driven selection on tree traits and trait plasticity across the climatic range of a riparian foundation species. Molecular Ecology 31, 5024–5040. https://doi.org/10.1111/mec.16645

Corbin, J.P.M., Best, R.J., Garthwaite, I.J., Cooper, H.F., Doughty, C.E., Gehring, C.A., Hultine, K.R., Allan, G.J., Whitham, T.G., 2024. Hyperspectral Leaf Reflectance Detects Interactive Genetic and Environmental Effects on Tree Phenotypes, Enabling Large-Scale Monitoring and Restoration Planning Under Climate Change. Plant Cell & Environment pce.15263. https://doi.org/10.1111/pce.15263

Coupel-Ledru, A., Pallas, B., Delalande, M., Boudon, F., Carrié, E., Martinez, S., Regnard, J.-L., Costes, E., 2019. Multi-scale high-throughput phenotyping of apple architectural and functional traits in orchard reveals genotypic variability under contrasted watering regimes. Hortic Res 6, 52. https://doi.org/10.1038/s41438-019-0137-3

Croft, H., Chen, J.M., Zhang, Y., 2014. The applicability of empirical vegetation indices for determining leaf chlorophyll content over different leaf and canopy structures. Ecological Complexity 17, 119–130. https://doi.org/10.1016/j.ecocom.2013.11.005

Čufar, K., Luis, M. de, Saz, M.A., Črepinšek, Z., Kajfež-Bogataj, L., 2012. Temporal shifts in leaf phenology of beech (Fagus sylvatica) depend on elevation. Trees - Structure and Function 26, 1091–1100. https://doi.org/10.1007/s00468-012-0686-7

Curran, P.J., 1989. Remote sensing of foliar chemistry. Remote Sensing of Environment 30, 271–278. https://doi.org/10.1016/0034-4257(89)90069-2

Curran, P.J., Windham, W.R., Gholz, H.L., 1995. Exploring the relationship between reflectance red edge and chlorophyll concentration in slash pine leaves. Tree Physiology 15, 203–206. https://doi.org/10.1093/treephys/15.3.203

Danusevicius, D., Masaitis, G., Mozgeris, G., 2014. Visible and near infrared hyperspectral imaging reveals significant differences in needle reflectance among Scots pine provenances. Silvae Genetica 63, 169–180. https://doi.org/10.1515/sg-2014-0022

De Kort, H., Vandepitte, K., Bruun, H.H., Closset-Kopp, D., Honnay, O., Mergeay, J., 2014. Landscape genomics and a common garden trial reveal adaptive differentiation to temperature across Europe in the tree species *Alnus glutinosa*. Molecular Ecology 23, 4709–4721. https://doi.org/10.1111/mec.12813

De Kort, H., Vander Mijnsbrugge, K., Vandepitte, K., Mergeay, J., Ovaskainen, O., Honnay, O., 2016. Evolution, plasticity and evolving plasticity of phenology in the tree species *Alnus glutinosa*. J of Evolutionary Biology 29, 253–264. https://doi.org/10.1111/jeb.12777

De Los Campos, G., Sorensen, D., Gianola, D., 2015. Genomic Heritability: What Is It? PLoS Genet 11, e1005048. https://doi.org/10.1371/journal.pgen.1005048

Demmig-Adams, B., Adams, W.I., 1996. Chlorophyll and Carotenoid Composition in Leaves of Euonymus kiautschovicus Acclimated to Different Degrees of Light Stress in the Field. Functional Plant Biol. 23, 649. https://doi.org/10.1071/PP9960649

Dengel, S., Grace, J., Aakala, T., Hari, P., Newberry, S.L., Mizunuma, T., 2013. Spectral characteristics of pine needles at the limit of tree growth in subarctic Finland. Plant Ecology & Diversity 6, 31–44. https://doi.org/10.1080/17550874.2012.754512

Deptuła, M., Piernik, A., Nienartowicz, A., Hulisz, P., Kamiński, D., 2020. Alnus glutinosa L. Gaertn. as potential tree for brackish and saline habitats. Global Ecology and Conservation 22, e00977. https://doi.org/10.1016/j.gecco.2020.e00977

Dittmar, C., Elling, W., 2006. Phenological phases of common beech (Fagus sylvatica L.) and their dependence on region and altitude in southern germany. European Journal of Forest Research 125, 181–188. https://doi.org/10.1007/s10342-005-0099-x

D'Odorico, P., Besik, A., Wong, C.Y.S., Isabel, N., Ensminger, I., 2020. High-throughput drone-based remote sensing reliably tracks phenology in thousands of conifer seedlings. New Phytologist 226, 1667–1681. https://doi.org/10.1111/nph.16488

D'Odorico, P., Schuman, M.C., Kurz, M., Csilléry, K., 2023. Discerning Oriental from European beech by leaf spectroscopy: Operational and physiological implications. Forest Ecology and Management 541, 121056. https://doi.org/10.1016/j.foreco.2023.121056

Donnelly, K., Cavers, S., Cottrell, J.E., Ennos, R.A., 2016. Genetic variation for needle traits in Scots pine (Pinus sylvestris L.). Tree Genetics & Genomes 12, 40. https://doi.org/10.1007/s11295-016-1000-4

Dounavi, A., Netzer, F., Celepirovic, N., Ivanković, M., Burger, J., Figueroa, A.G., Schön, S., Simon, J., Cremer, E., Fussi, B., Konnert, M., Rennenberg, H., 2016. Genetic and physiological differences of European beech provenances (F. sylvatica L.) exposed to drought stress. Forest Ecology and Management 361, 226–236. https://doi.org/10.1016/j.foreco.2015.11.014

Dungey, H.S., Dash, J.P., Pont, D., Clinton, P.W., Watt, M.S., Telfer, E.J., 2018. Phenotyping Whole Forests Will Help to Track Genetic Performance. Trends in Plant Science 23, 854–864. https://doi.org/10.1016/j.tplants.2018.08.005

Durrant, T.H., Rigo, D. de, Caudullo, G., 2016. Pinus sylvestris in Europe: distribution, habitat, usage and threats. European Atlas of Forest Tree Species.

Dutkowski, G.W., Silva, J.C.E., Gilmour, A.R., Lopez, G.A., 2002. Spatial analysis methods for forest genetic trials. Can. J. For. Res. 32, 2201–2214. https://doi.org/10.1139/x02-111

Dyderski, M.K., Paź, S., Frelich, L.E., Jagodziński, A.M., 2018. How much does climate change threaten European forest tree species distributions? Global Change Biology 24, 1150–1163. https://doi.org/10.1111/gcb.13925

Eismann, M., 2012. Hyperspectral Remote Sensing, 1st ed. ed, Press Monograph. Society of Photo-Optical Instrumentation Engineers (SPIE), Bellingham.

Eitel, J.U.H., Vierling, L.A., Litvak, M.E., Long, D.S., Schulthess, U., Ager, A.A., Krofcheck, D.J., Stoscheck, L., 2011. Broadband, red-edge information from satellites improves early stress detection in a New Mexico conifer woodland. Remote Sensing of Environment 115, 3640–3646. https://doi.org/10.1016/j.rse.2011.09.002

El-Hendawy, S., Al-Suhaibani, N., Mubushar, M., Tahir, M.U., Marey, S., Refay, Y., Tola, E., 2022. Combining Hyperspectral Reflectance and Multivariate Regression Models to Estimate Plant Biomass of Advanced Spring Wheat Lines in Diverse Phenological Stages under Salinity Conditions. Applied Sciences 12, 1983. https://doi.org/10.3390/app12041983

Eriksson, G., 2006. An introduction to forest genetics, 2. ed. ed. Genetic Center, Department of Plant Biology and Forest Genetics, SLU, Uppsala.

European Commission. Joint Research Centre., 2016. Robust modelling of the impacts of climate change on the habitat suitability of forest tree species. Publications Office, LU.

Faehn, C., Konert, G., Keinänen, M., Karppinen, K., Krause, K., 2024. Advancing hyperspectral imaging techniques for root systems: a new pipeline for macro- and microscale image acquisition and classification. Plant Methods 20, 171. https://doi.org/10.1186/s13007-024-01297-x

Falconer, D.S., Mackay, F.C.T., 1996. Introdutction to Quantitative Genetics, 4th ed. Harlow, Prentice Hall.

Faseela, P., Sinisha, A.K., Brestic, M., Puthur, J., 2020. Special issue in honour of Prof. Reto J. Strasser - Chlorophyll a fluorescence parameters as indicators of a particular abiotic stress in rice. Photosynthetica 58, 293–300. https://doi.org/10.32615/ps.2019.147

Feduck, C., McDermid, G., Castilla, G., 2018. Detection of Coniferous Seedlings in UAV Imagery. Forests 9, 432. https://doi.org/10.3390/f9070432

Feng, H., Guo, Z., Yang, W., Huang, C., Chen, G., Fang, W., Xiong, X., Zhang, H., Wang, G., Xiong, L., Liu, Q., 2017. An integrated hyperspectral imaging and genome-wide association analysis platform provides spectral and genetic insights into the natural variation in rice. Sci Rep 7, 4401. https://doi.org/10.1038/s41598-017-04668-8

Féret, J.-B., Le Maire, G., Jay, S., Berveiller, D., Bendoula, R., Hmimina, G., Cheraiet, A., Oliveira, J.C., Ponzoni, F.J., Solanki, T., De Boissieu, F., Chave, J., Nouvellon, Y., Porcar-Castell, A., Proisy, C., Soudani, K., Gastellu-Etchegorry, J.-P., Lefèvre-Fonollosa, M.-J., 2019. Estimating leaf mass per area and equivalent water thickness based on leaf optical properties: Potential and limitations of physical modeling and machine learning. Remote Sensing of Environment 231, 110959. https://doi.org/10.1016/j.rse.2018.11.002

Fghire, R., Anaya, F., Ali, O.I., Benlhabib, O., Ragab, R., Wahbi, S., 2015. Physiological and photosynthetic response of quinoa to drought stress. Chilean Journal of Agricultural Research 75, 174–183. https://doi.org/10.4067/S0718-58392015000200006

Fick, S.E., Hijmans, R.J., 2017. WorldClim 2: New 1-km spatial resolution climate surfaces for global land areas. International Journal of Climatology 37, 4302–4315. https://doi.org/10.1002/joc.5086

Field, C.B., Ball, J.T., Berry, J.A., 1989. Photosynthesis: principles and field techniques, in: Pearcy, R.W., Ehleringer, J.R., Mooney, H.A., Rundel, P.W. (Eds.), Plant Physiological Ecology: Field Methods and Instrumentation. Springer Netherlands, pp. 209–253. https://doi.org/10.1007/978-94-009-2221-1_11

Fiorani, F., Schurr, U., 2013. Future Scenarios for Plant Phenotyping. Annual Review of Plant Biology 64, 267–291. https://doi.org/10.1146/annurev-arplant-050312-120137

Fossdal, C.G., Krokene, P., Olsen, J.E., Strimbeck, R., Viejo, M., Yakovlev, I., Mageroy, M.H., 2024. Epigenetic stress memory in gymnosperms. Plant Physiology 195, 1117–1133. https://doi.org/10.1093/plphys/kiae051

Fotelli, M.N., Nahm, M., Radoglou, K., Rennenberg, H., Halyvopoulos, G., Matzarakis, A., 2009. Seasonal and interannual ecophysiological responses of beech (Fagus sylvatica) at its south-eastern distribution limit in Europe. Forest Ecology and Management 257, 1157–1164. https://doi.org/10.1016/j.foreco.2008.11.026

Gamon, J.A., Huemmrich, K.F., Wong, C.Y.S., Ensminger, I., Garrity, S., Hollinger, D.Y., Noormets, A., Peñuelas, J., 2016. A remotely sensed pigment index reveals photosynthetic phenology in evergreen conifers. Proc Natl Acad Sci USA 113, 13087–13092. https://doi.org/10.1073/pnas.1606162113

Gapare, W.J., Ivković, M., Liepe, K.J., Hamann, A., Low, C.B., 2015. Drivers of genotype by environment interaction in radiata pine as indicated by multivariate regression trees. Forest Ecology and Management 353, 21–29. https://doi.org/10.1016/j.foreco.2015.05.027

García-Plazaola, J.I., Becerril, J.M., 2001. Seasonal changes in photosynthetic pigments and antioxidants in beech (Fagus sylvatica) in a Mediterranean climate: Implications for tree decline diagnosis. Australian Journal of Plant Physiology 28, 225–232. https://doi.org/10.1071/pp00119

García-Plazaola, J.I., Esteban, R., Fernández-Marín, B., Kranner, I., Porcar-Castell, A., 2012. Thermal energy dissipation and xanthophyll cycles beyond the Arabidopsis model. Photosynth Res 113, 89–103. https://doi.org/10.1007/s11120-012-9760-7

Garillos-Manliguez, C.A., Chiang, J.Y., 2021. Multimodal Deep Learning and Visible-Light and Hyperspectral Imaging for Fruit Maturity Estimation. Sensors 21, 1288. https://doi.org/10.3390/s21041288

Georgopoulos, K., Bezemer, T.M., Vesterdal, L., Li, K., De Nobel, L., Gomes, S.I.F., 2025. Nondestructive Detection of *Frankia* in *ALNUS GLUTINOSA* With NIR Spectroscopy. Plant Enviro Interactions 6. https://doi.org/10.1002/pei3.70066

Gessler, A., Bottero, A., Marshall, J., Arend, M., 2020. The way back: recovery of trees from drought and its implication for acclimation. New Phytologist 228, 1704–1709. https://doi.org/10.1111/nph.16703

Gitelson, A., 2020. Towards a generic approach to remote non-invasive estimation of foliar carotenoid-to-chlorophyll ratio | Elsevier Enhanced Reader. Journal of Plant Physiology 153227. https://doi.org/10.1016/j.jplph.2020.153227

Gitelson, A.A., Solovchenko, A., 2018. Non-invasive quantification of foliar pigments: Possibilities and limitations of reflectance- and absorbance-based approaches. Journal of Photochemistry and Photobiology B: Biology 178, 537–544. https://doi.org/10.1016/j.jphotobiol.2017.11.023

Granlund, L., Keski-Saari, S., Kumpula, T., Oksanen, E., Keinänen, M., 2018. Imaging lichen water content with visible to mid-wave infrared (400–5500 nm) spectroscopy. Remote Sensing of Environment 216, 301–310. https://doi.org/10.1016/j.rse.2018.06.041

Grattapaglia, D., Plomion, C., Kirst, M., Sederoff, R.R., 2009. Genomics of growth traits in forest trees. Current Opinion in Plant Biology 12, 148–156. https://doi.org/10.1016/j.pbi.2008.12.008

Grattapaglia, D., Resende, M.D.V., 2011. Genomic selection in forest tree breeding. Tree Genetics & Genomes 7, 241–255. https://doi.org/10.1007/s11295-010-0328-4

Grattapaglia, D., Silva-Junior, O.B., Resende, R.T., Cappa, E.P., Müller, B.S.F., Tan, B., Isik, F., Ratcliffe, B., El-Kassaby, Y.A., 2018. Quantitative Genetics and Genomics Converge to Accelerate Forest Tree Breeding. Front. Plant Sci. 9, 1693. https://doi.org/10.3389/fpls.2018.01693

Griess, V.C., Acevedo, R., Härtl, F., Staupendahl, K., Knoke, T., 2012. Does mixing tree species enhance stand resistance against natural hazards? A case study for spruce. Forest Ecology and Management 267, 284–296. https://doi.org/10.1016/j.foreco.2011.11.035

Grubinger, S., Coops, N.C., O'Neill, G.A., 2023. Picturing local adaptation: Spectral and structural traits from drone remote sensing reveal clinal responses to climate transfer in common-garden trials of interior spruce (Picea engelmannii × glauca). Global Change Biology 29, 4842–4860. https://doi.org/10.1111/gcb.16855

Grubinger, S., Coops, N.C., O'Neill, G.A., Degner, J.C., Wang, T., Waite, O.J.M., Riofrío, J., Koch, T.L., 2025. Seasonal vegetation dynamics for phenotyping using multispectral drone imagery: Genetic differentiation, climate adaptation, and hybridization in a common-garden trial of interior spruce (Picea engelmannii × glauca). Remote Sensing of Environment 317, 114512. https://doi.org/10.1016/j.rse.2024.114512

Guerra-Hernández, J., Díaz-Varela, R.A., Ávarez-González, J.G., Rodríguez-González, P.M., 2021. Assessing a novel modelling approach with high resolution UAV imagery for monitoring health status in priority riparian forests. Forest Ecosystems 8. https://doi.org/10.1186/s40663-021-00342-8

Hamann, A., Koshy, M.P., Namkoong, G., Ying, C.C., 2000. Genotype×environment interactions in Alnus rubra: developing seed zones and seed-transfer guidelines with spatial statistics and GIS. Forest Ecology and Management 136, 107–119. https://doi.org/10.1016/S0378-1127(99)00284-4

Hampe, A., Petit, R.J., 2005. Conserving biodiversity under climate change: the rear edge matters. Ecology Letters 8, 461–467. https://doi.org/10.1111/j.1461-0248.2005.00739.x

Handa, I., Aerts, R., Berendse, F., Berg, M., Bruder, A., Butenschoen, O., Chauvet, E., Gessner, M., Jabiol, J., Makkonen, M., Mckie, B., Malmqvist, B., Peeters, E., Scheu, S., Schmid, B., Ruijven, J., Vos, V., Hättenschwiler, S., 2014. Consequences of biodiversity loss for litter decomposition across biomes. Nature 509, 218–221. https://doi.org/10.1038/nature13247

Haworth, M., Marino, G., Centritto, M., 2018. An introductory guide to gas exchange analysis of photosynthesis and its application to plant phenotyping and precision irrigation to enhance water use efficiency. Journal of Water and Climate Change 9. https://doi.org/10.2166/wcc.2018.152

Hazarika, R., Bolte, A., Bednarova, D., Chakraborty, D., Gaviria, J., Kanzian, M., Kowalczyk, J., Lackner, M., Lstibůrek, M., Longauer, R., Nagy, L., Tomášková, I., Schueler, S., 2021. Multi-actor perspectives on afforestation and reforestation strategies in Central Europe under climate change. Annals of Forest Science 78, 60. https://doi.org/10.1007/s13595-021-01044-5

Heide, O., 2003. High autumn temperature delays spring bud burst in boreal trees, counterbalancing the effect of climatic warming. Tree physiology 23, 931–936. https://doi.org/10.1093/treephys/23.13.931

Hejtmánek, J., Stejskal, J., Čepl, J., Lhotáková, Z., Korecký, J., Krejzková, A., Dvořák, J., Gezan, S.A., 2022. Revealing the Complex Relationship Among Hyperspectral

Reflectance, Photosynthetic Pigments, and Growth in Norway Spruce Ecotypes. Front. Plant Sci. 13, 721064. https://doi.org/10.3389/fpls.2022.721064

Hejtmánek, J., Stejskal, J., Provazník, D., Čepl, J., 2023. Understanding the role of ecotypic factors in the early growth of Pinus sylvestris L. J. For. Sci. 69, 539–549. https://doi.org/10.17221/102/2023-JFS

Henderson, C.R., 1975. Best Linear Unbiased Estimation and Prediction under a Selection Model. Biometrics 31, 423. https://doi.org/10.2307/2529430

Hlásny, T., Turčáni, M., 2013. Persisting bark beetle outbreak indicates the unsustainability of secondary Norway spruce forests: case study from Central Europe. Annals of Forest Science 70, 481–491. https://doi.org/10.1007/s13595-013-0279-7

Hong, Z., Fries, A., Wu, H.X., 2015. Age trend of heritability, genetic correlation, and efficiency of early selection for wood quality traits in Scots pine. Can. J. For. Res. 45, 817–825. https://doi.org/10.1139/cjfr-2014-0465

Houminer, N., Riov, J., Moshelion, M., Osem, Y., David-Schwartz, R., 2022. Comparison of Morphological and Physiological Traits between Pinus brutia, Pinus halepensis, and Their Vigorous F1 Hybrids. Forests 13, 1477. https://doi.org/10.3390/f13091477

Hrivnák, M., Krajmerová, D., Hrivnák, R., Slezák, M., Kochjarová, J., Jarolímek, I., Gömöry, D., 2023. Interplay between tree genetic variation, plant community composition and environment in forest communities dominated by black alder (Alnus glutinosa (L.) Gaertn.). Perspectives in Plant Ecology, Evolution and Systematics 60, 125748. https://doi.org/10.1016/j.ppees.2023.125748

Hu, G., Wang, T., Wan, M., Bao, W., Zeng, W., 2022. UAV remote sensing monitoring of pine forest diseases based on improved Mask R-CNN. International Journal of Remote Sensing 43, 1274–1305. https://doi.org/10.1080/01431161.2022.2032455

Hurme, P., Repo, T., Savolainen, O., Pääkkönen, T., 1997. Climatic adaptation of bud set and frost hardiness in Scots pine (*Pinus sylvestris*). Can. J. For. Res. 27, 716–723. https://doi.org/10.1139/x97-052

Hussain, S.B., Stinziano, J., Pierre, M.O., Vincent, C., 2024. Accurate photosynthetic parameter estimation at low stomatal conductance: effects of cuticular conductance and instrumental noise. Photosynth Res 160, 111–124. https://doi.org/10.1007/s11120-024-01092-8

Husson, C., Aguayo, J., Revellin, C., Frey, P., Ioos, R., Marçais, B., 2015. Evidence for homoploid speciation in Phytophthora alni supports taxonomic reclassification in this species complex. Fungal Genetics and Biology 77, 12–21. https://doi.org/10.1016/j.fgb.2015.02.013

Jacquemoud, S., Ustin, S., 2019. Leaf optical properties. Cambridge University Press, Cambridge. https://doi.org/10.1017/9781108686457

Jalink, H., Schoor, R., 2015. Role of Fluorescence Approaches to Understand Functional Traits of Photosynthesis. Phenomics in Crop Plants: Trends, Options and Limitations 181–194. https://doi.org/10.1007/978-81-322-2226-2_12

Jankowski, A., Wyka, T.P., Zytkowiak, R., Danusevičius, D., Oleksyn, J., 2019. Does climate-related in situ variability of Scots pine (Pinus sylvestris L.) needles have a genetic basis?

Evidence from common garden experiments. Tree Physiology 39, 573–589. https://doi.org/10.1093/treephys/tpy145

Jansen, M., Gilmer, F., Biskup, B., Nagel, K.A., Rascher, U., Fischbach, A., Briem, S., Dreissen, G., Tittmann, S., Braun, S., De Jaeger, I., Metzlaff, M., Schurr, U., Scharr, H., Walter, A., 2009. Simultaneous phenotyping of leaf growth and chlorophyll fluorescence via GROWSCREEN FLUORO allows detection of stress tolerance in Arabidopsis thaliana and other rosette plants. Functional Plant Biol. 36, 902. https://doi.org/10.1071/FP09095

Jiang, L., Dumroese, R.K., Liu, Y., Li, G., Lin, P., 2019. Short-day treatment affects growth, physiological parameters and needle proteome of Chinese pine (Pinus tabuliformis Carr.) seedlings. New Forests 50, 469–488. https://doi.org/10.1007/s11056-018-9671-3

Jin, X., 2012. Segmentation-based image processing system. U.S. Patent 8,260,048.

Jump, A.S., Hunt, J.M., Peñuelas, J., 2006. Rapid climate change-related growth decline at the southern range edge of Fagus sylvatica. Global Change Biology 12, 2163–2174. https://doi.org/10.1111/j.1365-2486.2006.01250.x

Kalaji, H.M., Govindjee, Bosa, K., Kościelniak, J., Żuk-Gołaszewska, K., 2011. Effects of salt stress on photosystem II efficiency and CO2 assimilation of two Syrian barley landraces. Environmental and Experimental Botany 73, 64–72. https://doi.org/10.1016/j.envexpbot.2010.10.009

Kalaji, H.M., Jajoo, A., Oukarroum, A., Brestic, M., Zivcak, M., Samborska, I.A., Cetner, M.D., Łukasik, I., Goltsev, V., Ladle, R.J., 2016. Chlorophyll a fluorescence as a tool to monitor physiological status of plants under abiotic stress conditions. Acta Physiologiae Plantarum 38, 102. https://doi.org/10.1007/s11738-016-2113-y

Kastally, C., Niskanen, A.K., Perry, A., Kujala, S.T., Avia, K., Cervantes, S., Haapanen, M., Kesälahti, R., Kumpula, T.A., Mattila, T.M., Ojeda, D.I., Tyrmi, J.S., Wachowiak, W., Cavers, S., Kärkkäinen, K., Savolainen, O., Pyhäjärvi, T., 2022. Taming the massive genome of Scots pine with PiSy50k, a new genotyping array for conifer research. The Plant Journal 109, 1337–1350. https://doi.org/10.1111/tpj.15628

Kattenborn, T., Schiefer, F., Zarco-Tejada, P., Schmidtlein, S., 2019. Advantages of retrieving pigment content [µg/cm2] versus concentration [%] from canopy reflectance. Remote Sensing of Environment 230, 111195. https://doi.org/10.1016/j.rse.2019.05.014

Kaur, S., Tiwari, V., Kumari, A., Chaudhary, E., Sharma, A., Ali, U., Garg, M., 2023. Protective and defensive role of anthocyanins under plant abiotic and biotic stresses: An emerging application in sustainable agriculture. Journal of Biotechnology 361, 12–29. https://doi.org/10.1016/j.jbiotec.2022.11.009

Kopačková-Strnadová, V., Koucká, L., Jelének, J., Lhotáková, Z., Oulehle, F., 2021. Canopy Top, Height and Photosynthetic Pigment Estimation Using Parrot Sequoia Multispectral Imagery and the Unmanned Aerial Vehicle (UAV). Remote Sensing 13, 705. https://doi.org/10.3390/rs13040705

Kothari, S., Beauchamp-Rioux, R., Blanchard, F., Crofts, A.L., Girard, A., Guilbeault-Mayers, X., Hacker, P.W., Pardo, J., Schweiger, A.K., Demers-Thibeault, S., Bruneau, A., Coops, N.C., Kalacska, M., Vellend, M., Laliberté, E., 2023. Predicting leaf traits

across functional groups using reflectance spectroscopy. New Phytologist 238, 549–566. https://doi.org/10.1111/nph.18713

Kowalski, T., 2006. *Chalara fraxinea* sp. nov. associated with dieback of ash (*Fraxinus excelsior*) in Poland. Forest Pathology 36, 264–270. https://doi.org/10.1111/j.1439-0329.2006.00453.x

Kowalski, T., Holdenrieder, O., 2009. Pathogenicity of Chalara fraxinea. Forest Pathology 39, 1–7. https://doi.org/10.1111/j.1439-0329.2008.00565.x

Kučerová, J., Konôpková, A., Pšidová, E., Kurjak, D., Jamnická, G., Slugenová, K., Gömöry, D., Ditmarová, L., 2018. Adaptive variation in physiological traits of beech provenances in Central Europe. IForest 11, 24–31. https://doi.org/10.3832/ifor2291-010

Kuhn, M., 2008. Building Predictive Models in*R*Using the**caret**Package. J. Stat. Soft. 28. https://doi.org/10.18637/jss.v028.i05

Kureel, N., Sarup, J., Matin, S., Goswami, S., Kureel, K., 2022. Modelling vegetation health and stress using hypersepctral remote sensing data. Modeling Earth Systems and Environment 8, 733–748. https://doi.org/10.1007/s40808-021-01113-8

Kurjak, D., Konôpková, A., Kmeť, J., Macková, M., Frýdl, J., Živčák, M., Palmroth, S., Ditmarová, Ľ., Gömöry, D., 2019. Variation in the performance and thermostability of photosystem II in European beech (Fagus sylvatica L.) provenances is influenced more by acclimation than by adaptation. European Journal of Forest Research 138, 79–92. https://doi.org/10.1007/s10342-018-1155-7

Kuznetsova, T., Lukjanova, A., Mandre, M., Lõhmus, K., 2011. Aboveground biomass and nutrient accumulation dynamics in young black alder, silver birch and Scots pine plantations on reclaimed oil shale mining areas in Estonia. Forest Ecology and Management 262, 56–64. https://doi.org/10.1016/j.foreco.2010.09.030

Lefèvre, F., Fady, B., Fallour-Rubio, D., Ghosn, D., Bariteau, M., 2004. Impact of founder population, drift and selection on the genetic diversity of a recently translocated tree population. Heredity 93, 542–550. https://doi.org/10.1038/sj.hdy.6800549

Leuschner, C., Backes, K., Hertel, D., Schipka, F., Schmitt, U., Terborg, O., Runge, M., 2001. Drought responses at leaf, stem and fine root levels of competitive Fagus sylvatica L. and Quercus petraea (Matt.) Liebl. trees in dry and wet years. Forest Ecology and Management 149, 33–46. https://doi.org/10.1016/S0378-1127(00)00543-0

Leverenz, J.W., Bruhn, D., Saxe, H., 1999. Responses of two provenances of Fagus sylvatica seedlings to a combination of four temperature and two CO2 treatments during their first growing season: Gas exchange of leaves and roots. New Phytologist 144, 437–454. https://doi.org/10.1046/j.1469-8137.1999.00541.x

Lévesque, M., Saurer, M., Siegwolf, R., Eilmann, B., Brang, P., Bugmann, H., Rigling, A., 2013. Drought response of five conifer species under contrasting water availability suggests high vulnerability of Norway spruce and European larch. Global Change Biology 19, 3184–3199. https://doi.org/10.1111/gcb.12268

Lhotáková, Z., Brodský, L., Kupková, L., Kopačková, V., Potůčková, M., Mišurec, J., Klement, A., Kovářová, M., Albrechtová, J., 2013. Detection of multiple stresses in Scots pine growing at post-mining sites using visible to near-infrared spectroscopy.

Environmental Science: Processes & Impacts 15, 2004. https://doi.org/10.1039/c3em00388d

Lhotáková, Z., Neuwirthová, E., Potůčková, M., Červená, L., Hunt, L., Kupková, L., Lukeš, P., Campbell, P., Albrechtová, J., 2025. Mind the leaf anatomy while taking ground truth with portable chlorophyll meters. Sci Rep 15. https://doi.org/10.1038/s41598-024-84052-5

Li, C., Czyż, E.A., Halitschke, R., Baldwin, I.T., Schaepman, M.E., Schuman, M.C., 2023. Evaluating potential of leaf reflectance spectra to monitor plant genetic variation. Plant Methods 19, 108. https://doi.org/10.1186/s13007-023-01089-9

Li, Y., Suontama, M., Burdon, R.D., Dungey, H.S., 2017. Genotype by environment interactions in forest tree breeding: review of methodology and perspectives on research and application. Tree Genetics & Genomes 13. https://doi.org/10.1007/s11295-017-1144-x

Li, Y., Yang, X., Tong, L., Wang, L., Xue, L., Luan, Q., Jiang, J., 2023. Phenomic selection in slash pine multi-temporally using UAV-multispectral imagery. Front. Plant Sci. 14, 1156430. https://doi.org/10.3389/fpls.2023.1156430

Linder, S., 1972. Seasonal variation of pigments in needles: a study of Scots pine and Norway spruce seedlings grown under different nursery conditions; Årstidsvariation av pigment i barr från plantor av tall och gran odlade under skilda plantskolebetingelser, Studia forestalia Suecica. Skogshögskolan, Stockholm.

Liu, K.-H., Yang, M.-H., Huang, S.-T., Lin, C., 2022. Plant Species Classification Based on Hyperspectral Imaging via a Lightweight Convolutional Neural Network Model. Front. Plant Sci. 13, 855660. https://doi.org/10.3389/fpls.2022.855660

Lobo, F. de A., Barros, M.P. de, Dalmagro, H.J., Dalmolin, Â.C., Pereira, W.E., Souza, É.C. de, Vourlitis, G.L., Ortíz, C.E.R., 2013. Fitting net photosynthetic light-response curves with Microsoft Excel - a critical look at the models. Photosynthetica 51, 445–456. https://doi.org/10.1007/s11099-013-0045-y

Lstibůrek, M., Bittner, V., Hodge, G.R., Picek, J., Mackay, T.F.C., 2018. Estimating Realized Heritability in Panmictic Populations. Genetics 208, 89–95. https://doi.org/10.1534/genetics.117.300508

Lukyanets, V., Rumiantsev, M., Tarnopilska, O., Kobets, O., Musienko, S., Obolonyk, I., Bondarenko, V., Pozniakova, S., 2022. Distribution, productivity and natural regeneration of black alder (*Alnus glutinosa* (L.) Gaertn.) in Ukrainian Polissya. Folia Oecologica 49, 137–147. https://doi.org/10.2478/foecol-2022-0016

Luoranen, J., Rikala, R., 2012. Early season short-day treatment did not affect the field performance of *Pinus sylvestris* container seedlings in summer planting. Scandinavian Journal of Forest Research 27, 420–423. https://doi.org/10.1080/02827581.2012.670728

Lynch, M., Walsh, B., 1998. Genetics and analysis of quantitative traits. Sinauer, Sunderland, Mass.

Magri, D., Vendramin, G.G., Comps, B., Dupanloup, I., Geburek, T., Gömöry, D., Latałowa, M., Litt, T., Paule, L., Roure, J.M., Tantau, I., Knaap, W.O.V.D., Petit, R.J., Beaulieu, J.L.D., 2006. A new scenario for the Quaternary history of European beech populations:

Palaeobotanical evidence and genetic consequences. New Phytologist 171, 199–221. https://doi.org/10.1111/j.1469-8137.2006.01740.x

Marguerit, E., Bouffier, L., Chancerel, E., Costa, P., Lagane, F., Guehl, J.-M., Plomion, C., Brendel, O., 2014. The genetics of water-use efficiency and its relation to growth in maritime pine. Journal of Experimental Botany 65, 4757–4768. https://doi.org/10.1093/jxb/eru226

Mathur, S., Mehta, P., Jajoo, A., 2013. Effects of dual stress (high salt and high temperature) on the photochemical efficiency of wheat leaves (Triticum aestivum). Physiology and Molecular Biology of Plants 19, 179–188. https://doi.org/10.1007/s12298-012-0151-5

Mazis, A., Choudhury, S.D., Morgan, P.B., Stoerger, V., Hiller, J., Ge, Y., Awada, T., 2020. Application of high-throughput plant phenotyping for assessing biophysical traits and drought response in two oak species under controlled environment. Forest Ecology and Management 465, 118101. https://doi.org/10.1016/j.foreco.2020.118101

Mckinney, L., Nielsen, L., Collinge, D., Thomsen, I., Hansen, J., Kjaer, E., 2014. The ash dieback crisis: Genetic variation in resistance can prove a long-term solution. Plant Pathology 63. https://doi.org/10.1111/ppa.12196

Meng, F., Cao, R., Yang, D., Niklas, K.J., Sun, S., 2014. Trade-offs between light interception and leaf water shedding: A comparison of shade- and sun-adapted species in a subtropical rainforest. Oecologia 174, 13–22. https://doi.org/10.1007/s00442-013-2746-0

Miettinen, I., Zhang, C., Alonso, L., Fernández-Marín, B., García-Plazaola, J.I., Grebe, S., Porcar-Castell, A., Atherton, J., 2025. Hyperspectral Imaging Reveals Differential Carotenoid and Chlorophyll Temporal Dynamics and Spatial Patterns in Scots Pine Under Water Stress. Plant Cell & Environment 48, 1535–1554. https://doi.org/10.1111/pce.15225

Mishra, A., 2018. Chlorophyll Fluorescence: A Practical Approach to Study Ecophysiology of Green Plants, in: Advances in Plant Ecophysiology Techniques. pp. 77–97. https://doi.org/10.1007/978-3-319-93233-0_5

Mode, C.J., Robinson, H.F., 1959. Pleiotropism and the Genetic Variance and Covariance. Biometrics 15, 518. https://doi.org/10.2307/2527650

Montes, C.M., Fox, C., Sanz-Sáez, Á., Serbin, S.P., Kumagai, E., Krause, M.D., Xavier, A., Specht, J.E., Beavis, W.D., Bernacchi, C.J., Diers, B.W., Ainsworth, E.A., 2022. High-throughput characterization, correlation, and mapping of leaf photosynthetic and functional traits in the soybean (*Glycine max*) nested association mapping population. Genetics iyac065. https://doi.org/10.1093/genetics/iyac065

Mottus, M., Sulev, M., Hallik, L., 2014. Seasonal Course of the Spectral Properties of Alder and Birch Leaves. IEEE J. Sel. Top. Appl. Earth Observations Remote Sensing 7, 2496–2505. https://doi.org/10.1109/jstars.2013.2294242

Murchie, E., Lawson, T., 2013. Chlorophyll Fluorescence Analysis: A Guide to Good Practice and Understanding some new Applications. Journal of experimental botany 64, 3983–3998. https://doi.org/10.1093/jxb/ert208

Neale, D.B., Kremer, A., 2011. Forest tree genomics: growing resources and applications. Nat Rev Genet 12, 111–122. https://doi.org/10.1038/nrg2931

Neuwirthová, E., Kuusk, A., Lhotáková, Z., Kuusk, J., Albrechtová, J., Hallik, L., 2021. Leaf Age Matters in Remote Sensing: Taking Ground Truth for Spectroscopic Studies in Hemiboreal Deciduous Trees with Continuous Leaf Formation. Remote Sensing 13, 1353. https://doi.org/10.3390/rs13071353

Nielsen, C.N., Jørgensen, F.V., 2003. Phenology and diameter increment in seedlings of European beech (Fagus sylvatica L.) as affected by different soil water contents: variation between and within provenances. Forest Ecology and Management 174, 233–249. https://doi.org/10.1016/S0378-1127(02)00042-7

Niinemets, Ü., 2010. Responses of forest trees to single and multiple environmental stresses from seedlings to mature plants: Past stress history, stress interactions, tolerance and acclimation. Forest Ecology and Management 260, 1623–1639. https://doi.org/10.1016/j.foreco.2010.07.054

Niinemets, Ü., Tamm, Ü., 2005. Species differences in timing of leaf fall and foliage chemistry modify nutrient resorption efficiency in deciduous temperate forest stands. Tree Physiology 25, 1001–1014. https://doi.org/10.1093/treephys/25.8.1001

Novikova, T.N., Milyutin, L.I., 2006. Variation in certain characters and properties of scotch pine needles in geographic cultures. Russian Journal of Ecology 37, 90–96. https://doi.org/10.1134/S1067413606020044

Nozzolillo, C., Isabelle, P., Andersen, Ø.M., Abou-Zaid, M., 2002. Anthocyanins of jack pine *(Pinus banksiana)* seedlings. Can. J. Bot. 80, 796–801. https://doi.org/10.1139/b02-056

Odén, P.-C., Dunberg, A., 1984. Abscisic acid in shoots and roots of Scots pine (Pinus sylvestris L.) seedlings grown in controlled long-day and short-day environments. Planta 161, 148–155. https://doi.org/10.1007/BF00395475

Ols, C., Bontemps, J.-D., 2021. Pure and even-aged forestry of fast-growing conifers under climate change: on the need for a silvicultural paradigm shift. Environ. Res. Lett. 16, 024030. https://doi.org/10.1088/1748-9326/abd6a7

Omari, M.K., Lee, J., Faqeerzada, M.A., Joshi, R., Park, E., Cho, B.-K., 2020. Digital image-based plant phenotyping: a review. Korean J. Agric. Sci. 47, 119–130. https://doi.org/10.7744/kjoas.2020004

Onokpise, O.U., Hall, R.B., 1994. Evaluating European black alder (Alnus glutinosa (L.) Gaertn.) provenances for short rotation forestry. The Commonwealth Forestry Review 73, 113–120.

Oukarroum, A., Schansker, G., Strasser, R.J., 2009. Drought stress effects on photosystem i content and photosystem II thermotolerance analyzed using Chl a fluorescence kinetics in barley varieties differing in their drought tolerance. Physiologia Plantarum 137, 188–199. https://doi.org/10.1111/j.1399-3054.2009.01273.x

Pakharkova, N.V., Kuzmina, N.A., Kuzmin, S.R., Efremov, A.A., 2014. Morphophysiological traits of needles in different climatypes of Scots pine in provenance trial. Contemporary Problems of Ecology 7, 84–89. https://doi.org/10.1134/S1995425514010107

Pan, J., Jacobs, D., Li, G., 2017. Combined effects of short-day treatment and fall fertilization on growth, nutrient status, and spring bud break of Pinus tabulaeformis seedlings. iForest 10, 242–249. https://doi.org/10.3832/ifor2178-009

Parammal, F., K, S. a, Brestic, M., Puthur, J., 2019. Special issue in honour of Prof. Reto J. StrasserChlorophyll a fluorescence parameters as indicators of a particular abiotic stress in rice. Photosynthetica 58. https://doi.org/10.32615/ps.2019.147

Pashkovskiy, P., Ivanov, Y., Ivanova, A., Kartashov, A., Zlobin, I., Lyubimov, V., Ashikhmin, A., Bolshakov, M., Kreslavski, V., Kuznetsov, V., Allakhverdiev, S.I., 2023. Effect of Light of Different Spectral Compositions on Pro/Antioxidant Status, Content of Some Pigments and Secondary Metabolites and Expression of Related Genes in Scots Pine. Plants 12, 2552. https://doi.org/10.3390/plants12132552

Patterson, H.D., Thompson, R., 1971. Recovery of inter-block information when block sizes are unequal. Biometrika 58, 545–554. https://doi.org/10.1093/biomet/58.3.545

Perboni, A.T., Cassol, D., Silva, F.S.P. da, Silva, D.M., Bacarin, M.A., 2012. Chlorophyll a fluorescence study revealing effects of flooding in canola hybrids. Biologia 67, 338–346. https://doi.org/10.2478/s11756-012-0006-0

Pieruschka, R., Schurr, U., 2019. Plant Phenotyping: Past, Present, and Future. Plant Phenomics 2019, 7507131. https://doi.org/10.34133/2019/7507131

Pietrzykowski, M., Woś, B., 2021. The Impact of Climate Change on Forest Tree Species Dieback and Changes in Their Distribution, in: Choudhary, D.K., Mishra, A., Varma, A. (Eds.), Climate Change and the Microbiome: Sustenance of the Ecosphere. Springer International Publishing, Cham, pp. 447–460. https://doi.org/10.1007/978-3-030-76863-8_23

Pliûra, A., 2004. Possibilities for adaptation of Alnus glutinosa L. to changing environment. Biologija, 1 6–12. https://doi.org/10.6001/biologija.vi1.501

Porra, R., Thompson, W., Kriedemann, P., 1989. Determination of Accurate Extinction Coefficients and Simultaneous-Equations for Assaying Chlorophyll-a and Chlorophyll-B Extracted with 4 Different Solvents - Verification of the Concentration. Biochimica Et Biophysica Acta 975, 384–394. https://doi.org/10.1016/S0005-2728(89)80347-0

Porter, R.B., Lacourse, T., Hawkins, B.J., Yanchuk, A., 2013. Adaptive variation in growth, phenology, cold tolerance and nitrogen fixation of red alder (Alnus rubra Bong.). Forest Ecology and Management 291, 357–366. https://doi.org/10.1016/j.foreco.2012.11.017

Pott, R., 1997. Invasion of beech and establishment of beech forests in Europe. Annali Di Botanica 55, 27–58. https://doi.org/10.4462/annbotrm-9024

Poupon, V., Gezan, S.A., Schueler, S., Lstibůrek, M., 2023. Genotype x environment interaction and climate sensitivity in growth and wood density of European larch. Forest Ecology and Management 545, 121259. https://doi.org/10.1016/j.foreco.2023.121259

Primka, E.J., Smith, W.K., 2019. Synchrony in fall leaf drop: chlorophyll degradation, color change, and abscission layer formation in three temperate deciduous tree species. American Journal of Botany 106, 377–388. https://doi.org/10.1002/ajb2.1247

Provazník, D., Stejskal, J., Hansen, O.K., Čepl, J., Erichsen, E.R., Hansen, J.K., 2024. Addressing the altitudinal and geographical gradient in European beech via photosynthetic parameters: a case study on Calabrian beech transplanted to Denmark. Frontiers in Forests and Global Change 7. https://doi.org/10.3389/ffgc.2024.1369464

Provazník, D., Stejskal, J., Lhotáková, Z., Čepl, J., Neuwirthová, E., Nofrizal, A.Y., Korecký, J., Červená, L., Kupková, L., Klápště, J., Hansen, J.K., Gezan, S.A., Campbell, P.,

Lstibůrek, M., Albrechtová, J., 2025. Needle- and Canopy-Level Genetic Variation in Scots Pine (*Pinus sylvestris* L.) Revealed by Hyperspectral Phenotyping Across Sites and Seasons. Evolutionary Applications 18, e70176. https://doi.org/10.1111/eva.70176

Pšidová, E., Živčák, M., Stojnić, S., Orlović, S., Gömöry, D., Kučerová, J., Ditmarová, Ľ., Střelcová, K., Brestič, M., Kalaji, H.M., 2018. Altitude of origin influences the responses of PSII photochemistry to heat waves in European beech (Fagus sylvatica L.). Environmental and Experimental Botany 152, 97–106. https://doi.org/10.1016/j.envexpbot.2017.12.001

Pulkkinen, P., Varis, S., Jaatinen, R., Leppänen, A., Pakkanen, A., 2011. Increasing survival and growth of Scots pine seedlings with selection based on autumn coloration. Silva Fenn. 45. https://doi.org/10.14214/sf.93

QGIS Development Team, 2024. QGIS Geographic Information System.

R Core Team, 2014. R: A language and environment for statistical computing.

Redondo, M.A., Stenlid, J., Oliva, J., 2020. Genetic Variation Explains Changes in Susceptibility in a Naïve Host Against an Invasive Forest Pathogen: The Case of Alder and the *Phytophthora alni* Complex. Phytopathology® 110, 517–525. https://doi.org/10.1094/PHYTO-07-19-0272-R

Rehschuh, R., Cecilia, A., Zuber, M., Faragó, T., Baumbach, T., Hartmann, H., Jansen, S., Mayr, S., Ruehr, N., 2020. Drought-Induced Xylem Embolism Limits the Recovery of Leaf Gas Exchange in Scots Pine. Plant Physiol. 184, 852–864. https://doi.org/10.1104/pp.20.00407

Reich, P.B., Sendall, K.M., Stefanski, A., Rich, R.L., Hobbie, S.E., Montgomery, R.A., 2018. Effects of climate warming on photosynthesis in boreal tree species depend on soil moisture. Nature 562, 263–267. https://doi.org/10.1038/s41586-018-0582-4

Repo, T., Zhang, G., Ryyppö, A., Rikala, R., Vuorinen, M., 2000. The relation between growth cessation and frost hardening in Scots pines of different origins. Trees 14, 456–464. https://doi.org/10.1007/s004680000059

Reynolds, P., Frochot, H., Reynolds, P.E., 2003. Photosynthetic acclimation of beech seedlings to full sunlight following a major windstorm event in France. Annals of Forest Science 60, 701–709. https://doi.org/10.1051/forest:2003064ï

Richardson, A.D., Berlyn, G.P., 2002. Changes in foliar spectral reflectance and chlorophyll fluorescence of four temperate species following branch cutting. Tree Physiol. 22, 499–506.

Robson, T.M., Rasztovits, E., Aphalo, P.J., Alia, R., Aranda, I., 2013. Flushing phenology and fitness of European beech (Fagus sylvatica L.) provenances from a trial in La Rioja, Spain, segregate according to their climate of origin. Agricultural and Forest Meteorology 180, 76–85. https://doi.org/10.1016/j.agrformet.2013.05.008

Robson, T.M., Sánchez-Gómez, D., Cano, F.J., Aranda, I., 2012. Variation in functional leaf traits among beech provenances during a Spanish summer reflects the differences in their origin. Tree Genetics and Genomes 8, 1111–1121. https://doi.org/10.1007/s11295-012-0496-5

Rodríguez-González, P.M., Campelo, F., Albuquerque, A., Rivaes, R., Ferreira, T., Pereira, J.S., 2014. Sensitivity of black alder (Alnus glutinosa [L.] Gaertn.) growth to

hydrological changes in wetland forests at the rear edge of the species distribution. Plant Ecol 215, 233–245. https://doi.org/10.1007/s11258-013-0292-9

Rojo, J., Fernández-González, F., Lara, B., Bouso, V., Crespo, G., Hernández-Palacios, G., Rodríguez-Rojo, M.P., Rodríguez-Torres, A., Smith, M., Pérez-Badia, R., 2021. The effects of climate change on the flowering phenology of alder trees in southwestern Europe. Mediterr. Bot. 42, e67360. https://doi.org/10.5209/mbot.67360

Roman, A., Ursu, T., 2016. Multispectral satellite imagery and airborne laser scanning techniques for the detection of archaeological vegetation marks. pp. 141–152.

Rötzer, T., Grote, R., Pretzsch, H., 2004. The timing of bud burst and its effect on tree growth. International Journal of Biometeorology 48, 109–118. https://doi.org/10.1007/s00484-003-0191-1

Russell, M.B., Woodall, C.W., D'Amato, A.W., Domke, G.M., Saatchi, S.S., 2014. Beyond mean functional traits: Influence of functional trait profiles on forest structure, production, and mortality across the eastern US. Forest Ecology and Management 328, 1–9. https://doi.org/10.1016/j.foreco.2014.05.014

Rutkowski, P., Konatowska, S.M., 2019. TREE-SOIL-WATER RELATIONSHIPS IN EUROPEAN BLACK ALDER FOREST - CASE STUDY.

Rweyongeza, D.M., Yeh, F.C., Dancik, B.P., Dhir, N.K., 2003. Genetic Variation in Height, Branch and Needle Lengths of Pinus sylvestris L. from Siberia Tested in Alberta, Canada 2003.

Savolainen, O., Bokma, F., García-Gil, R., Komulainen, P., Repo, T., 2004. Genetic variation in cessation of growth and frost hardiness and consequences for adaptation of Pinus sylvestris to climatic changes. Forest Ecology and Management 197, 79–89. https://doi.org/10.1016/j.foreco.2004.05.006

Savolainen, O., Lascoux, M., Merilä, J., 2013. Ecological genomics of local adaptation. Nat Rev Genet 14, 807–820. https://doi.org/10.1038/nrg3522

Schieber, B., Janík, R., Snopková, Z., 2013. Phenology of common beech (Fagus sylvatica L.) along the altitudinal gradient in Slovak Republic (Inner Western Carpathians). JOURNAL OF FOREST SCIENCE 59, 176–184. https://doi.org/10.17221/82/2012-JFS

Schindelin, J., Arganda-Carreras, I., Frise, E., Kaynig, V., Longair, M., Pietzsch, T., Preibisch, S., Rueden, C., Saalfeld, S., Schmid, B., Tinevez, J.-Y., White, D.J., Hartenstein, V., Eliceiri, K., Tomancak, P., Cardona, A., 2012. Fiji: an open-source platform for biological-image analysis. Nat Methods 9, 676–682. https://doi.org/10.1038/nmeth.2019

Sederoff, R., Myburg, A., Kirst, M., 2009. Genomics, Domestication, and Evolution of Forest Trees. Cold Spring Harbor Symposia on Quantitative Biology 74, 303–317. https://doi.org/10.1101/sqb.2009.74.040

Seeley, M.M., Thomson, E., Allan, G.J., Wiebe, B.C., Whitham, T.G., Hultine, K.R., Cooper, H.F., Asner, G.P., Doughty, C.E., 2024. Disentangling heritability and plasticity effects on *Populus fremontii* leaf reflectance across a temperature gradient. https://doi.org/10.1101/2024.10.21.619129

Semerci, A., Semerci, H., Çalişkan, B., Çiçek, N., Ekmekçi, Y., Mencuccini, M., 2017. Morphological and physiological responses to drought stress of European provenances of Scots pine. Eur J Forest Res 136, 91–104. https://doi.org/10.1007/s10342-016-1011-6

Seyednasrollah, B., Bowling, D.R., Cheng, R., Logan, B.A., Magney, T.S., Frankenberg, C., Yang, J.C., Young, A.M., Hufkens, K., Arain, M.A., Black, T.A., Blanken, P.D., Bracho, R., Jassal, R., Hollinger, D.Y., Law, B.E., Nesic, Z., Richardson, A.D., 2021. Seasonal variation in the canopy color of temperate evergreen conifer forests. New Phytologist 229, 2586–2600. https://doi.org/10.1111/nph.17046

Shoshany, M., Spond, H., Bar, D.E., 2019. Overcast versus clear-sky remote sensing: comparing surface reflectance estimates. International Journal of Remote Sensing 40, 6737–6751. https://doi.org/10.1080/01431161.2019.1591649

Sigala, J.A., Uscola, M., Oliet, J.A., Jacobs, D.F., 2020. Drought tolerance and acclimation in Pinus ponderosa seedlings: the influence of nitrogen form. Tree Physiology 40, 1165–1177. https://doi.org/10.1093/treephys/tpaa052

Šindelář, J., Frýdl, J., Novotný, P., 2007. Towards the Scots pine (Pinus sylvestris L.) regional populations (ecotypes) characteristics in the Czech Republic. Výzkumný ústav lesního hospodářství a myslivosti, v. v. i.

Singh, M., Nara, U., Kumar, A., Thapa, S., Jaswal, C., Singh, H., 2021. Enhancing genetic gains through marker-assisted recurrent selection: from phenotyping to genotyping. Cereal Research Communications. https://doi.org/10.1007/s42976-021-00207-4

Slovíková, K., Bednářová, E., 2014. Monitoring of vegetative phenological stages in European beech (Fagus sylvatica l.) growing in a mixed stand. Acta Universitatis Agriculturae et Silviculturae Mendelianae Brunensis 62, 1109–1115. https://doi.org/10.11118/actaun201462051109

Song, G., Wang, Q., 2022. Developing Hyperspectral Indices for Assessing Seasonal Variations in the Ratio of Chlorophyll to Carotenoid in Deciduous Forests. Remote Sensing 14, 1324. https://doi.org/10.3390/rs14061324

Song, Q., Zhu, X.-G., 2024. Techniques for photosynthesis phenomics: gas exchange, fluorescence, and reflectance spectrums. Crop and Environment 3, 147–158. https://doi.org/10.1016/j.crope.2024.05.002

Song, Z., Xu, C., Luan, Q., Li, Y., 2024. Multitemporal UAV study of phenolic compounds in slash pine canopies. Remote Sensing of Environment 315, 114454. https://doi.org/10.1016/j.rse.2024.114454

Sonobe, R., Yamashita, H., Mihara, H., Morita, A., Ikka, T., 2020. Estimation of Leaf Chlorophyll a, b and Carotenoid Contents and Their Ratios Using Hyperspectral Reflectance. Remote Sensing 12, 3265. https://doi.org/10.3390/rs12193265

Stejskal, J., Čepl, J., Neuwirthová, E., Akinyemi, O.O., Chuchlík, J., Provazník, D., Keinänen, M., Campbell, P., Albrechtová, J., Lstibůrek, M., Lhotáková, Z., 2023. Making the Genotypic Variation Visible: Hyperspectral Phenotyping in Scots Pine Seedlings. Plant Phenomics 5, 0111. https://doi.org/10.34133/plantphenomics.0111

Strasser, R.J., Merope, T.-M., Srivastava, A., 2004. Analysis of the Chlorophyll a Fluorescence Transient, in: Christos, G., Papageorgiou, G. (Eds.), Chlorophyll a Fluorescence: A

Signature of Photosynthesis. Springer Netherlands, pp. 321–362. https://doi.org/10.1007/978-1-4020-3218-9_12

Strasser, R.J., Tsimilli-Michael, M., Qiang, S., Goltsev, V., 2010. Simultaneous in vivo recording of prompt and delayed fluorescence and 820-nm reflection changes during drying and after rehydration of the resurrection plant Haberlea rhodopensis. Biochimica et Biophysica Acta (BBA) - Bioenergetics 1797, 1313–1326. https://doi.org/10.1016/j.bbabio.2010.03.008

Švik, M., Lukeš, P., Lhotáková, Z., Neuwirthová, E., Albrechtová, J., Campbell, P.E., Homolová, L., 2023. Retrieving plant functional traits through time series analysis of satellite observations using machine learning methods. International Journal of Remote Sensing 44, 3083–3105. https://doi.org/10.1080/01431161.2023.2216847

Tamayo, P.R., Weiss, O., Sánchez-Moreiras, A.M., 2001. Gas Exchange Techniques in Photosynthesis and Respiration Infrared Gas Analyser, in: Roger, M.J.R. (Ed.), Handbook of Plant Ecophysiology Techniques. Springer Netherlands, pp. 113–139. https://doi.org/10.1007/0-306-48057-3_8

Tao, X., Li, Y., Yan, W., Wang, M., Tan, Z., Jiang, J., Luan, Q., 2021. Heritable variation in tree growth and needle vegetation indices of slash pine (Pinus elliottii) using unmanned aerial vehicles (UAVs). Industrial Crops and Products 173, 114073. https://doi.org/10.1016/j.indcrop.2021.114073

Taulavuori, E., Taulavuori, K., Niinimaa, A., Laine, K., 2010. Effect of Ecotype and Latitude on Growth, Frost Hardiness, and Oxidative Stress of South to North Transplanted Scots Pine Seedlings. International Journal of Forestry Research 2010, 1–16. https://doi.org/10.1155/2010/162084

Taulavuori, K., 2006. A simple method to visualize the mechanism why Alnus glutinosa remains green during autumn colouration of Sorbus aucuparia. Trees 20, 28–33. https://doi.org/10.1007/s00468-005-0009-3

Tilman, D., Wedin, D., Knops, J., 1996. Productivity and Sustainability Influenced by Biodiversity in Grassland Ecosystem. Nature 379. https://doi.org/10.1038/379718a0

Toivonen, A., Rikala, R., Repo, T., Smolander, H., 1991. Autumn colouration of first year *Pinus sylvestris* seedlings during frost hardening. Scandinavian Journal of Forest Research 6, 31–39. https://doi.org/10.1080/02827589109382644

Tsuchikawa, S., Kobori, H., 2015. A review of recent application of near infrared spectroscopy to wood science and technology. J Wood Sci 61, 213–220. https://doi.org/10.1007/s10086-015-1467-x

Usta, A., Yılmaz, M., Malkoçoğlu, S., Serdar, B., Yılmaz, S., Bozlar, T., 2014. ANATOMY OF BLACK ALDER (Alnus glutinosa (L.) Gaertner subsp. barbata (C.A. Meyer) Yalt) FROM TWO DIFFERENT. Fresenius Environmental Bulletin 23.

Vacek, Z., Vacek, S., Cukor, J., Bulušek, D., Slávik, M., Lukáčik, I., Štefančík, I., Sitková, Z., Eşen, D., Ripullone, F., Yildiz, O., Sarginci, M., D'Andrea, G., Weatherall, A., Šimůnek, V., Hájek, V., Králíček, I., Prausová, R., Bieniasz, A., Prokůpková, A., Putalová, T., 2022. Dendrochronological data from twelve countries proved definite growth response of black alder (*Alnus glutinosa* [L.] Gaertn.) to climate courses across its distribution range. Central European Forestry Journal 68, 139–153. https://doi.org/10.2478/forj-2022-0003

VanRaden, P.M., 2008. Efficient Methods to Compute Genomic Predictions. Journal of Dairy Science 91, 4414–4423. https://doi.org/10.3168/jds.2007-0980

Verbylaitė, R., Aravanopoulos, F.A., Baliuckas, V., Juškauskaitė, A., Ballian, D., 2023. Can a Forest Tree Species Progeny Trial Serve as an Ex Situ Collection? A Case Study on Alnus glutinosa. Plants 12, 3986. https://doi.org/10.3390/plants12233986

Vilhar, U., Beuker, E., Mizunuma, T., Skudnik, M., Lebourgeois, F., Soudani, K., Wilkinson, M., 2013. Tree Phenology, in: Developments in Environmental Science. Elsevier, pp. 169–182. https://doi.org/10.1016/B978-0-08-098222-9.00009-1

Virlet, N., Costes, E., Martinez, S., Kelner, J.-J., Regnard, J.-L., 2015. Multispectral airborne imagery in the field reveals genetic determinisms of morphological and transpiration traits of an apple tree hybrid population in response to water deficit. Journal of Experimental Botany 66, 5453–5465. https://doi.org/10.1093/jxb/erv355

Visscher, P.M., Goddard, M.E., 2015. A General Unified Framework to Assess the Sampling Variance of Heritability Estimates Using Pedigree or Marker-Based Relationships. Genetics 199, 223–232. https://doi.org/10.1534/genetics.114.171017

Vitasse, Y., Delzon, S., Dufrêne, E., Pontailler, J.Y., Louvet, J.M., Kremer, A., Michalet, R., 2009. Leaf phenology sensitivity to temperature in European trees: Do within-species populations exhibit similar responses? Agricultural and Forest Meteorology 149, 735–744. https://doi.org/10.1016/j.agrformet.2008.10.019

Vornam, B., Decarli, N., Gailing, O., 2004. Spatial Distribution of Genetic Variation in a Natural Beech Stand (Fagus sylvatica L.) Based on Microsatellite Markers. Conservation Genetics - CONSERV GENET 5, 561–570. https://doi.org/10.1023/B:COGE.0000041025.82917.ac

Walsh, B., Lynch, M., 2018. Evolution and Selection of Quantitative Traits. Oxford University Press. https://doi.org/10.1093/oso/9780198830870.001.0001

Wang, Q., Fleisher, D.H., Timlin, D., Reddy, V.R., Chun, J.A., 2012. Quantifying the measurement errors in a portable open gas-exchange system and their effects on the parameterization of Farquhar et al. model for C3 leaves. Photosynthetica 50, 223–238. https://doi.org/10.1007/s11099-012-0012-z

Webber, J., 2008. Experimental studies on factors influencing the transmission of Dutch elm disease. Investigación agraria. Sistemas y recursos forestales, ISSN 1131-7965, Vol. 13, Nº 1, 2004, pags. 197-206 13.

Wellburn, A.R., 1994. The Spectral Determination of Chlorophylls a and b, as well as Total Carotenoids, Using Various Solvents with Spectrophotometers of Different Resolution. Journal of Plant Physiology 307–313.

White, T., Adams, T., Neale, D., 2007. Forest Genetics. CABI Pub, Wallingford, UK ; Cambridge, MA.

Wong, C.Y.S., D'Odorico, P., Bhathena, Y., Arain, M.A., Ensminger, I., 2019. Carotenoid based vegetation indices for accurate monitoring of the phenology of photosynthesis at the leaf-scale in deciduous and evergreen trees. Remote Sensing of Environment 233, 111407. https://doi.org/10.1016/j.rse.2019.111407

Xie, C.-Y., 2008. Ten-year results from red alder (Alnus rubra Bong.) provenance-progeny testing and their implications for genetic improvement. New Forests 36, 273–284. https://doi.org/10.1007/s11056-008-9098-3

Yakovlev, I., Fossdal, C.G., Skrøppa, T., Olsen, J.E., Jahren, A.H., Johnsen, Ø., 2012. An adaptive epigenetic memory in conifers with important implications for seed production. Seed Sci. Res. 22, 63–76. https://doi.org/10.1017/s0960258511000535

Yang, J., Benyamin, B., McEvoy, B.P., Gordon, S., Henders, A.K., Nyholt, D.R., Madden, P.A., Heath, A.C., Martin, N.G., Montgomery, G.W., 2010. Common SNPs explain a large proportion of the heritability for human height. Nature genetics 42, 565–569.

Yigit, N., Öztürk, A., Sevik, H., Özel, H.B., Kshkush, F.E.R., Işık, B., 2023. Clonal variation based on some morphological and micromorphological characteristics in the Boyabat (Sinop/Turkey) black pine (Pinus nigra subsp. pallasiana (Lamb.) Holmboe) seed orchard. BioRes 18, 4850–4865. https://doi.org/10.15376/biores.18.3.4850-4865

Yuan, J., Xu, M., Duan, W., Fan, P., Li, S., 2013. Effects of Whole-root and Half-root Water Stress on Gas Exchange and Chlorophyll Fluorescence Parameters in Apple Trees. Journal of the American Society for Horticultural Science 138, 395–402. https://doi.org/10.21273/JASHS.138.5.395

Zang, C., Hartl-Meier, C., Dittmar, C., Rothe, A., Menzel, A., 2014. Patterns of drought tolerance in major European temperate forest trees: climatic drivers and levels of variability. Global Change Biology 20, 3767–3779. https://doi.org/10.1111/gcb.12637

Zhang, Y., Wu, J., Wang, A., 2022a. Comparison of various approaches for estimating leaf water content and stomatal conductance in different plant species using hyperspectral data. Ecological Indicators 142, 109278. https://doi.org/10.1016/j.ecolind.2022.109278

Zhang, Y., Wu, J., Wang, A., 2022b. Comparison of various approaches for estimating leaf water content and stomatal conductance in different plant species using hyperspectral data. Ecological Indicators 142, 109278. https://doi.org/10.1016/j.ecolind.2022.109278

Zheng, Y., Feng, M., Li, Xue, Huang, X., Chen, G., Bai, W., Xu, X., Li, J., Li, Xiaohong, Leng, B., Sun, H., He, C., Chen, Y., 2023. Phenotypic Variation Analysis and Excellent Clone Selection of Alnus cremastogyne from Different Provenances. Plants 12, 3259. https://doi.org/10.3390/plants12183259

Zobel, B.J., Talbert, B.J., 1984. Applied Forest Tree Improvement. John Wiley & Sons.

Attachments

Attachment 1 - Experiment 1 – Soil Analyses in Seed Orchards

	1988		2015	
	Plasy	Nepomuk	Plasy	Nepomuk
exchange acidity of soil - pH	3.3	3.6	3.7	3.8
Calcium content (mg Ca/kg)	263	293	441	660
Magnesium content (mg Mg/kg)	50	41	53	121
Phosphorous content (mg P/kg)	11	36	19	9
Potassium content (mg K/kg)	20	43	83	92
Carbon content (% C)	-	-	1.7	1.3
Nitrogen content (% N)	0.05	0.08	0.11	0.16
Hummus content (%)	1.7	1.61	3	2.2
C:N ratio	20	8	14	8

Supplementary Table 1: Soil Analyses Results from Plasy and Nepomuk seed orchards from 1988 and 2015. The Forestry and Game Management Research Institute prepared data from 1988. For the 2015 data, n=6 (Nepomuk), n=7 (Plasy). All element concentrations are expressed on a dry-soil basis (mg/kg oven-dry soil). The hyphen symbol indicates that the analysis was not performed.

Attachment 2 - Experiment 1 – Seed Orchard Layouts

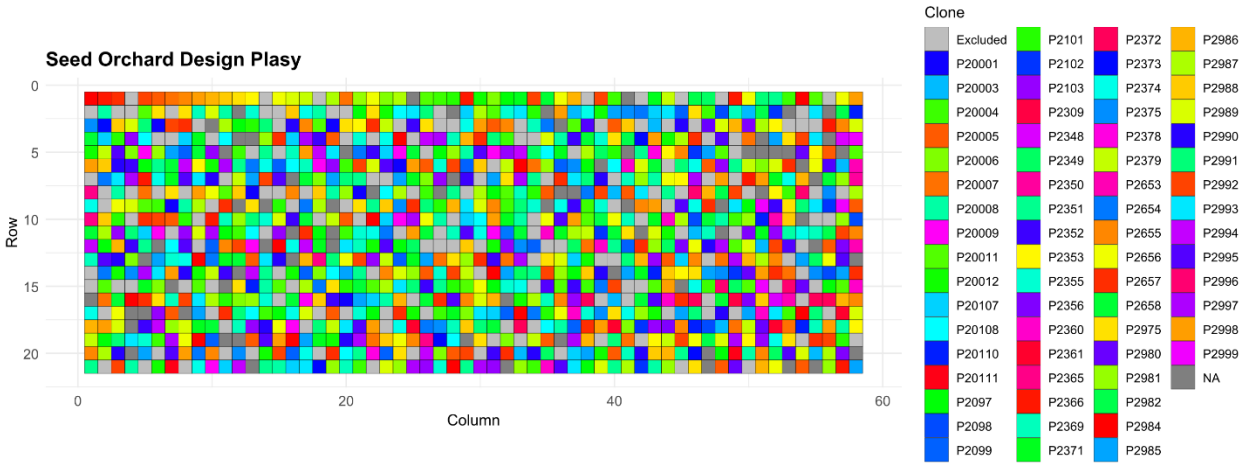

Supplementary Figure 1:Spatial visualization of the Plasy seed orchard design and the clones utilized for the analyses.

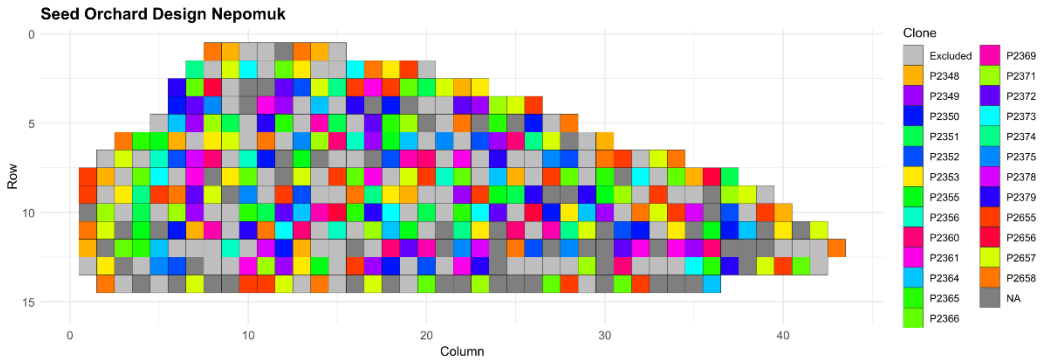

Supplementary Figure 2: Spatial visualization of the Nepomuk seed orchard design and the clones utilized for the analyses.

Attachment 3 - Experiment 2 – Experimental Layout

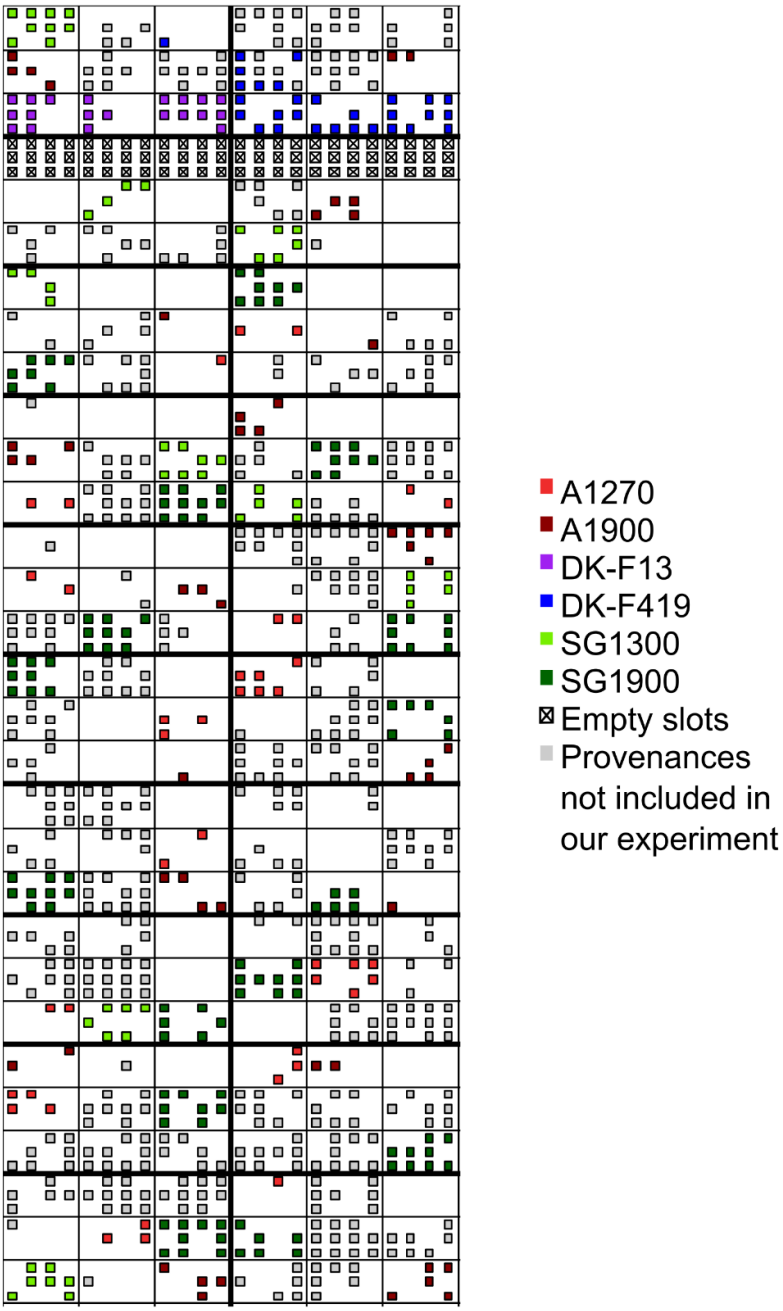

Supplementary Figure 3: Spatial design of the common garden in Experiment 2 in September 2018. Published in (Provazník et al., 2024).

Attachment 4 – Experiment 4 – Experimental Layouts of Each Site

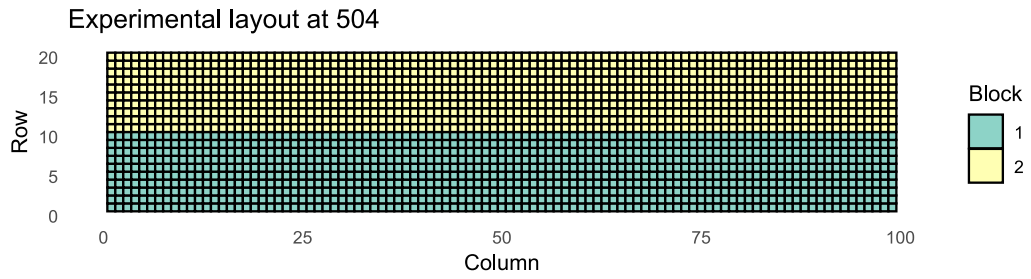

Supplementary Figure 4: Experimental layout at the 504 site.

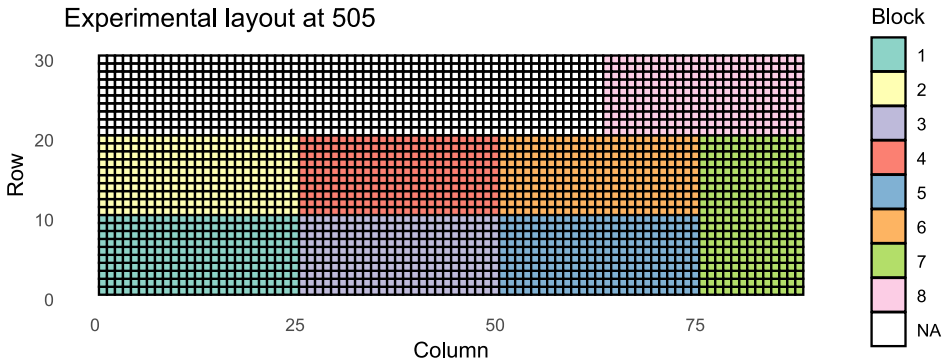

Supplementary Figure 5: Experimental layout at the 505 site. The white positions marked as NA were left empty.

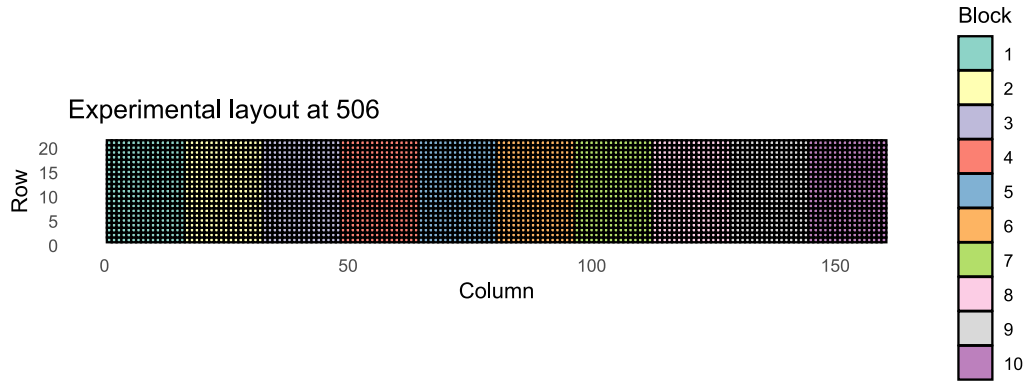

Supplementary Figure 6: Experimental layout at the 506 site.

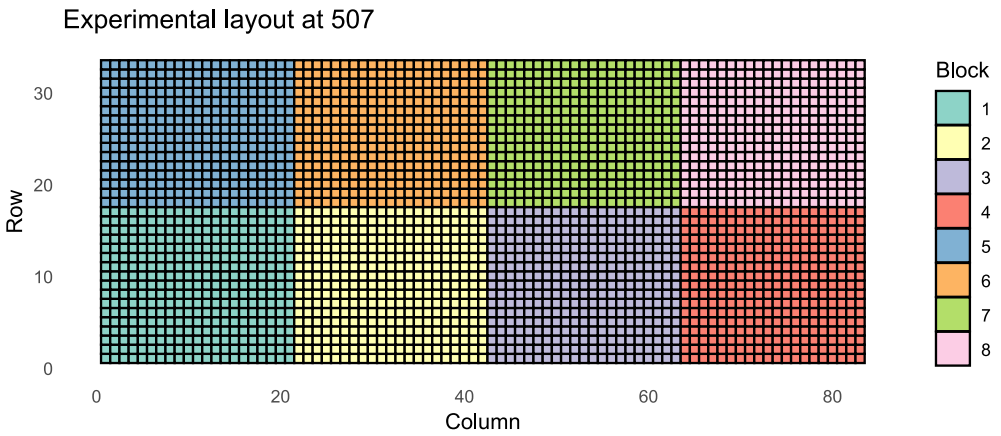

Supplementary Figure 7: Experimental layout at the 507 site.